Generalized Riemann Problems in Dispersive Hydrodynamics

by

Patrick Sprenger

B.S. Seattle University, 2014

M.S. University of Colorado Boulder, 2018

A thesis submitted to the

Faculty of the Graduate School of the

University of Colorado in partial fulfillment

of the requirements for the degree of

Doctor of Philosophy

Department of Applied Mathematics

2019

This thesis entitled:
Generalized Riemann Problems in Dispersive Hydrodynamics
written by Patrick Sprenger
has been approved for the Department of Applied Mathematics

Professor Mark Hoefer

Professor Bengt Fornberg

Professor Ian Grooms

Professor Keith Julien

Professor Patrick Weidman

Date

The final copy of this thesis has been examined by the signatories, and we find that both the content and the form meet acceptable presentation standards of scholarly work in the above mentioned discipline.

Sprenger, Patrick (Ph.D., Applied Mathematics)

Generalized Riemann Problems in Dispersive Hydrodynamics

Thesis directed by Professor Mark Hoefer

Nonlinear, dispersive wave phenomena occur in a variety of physical contexts, both in nature and the laboratory. Mathematically, their dynamics can be modeled by a dispersive hydrodynamic system—a first order system of conservation laws modified by dispersion. In appropriate physical regimes, a multi-scale asymptotic expansion can by employed to derive a scalar equation from which we can infer approximate dynamics of the overarching system.

We first study scalar models of dispersive hydrodynamics when dispersion is of higher order. Higher order dispersion in nonlinear, real-valued, local scalar equations can manifest when spatial derivatives are higher than third order. The primary mathematical framework we utilize is Whitham modulation theory, an asymptotic method to describe the slow modulations of a periodic wave's parameters. We identify three new classes of DSWs solutions to the Kawahara equation—a weakly nonlinear model that contains both third and fifth order dispersive terms. Numerical and asymptotic studies of the DSW solutions to the Kawahara equation motivate a further comprehensive study of the Whitham modulation equations for the fifth order Korteweg-de Vries (KdV5) equation. We compute various heteroclinic traveling waves that are shown to correspond to weak, discontinuous shock solutions of the KdV5-Whitham modulation system in the zero dispersion limit. The discontinuous shock solutions are shown to arise from a so-called generalized Riemann problem. The existence of heteroclinic traveling waves of the governing equation allow us to define the admissibility of discontinuous, weak solutions of the Whitham modulation equations, which we term **Whitham shocks**. Furthermore, the structure of the modulation equations, e.g. hyperbolicity or ellipticity, determine the modulational (in)stability of the heteroclinic traveling wave corresponding to an admissible Whitham shock. We then revisit the DSW solution of the

KdV5 equation and demonstrate that it can be described in terms of a shock-rarefaction solution of the KdV5-Whitham modulation system. We conclude this portion with a discussion of how our results can be applied to other model dispersive hydrodynamic systems.

We then investigate the interaction of a soliton and an evolving mean flow in bi-directional dispersive hydrodynamic media. The model equation is the defocusing nonlinear Schrödinger equation. Utilizing Whitham modulation theory and posing a generalized Riemann problem for an initial jump in the mean flow and the soliton amplitude, a simple wave solution of the diagonalized NLS-Whitham modulation equations is obtained. This yields algebraic relationships between far-field initial data and the solitary wave amplitude from which we may infer the long-time soliton dynamics including the hydrodynamic trapping or transmission of the soliton by a, possibly, oscillatory mean flow.

Dedication

To my mom and dad, in sincere thanks of their ongoing love and support.

Acknowledgements

Mark Hoefer, I could not ask for a better adviser. Among the technical skills I have developed directly as a result of your mentoring, I have also learned how to take the struggles of research in stride. Working with you has been a productive, humbling, and above all else, enjoyable experience.

Noel Smyth, I will forever remember my time spent working with you in Edinburgh. Thank you for welcoming me into your home and treating me like family.

My committee members: Professors Ian Grooms, Keith Julien, Bengt Fornberg, and Patrick Weidman. Your input and recommendations greatly improved this thesis.

Ezio Iacocca, you have been a great friend and mentor. I enjoyed our many lunchtime scientific and personal discussions.

Members of the Dispersive Hydrodynamics Laboratory, and in particular, Adam Binswanger. It was a pleasure to work and learn with all of you.

Audra, thank you for you unwavering love and support throughout the highs and lows of graduate school. May we continue to grow together.

All my friends at CU and in Boulder, you filled my life outside of graduate school with unforgettable experiences.

Contents

Chapter

1 Introduction **1**

1.1 Dispersive nonlinear waves: periodic and solitary waves 3

1.2 Resolution of singularities: dissipative and dispersive shock waves 5

1.2.1 Dissipative regularization: Burgers equation 9

1.2.2 Dispersive regularization: Korteweg-de Vries 10

1.3 Outline of this thesis 16

2 Derivation of fifth order KdV equations and computations of their traveling wave solutions **20**

2.1 Derivation of fifth order equations of KdV type 21

2.1.1 Multiple scale derivation of the Korteweg-de Vries and Kawahara equations 22

2.1.2 Water waves 28

2.1.3 Nonlinear fiber optics 30

2.1.4 Other systems 31

2.2 Traveling wave solutions 33

2.2.1 Solitary waves 35

2.2.2 Periodic waves 40

3 Whitham modulation equations for the Kawahara and KdV5 equations **46**

3.1 Whitham modulation equations: Derivation 47

3.1.1 Averaged conservation laws 48

3.1.2 Averaged Lagrangian 52

3.2 Properties of the weakly nonlinear Whitham Modulation equations 54

3.2.1 Hyperbolicity/ellipticity 54

3.2.2 Genuine nonlinearity 56

3.2.3 Simple waves 58

3.3 Whitham modulation equations for the KdV5 equation 58

3.3.1 Numerical computations of fully nonlinear KdV5-Whitham modulation equations 59

3.4 Conclusions 61

4 Numerical and asymptotic studies of wavebreaking in the Kawahara equation **63**

4.1 Dispersive shock waves in the Kawahara equation 64

4.1.1 Numerical evolution of step-like initial data 66

4.1.2 Non-convex dispersion with large jumps: TDSWs 67

4.1.3 Non-convex dispersion with small jumps: RDSWs 76

4.1.4 Non-convex dispersion with intermediate jumps: crossover regime . . 81

4.1.5 Convex dispersion 83

4.2 Conclusions 88

5 Discontinuous shock solutions of the KdV5-Whitham modulation equations **91**

5.1 Whitham shocks 93

5.2 Heteroclinic and homoclinic traveling waves 97

5.2.1 Solitary wave to periodic wave 97

5.2.2 Periodic wave to periodic wave 102

5.2.3 Two copropagating shock solutions 107

5.3 Conclusions 111

6 Applications and Extensions **114**

6.1 Dam break problem for the KdV5-Whitham modulation equations: traveling dispersive shock waves revisited 114

6.2 Traveling waves in gravity-capillary water waves 118

7 Hydrodynamic optical soliton tunneling **124**

7.1 Background 124

7.2 Problem formulation 127

7.2.1 NLS-Whitham modulation equations 128

7.2.2 Hydrodynamic soliton tunneling: setup 130

7.3 Hydrodynamic soliton tunneling: results 133

7.4 Conclusions 143

8 Conclusions and Future work **148**

Bibliography **152**

Appendix

A Stokes wave approximation **163**

B Numerical methods **166**

B.1 Traveling wave computations 166

B.1.1 Periodic solutions 166

B.1.2 Solitary wave solutions 167

B.2 Heteroclinic and homoclinic traveling waves 172

Tables

Table

5.1 Three distinct Whitham shock loci and right (+) characteristic velocities for (5.19) when the right periodic wave φ_+ is approximated by a weakly nonlinear Stokes wave (5.23). 99

5.2 Three distinct Whitham shock loci and right characteristic velocities using numerically computed periodic traveling waves. Compare with the approximate loci in Table 5.1. 99

Figures

Figure

1.1 Sample traveling wave solutions of the KdV equation. Black curves are periodic, elliptic function solutions (1.7) with zero mean, $\overline{u} = 0$. The solid red curve is the soliton solution of KdV with unit amplitude $a = 1$ and mean $\overline{u} = 0$. 4

1.2 Wavebreaking in the Hopf equation (1.11) with initial data $u_0(x) = e^{-x^2}$. The solution is shown at $t = 0$ (red dashed) and at $t = t_{\rm B} \approx 1.15$ (gray). The profile at $t = 2$ obtained via the method of characteristics is the black curve. 7

1.3 Dispersive shock wave solution to the KdV equation (1.2) for the initial data (1.15) with $u_l = 1$ and $u_r = 0$ and $w = 10$ at $t = 100$. 11

1.4 DSW solution of the KdV Riemann problem found by GP. (a) Solution in the physical domain at $t = 100$ (b) Riemann invariant, self-similar solution to Eq. (1.29) at $x/t = v_+ = 2/3$ we observe the coalescence $r_2 \to r_3^-$ and we observe the limit $r_2 \to r_1^+$ when $x/t = v_- = -1$. 14

1.5 Expanding KdV-like DSWs for (a) positive dispersion curvature ($\sigma = -1$) and (b) negative dispersion curvature ($\sigma = +1$), exhibiting dispersion curvature dependent orientation and polarity. 15

1.6 DSW solution of the KdV5 equation (1.4) with unit step initial data $u_l = 1$ and $u_r = 0$ at $t = 500$ 16

2.1 Numerically computed solitary wave profiles (insets) and speed-amplitude relation for the Kawahara equation with $\sigma = -1$ (solid) and the KdV equation (dashed). 37

2.2 Numerically computed solitary wave profiles (insets) and speed-amplitude relation for the Kawahara equation with $\sigma = +1$ (solid) and the KdV equation (dashed). The linear wave spectrum is denoted on the vertical axis by the thick black curve. The "band gap" where no solitary waves exist is the shaded region. 38

2.3 Characteristic roots, r, of the linearized, traveling wave equation (2.36) with $\sigma = +1$. 39

2.4 Numerically computed solitary wave solution of the KdV5 equation (1.4) with amplitude $a = 1$ and velocity $c \approx -0.3652$. 40

2.5 Zero mean periodic solutions of the Kawahara equation for $\sigma = -1$ with amplitudes, $a \in \{0.25, 0.5, \ldots, 1.75, 2\}$ for various wavenumbers (a) $k = 1$, (b) $k = 0.5$, and (c) $k = 0.2$ 43

2.6 Zero mean periodic solutions of the Kawahara equation for $\sigma = +1$ with amplitudes, $a \in \{0.25, 0.5, \ldots, 1.75, 2\}$ for various wavenumbers (a) $k = 1.2$, (b) $k = 1$, and (c) $k = 0.5$ 44

2.7 Numerically computed periodic traveling waves $\tilde{\varphi}(\theta, \tilde{k})$ with zero mean and unit amplitude. (a) Example periodic waves. (b) Comparison of numerically computed phase velocity $\tilde{c}$ for the family of periodic waves (black solid curve) compared with the Stokes approximation Eq. (2.41) (red dashed curve). Insets: example zero mean, unit amplitude periodic traveling waves for two different phase velocities. 45

3.1 Sketch of a nonlinear periodic wave with modulation parameters identified graphically. 47

3.2 Magnitude of imaginary part of the eigenvalues of the weakly nonlinear modulation equations of the Kawahara equation. (a) imaginary part of the eigenvalues expansions (3.27)–(3.28) (b) eigenvalues of the coefficient matrix (3.17). 55

3.3 (a) Eigenvalues of $\mathcal{A}$ for $\overline{u} = 0$, and $a = 1$ as a function of wavenumber $\tilde{k}$ shown in black curves. The eigenvalues from weakly nonlinear theory (3.29)–(3.31) are identified by dashed red curves. Gray, banded regions denote the domain of the 2-wave curves, which solve the ODE (3.35) in (b) and (c). (b) Example 2-wave curve for $0 < \tilde{k} \lesssim 0.15$. (c) Example 2-wave curve for $0.65 \lesssim \tilde{k} < 1$. . 61

4.1 Non-convex Kawahara dispersion relation for $\sigma = +1$ along with example numerical simulations for step initial data. The RDSW, crossover regime, and TDSW can be identified with properties of the dispersion curvature and the existence of solitary wave structures. 65

4.2 Kawahara traveling DSW resulting from the initial step $\Delta = 1$ for the non-convex case $\sigma = +1$. Initial data is shown in the top figure with the dashed curve. 68

4.3 Trailing edge comparison with Kawahara ($\sigma = +1$) solitary waves. (a) Computed TDSW (pluses) and solitary wave (solid) amplitude-speed relations. (b) Overlay of solitary wave on TDSW leading edge with $\Delta = 1$. 69

4.4 (+) Comparison of TDSW harmonic leading edge speed extracted from numerical simulations with the linear group velocity (solid). 69

4.5 Trailing edge of the TDSW evolving from the GP problem (4.1) with $\Delta = 1$ at $t = 100$. The parameters of the nonlinearly resonant periodic wave are identified: mean $\overline{u}$, amplitude $\bar{a}$ and wavenumber $\bar{k}$. 70

4.6 Comparisons of asymptotic predictions of nonlinear wavetrain features: (a) the amplitude of the nonlinear wavetrain, (b) the square of the wavenumber of the nonlinear wavetrain, and (c) the speed of the traveling wave. All figures compare values from computed traveling wave solutions (solid), asymptotic predictions (dashed), and data extracted from numerical simulations of the GP problem (pluses). 74

4.7 (a) Superimposed traveling wave solution to the dynamical system (4.8) with boundary conditions (4.19) (solid) on a TDSW computed from the GP problem with $\Delta = 1$ (dashed) at $t = 150$. (b) Absolute error between the two solutions. 75

4.8 Numerically computed Kawahara radiating DSWs in the small jump regime. (a) The solution at $t \approx 8573$ for jump $\Delta = 0.06$. The radiation is not visible due to its small amplitude. (b) Zoomed in view of radiation for RDSW in panel (a). (c) RDSW leading edge from (a) with an overlay of a numerically computed Kawahara solitary wave of the same speed. (d) Comparison of the leading edge amplitude a_+ versus Δ incorporating predictions from Kawahara DSW fitting (solid) and extracted values from numerical simulations (pluses). 77

4.9 Comparison of amplitude of the radiation in the small amplitude RDSW with Analytical prediction from (4.32) (solid) and extracted values from numerical simulations (pluses). 81

4.10 Crossover Kawahara DSW dynamics for the intermediate jump value $\Delta = 0.3$ with $\sigma = +1$. Initial data is the dashed curve. 83

4.11 Development of a classical Kawahara DSW with initial jump $\Delta = 1$ and convex dispersion $\sigma = -1$. Approximate initial data is shown in the top figure with the dashed curve. 84

4.12 Comparison of DSW trailing edge properties to Kawahara solitary waves. (a) Speed-amplitude relation of Kawahara solitary wave (solid) and DSW trailing edge from numerical simulation (pluses) for $\sigma = +1$. (b) Overlay of numerically computed solitary wave with coincident velocity to the DSW trailing edge for $\Delta = 1$. 85

4.13 Kawahara DSW trailing edge wavenumber (a) and DSW leading edge speed, (b) for varying jump height. Comparison between Whitham theory predictions for the Kawahara equation (solid), Whitham theory for the KdV equation (dashed) and numerical simulation of the Kawahara equation (pluses). . 87

4.14 Development of a Kawahara TDSW with initial jump $\Delta = 5$ and convex dispersion $\sigma = -1$. Approximate initial data is shown in the top figure with the dashed curve. 87

5.1 Numerical simulation of the Riemann problem (5.1) with $\Delta = 1$ for the KdV5 equation (1.4). (a) Solution at $t = 1000$ (solid) for a TDSW and the initial step (dashed). (b) A zoom in of the trailing edge that resembles an equilibrium heteroclinic to a periodic orbit traveling wave solution to the KdV5 equation [64]. 92

5.2 Computed traveling wave solutions corresponding to the periodic wave and mean values from the Whitham shock locus in Table 5.2, matched by the symbols in the lower left corner. 100

5.3 Whitham shock structure via heteroclinic TW solutions (solid). The left solitary wave (dashed red for $x < 0$) and right periodic wave (dashed blue for $x > 0$) from the Whitham shock loci reported in Table 5.2 are overlaid on the heteroclinic TW solution. The symbols in the lower left corners coincide with those in Fig. 5.2 and Table 5.2. 101

5.4 Characteristics of the KdV5-Whitham modulation equations for the Whitham shock locus ▲ in Table 5.2. (a) Weakly compressive 1-wave characteristics Γ_1, (b) Weakly expansive 2-wave characteristics Γ_2, and (c) Decelerating 3-wave characteristic family Γ_3. The shock is identified by the thick, red line. . . . 102

5.5 Characteristics of the KdV5-Whitham modulation equations for the solution ■ in Table 5.2. (a) Weakly compressive 1-wave characteristics Γ_1, (b) Weakly expansive 2-wave characteristics Γ_2, and (c) Accelerating 3-wave characteristic family Γ_3. The shock is identified by the thick, red line. 102

5.6 Continuation curves of admissible periodic to periodic Whitham shock solutions (5.28) and corresponding heteroclinic traveling wave solutions. (a),(c),(e) Shock loci for the periodic wave parameters $k_-(\overline{u}_-)$, $a_+(\overline{u}_-)$, $k_+(\overline{u}_-)$, and $V(\overline{u}_-)$. (b), (d), (f) Example heteroclinic solutions corresponding to the shock curves (a), (c), and (e) respectively. Gray, shaded areas in (a), (c) and (e) correspond to complex characteristic velocities and modulational instability. The zoomed-in inset in Figure (e) demonstrates that the amplitude is not constant across the solution curve. 105

5.7 (a)-(c) Characteristic families of the undercompressive Whitham shock in Fig. 5.6(b) with $\overline{u}_+ = 0.6$ where $\lambda_1^{(\pm)} < V < \lambda_2^{(\pm)} < \lambda_3^{(\pm)}$. The shock trajectory is depicted with the thick red curve. 106

5.8 Numerically computed normalized Whitham shock velocity $(V - \overline{u})/a$ (blue, dashed) and normalized, purely real characteristic velocities $(\lambda_1 - \overline{u})/a < (\lambda_2 - \overline{u})/a$ (black dots). The inset is a zoomed in view of the phase velocity and characteristics velocities for small $a^{-1/4}k$. 106

5.9 Double Whitham shock solution satisfying the jump conditions (5.7)–(5.9) from the interior periodic wave $(0, 1, k_{\rm i})$ to the outer solitary wave $(\overline{u}_{\rm o}, a_{\rm o}, 0)$. The shocks are identified by the solid black curves and the solution (shock structure) in physical space is shown in gray. 108

5.10 Evolution of perturbed homoclinic traveling wave solutions whose oscillatory parameters in Eq. (5.30) with $n = 25$ lie on the Whitham shock loci in Table 5.2. Initial data at $t = 0$ is evolved to $t = 2000$. (a) Double Whitham shocks ▲ in Table 5.2 with real characteristics. (b) Double Whitham shocks ● with complex characteristics. (c) Double Whitham shocks ■ with real characteristics. 109

5.11 Evolution of perturbed traveling waves corresponding to co-propagating Whitham shocks shown at initial time $t = 0$ and final time $t = 1500$. Parameter values are selected from those depicted in Figure 5.6. (a) traveling wave with parameters in Fig. 5.6(a) with $\overline{u}_{\rm o} = \overline{u}_{-} = 0.6$. (b) traveling wave with parameters in Fig. 5.6(a) with $\overline{u}_{\rm o} = \overline{u}_{-} = -0.3$. (c) traveling wave with parameters in Fig. 5.6(c) with $\overline{u}_{\rm o} = \overline{u}_{-} = 0.15$. (d) traveling wave with parameters in Fig. 5.6(e) with $\overline{u}_{\rm o} = \overline{u}_{-} = 0.1$. 110

6.1 Direct numerical simulation the initial value problem (5.1) with smoothed step data (dashed red) at $t = 1000$ (solid black). Three distinct velocities $V_{\rm s}$, $V_{\rm i}$, and V_{+} are identified. 118

6.2 Extracted modulation parameters (a) mean, (b) amplitude, and (c) wavenumber extracted from numerical simulations of (5.1) (circles) with the shock-rarefaction solution of the Whitham modulation equations at $t = 1000$ (solid curves). 118

6.3 (a)-(c)Traveling wave parameter values, a_{+}, k_{+} and V, respectively from computations of the jump conditions (6.7)–(6.9) (solid, black curves) compared against numerical computations of traveling waves from [121] (red circles). . 121

6.4 Solutions arising from step-like initial data (5.10) for the Whitham equation (6.10) matching the phase velocity, $c(k)$ for linear gravity-capillary water waves. The initial step has an amplitude of $\Delta = 0.25$ at $x = 0$ and the simulations are shown on the same axes at $t = 2000$ for various Bond numbers, B, specified in each subfigure. 123

7.1 Hydrodynamic soliton tunneling configurations. (a) soliton-RW collision (b) soliton-DSW collision (c) RW overtaking soliton (d) DSW overtaking soliton. 131

7.2 Hydrodynamic soliton tunneling configuration of the Riemann invariants for soliton-RW interactions. 135

7.3 Time reversibility of initial data $(\overline{\rho}_+, a_+)$ and $(\overline{\rho}_-, a_+)$ with $\overline{\rho}_+ < \overline{\rho}_-$. Forward temporal evolution results in soliton interaction with a 4-DSW (upper half plane) and backward evolution results in soliton interaction with a 1-RW. Soliton trajectories are depicted with solid and dashed curves. 136

7.4 Sketch of configurations demonstrating hydrodynamic reciprocity. Horizontal arrows refer to temporal evolution and vertical arrows connote the transformation to the reciprocal initial condition. 137

7.5 Comparison between the tunneling relation (7.29) (solid curves) and direct numerical simulations of the NLS equation (dots) with smoothed, step initial data defined by $\overline{\rho}_+ > 0$ and a soliton of amplitude a_+. (a) The overtaking cases in Fig. 7.1(c,d). (b) The collision cases in Fig. 7.1(a,b). Filled dots correspond to the emergence of a black soliton. The grey regions correspond to soliton-DSW tunneling and white regions correspond to soliton-RW tunneling. 139

7.6 Numerical simulation of hydrodynamically trapped solitons. (a) Soliton of amplitude $a_- = 0.25$ sent into a 4-DSW with $\overline{\rho}_+ = 0.5$. (b) Soliton of amplitude $a_+ = 1$ overtaken by RW with $\rho_+ = 4$. 145

7.7 Tracking a soliton through a RW and DSW via equations (7.35) and (7.39). (a) $\overline{\rho}_+ = 2$, $a_+ = 1$ and the sign of r_3 in Eq. (7.25) is "−". (b) $\overline{\rho}_+ = 0.5$, $a_+ = 0.5$, the r_3 sign is "−". (c) $\overline{\rho}_+ = 2$, $a_+ = 2$, the sign of r_3 is "+". (d) $\overline{\rho}_+ = 0.5$, $a_+ = 0.4$, the sign of r_3 is "+". Predictions from Eqs. (7.35) and (7.39) are the red dashed curves, the contours are from direct numerical simulation of Eq. (7.1). 146

7.8 Examples of the emergence of a black soliton after tunneling in the characteristic plane. The initial configurations are (a) RW collision case with $\overline{\rho}_+ = 2$, (b) DSW overtaking case with $\overline{\rho}_+ = 0.6$. Initial soliton amplitudes are chosen so that $a_- = 1$ in (7.29). Numerically computed soliton trajectories (contours) are compared against theoretical predictions of Eqs. (7.35) and (7.39). The snapshots of the intensity ρ at $t = 225$ are shown above the contour plots. . . 147

B.1 Validation of the spectral renormalization method for computing the soliton solution of the KdV equation (2.37) with $c = 1/3$. (a) Numerically computed solitary wave solution (black, solid) superimposed with the true solution (dashed, red). (b) The absolute error between the numerically computed solution and the true solution depicted in panel (a). (c) The amplitude of the Fourier coefficients of the numerically computed solution, $|\hat{u}|$ as a function of wavenumber k. (d) The relative error between iterations, $\max_k |\hat{w}_m - \hat{w}_{m-1}|$. 170

B.2 Example of the use of the Newton-CG method to compute the soliton solution of the KdV equation with velocity $c = 1/3$. (a) Numerically computed solitary wave solution (black, solid) superimposed with the true solution (dashed, red). (b) The absolute error between the numerically computed solution and the true solution depicted in panel (a). (c) The residual of $L_0[u_n]$ at each step of the iterative scheme (B.9), n. 173

B.3 Depiction of initial guess given to numerical method with an even reflection across the origin, identified by the vertical, dashed line. 174

B.4 Numerically computed periodic-to-periodic heteroclinic traveling wave corresponding to Whitham shock with parameters $\overline{u}_- = 0.75$, $a_- \approx 1.51$, $k_- \approx 0.206$, $k_+ \approx .809$. The number of oscillation periods are $n_- = 2$ and $n_+ = 10$. 176

B.5 Number of collocation points versus maximum residual error (red dots) for various periodic-periodic heteroclinic traveling waves plotted versus a reference line N^{-5} to demonstrate fifth order convergence. (a) Maximum residual error of a periodic-periodic heteroclinic traveling wave with approximate parameters $(\overline{u}_-, a_-, k_-) \approx (0.25, 1.37, 0.59)$ and $(\overline{u}_+, a_+, k_+) \approx (0, 1, 0.77)$ with $n_- = 12$ and $n_+ = 12$. (b) Maximum residual error of a periodic-periodic heteroclinic traveling wave with approximate parameters $(\overline{u}_-, a_-, k_-) \approx (-0.15, 1.02, 0.45)$ and $(\overline{u}_+, a_+, k_+) \approx (0, 1, 0.26)$ with $n_- = 5$ and $n_+ = 7$. Insets are computed heteroclinic traveling wave solutions with the smallest residual reported. . . 176

Chapter 1

Introduction

Dispersive hydrodynamics describe the evolution of a conservative fluid—or fluid like flow. The mathematical description of these systems consists of hyperbolic partial differential equations modified by wave dispersion rather than dissipation. The equations can be written in the form

$$\mathbf{u}_t + \nabla \cdot \mathbf{F}(\mathbf{u}) = \nabla \cdot \mathbf{D}[\mathbf{u}]. \tag{1.1}$$

Where $\mathbf{u} \in \mathbb{R}^n$ is a vector consisting of the hydrodynamic quantities, e.g. the fluid velocity, density, temperature, etc. The flux tensor $\mathbf{F}(\mathbf{u})$ contains convective and nonlinear terms, and $\mathbf{D}$ is an integro-differential dispersive operator such that $\mathbf{u}$ is conserved in time. Physical systems aptly described by Eq. (1.1) range from the familiar (surface and internal water waves) to the exotic (superfluids, nonlinear photonics, magnetic spin waves) [47]. The evolution of linear waves is determined by the linear dispersion relation, which is computed upon seeking an approximate harmonic solution to Eq. (1.1) of the form

$$\mathbf{u} = \mathbf{u}_0 + \epsilon \mathbf{u_1} e^{i(\mathbf{k}\cdot\mathbf{r} - \omega t)},$$

where $\mathbf{u}_0$, $\mathbf{u}_1$ are constants and $0 < \epsilon \ll 1$, $\mathbf{k}$ is an n-dimensional vector of spatial wavenumbers in the coordinates $\mathbf{r}$. The linearized equation is solved if the wave frequency, ω and spatial wavenumber k are related via

$$D(\omega, k; \mathbf{u}_0) = 0.$$

referred to as the **dispersion relation**. In general, for a dispersive hydrodynamic system with $\mathbf{u} \in \mathbb{R}^n$, the dispersion relation has up to n distinct branches $\omega_j = \omega_j(k, \mathbf{u}_0)$. For a scalar system, $\mathbf{u} \in \mathbb{R}$, (1.1) is **dispersive** if ω is real valued and ω_{kk} is not identically zero.

To shed light on the structure of nonlinear solutions to (1.1), we introduce a multi-scale, long wave expansion involving successively smaller terms. The universal, weakly nonlinear scalar model is the Koreteweg-de Vries (KdV) equation for a *single* hydrodynamic variable u

$$u_t + uu_x + \sigma u_{xxx} = 0, \tag{1.2}$$

where $\sigma = \pm 1$. In a long wave expansion with successively smaller terms, cubic dispersion dominates, which is why the KdV equation is said to be universal [1]. However, when successive terms are comparable, e.g., third and fifth order dispersion near an inflection point [121] in ω, then higher order dispersion (larger than third order) is operable. For a majority of this thesis, a long wave, nonlinear model encapsulating the competition between third and fifth order dispersion will be used. The model is the Kawahara equation [72] given by

$$u_t + uu_x + \sigma u_{xxx} + u_{xxxxx} = 0. \tag{1.3}$$

Alternatively, physical parameters may be such that third order dispersion is not operable. In this case, fifth order dispersion dominates and the scalar model equation approximating solutions to (1.1) is the fifth order Korteweg-de Vries (KdV5) equation

$$u_t + uu_x + u_{xxxxx} = 0. \tag{1.4}$$

Higher order dispersion is relevant in a variety of physical systems including gravity-capillary water waves [65, 37, 102] and flexural ice sheets on a free surface water wave [100, 58, 38], nonlinear optical systems [132, 136, 120, 48], and Bose-Einstein condensates [73]. Nonlinear PDEs with higher order or nonlocal dispersion admit solutions wholly different

from their lower order dispersive counterparts. The variety of novel solutions will be pivotal in the results presented later in this thesis. Our investigation of higher order dispersive systems will begin by reviewing some well known results for the Korteweg-de Vries equation (1.2). Solutions and their dynamics will be compared and contrasted with those that occur in scalar models for dissipative and higher order dispersive systems.

1.1 Dispersive nonlinear waves: periodic and solitary waves

In this section we review the well known solutions of the KdV equation, in particular periodic and solitary traveling wave solutions (cf. references [47, 140]). Traveling wave solutions to Eq. (1.2) are sought in the form $u = f(\xi)$ where $\xi = x - ct$, and c is the wave velocity. Substitution of the traveling wave ansatz into the KdV equation (1.2) results in the ordinary differential equation

$$-cf' + ff' + f''' = 0. \tag{1.5}$$

Upon integrating twice, the traveling wave ODE reduces to a first order system

$$f' = (\lambda_1 - f)(\lambda_2 - f)(\lambda_3 - f), \tag{1.6}$$

where λ_i, $i = 1, 2, 3$ are specified in terms of two integration constants and the wave velocity c. It is convenient to cast the constants λ_i in terms of new constants defined by

$$r_1 = \frac{\lambda_1 + \lambda_2}{2}, \quad r_2 = \frac{\lambda_1 + \lambda_3}{2}, \quad r_3 = \frac{\lambda_2 + \lambda_3}{2}.$$

The solution of Eq. (1.6) is

$$u(x,t) = r_1 + r_2 - r_3 + 2(r_3 - r_1)\mathrm{dn}^2\left(\sqrt{\frac{r_1 - r_3}{6}}\xi; m\right), \tag{1.7}$$

$$m = \frac{r_2 - r_1}{r_3 - r_1}, \qquad c = \frac{r_1 + r_2 + r_3}{3} \tag{1.8}$$

where dn is a Jacobi elliptic function, with modulus m [24]. Various periodic solutions of the KdV equation are shown in Fig. 1.1. Periodic traveling waves possess three parameters:

mean $\overline{u}$, amplitude a and wavenumber k given explicitly by

$$\begin{aligned} a &= 2(r_2 - r_1) \\ k &= \frac{\pi\sqrt{r_3 - r_2}}{2\sqrt{3}K(m)}, \\ \overline{u} &= r_1 + r_2 - r_3 + 2\,(r_3 - r_1)\,\frac{E(m)}{K(m)}, \end{aligned}$$

where $K(m)$ and $E(m)$ are complete elliptic integrals of the first and second kind, respectively.

In the limit as $r_2 \to r_3$, the periodic solution (1.7) transitions to the celebrated soliton solution [145]

$$u(x,t) = \overline{u} + a\mathrm{sech}^2\left(\sqrt{\frac{a}{12}}(x - ct + x_0)\right), \tag{1.9}$$

where the soliton velocity is given by $c = \frac{a}{3} + \overline{u}$.

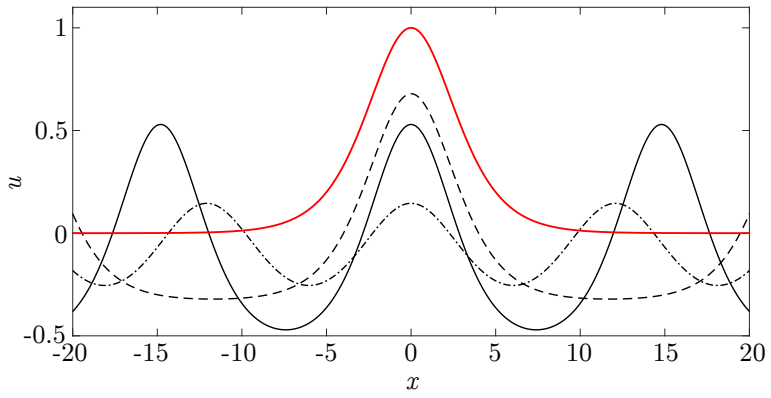

Figure 1.1: Sample traveling wave solutions of the KdV equation. Black curves are periodic, elliptic function solutions (1.7) with zero mean, $\overline{u} = 0$. The solid red curve is the soliton solution of KdV with unit amplitude $a = 1$ and mean $\overline{u} = 0$.

Soliton (solitary wave) and periodic traveling wave solutions of higher order dispersive systems can be quite different from those discussed here for the KdV equation. Here we will briefly summarize some relevant results regarding the traveling wave solutions for, primarily,

the Kawahara (1.3) and KdV5 (1.4) equations. Traveling wave solutions of the Kawahara equation (1.3) satisfy the fourth order ODE

$$-cf + \frac{1}{2}f^2 + \sigma f'' + f^{(4)} = A, \tag{1.10}$$

where $A \in \mathbb{R}$. Kawahara's original study of equation (1.3) included numerical computations of traveling waves satisfying (1.10) such as solitary wave solutions that do not decay monotonically from their peak [72]. Further analysis of the traveling wave ODE revealed various other solitary waves, periodic waves and solutions not falling into either category. Periodic and solitary wave solutions of the Kawahara equation can be understood by analyzing the ODE (1.10), or the equivalent fourth order dynamical system. Traveling waves wholly different from the KdV periodic wave (1.7) and KdV soliton (2.37) include multi-mode periodic waves (traveling waves in which two wavenumbers are resonant) [128, 52, 112], solitary waves consisting of multiple pulses [29], solitary waves with decaying oscillatory tails [72, 55], and solitary waves accompanied by co-propagating small, but finite, amplitude oscillations spatially extending to infinity [66, 6, 30]. This rich zoology of traveling waves can be attributed to additional degrees of freedom inherent in the fourth order system (1.10).

1.2 Resolution of singularities: dissipative and dispersive shock waves

In this section, we discuss the physical mechanisms that resolve singularities arising from nonlinearity in the governing equation. The regularization considered here may be due to dissipative (viscous) effects or conservative dispersive effects. We will show through canonical examples that dissipative and dispersive regularizations are fundamentally different and discuss the mathematical methods one can utilize to describe the ensuing shock wave. We will conclude this section with motivating numerical examples of shock waves that arise in the Korteweg-de Vries (1.2) and the fifth order Korteweg-de Vries (1.4) equations to elucidate some of the effects of purely higher order dispersion on dynamic nonlinear solutions.

The simplest initial value problem exhibiting finite time singularities consists of the

inviscid Burgers or Hopf equation

$$u_t + uu_x = 0 \tag{1.11}$$

with the initial data

$$u(x,0) = u_0(x), \tag{1.12}$$

where $u_0 \in C^1(\mathbb{R})$ for a classical solution. The solution of Equation (1.11) with initial data (1.12) originally found by Poisson [110] is defined implicitly by

$$u(x,t) = u_0(x - ut). \tag{1.13}$$

In the implicit solution, larger amplitude portions of the solution move faster than the small amplitude portions which results in self-steepening and finite time wavebreaking for nonmonotonically increasing initial data–i.e. an infinitely steep solution or gradient catastrophe. The time of breaking depends on the form of the initial data, and can be computed explicitly by taking partial derivatives of (1.13) $u_x = \frac{u_0'(x)}{1+u_0'(x)t}$, which implies

$$t_{\mathrm{B}} = -\frac{1}{\min u_0'(x)}.$$

If we continue to trace out the solution past the breaking time, we see a curve that is triple valued for a range of x values; this phenomenon is depicted in Figure 1.2.

To consider solutions with low regularity, we study the weak form of Eq. (1.11)

$$\int_0^\infty \int_{\mathbb{R}} \left(\phi_t u + \frac{1}{2} u^2 \phi_x \right) dx dt + \int_{\mathbb{R}} \phi(x,0) u(x,0) dx = 0, \tag{1.14}$$

where ϕ is any test function in $C^\infty(\mathbb{R} \times [0,\infty))$ with compact support. The weak form of the inviscid Burgers equation (1.14) is amenable to the discontinuous initial data

$$u(x,0) = \begin{cases} u_l & x < 0 \\ \\ u_r & x > 0 \end{cases}, \tag{1.15}$$

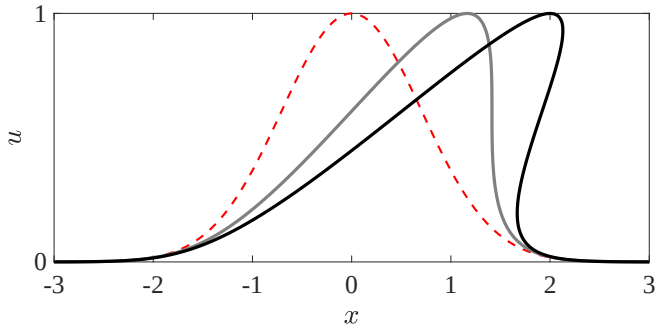

Figure 1.2: Wavebreaking in the Hopf equation (1.11) with initial data $u_0(x) = e^{-x^2}$. The solution is shown at $t = 0$ (red dashed) and at $t = t_{\mathrm{B}} \approx 1.15$ (gray). The profile at $t = 2$ obtained via the method of characteristics is the black curve.

which is referred to as the **Riemann problem**. We seek a solution of the form

$$u(x,t) = \begin{cases} u_l & x < Vt \\ \\ u_l & x > Vt \end{cases}, \tag{1.16}$$

and choose a test function, ϕ whose support encapsulates the curve $x = Vt$. Let Ω_l and Ω_r denote the disjoint regions of the support of ϕ separated by the curve $x = Vt$. Inserting the discontinuous solution (1.16) into Eq. (1.14) gives

$$\int_{\Omega_l} \left(\phi_t u_l + \frac{1}{2} u_l^2 \phi_x \right) dxdt + \int_{\Omega_+} \left(\phi_t u_r + \frac{1}{2} u_r^2 \phi_x \right) dxdt + \int_{\mathbb{R}} \phi(x,0) u(x,0) dx = 0. \tag{1.17}$$

Integrating by parts, we find that

$$\int_{x=Vt} \phi \left(-u_l + \frac{1}{2V} u_l^2 \right) dx - \int_{x=Vt} \phi \left(-u_r + \frac{1}{2V} u_r^2 \right) dx = 0, \tag{1.18}$$

which can be rewritten as

$$\int_{x=Vt} \phi \left(-(u_l - u_r) + \frac{1}{2V} (u_l^2 - u_r^2) \right) dx = 0. \tag{1.19}$$

Since the test function, ϕ is arbitrary, then we find that the shock velocity is

$$V = \frac{u_l + u_r}{2}, \tag{1.20}$$

The shock velocity is determined solely by the far-field values and satisfies the so-called Rankine-Hugoniot jump conditions. Systems of conservation laws with one spatial dimension take the form

$$\mathbf{u}_t + \mathbf{F}(\mathbf{u})_x = 0, \tag{1.21}$$

where $\mathbf{F} : \mathbb{R}^n \to \mathbb{R}^n$ is a C^2 function. Discontinuous solutions of the form

$$\mathbf{u}(x,t) = \begin{cases} \mathbf{u}_l & x < Vt \\ \\ \mathbf{u}_r & x > Vt \end{cases}, \tag{1.22}$$

satisfy the Rankine-Hugoniot relation

$$-V[\![\mathbf{u}]\!] + [\![\mathbf{F}(\mathbf{u})]\!] = 0, \tag{1.23}$$

where $[\![\cdot]\!]$ denotes the difference in a quantity evaluated at $\mathbf{u}_r$ and $\mathbf{u}_l$ respectively.

Rigorous investigations of the discontinouous data (1.15) by Lax [81] established the entropy conditions that define the **admissibility** of a weak, discontinuous solution, and ultimately the uniqueness of weak solutions. Fundamentally, the Lax entropy condition requires that the characteristics impinge upon the discontinuity. For Eq. (1.24), the characteristic velocities are given simply by u. Therefore, for the discontinuous solution (1.27) to be an admissible weak solution of Eq. (1.24) we require

$$u_r < V < u_l.$$

More simply stated, the discontinuous solution (1.27) is admissible provided that $u_l > u_r$.

Finite time singularity formation may be prevented by appending to the conservation law (1.11) additional physical terms that can be dissipative or dispersive. These terms compete with the self-steepening and prevent the formation of gradient catastrophe. In what follows, we present the classical mathematical description of dissipative and dispersive regularizations of gradient catastrophe and discuss what occurs when higher order dissipative or dispersive terms are in effect.

1.2.1 Dissipative regularization: Burgers equation

The Burgers equation is the canonical scalar model equation for nonlinear, dissipative wave dynamics and is given by

$$u_t + uu_x = \nu u_{xx}, \tag{1.24}$$

where $\nu > 0$ is the measure of dissipation. Let us seek a traveling wave heteroclinic solution of (1.24) of the form $u = f(\xi)$, $\xi = x - Vt$ with the far-field boundary conditions

$$f(\xi) \to u_l, \quad \xi \to -\infty$$
$$f(\xi) \to u_r, \quad \xi \to +\infty.$$

such that $f'(\xi) \to 0$ as $|\xi| \to \infty$. The traveling wave profile is then given by a solution to the ODE

$$-Vf' + ff' = \nu f'',$$

and a single integration from $\xi = -\infty$ gives

$$f' = \frac{1}{2\nu}(f^2 - u_l^2) - \frac{V}{\nu}(f - u_l). \tag{1.25}$$

Applying the boundary condition as $\xi \to +\infty$, we find the traveling wave velocity is given by

$$V = \frac{u_l + u_r}{2}. \tag{1.26}$$

Additionally, a phase plane analysis reveals that a heteroclinic solution satisfying the boundary conditions exist only if $u_l > u_r$. Integrating the first order equation (1.25), we find

$$f(\xi) = \frac{u_r + u_l e^{\frac{u_r - u_l}{2\nu}(\xi - \xi_0)}}{1 - e^{\frac{u_r - u_l}{2\nu}(\xi - \xi_0)}}$$

where ξ_0 is a constant of integration. The traveling wave solution for $u(x,t)$ can be written as a hyperbolic trigonometric function upon replacing $\xi = x - Vt$

$$u(x,t) = \frac{u_r + u_l}{2} + \frac{u_l - u_r}{2} \tanh\left(\frac{u_r - u_l}{4\nu}(x - Vt)\right), \tag{1.27}$$

where V is given by Eq. (1.20).

As the viscous term $\nu \to 0$, the hyperbolic tangent profile converges strongly to a weak solution of the Hopf equation (1.16). In fact, higher order dissipative regularizations admit smooth solutions that converge to the weak solution (1.16) in the vanishing-viscosity limit [125]. The convergence of a heteroclinic traveling waves to a weak, discontinuous solution affords us an alternative definition of admissible weak shocks (1.16). A weak shock is said to be admissible if it is the inviscid limit ($\nu \to 0$) of a heteroclinic traveling wave solution of the Burgers equation, i.e. the solution given by (1.27).

We will now briefly address the question of higher order dissipative effects on the shock solution so that these may be contrasted with the wavefronts that arise from dispersive regularization.

1.2.2 Dispersive regularization: Korteweg-de Vries

In this section, we outline the nonlinear wave patterns that arise from a smooth connection of disparate constant states that, for the Hopf equation, would result in finite time gradient catastrophe. To this end, we pose smoothed, decreasing initial data to the Korteweg-de Vries equation (1.2) with $\sigma = 1$ of the form

$$u(x,0) = \frac{u_r + u_l}{2} - \frac{u_r - u_l}{2} \tanh\left(\frac{x}{w}\right), \tag{1.28}$$

where $w > 0$ is the width of the initial discontinuity. Without loss of generality, we take $u_l = 1$ and $u_r = 0$. Numerical simulations of the initial value problem (1.2), (1.28) reveal a structure wholly different from the dynamics discussed in the previous section (cf. Eq. (1.27)). Figure 1.3 shows the evolution of the smoothed initial data, revealing a dynamically

expanding structure markedly different from the tanh profile (1.27) admitted by Burgers equation.

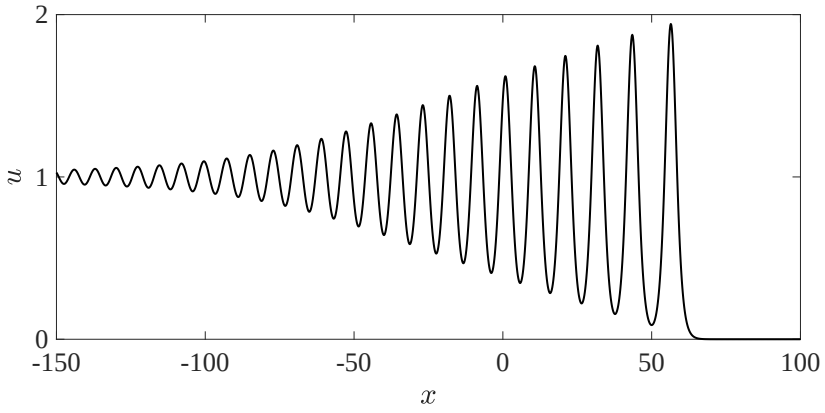

Figure 1.3: Dispersive shock wave solution to the KdV equation (1.2) for the initial data (1.15) with $u_l = 1$ and $u_r = 0$ and $w = 10$ at $t = 100$.

The wavetrain arising from gradient catastrophe consists of a slowly modulated, oscillatory wavetrain that limits to an approximate solitary wave at the front and a nearly linear, sinusoidal wave at the trailing edge. Structures resembling those in Fig. 1.3 arise in a variety of nonlinear dispersive systems and are hitherto referred to as **dispersive shock waves** (DSWs). Mathematically, classical DSWs in scalar systems can be described in terms of a continuous, solution of the Whitham modulation equations. In what follows, we outline the typical mathematical framework that can be used to describe the classical DSW solution of the KdV equation shown in Figure 1.3.

In their seminal 1974 paper, Gurevich and Pitaevskii (GP) considered the Riemann problem (1.15) for the KdV equation (1.2) with $u_l > u_r$ [57]. Here they utilized Whitham's averaging theory and employed matching conditions to determine the details of the DSW structure. We will briefly outline the procedure to obtain the KdV-Whitham equations and highlight the GP results.

The solution of the GP problem utilizes the Whitham modulation equations, a set of

first order, quasilinear equations that describe the evolution of a periodic wave's parameters on spatial and temporal scales longer than those over one oscillation period. For the KdV equation, Whitham's original derivation consisted of averaging conservation laws of (1.2) over the periodic solution (1.7) [138]. Specific details of the derivation can be found in a number of works [140, 71, 47]. In a series of papers, Lax, Levermore [82, 83, 84] and Venakides [130, 131] utilized the inverse scattering transform to prove that the KdV-Whitham system (and their multiphase generalizations [49]) describe the zero dispersion limit of the KdV equation. The limit was shown to be weak in the L^2 sense and thus provides a rigorous justification for Whithams averaging approach.

The KdV-Whitham modulation equations can be cast in diagonal Riemann invariant form via the parameters r_i, $i = 1, 2, 3$ and are given by

$$\frac{\partial r_i}{\partial t} + V_i(r_1, r_2, r_3)\frac{\partial r_I}{\partial x} = 0, \tag{1.29}$$

where the velocities are explicit functions of the Riemann invariants $r_1 \leq r_2 \leq r_3$. Of particular importance in the description of DSWs is the second Riemann invariant, r_2. The corresponding velocity of the characteristic family is

$$V_2 = \frac{r_1 + r_2 + r_3}{3} - \frac{2}{3}(r_2 - r_1)\frac{(1-m)K(m)}{E(m) - (1-m)K(m)}, \tag{1.30}$$

where K and E are the complete elliptic integrals of the first and second kind respectively and m is the elliptic modulus defined in (1.7). In the solitary wave limit, it can be shown that the second two Riemann invariants and their velocities coalesce, i.e. $r_2 \to r_3$ and $V_2 \to V_3$. Another special reduction of the KdV-Whitham equations that we will use is the linear wave limit where $r_2 \to r_1$, which is useful in the modulation description of the DSW solution to KdV. GP constructed the DSW via a simple wave solution of the diagonal system (1.29) where $r_1 = 0$ and $r_3 = 1$, while r_2 is a centered rarefaction wave. At the leading edge of the DSW, the modulus tends to 1 so that the leading edge is well approximated by a soliton solution of the KdV equation (2.37). The corresponding limit of the Riemann invariants

is $r_2 \to r_3 = 1$.. At the trailing edge of the KdV DSW, the amplitude of the modulated periodic wave tends to zero, which is consistent with the limit $r_2 \to r_1 = 0$.

These limits define the boundary of the single phase wavetrain. The leading edge velocity is denoted by v_+ and the trailing edge velocity denoted by v_-. The leading, solitary wave velocity and trailing, harmonic wave velocities are given by

$$v_+ = \lim_{r_2 \to r_3^-} V_2 = \frac{1}{3}(r_1 + 2r_3)$$

$$v_- = \lim_{r_2 \to r_1^+} V_2 = 2r_1 - r_3.$$

For the initial data $u_l = 1$ and $u_r = 0$, the leading and trailing velocities are $v_+ = \frac{2}{3}$ and $v_- = -1$ respectively. Note that this is quite different from the Burgers traveling wave solution, Eq. (1.16), which is a fixed front moving with a single velocity. The DSW solution found by GP is therefore given by [57]

$$r_2(x,t) = \begin{cases} 0 & x < v_- t \\ V_2^{-1}(x/t) & v_- t \le x \le v_+ t \\ 1 & x > v_+ t \end{cases}. \tag{1.31}$$

In Figure 1.4(a), we plot the GP solution of the KdV equation in the physical domain and the solution of the KdV-Whitham system (1.29) in Figure 1.4(b).

Due to its dynamically expanding, distinct edge behavior, a DSW exhibits an orientation d and polarity p, identifying the location and polarity of the solitary wave edge. For the KdV equation (1.2), these are determined by the third order dispersion parameter σ. The DSW has $d = +1$ ($d = -1$) if the solitary wave edge is rightmost (leftmost) and $p = +1$ ($p = -1$) if the solitary wave edge is a wave of elevation (depression) with respect to its adjacent, slowly varying background (cf. Fig. 1.5). The linear dispersion relation on a background $\overline{u}$ for (1.2) is $\omega(k, \overline{u}) = k\overline{u} - \sigma k^3$. As shown in Fig. 1.5, the KdV DSW for eq. (1.2) has $d = p = -\operatorname{sgn}\omega_{kk} = \operatorname{sgn}\sigma$.

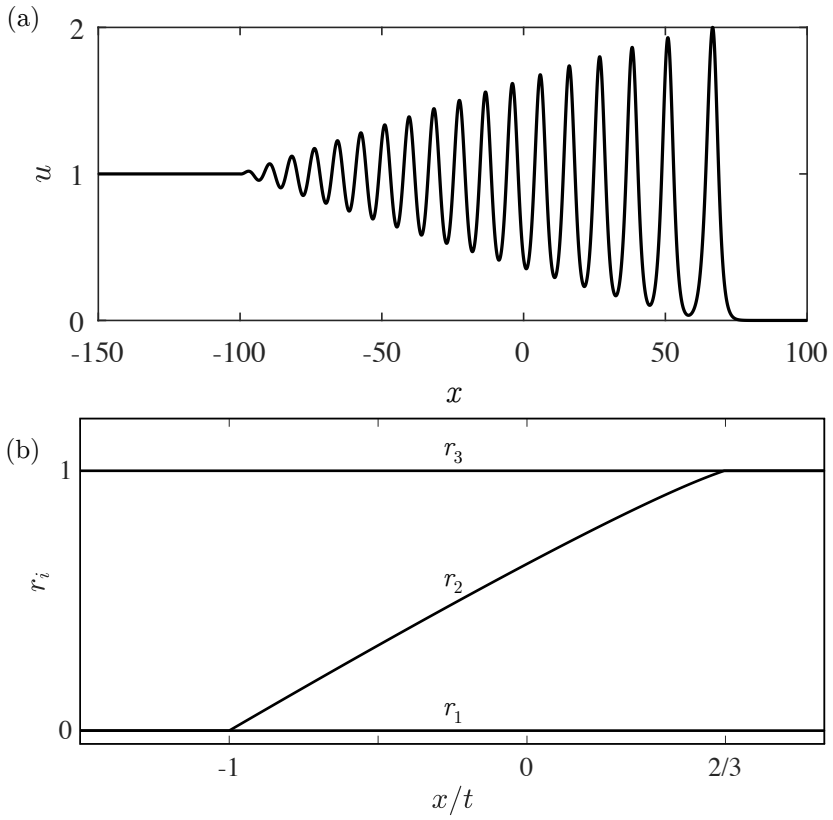

Figure 1.4: DSW solution of the KdV Riemann problem found by GP. (a) Solution in the physical domain at $t = 100$ (b) Riemann invariant, self-similar solution to Eq. (1.29) at $x/t = v_+ = 2/3$ we observe the coalescence $r_2 \to r_3^-$ and we observe the limit $r_2 \to r_1^+$ when $x/t = v_- = -1$.

1.2.2.1 Higher order dispersive regularization

In this section, we observe the difference in DSW structure arising from the long time evolution to the smooth, step-like initial data (1.28) given to a higher order dispersive equation, which is the subject of much of this thesis. The concise higher order dispersive equation is the KdV5 equation (1.4). A numerical simulation for a smoothed initial step (1.28) with $u_l = 1$ and $u_r = 0$ and $w = 10$ is shown in Fig. 1.6 at $t = 100$. This solution differs substantially from the classical, KdV DSW solution with positive dispersion, cf. Figure 1.5(a). In what follows, we will outline some particular features that distinguish

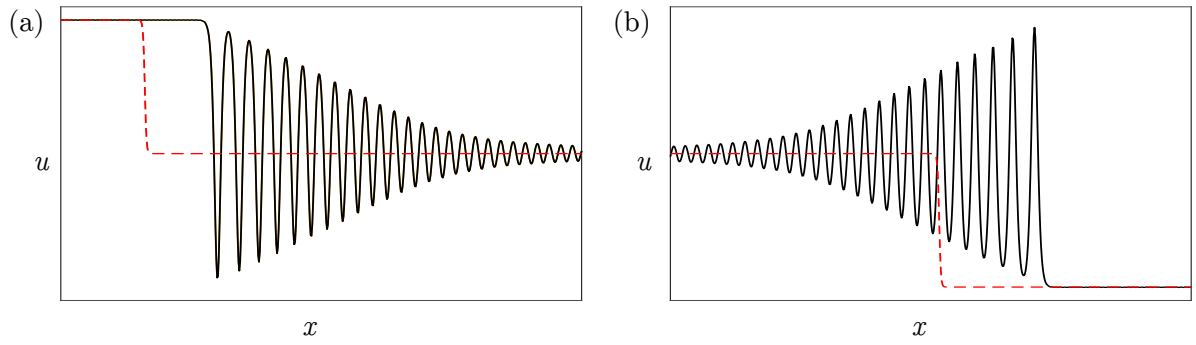

Figure 1.5: Expanding KdV-like DSWs for (a) positive dispersion curvature ($\sigma = -1$) and (b) negative dispersion curvature ($\sigma = +1$), exhibiting dispersion curvature dependent orientation and polarity.

the KdV5 DSW from the DSW solution of the KdV equation.

The KdV5 DSW consists of a rapid transition from the left equilibrium, $u_l = 1$ to a nearly uniform wavetrain. Ahead of this wavetrain is a slowly modulated oscillatory wave that gradually transitions to the rightmost constant level ahead, $u_r = 0$, as the wavetrain amplitude tends to zero. As the leading, modulated periodic wavetrain traversed from its linear edge (right to left) its increasing amplitude and decreasing wavenumber eventually terminate into the periodic wavetrain as seen in Figure 1.6. Since the modulated wavetrain terminates at a periodic wave, rather than a constant level, we term the leading modulated periodic wave a partial DSW. However, the KdV5 DSW shares some similarities with the KdV DSWs in Fig. 1.5. The dispersion relation of the KdV5 equation (1.4) on a background $\overline{u}$ is $\omega(k;\overline{u}) = \overline{u}k + k^5$, which has positive curvature.

Nonclassical DSWs in systems with higher order dispersion have been observed in a variety of systems, and the defining feature is the **rapid** transition—on the order of one oscillation wavelength—from the equilibrium to the intermediate periodic wavetrain and a partial DSW bringing the nearly uniform wavetrain to the constant level [122, 64, 31, 9]. The work presented in this thesis aims to describe the nonclassical DSWs such as those shown in

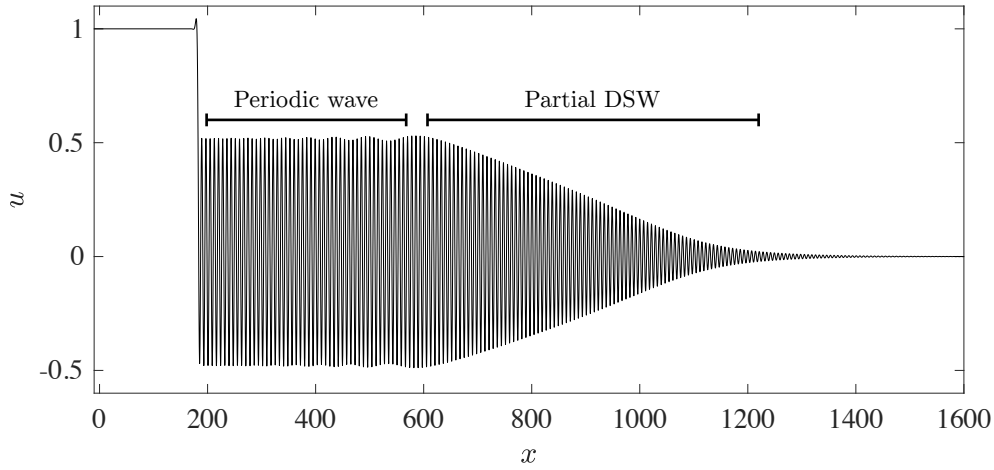

Figure 1.6: DSW solution of the KdV5 equation (1.4) with unit step initial data $u_l = 1$ and $u_r = 0$ at $t = 500$

Figure 1.6 utilizing the mathematical framework of Whitham modulation theory. We may state one main result here, that will be revisited in Chapter 6. The nonclassical DSW solution of the KdV5 equation (1.4) can be described in terms of a *shock-rarefaction* solution of the Whitham modulation equations—to be contrasted with the continuous rarefaction solution (1.31) of the Whitham equations used to describe the KdV-DSW modulation in Figure 1.4.

1.3 Outline of this thesis

In **Chapter 2**, we derive the Kawahara equation (1.3) from a class of dispersive Eulerian systems that represent conservation of mass and momentum modified by dispersion. The Kawahara equation is shown to arise generically when third order terms that arise from a long wave, multi-scale expansion are small and hence compensated by higher order fifth order terms. In this chapter, we compute solitary and periodic solutions to the Kawahara (1.3) and KdV5 (1.4) equations and discuss their structure. The Kawahara equation admits a Galilean symmetry so that the three parameter family of solutions with mean $\overline{u}$, amplitude a and wavenumber k can be uniquely determined by a two parameter family in a and k where

solutions have zero mean. We utilize an additional, scaling symmetry of the KdV5 equation show that the three parameter family can be obtained by rescaling a one parameter family of periodic solutions with unit amplitude, zero mean and wavenumber k.

In **Chapter 3**, we derive the Kawahara-Whitham modulation equations using two equivalent methods that were first implemented by Whitham himself. The Kawahara-Whitham modulation equations are written in an approximate but explicit form by utilizing a weakly nonlinear Stokes wave. Within the weakly nonlinear regime, we find that Kawahara-Whitham modulation equations become elliptic for a range of periodic wave parameters. Here, we also study the KdV5-Whitham modulation system in extensive detail. Utilizing approximate expressions for periodic waves in the weakly nonlinear regime and numerically computed periodic waves in the strongly nonlinear regime, we are able to characterize the modulation equations for a large parameter range. We find that for a small range in wavenumber, the modulation equations are elliptic, and the periodic waves are therefore modulationally unstable. This feature is not captured by the weakly nonlinear calculations. We further determine regions of genuine nonlinearity and discuss simple wave solutions of the KdV5-Whitham equations which have implications for the work presented in later chapters.

In **Chapter 4**, we use numerical and asymptotic methods to study the long term evolution of DSWs in the Kawahara equation (1.3). When the dispersion curve is non-convex (i.e. $\sigma = +1$ in Eq. (1.3)), we observe and classify three types of non-classical DSWs depending on the amplitude of the smoothed, step-like initial jump. For large jumps, we find **traveling dispersive shock waves** (TDSWs) characterized by a non-monotonic, depression solitary wave trailing edge. Rather than complete a full oscillation, the solitary wave is partial and connects to a periodic nonlinear wavetrain that is brought to the leading mean by a partial DSW (cf. Figure 1.6). For small amplitude jumps, the DSW is a KdV-like DSW with a leading edge elevation solitary wave that is in resonance with short, forward-propagating linear waves. These are termed **radiating dispersive shock waves** (RDSWs). Moderate jumps result in DSWs resembling both the TDSW and the RDSW, though complex

nonlinear wave-mixing make determining the ensuing wavepattern's properties difficult. For a convex dispersion relation, we numerically observe a classical KdV-like DSW until the jump magnitude is sufficiently large. For extremely large jumps, we observe a TDSW due to the dominance of the fifth order dispersion term in the Kawahara equation.

Chapter 5 is motivated by numerical experiments in the previous chapter, as well as numerical computation of DSW solutions of the KdV5 equation (1.4) (cf. Fig. 1.6). The traveling wave at the trailing edge is further scrutinized, and we find that it can be described as a **discontinuous** shock solution of the KdV5-Whitham modulation equations. In this section, a broader theme emerges and a host of novel heteroclinic and homoclinic traveling wave solutions as well as a Whitham modulation theory framework to interpret them is established. We introduce the notion of a **Whitham shock**–a discontinuous shock solution of the KdV5-Whitham equation whose admissibility coincides with the existence of a traveling wave consisting of a rapid transition from one periodic wave to a different periodic wave that co-propagate at a fixed velocity. These solutions arise from a **generalized Riemann problem** for the KdV5-Whitham equations. We then prove that if a traveling wave exists connecting two periodic waves, their parameters are determined by the Rankine-Hugoniot jump conditions applied to the Whitham modulation equations. Since the traveling wave is comprised of two periodic waves, we can determine the modulational stability or instability of the heteroclinic wave based on the hyperbolicity or ellipticity of the modulation equations. Families of traveling waves are computed and evolved numerically to corroborate the stability results from modulation theory.

Chapter 6 explores applications of Whitham shocks to various problems. Here we revisit the TDSW solution of the KdV5 equation (1.4) and show that it is described by a shock-rarefaction solution of the modulation equations. We also revisit the traveling wave portion of the TDSW solution of the Kawahara equation and show that its parameters can be identified by the Rankine-Hugoniot relations of the Kawahara-Whitham system. The chapter concludes with numerical experiments of smoothed, step-like initial data of the

Whitham equation–a nonlocal, scalar model whose dispersion matches that for free surface gravity-capillary water waves.

Chapter 7 shifts focus to another application of Whitham modulation theory and investigates how a soliton interacts with an extended hydrodynamic state–a rarefaction wave or DSW–using the Nonlinear Schrödinger equation as the model. We refer to this phenomenon as **soliton tunneling**. We show that the soliton amplitude can be treated as a **field** so that the physical configuration corresponds to a generalized Riemann problem for the Whitham modulation equations. One of the fundamental results of hydrodynamic soliton tunneling is **hydrodynamic reciprocity** whereby the tunneling through rarefaction waves and DSWs is described by the same set of conditions in spite of the very different interaction dynamics.

In **Chapter 8**, we summarize the results presented in this thesis. Open questions and future research directions will also be addressed.

Chapter 2

Derivation of fifth order KdV equations and computations of their traveling wave solutions

Throughout this thesis, we consider a nonlinear dispersive equation consisting of higher order dispersive terms, which may arise as a model equation describing the propagation of nonlinear waves in a variety of physical systems. For example, gravity-capillary water waves [65, 37, 102] and flexural ice sheets deformed by a water wave [100, 58, 38], nonlinear optical systems [132, 136, 120, 48], and Bose-Einstein condensates [73] all exhibit a change in dispersion curvature for sufficiently short waves, therefore necessitating a higher order model. In this chapter, we demonstrate that when third order dispersion is sufficiently weak, it can balance with fifth order dispersion so that the Kawahara equation emerges as a universal, weakly nonlinear dispersive model. The universality of the Kawahara equation for systems which balance third and fifth order dispersion can be derived from a general dispersive Eulerian system using a standard, multiple-scale expansion via the method of multiple scales. Depending on the physical parameter regime, the long wave approximate model can exhibit a structural change in the linear dispersion, so that two linear waves with distinct wavenumbers may propagate with the same phase velocity—a linear resonance. We observe some ramifications of the linear resonance on steady traveling waves. These come from computations of periodic and solitary waves by numerical and asymptotic procedures. The periodic solutions along with conservation laws of solutions to the Kawahara equation are used to compute the Whitham modulation equations and their structure in Chapter 3,

and computed solitary waves will be useful in describing the DSW solutions of the Kawahara equation explored numerically and asymptotically in Chapter 4. In Chapter 5 we use the numerically computed library of periodic solutions as components to heteroclinic and homoclinic traveling wave solutions of the KdV5 equation (1.4).

2.1 Derivation of fifth order equations of KdV type

The canonical models studied throughout this thesis that incorporate higher order dispersion will be the Kawahara (1.3) and fifth order KdV (1.4) equations. Our study begins by deriving the canonical models via a multiple scales applied to a general 2×2 dispersive Eulerian system

$$\rho_t + (\rho u)_x = D_1[\rho, u]_x, \tag{2.1}$$

$$(\rho u)_t + \left(\rho u^2 + P(\rho)\right)_x = D_2[\rho, u]_x, \tag{2.2}$$

where $\rho = \rho(x,t)$ corresponds to the fluid density, $u = u(x,t)$ the fluid velocity, and the pressure law is given by $P(\rho)$. The integro-differential operators D_1, D_2 acting on ρ, u in Eqs. (2.1) and (2.2) are assumed to be of the second order or higher, yielding a real valued dispersion relation. Dubrovin et al. [42] studied general Hamiltonian perturbations, D_1, D_2 of the dispersionless conservation laws (2.1)–(2.2). In general, the Hamiltonian perturbations take the form of so-called differential polynomials in the spatial derivatives. More specifically, the dispersive operators are expanded in a series containing only odd numbers of spatial derivatives on the hydrodynamic variables ρ and u. For our purposes, we will suppose that D_1 and D_2 expand to have the same structure.

Eulerian systems (2.1) and (2.2) serve as models of dispersive fluid-like systems, e.g. water waves. However, less familiar physical systems such as light propagation in a nonlinear optical medium are well modeled by Eqs. (2.1)–(2.2); in this setting ρ corresponds to the light intensity, u is the phase gradient of the complex carrier wave envelope and $P(\rho)$ is the intensity dependent refractive index of the nonlinear optical medium. We assume strict

hyperbolicity $P'(\rho) > 0$ and genuine nonlinearity $[\rho^2 P'(\rho)]' > 0$ of the dispersionless system ((2.2), (2.1) with $D_{1,2} = 0$) so that weakly nonlinear dynamics exhibit quadratic, convex flux [47]. We compute the dispersion relation by linearizing about the background state (ρ_0, u_0) with a small amplitude harmonic perturbation

$$\rho = \rho_0 + Ae^{i\theta}, \quad u = u_0 + Be^{i\theta}, \tag{2.3}$$

where $\theta = kx - \omega t$ and $|A|, |B| \ll 1$ are of the same order. Substitution of this ansatz into eq. (2.1) and eq. (2.2) yields a homogeneous algebraic system of linear equations for A and B that are only solvable for two distinct frequency branches of the dispersion relation $\omega_\pm(k)$ due to the assumed structure of the operators D_1 and D_2 in Eqs. (2.1)–(2.2). The dispersion relation exhibits the long wave $(0 < k \ll 1)$ behavior for unidirectional waves

$$\omega_\pm(k) = u_0 k \pm \Big(c_0 k - \alpha k^3 + \beta k^5 + o(k^5) \Big), \tag{2.4}$$

where $c_0 = \sqrt{P'(\rho_0)}$ is the long wave speed of sound and α, β are the third and fifth order dispersion coefficients, respectively. The $\pm$ allows for wave propagation to the left or right with respect to the background flow u_0, respectively. In general, these coefficients will depend on ρ_0, u_0 and potentially other physical parameters.

2.1.1 Multiple scale derivation of the Korteweg-de Vries and Kawahara equations

For illustrative and comparative purposes, we recall the multiple scale derivation of the Korteweg-de Vries equation (1.2), which arises generically supposing that weak nonlinearity and third order dispersion are in balance [103]. We seek approximate uni-directional solutions to the dispersive hydrodynamic system (2.1) and (2.2) via multiple-scales in the form

$$\begin{aligned} &\tau = \epsilon^{3/2} t, \quad \eta = \epsilon^{1/2} \left(x - (u_0 + c_0) t \right), \\ &\rho = \rho_0 + \epsilon \rho_1(\eta, \tau) + \epsilon^2 \rho_2(\eta, \tau) + \epsilon^3 \rho_3(\eta, \tau) + o(\epsilon^4), \\ &u = u_0 + \epsilon u_1(\eta, \tau) + \epsilon^2 u_2(\eta, \tau) + \epsilon^3 u_3(\eta, \tau) + o(\epsilon^4), \end{aligned} \tag{2.5}$$

where $0 < \epsilon \ll 1$ is a small, amplitude scale and $c_0 = c_0(\rho_0, u_0)$ is a velocity to be determined. We also assume the far field boundary conditions

$$\rho(x,t) \to \rho_0, \quad u(x,t) \to u_0, \quad x \to \infty. \tag{2.6}$$

The non-integer powers of ϵ appearing in the spatial and temporal scales in Eq. (2.5) are chosen so that we balance third order dispersion and quadratic nonlinearity that naturally appear in the dispersive Euler equations (2.1)–(2.2). Spatial and temporal derivatives are modified according to

$$\partial_t \to \epsilon^{3/2}\partial_\tau - (u_0 + c_0)\epsilon^{1/2}\partial_\eta, \tag{2.7}$$

$$\partial_x \to \epsilon^{1/2}\partial_\eta. \tag{2.8}$$

Inserting the multiple scales expansion into the dispersive operators D_1 and D_2, we find the expansions

$$\begin{aligned} D_1[\rho,u]_x &= \epsilon^{5/2}\left[f_1(\rho_0,u_0)\rho_{1,\eta\eta\eta} + f_2(\rho_0,u_0)u_{1,\eta\eta\eta}\right] + o(\epsilon^{5/2}), \\ D_2[\rho,u]_x &= \epsilon^{5/2}\left[g_1(\rho_0,u_0)\rho_{1,\eta\eta\eta} + g_2(\rho_0,u_0)u_{1,\eta\eta\eta}\right] + o(\epsilon^{5/2}), \end{aligned} \tag{2.9}$$

where the functions f_i, g_i are problem dependent. More general dispersive/nonlinear dispersive perturbations may be included by considering alternative balances or terms that preserve a Hamiltonian structure [42, 41]. Now we will proceed with the multi-scale expansion that leads to the KdV equation (1.2).

The KdV equation is found by inserting the asymptotic series (2.5), the spatiotemporal scales (2.7) and (2.8) and operator expansions (2.9) into the general dispersive Eulerian system (2.1)–(2.2) and gathering terms at increasing orders in ϵ. The leading order nontrivial problem at $\mathcal{O}(\epsilon^{3/2})$ is

$$\begin{aligned} \mathcal{L}\begin{bmatrix}\rho_1 \\ u_1\end{bmatrix} &= 0, \\ \rho_1, u_1 \to 0 \text{ as } \eta \to \infty, & \end{aligned} \tag{2.10}$$

where the linear operator is defined as

$$\mathcal{L} = \begin{bmatrix} -c_0 & \rho_0 \\ -u_0 c_0 + P'(\rho_0) & (u_0 - c_0)\rho_0 \end{bmatrix} \partial_\eta. \tag{2.11}$$

The leading order problem (2.10) admits a nontrivial, decaying family of solutions

$$\rho_1 = \pm \frac{\rho_0}{c_0} u_1, \tag{2.12}$$

so long as $c_0 = \pm\sqrt{\rho_0}$. For the remainder of the calculation, we will consider right moving waves so that we take the "+" branch of c_0. Equating terms at $\mathcal{O}(\epsilon^{5/2})$ gives

$$\begin{aligned} \mathcal{L} \begin{bmatrix} \rho_2 \\ u_2 \end{bmatrix} = & \begin{bmatrix} -\rho_{1,\tau} - (\rho_1 u_1)_\eta \\ -\rho_0 u_{1,\tau} - u_0 \rho_{1,\tau} - (u_0 - c_0)(\rho_1 u_1)_\eta - 2\rho_0 u_1 u_{1,\eta} - P''(\rho_0)\rho_1 \rho_{1,\eta} \end{bmatrix}, \\ & + \begin{bmatrix} f_1 & f_2 \\ g_1 & g_2 \end{bmatrix} \begin{bmatrix} \rho_{1,\eta\eta\eta} \\ u_{1,\eta\eta\eta} \end{bmatrix} \end{aligned} \tag{2.13}$$

where f_i and g_i are the same coefficients that appear upon expanding the differential operators (2.9). The system (2.13) is solvable so long as the right hand side is orthogonal to the kernel of the adjoint of the operator $\mathcal{L}$, $\ker \mathcal{L}^\dagger$. A calculation reveals that

$$\ker \mathcal{L}^\dagger = \begin{bmatrix} c_0 - u_0 \\ 1 \end{bmatrix} F(\eta),$$

where $F(\eta)$ is an arbitrary, smooth function of η. Under this restriction along with the leading order relation (2.12) one finds that u_1 satisfies

$$\begin{aligned} u_{1,\tau} + n u_1 u_{1,\eta} + \alpha u_{1,\eta\eta\eta} = 0, \\ n = 1 + \rho_0 \frac{c_0'}{c_0^2}, \quad \alpha = -\frac{1}{2\rho_0} \left[(c_0 - u_0) \left(\frac{\rho_0}{c_0} f_1 + f_2 \right) + \frac{\rho_0}{c_0} g_1 + g_2 \right], \end{aligned} \tag{2.14}$$

which can be rewritten exactly as the Korteweg-de Vries equation (1.2). Let us suppose that we operate within a parameter regime such that the third order derivative coefficient, α, is

sufficiently small and the KdV equation is no longer asymptotically consistent with regards to the spatiotemporal scales in the multi-scale expansion (2.5). In this parameter regime, Equation (2.14) reduces to the Hopf equation (1.11), which is no longer a valid physical model due to finite time singularity formation. From here on, we consider the case where higher order dispersion is incorporated to maintain asymptotic ordering of the scalar model equation. The long-wave dispersion (2.4) reveals that this asymptotic imbalance may be avoided by incorporating higher order, i.e. fifth order, dispersive terms. In this regime, third and fifth order dispersion are balanced so long as $\alpha \sim k^2 \ll 1$, where k is a typical wavenumber in the problem. The maximal balance of quadratic nonlinearity, and cubic and quintic dispersion therefore occurs when $\alpha \sim \epsilon^{1/2}$. Under this balance, we modify the spatial and temporal scales in the multiple scale expansion to incorporate the long waves. The multiple scales expansion, again in the amplitude parameter $0 < \epsilon \ll 1$, consists of

$$\begin{aligned} &\tau' = \epsilon^{5/4} t, \quad \eta' = \epsilon^{1/4} \left(x - (u_0 + c_0) t \right), \\ &\rho = \rho_0 + \epsilon \rho_1(\eta', \tau') + \epsilon^{3/2} \rho_2(\eta', \tau') + \epsilon^2 \rho_3(\eta', \tau') + o(\epsilon^2), , \\ &u = u_0 + \epsilon u_1(\eta', \tau') + \epsilon^{3/2} u_2(\eta', \tau') + \epsilon^2 u_3(\eta', \tau') + o(\epsilon^2), \end{aligned} \tag{2.15}$$

where τ' and η' are denoted with primes to distinguish from the multiple scales that result in the KdV equation (2.5). To simplify notation throughout the remainder of this calculation we will drop the primes. As before, it is useful to introduce the expansion of the dispersion operators

$$\begin{aligned} D_1[\rho, u]_x &= \epsilon^{7/4} \left[f_1(\rho_0, u_0) \rho_{1,\eta\eta\eta} + f_2(\rho_0, u_0) u_{1,\eta\eta\eta} \right] \\ &\quad + \epsilon^{9/4} \left[f_3(\rho_0, u_0) \rho_{1,\eta\eta\eta\eta\eta} + f_4(\rho_0, u_0) u_{1,\eta\eta\eta\eta\eta} \right] + o(\epsilon^{9/4}), \\ D_2[\rho, u]_x &= \epsilon^{7/4} \left[g_1(\rho_0, u_0) \rho_{1,\eta\eta\eta} + g_2(\rho_0, u_0) u_{1,\eta\eta\eta} \right] \\ &\quad + \epsilon^{9/4} \left[g_3(\rho_0, u_0) \rho_{1,\eta\eta\eta\eta\eta} + g_4(\rho_0, u_0) u_{1,\eta\eta\eta\eta\eta} \right] + o(\epsilon^{9/4}). \end{aligned} \tag{2.16}$$

As before, we insert the multiple scale expansion (2.15) into Eqs. (2.1) and (2.2) and assume the boundary conditions (2.6). The procedure to obtain the Kawahara equation is largely identical to that to obtain the KdV, with some idiosyncrasies which will be given additional

attention. The leading order appears by equating terms at $\mathcal{O}(\epsilon^{5/4})$, which gives an identical relation to (2.12) and the same result $c_0 = \pm\sqrt{P'(\rho_0)}$, where we will again restrict ourselves to the "+" branch in order to consider only right moving waves. Equating terms at $\mathcal{O}\left(\epsilon^{7/4}\right)$

$$\mathcal{L}\begin{bmatrix}\rho_2\\ u_2\end{bmatrix} = \begin{bmatrix}f_1 & f_2\\ g_1 & g_2\end{bmatrix}\begin{bmatrix}\rho_{1,\eta\eta\eta}\\ u_{1,\eta\eta\eta}\end{bmatrix}, \tag{2.17}$$

where $\mathcal{L}$ is the linear operator defined in (2.11). We remove secular terms by enforcing the solvability condition

$$\left[(c_0-u_0)\left(\frac{\rho_0}{c_0}f_1+f_2\right)+\frac{\rho_0}{c_0}g_1+g_2\right]u_{1,\eta\eta\eta} = \mathcal{O}\left(\epsilon^{1/2}\right). \tag{2.18}$$

The perturbation of the secularity condition at $\mathcal{O}(\epsilon^{7/4})$ encapsulates the maximal balance chosen so that third and fifth order dispersion are of comparable magnitude, as a result the terms in Eq. (2.18) appear at the subsequent order in ϵ. Enforcing the requirement that no secular terms are present, Equation (2.17) can be solved for the homogeneous solution which allows us to conclude

$$\rho_2 = u_2 = 0,$$

since their behavior can be absorbed into the leading order solutions ρ_1 and u_1. Equating terms at $O(\epsilon^{9/4})$ gives

$$\begin{aligned}\mathcal{L}\begin{bmatrix}\rho_3\\ u_3\end{bmatrix} = &\begin{bmatrix}-\rho_{1,\tau}-(\rho_1u_1)_\eta\\ -\rho_0u_{1,\tau}-u_0\rho_{1,\tau}-(u_0-c_0)(\rho_1u_1)_\eta-2\rho_0u_1u_{1,\eta}-P''(\rho_0)\rho_1\rho_{1,\eta}\end{bmatrix}\\ &+\begin{bmatrix}f_3 & f_4\\ g_3 & g_4\end{bmatrix}\begin{bmatrix}\rho_{1,\eta\eta\eta\eta\eta}\\ u_{1,\eta\eta\eta\eta\eta}\end{bmatrix}.\end{aligned} \tag{2.19}$$

The solvability of (2.19) along with (2.12) implies that u_1 satisfies the Kawahara equation

$$u_{1,\tau}+nu_1u_{1,\eta}+\tilde{\alpha}u_{1,\eta\eta\eta}+\beta u_{1,\eta\eta\eta\eta\eta} = 0, \tag{2.20}$$

where n is defined as in the KdV equation (2.14), and $\tilde{\alpha} = \epsilon^{1/2}\alpha$ from Eq. (2.14). The coefficient of the fifth order dispersion term is then given by

$$\beta = -\frac{1}{2\rho_0}\left[(c_0 - u_0)\left(\frac{\rho_0}{c_0}f_3 + f_4\right) + \frac{\rho_0}{c_0}g_3 + g_4\right].$$

Assuming $\tilde{\alpha} \neq 0$ and $\beta \neq 0$, equation (2.20) can be cast to the normalized form (1.3) by introducing the scaled variables

$$x' = \left|\frac{\tilde{\alpha}}{\beta}\right|^{1/2}\eta, \quad t' = \beta\left|\frac{\tilde{\alpha}}{\beta}\right|^{5/2}\tau, \quad u' = \frac{n\beta}{\tilde{\alpha}^2}u_1, \tag{2.21}$$

and dropping primes recovers the Kawahara equation (1.3)

$$u_t + uu_x + \sigma u_{xxx} + u_{xxxxx} = 0.$$

The key parameter in the Kawahara equation (1.3) that encapsulates the competition between third and fifth order dispersion is

$$\sigma = -\mathrm{sgn}(\tilde{\alpha}\beta), \tag{2.22}$$

so that if α and β have the same sign, the dispersion relation has purely positive curvature. However, if α and β have differing signs, the dispersion relation is non-convex. The non-convex dispersion results in linear and nonlinear resonances that have implications on the waves investigated in Chapter 4.

Physical parameter regimes may result in situations such that the third order dispersion coefficient $\alpha = 0$. In this scenario, we introduce the variables

$$\tilde{x} = \left|\frac{\beta}{n}\right|^{1/4}\eta, \quad \tilde{t} = \left|\frac{\beta}{n^5}\right|^{1/4}\tau, \tilde{u} = u_1$$

in (2.20) with $\alpha = 0$. Upon dropping the tildes from the variables, the weakly nonlinear model equation is the fifth order KdV (KdV5) equation (1.4)

$$u_t + uu_x + u_{xxxxx} = 0.$$

The following sections demonstrate the ubiquity of the Kawahara equation (1.3) and the KdV5 equation (1.4) when describing long wave dynamics in various physical systems. Illuminating examples in both gravity-capillary water waves and fiber optics are provided in sections 2.1.2 and 2.1.3, respectively. Other systems that are not explicitly cast as a dispersive Eulerian system (2.1)–(2.2) (which can be described by the Kawahara and KdV5 equations) will also be presented including applications to light propagation in liquid crystals, ultra-cold atoms, and elastic ice sheets capping water. Additionally, we will address how the Kawahara equation can emerge as a model for nonlocal, Whitham type models [141] and from steady, ultra-shallow, supercritical flows [18].

2.1.2 Water waves

Irrotational, gravity-capillary free surface water waves in $1+1$ dimensions are modeled by the Euler equations [70], which are given in non-dimensional form by

$$\delta^2\phi_{xx} + \phi_{zz} = 0, \qquad -1 < z < \epsilon\eta \tag{2.23}$$

$$\phi_z = 0, \qquad z = -1 \tag{2.24}$$

$$\eta_t + \epsilon\phi_x\eta_x - \delta{-}2\phi_z = 0, \qquad \text{on } z = \epsilon\eta \tag{2.25}$$

$$\phi_t + \frac{\epsilon}{2}(\phi_x^2 + \delta^{-2}\phi_z^2) + \eta = \delta^2 B\frac{(1+\epsilon^2\delta^2)\eta_{xx}}{(1+\epsilon^2\delta^2\eta_x^2)^{3/2}} \qquad \text{on } z = \epsilon\eta. \tag{2.26}$$

where ϕ is the velocity potential, e.g. $\nabla\phi$ recovers the vector of the velocity components, $\eta = \eta(x,t)$ is the free surface and $\epsilon = a/h$ is the ratio of a typical wave amplitude related to depth (a parameter determining the nonlinearity) and $\delta = \lambda/h$ is the ratio of a typical wavelength and the undisturbed water depth. The Bond number, B, is a ratio of capillary (surface tension) forces to gravity forces given by

$$B = \frac{\tau}{\rho g h^2},$$

where τ is the coefficient of surface tension, ρ is the density of the fluid, g the gravitational acceleration constant and h is the depth of the fluid. Waves propagating in the positive

x-direction are described by the linear dispersion relation

$$\omega(k) = \pm\sqrt{(k(1+Bk^2)\tanh k}, \tag{2.27}$$

$$\sim k + \frac{1}{6}(3B-1)k^3 + \frac{1}{360}\left(19 - 30B - 45B^2\right)k^5 + o(k^5). \tag{2.28}$$

In [65], the authors derived the Kawahara equation directly from the Euler equations as a model for shallow water waves for Bond number near $\frac{1}{3}$. In what follows, we will demonstrate an alternative derivation based on the methodology for general dispersive Eulerian systems.

In order to accurately capture the competing effects of third and fifth order dispersion in water waves, we use a model for fully nonlinear water waves that expands upon the models of fully nonlinear, long gravity waves derived independently by Serre [118], Su and Gardner [124], and Green and Naghdi [54] . We refer to these as the extended Green-Naghdi equations [102]. Dias and Milewski [37] derived a fully nonlinear model incorporating surface tension effects. Combining the results of both works, the extended, generalized Serre equations which include terms to match the dispersion relation up to $\mathcal{O}(k^5)$ and surface tension effects (2.28) takes the form of (2.1) and (2.2) where the dispersive operators and pressure law are

$$\begin{aligned} D_1(\rho,u) &= 0, \\ D_2(\rho,u) &= \frac{\rho^3}{3}\left(u_{xt} + uu_{xx} - u_x^2\right) - B\left[\frac{1}{2}\rho_x^2 - \rho\rho_{xx}\right] \\ &\quad + \left[\frac{\rho^5}{45}\left(u_{xxt} + uu_{xxx} - 5u_xu_{xx}\right)\right]_x - 3\rho^5u_{xx}^2, \\ P(\rho) &= \frac{\rho^2}{2}. \end{aligned} \tag{2.29}$$

The dependent variables $\rho(x,t)$ and $u(x,t)$ are the nondimensional water free surface height and vertically averaged horizontal velocity component, respectively. The bond number, B, is exactly as it appeared in the water wave problem (2.25). The dispersion relation for eqs. (2.1), (2.2) with (2.29) on the undisturbed, static background $\rho_0 = 1$ and $u_0 = 0$ has the long wave expansion identical to (2.28) up to $\mathcal{O}(k^5)$.

Utilizing the derivation of the Kawahara equation outlined in the previous section, we find the coefficients for the Kawahara equation (2.20)

$$n = \frac{3}{2}, \quad \tilde{\alpha} = \frac{1}{6}(1 - 3B), \quad \beta = \frac{1}{360}(19 - 30B - 45B^2),$$

As noted in our derivation, the Kawahara equation is valid when $\tilde{\alpha}$ is small, therefore we are considering B close to $1/3$. Note that we have also assumed that $\beta = \mathcal{O}(1)$. Since β is zero when $B = (2\sqrt{30} - 5)/15 \approx 0.40$, we require $B < 0.4$ for the asymptotic validity of the scaled Kawahara equation (2.20) with parameter

$$\sigma = -\text{sgn}(\alpha\beta) = \text{sgn}\,(1 - 3B)\,. \tag{2.30}$$

When $B < 1/3$, gravity effects dominate surface tension effects and we have $\sigma = +1$. Note that the coefficients shown here differ from those appearing in the derivation of the Kawahara equation directly from the Euler equations (2.23)–(2.26) presented by Hunter and Scheurle [65], where the authors expanded β near $B = 1/3$ and report $\beta \sim \frac{1}{90}$.

2.1.3 Nonlinear fiber optics

The effect of higher order dispersive terms in the Nonlinear Schrödinger equation and associated experiments were studied in the series of papers [32, 31, 33, 34, 95] within the context of light propagation in optical fibers with higher order dispersion effects. Further readings can be found in the monograph [9] (in Russian) for applications in continuum mechanics. The equation of interest is a higher order NLS equation

$$i\psi_t + \frac{1}{2}\psi_{xx} + i\frac{\beta_3}{6}\psi_{xxx} - |\psi|^2\psi = 0, \tag{2.31}$$

where ψ is the complex envelope of a weakly nonlinear carrier wave and β_3 is a parameter modeling higher order dispersive effects in the fiber. The variables x, t are used here to maintain consistency with (2.1) and (2.2) but physically correspond to nondimensionalized time and negative distance along the fiber, respectively. The Madelung transformation

$\psi = \sqrt{\rho}e^{i\phi}$, $u = \phi_x$ can be utilized to write eq. (2.31) as a generalized dispersive Eulerian system

$$\rho_t + \left(\rho u - \frac{1}{2}\beta_3 \rho u^2\right)_x = D_1[\rho, u]_x,$$
$$(\rho u)_t + \left(\rho u^2 - \frac{1}{2}\beta_3 \rho u^3 + \frac{1}{2}\rho^2\right)_x = D_2[\rho, u]_x,$$

where

$$D_1[\rho, u] = \beta_3 \left(\frac{1}{6}\rho_{xx} - \frac{1}{8}\frac{\rho_x^2}{\rho}\right),$$
$$D_2[\rho, u] = \frac{1}{4}\rho \left(\log(\rho)\right)_{xx} + \frac{\beta_3}{12}\left(\frac{9\rho_x^2 u}{2\rho} - 5\rho_{xx}u - \rho_x u_x - 2\rho u_{xx}\right).$$

Note that the flux terms in the dispersionless limit are modified due to the Madelung transformation of the third order dispersion term in (2.31) which vanish in the singular limit $\beta_3 \to 0$. Utilizing the same method as our general derivation of the Kawahara equation for dispersive Eulerian equations, we obtain eq. (2.20) with coefficients

$$n = \frac{3 - \beta_3\left(6u_0 - 3u_0^2\beta_3 + \sqrt{\rho_0 - \rho_0 u_0 \beta_3}\right)}{2\left(1 - u_0\beta_3\right)},$$
$$\alpha = \frac{(7u_0\beta_3 - 3)\sqrt{\rho_0 - \rho_0 u_0 \beta_3}}{24\rho_0},$$
$$\beta = \frac{\sqrt{\rho_0 - \rho_0 u_0 \beta_3}\left(-9 + 51u_0\beta_3 + 16\rho_0\beta_3^2 - 91u_0^2\beta_3^2 + 49u_0^3\beta_3^3\right)}{1152\rho_0^2\left(u_0\beta_3 - 1\right)}.$$

Unlike the applications to water waves, a nonzero background velocity u_0 is required in order to achieve a balance between third and fifth order dispersion. We note that the numerical simulations in [31] consider the cases $\rho_0 = 0.5$, $u_0 \in (-0.586, -0.543)$, and $\beta_3 \in (-0.35, 1)$, corresponding to $\sigma = -\text{sgn}\alpha\beta = +1$, the non-convex dispersion case.

2.1.4 Other systems

El and Smyth derived the Kawahara equation (1.3) as a weakly nonlinear model for the intensity of light propagating through a nematic liquid crystal [48]. If the elastic response of the nematic liquid crystal is sufficiently large, the linear dispersion relation incorporates

short wave effects and we expect a regime where the Kawahara equation is an operable approximate model. The Kawahara equation derived has third order dispersion coefficient $\sigma = 1$. Further work in nematic liquid crystals has resulted in a detailed classification of DSWs arising from step initial data [10] where the authors observe dispersive shocks identical to those we observe in the Kawahara equation (and related systems) throughout this thesis.

In the last decade, with the development of spin-orbit coupled Bose-Einstein condensates (BECs) [87, 88], experimental methodologies now exist to engineer the dispersion experienced by the wave functions of two nonlinearly coupled spin states. Depending on the coupling strength, the dispersion curve can be altered from convex to non-convex—analogous to the change in dispersion curvature that can occur for the Kawahara equation as σ changes sign. If the BEC is confined in a quasi-one-dimensional parabolic trap, the mean-field dynamics may be modeled by two coupled nonlinear Schrödinger equations (see, e.g., [5] and references therein), which may exhibit non-convex dispersion. Similar engineering of the dispersion relation has been established recently in thin film magnonic crystals [113].

The Kawahara equation may also arise in the modeling of free surface water waves developing under a thin, elastic ice sheet. For long waves and a sufficiently large elasticity parameter, Young's modulus, the Kawahara equation is an employable model [38, 100, 67].

2.1.4.1 Scalar, nonlocal equations

In 1967, Whitham proposed a model for surface water waves that incorporates weak nonlinearity and a general, linear dispersion relation $\omega(k)$. The so-called Whitham equation is

$$u_t + nuu_x + \mathcal{K} * u_x = 0, \quad \mathcal{K}(x) = \frac{1}{2\pi}\int_{\mathbb{R}} \frac{\omega(k)}{k} e^{ikx} dk, \tag{2.32}$$

where $\mathcal{K} * u_x$ is the convolution

$$\mathcal{K} * u_x = \frac{\partial}{\partial x}\left[\int_{\mathbb{R}} \mathcal{K}(x-y)u(y,t)dy\right].$$

Originally, the model (6.10) was proposed to model free surface, gravity water waves so that $\omega(k) = \sqrt{k \tanh k}$, though the kernel $\mathcal{K}$ can be any polynomial, rational, or even transcendental function depending on the application if the convolution is interpreted in the distributional sense. In fact, recent papers have studied the Whitham equation for gravity-capillary water waves [26, 39, 27] and for water waves under elastic ice sheets [38].

If the dispersion relation in the convolution kernel $\mathcal{K}$ is odd and analytic, then it has the long wave expansion

$$\omega \sim c_0 k - \alpha k^3 + \beta k^5 + o(k^5),$$

and

$$\mathcal{K} = \frac{1}{2\pi} \int_{\mathbb{R}} \left(c_0 + \alpha k^2 + \beta k^4 + \ldots\right) e^{ikx} dk, \tag{2.33}$$

must now be viewed in a distributional sense so that $\mathcal{K}(x)$ is the sum of delta functions and its distributional derivatives. In the Fourier domain, multiplication by polynomials of k correspond to differentiation with respect to x. Therefore, under the long wave expansion of $\mathcal{K}$, we find

$$\begin{aligned}\left[\frac{1}{2\pi} \int_{\mathbb{R}} \left(c_0 + \alpha k^2 + \beta k^4 + \ldots\right) e^{ikx} dk\right] * u_x &= \frac{i}{2\pi} \int_{\mathbb{R}} \left(c_0 k - \alpha k^3 + \beta k^5 + \ldots\right) \hat{u}(k) e^{ikx} dk \\ &= c_0 u_x + \alpha u_{xxx} + \beta u_{xxxxx} + \ldots,\end{aligned} \tag{2.34}$$

where $\hat{u}$ is the Fourier transform of u. For appropriately long waves, the Whitham equation (2.32) reduces to the Kawahara equation obtained from the multiple scales expansion (2.20). We will revisit the nonlocal model equation (2.32) in Chapter 6 as an extension of the theory developed in this thesis.

2.2 Traveling wave solutions

This section is dedicated to numerical computations of solitary and periodic traveling wave solutions of the Kawahara equation (1.3). Extensive previous works have demonstrated

that the structure of solutions arising from higher order equations are quite distinct from their counterparts in systems with weaker dispersion. We will briefly outline exotic solutions that arise from higher order dispersion, but the following examples are by no means comprehensive. Examples include multi-mode periodic waves (traveling waves with two resonant wavenumbers present) [128, 52, 112], solitary waves consisting of multiple pulses [29], solitary waves with decaying oscillatory tails [72, 55], and solitary waves accompanied by co-propagating small, but finite, amplitude oscillations spatially extending to infinity [66, 6, 30]. The zoology of traveling waves (TWs) can be attributed to additional degrees of freedom inherent in the higher order ODE that results from a traveling wave ansatz. Periodic solutions will be utilized to formulate the Whitham modulation equations and determine their properties. In chapter 5 we will utilize the Whitham modulation equations to compute new traveling wave solutions and add to the variety of solutions that occur in higher order dispersive systems.

We seek a solution in the form of a traveling wave $u(x,t) = f(\xi;c)$ where ξ is the traveling wave coordinate $\xi = x - ct$, and c is the traveling wave velocity. Inserting the traveling wave ansatz, we arrive at the ordinary differential equation

$$-cf' + \frac{1}{2}\left(f^2\right)' + \sigma f''' + f^{(5)} = 0, \tag{2.35}$$

where $f' = \frac{df}{d\xi}$. A single integration yields the fourth order equation

$$-cf + \frac{1}{2}f^2 + \sigma f'' + f^{(4)} = A, \tag{2.36}$$

where A is a constant of integration. In the following sections, we compute both solitary and periodic solutions of Eq. (2.36) using a variety of methods which primarily utilize a projection onto Fourier modes. Details and validation of the numerical methods are given in Appendix B.

2.2.1 Solitary waves

The structure of solitary wave solutions to the Kawahara equation (1.3) are well known [14, 55, 72]. In what follows, we outline relevant properties of these solutions for $\sigma = \pm 1$. When $\sigma = +1$, solitary waves are unstable when embedded in the continuous spectrum, i.e., when they exhibit a resonance for velocities $c > 0$ [126]. However, there are stable solitary waves with velocities distinct from those appearing in the continuous spectrum when $c < -\frac{1}{4}$ [25]. The stable solitary waves are oscillatory from their peak and rapidly tend to their far-field equilibrium. Our investigation of solitary wave solutions focuses upon their numerical and asymptotic calculation due to the fact that, for the fifth order problem, solitary waves cannot easily be computed in closed form. However, some closed form solutions have been discovered when $\sigma = -1$ [98, 61, 97, 77].

A key quantity of interest is the amplitude-speed relation for these solitary waves, which will prove useful in the study of DSWs in Chapter 4.

The nonlinear equation (2.36) is appended with the boundary conditions that enforce decay in $f(\xi)$ and all its derivatives as $|\xi| \to \infty$ so that any constants of integration are 0 (i.e. $A = 0$ in Eq. (2.36)). The boundary-value problem is solved using a variety of methods, namely the Newton conjugate gradient method [143], the spectral renormalization method [3], or with Matlab's boundary value solver bvp5c for the solitary wave profile f corresponding to the speed c. An outline of the Newton conjugate gradient method and the spectral renormalization method are provided in Appendix B. For comparative purposes, it is helpful to recall the well-known soliton solution of the KdV equation (1.2)

$$f(\xi; c) = a\sigma \mathrm{sech}^2\left(\sqrt{\frac{a}{12}}\xi\right), \quad c(a) = \frac{a\sigma}{3}, \quad a > 0. \tag{2.37}$$

The monotonic Kawahara solitary waves are well-approximated by the KdV solution (2.37) in the small amplitude regime [14]. Here, monotonic refers to the decay profile on either side of the solitary wave peak–a convention presented in [72]. Higher order dispersion acts as a small perturbation to the KdV solitary wave. This effect is understood by integrating (2.36)

again and enforcing the decay of f and its derivatives to obtain

$$‘ - \frac{c}{2}f^2 + \frac{1}{6}f^3 + \frac{\sigma}{2}\left(f'\right)^2 + f'f''' - \frac{1}{2}\left(f''\right)^2 = 0. \tag{2.38}$$

Evaluating at the solitary wave extremum taken to be at $\xi = 0$ yields the correction to the KdV speed-amplitude relation (2.37)

$$\begin{aligned} c(a) &= \frac{a\sigma}{3} - \left(\frac{f''(0;c)}{a}\right)^2, \\ &\sim \frac{a\sigma}{3} - \frac{a^2}{36}, \end{aligned} \tag{2.39}$$

where the approximate speed correction is found upon inserting the KdV solitary wave profile (2.37). Note that the speed correction in Eq. 2.39 is strictly negative, independent of the sign of σ.

We first compute solitary wave solutions of the Kawahara equation (1.3) with $\sigma = +1$. Numerical computations are carried out on the computational domain $\xi \in [-50\pi, 50\pi]$ with $N = 2048$ discretized collocation points for the branch bifurcating from $c = -1/4$ while computation of elevation solitary waves are carried out via Matlab's bvp5c on a domain of $[0, 100]$, where we may reflect the numerically computed wave across its peak at $\xi = 0$ to determine the solitary wave profile. Numerical experiments also demonstrate that increasing the size of the computational domain or increasing the spatial resolution does not significantly modify the localized wave profile.

The Kawahara solitary wave amplitude-speed relation and sample solitary waves for the case of convex dispersion $\sigma = -1$ are shown in Fig. 2.1.

In the regime of non-convex dispersion, $\sigma = +1$, we find two distinct branches of solitary wave solutions that are depicted in Fig. 2.2. The case with wave velocities $c > 0$ corresponds to elevation solitary waves qualitatively resembling the soliton solution of the KdV equation (2.37), whose amplitude-speed relation and profiles are depicted by the blue, dashed curve in Fig. 2.2. We note that the Kawahara speed-amplitude relation for $\sigma = +1$ rapidly departs from the KdV relation in Figure 2.2 relative to the deviation shown in 2.1 for

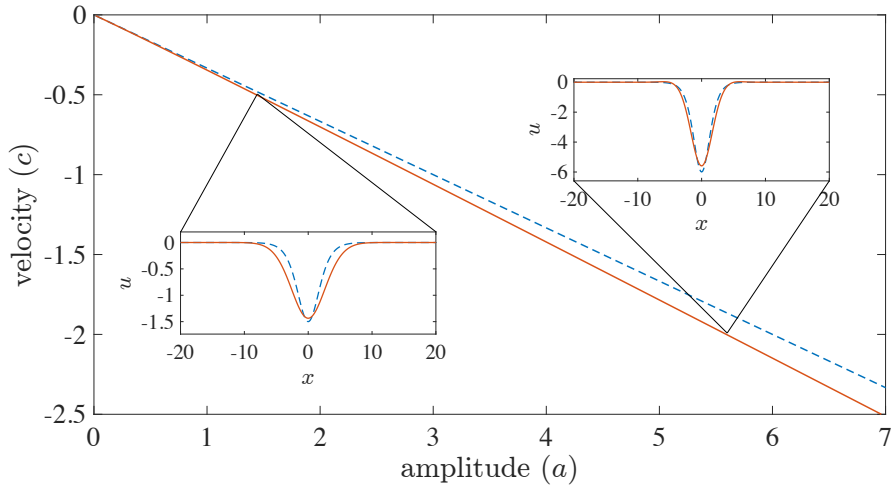

Figure 2.1: Numerically computed solitary wave profiles (insets) and speed-amplitude relation for the Kawahara equation with $\sigma = -1$ (solid) and the KdV equation (dashed).

$\sigma = -1$. The elevation solitary waves are embedded in the continuous wave spectrum, which consists of all possible linear phase velocities for vanishing periodic waves on zero background mean: $\omega/k = -k^2 + k^4 > -\frac{1}{4}$. The linear wave phase velocities are shown in Fig. 2.2 with the solid, coiled curve on the ordinate. Previous observations of these elevation waves [14] have shown that a resonance between the solitary wave and small amplitude waves with the same phase velocity occurs as a result of embedding in the continuous spectrum. The ensuing radiation decreases the amplitude of the solitary wave core as the solution propagates, which is a property of embedded solitary waves in a more general setting [126].

When $c < -\frac{1}{4}$, the solitary waves are depression waves with non-monotonic decay to the far-field equilibrium. A stability analysis of the solitary wave solutions demonstrated that this solitary wave solution branch is stable [25] and previous numerical experiments corroborate this result even in the case of inelastically interacting oscillatory solitary waves [96]. The bifurcation point $c = -1/4$ can be determined by a linear analysis of equation (2.36). Linearization about a constant background results in a fourth order, linear equation

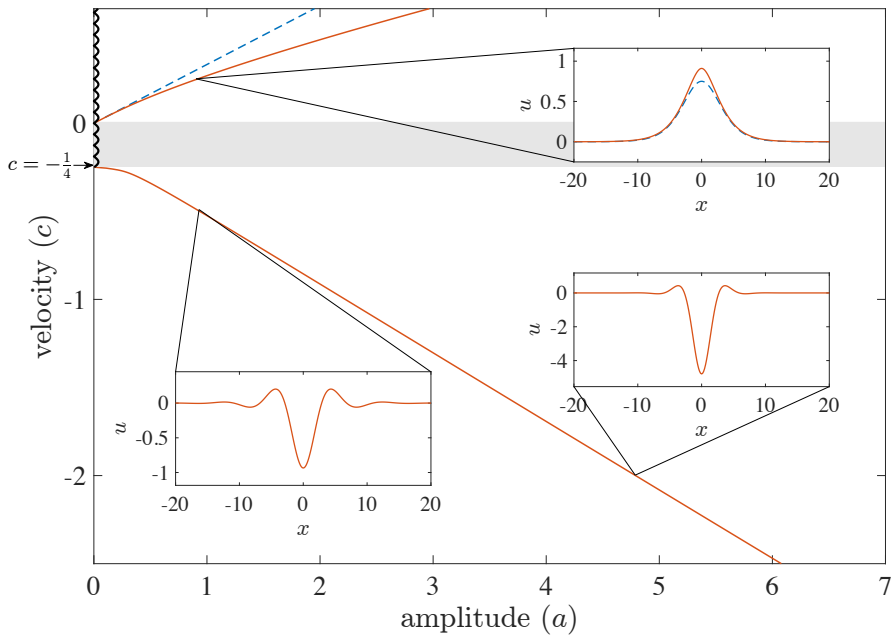

Figure 2.2: Numerically computed solitary wave profiles (insets) and speed-amplitude relation for the Kawahara equation with $\sigma = +1$ (solid) and the KdV equation (dashed). The linear wave spectrum is denoted on the vertical axis by the thick black curve. The "band gap" where no solitary waves exist is the shaded region.

with characteristic roots

$$r_{\pm}^2 = \frac{-1 \pm \sqrt{1+4c}}{2},$$

which are sketched in Fig. 2.3 for varying c. Note that the characteristic roots are complex with nonzero real part for $c < -\frac{1}{4}$ and purely imaginary for $-\frac{1}{4} < c < 0$ (what we term the solitary wave band gap in Fig. 2.2). Consequently, solitary waves with negative velocity can only exist for $c < -\frac{1}{4}$. A more detailed, asymptotic analysis of weakly nonlinear, modulated waves for $0 < -\frac{1}{4} - c \ll 1$ demonstrates a bifurcation of oscillatory, envelope solitary waves, hence the non-monotonic profiles in Figure 2.2 for $c < -\frac{1}{4}$ [55, 25]. In fact, for c sufficiently near, but below 1/4, the oscillatory solitary wave envelope is well described by the nonlinear Schrödinger equation [55]. For $c > 0$, the characteristic roots are purely real or purely imaginary. Here, the unstable/stable manifolds (real roots) correspond to the exponential decay of an embedded solitary wave while the stable manifolds (the imaginary characteristic roots) correspond to the oscillatory radiation tails of vanishing amplitude [126].

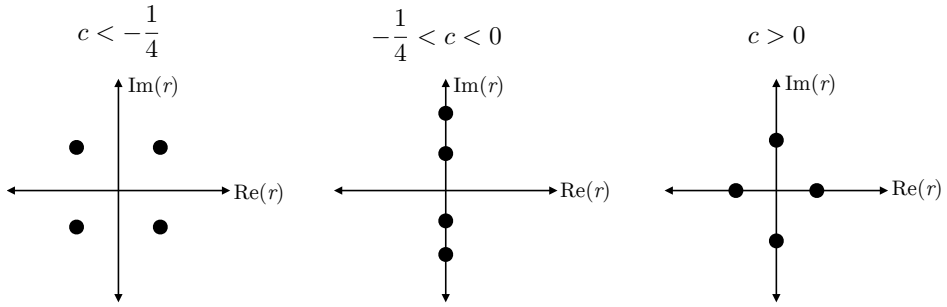

Figure 2.3: Characteristic roots, r, of the linearized, traveling wave equation (2.36) with $\sigma = +1$.

We now briefly shift our focus to numerical computation of solitary wave solutions of the KdV5 equation equation (1.4). These are useful in numerical computation of heteroclinic traveling waves in section 5.2.1. We implement an identical procedure as we used to compute solitary wave solutions of the Kawahara equation utilizing the spectral renormalization

method [3] for the Kawahara equation with $\sigma = 0$ in the computations. The structure of the solitary wave is shown in Fig. 2.4 with an amplitude of $a = \max u - \min u = 1$ and velocity $c \approx -0.3652$, where the wave amplitude. The invariance of the KdV5 equation under amplitude scaling yields the approximate amplitude speed relation

$$c_{\mathrm{s}}(a) \approx -0.3652a.$$

Compared to the depression solitary waves of the Kawahara equation whose amplitude-speed relation is depicted in Fig. 2.2, KdV5 depression, oscillatory solitary traveling waves propagate at a slightly higher velocity than similar solutions of the Kawahara equation. However, as the wave amplitude increases, fifth order dispersion dominates third order dispersion in the Kawahara equation, so that the relative difference between the two velocities decreases.

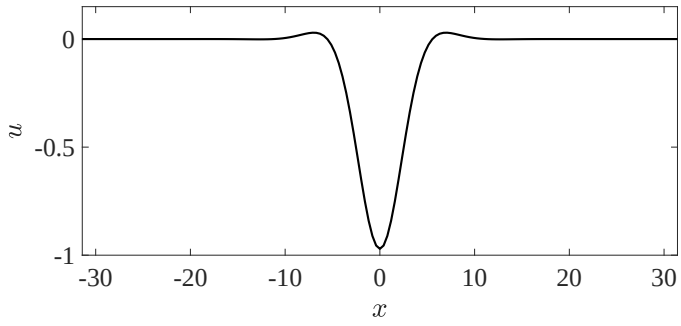

Figure 2.4: Numerically computed solitary wave solution of the KdV5 equation (1.4) with amplitude $a = 1$ and velocity $c \approx -0.3652$.

2.2.2 Periodic waves

Periodic solutions to the Kawahara equation and their stability are also well known within the literature. Here we will discuss the results from the literature that are directly related to this thesis and provide asymptotic and numerical computations of periodic traveling waves. Upon computing periodic solutions of the Kawahara equation, we may identify three

independent parameters, the mean denoted by $\overline{u}$, amplitude a and wavenumber k, which, in turn, uniquely determine the wave velocity $c = c(\overline{u}, a, k)$.

Here we will briefly comment on known results regarding periodic solutions of the Kawahara equation (1.3), although this brief explanation is by no means exhaustive. Existence of periodic solutions to the Kawahara equation has been rigorously established for $\sigma = 1$ by Haragus et al. [60] for small amplitude periodic waves. Further, more general homoclinic orbits have been computed for Kawahara and related systems for quite general settings (see, e.g. the review article by Champneys and references therein [29]). Tritchtchenko et al. [129] utilized numerical methods based on a Floquet-Bloch decomposition. Here they characterize both the stability of small amplitude periodic solutions of (1.3) for either sign of the third order dispersion parameter, σ.

We first obtain approximate periodic solutions to (1.3) via a weakly nonlinear Stokes frequency shift calculation [140] and through numerical computations. To this end, we seek an approximate form for the periodic wave solution to (2.35) of the form $f(\theta) = \varphi(\theta)$, $\theta = k\xi$ and its phase speed c as series expansions in the small, finite amplitude parameter a

$$\varphi = \overline{u} + a\varphi_1 + a^2\varphi_2 + \ldots, \quad c = c_0 + a^2 c_2 + \ldots, \quad 0 < a \ll 1.$$

Inserting the asymptotic approximation and equating like powers of a, we obtain the periodic wave and phase velocity up to $\mathcal{O}(a^2)$

$$\varphi = \overline{\varphi} + \frac{a}{2}\cos\theta + \frac{a^2}{48k^2\left(\sigma - 5k^2\right)}\cos 2\theta \tag{2.40}$$

$$c = \overline{u} - \sigma k^2 + k^4 - \frac{a^2}{96k^2\left(5k^2 - \sigma\right)}. \tag{2.41}$$

We now perform computations of periodic solutions of the Kawahara equation (1.3). We seek solutions to Eq. (2.35) of the form $f(k\xi) = \varphi(\theta)$, where f is a periodic solution of Eq. (2.38) with period $\frac{2\pi}{k}$. We may therefore approximate solutions as a truncated Fourier

series

$$\varphi(\theta) = \overline{u} + \sum_{n=-N/2}^{n=N/2-1} a_n e^{in\theta} \tag{2.42}$$

with N terms chosen so that $|a_N|, |a_{N/2=1}|$ are below a specified, small tolerance (typically $\mathcal{O}(10^{-14})$. For instance, parameters $(\overline{u}, a, k) = (0, 1, 1)$ requires $N = 2^6$ and $(\overline{u}, a, k) = (0, 1, 0.1)$ necessitates $N = 2^8$ modes to maintain spectral accuracy (Fourier coefficients decaying to $\mathcal{O}(10^{-15})$). Inserting the approximation (2.42) into Eq. (2.35) results in a nonlinear algebraic system that is solved with Matlab's optimization routine fsolve for a fixed value of c.

The Kawahara equation admits the Galilean symmetry

$$u(x,t) \to u(x - u_0 t, t) + u_0, \quad u_0 \in \mathbb{R}, \tag{2.43}$$

so that we may compute periodic solutions with zero mean without loss of generality. Figures 2.5 and 2.6 show sample periodic solutions for $\sigma = -1$ and $\sigma = +1$ respectively. Samples of the two-parameter family of periodic solutions are shown with fixed wavenumbers on each set of axes, while amplitude is varied in the range $(0.25, 2)$ with steps of 0.25. The periodic solutions reflect the structural change in the solutions of the Kawahara equation for $\sigma = \pm 1$. When $\sigma = -1$ the dispersion relation is convex, and solutions resemble the cnoidal solutions of the KdV equation(1.7). On the other hand, non-convex dispersion, $\sigma = +1$, exhibits periodic solutions which that are non-monotonic from their trough to their half-period.

We conclude this section with numerical computations of periodic solutions of the KdV5 equation (1.4). In contrast to the two parameter family of solutions computed for the Kawahara equation, the absence of the third derivative affords the additional symmetry

$$u \to bu, \quad x \to b^{-1/4} x, \quad t \to b^{-5/4} t \tag{2.44}$$

in addition to the Galilean symmetry Eq. (2.43) so that we obtain the three parameter family of solutions by scaling a one parameter family of solutions in k with unit amplitude

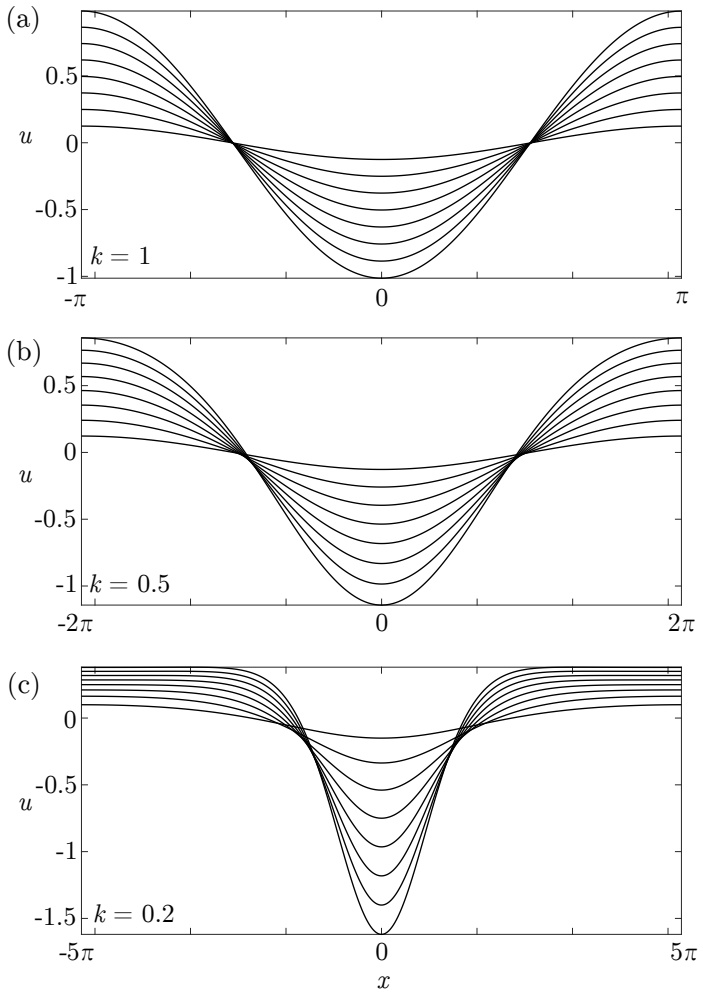

Figure 2.5: Zero mean periodic solutions of the Kawahara equation for $\sigma = -1$ with amplitudes, $a \in \{0.25, 0.5, \ldots, 1.75, 2\}$ for various wavenumbers (a) $k = 1$, (b) $k = 0.5$, and (c) $k = 0.2$.

and zero mean. The three-parameter family of periodic traveling waves can be generated from the one-parameter family $\left\{(\tilde{\varphi}(\theta;\tilde{k}), \tilde{c}(\tilde{k}))\right\}_{\tilde{k}\geq 0}$ by

$$\begin{aligned} \varphi(\theta;\overline{u},a,k) &= \overline{u} + a\tilde{\varphi}(a^{1/4}\theta - a^{1/4}k\overline{u}t; a^{-1/4}k), \\ c(\overline{u},a,k) &= a\tilde{c}(a^{-1/4}k) + \overline{u}, \end{aligned} \tag{2.45}$$

for any $a > 0$, $k > 0$, $\overline{u} \in \mathbb{R}$. Note that $\tilde{\varphi}(\theta;\tilde{k}) = \varphi(\theta; 0, 1, \tilde{k})$ and $\tilde{c}(\tilde{k}) = c(0, 1, \tilde{k})$.

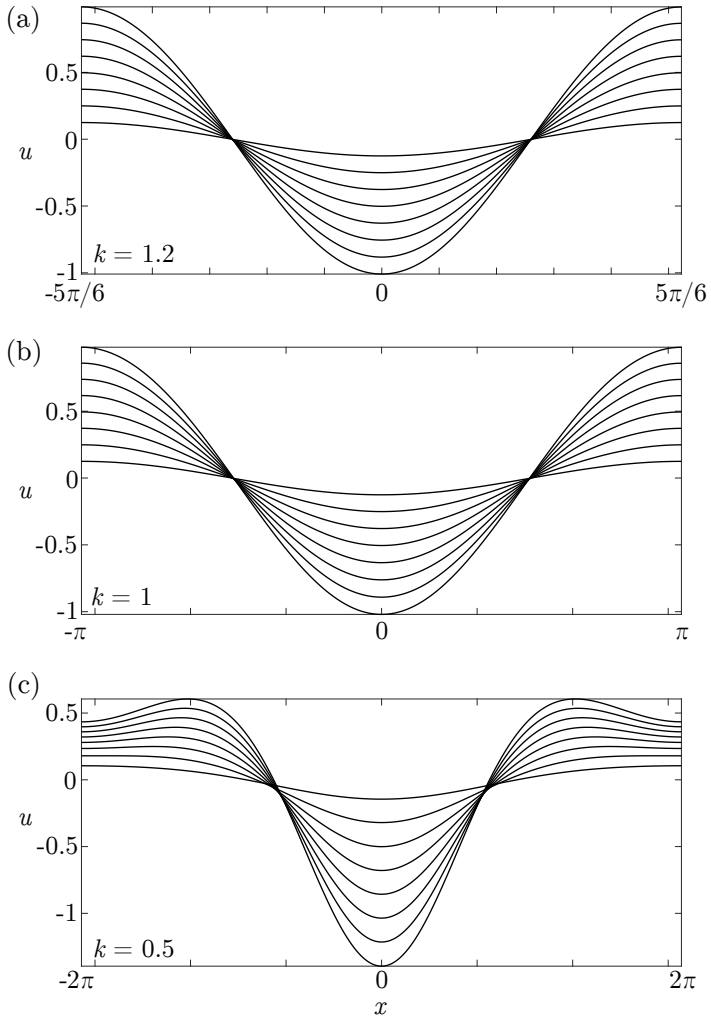

Figure 2.6: Zero mean periodic solutions of the Kawahara equation for $\sigma = +1$ with amplitudes, $a \in \{0.25, 0.5, \ldots, 1.75, 2\}$ for various wavenumbers (a) $k = 1.2$, (b) $k = 1$, and (c) $k = 0.5$.

Examples of periodic traveling wave solutions and their corresponding nonlinear dispersion curve are given in Fig. 2.7. Small $\tilde{k}$ corresponds to a well separated, solitary wave train. One measure for the validity of the Stokes approximation is the accuracy of the phase velocity (2.41), which compares favorably with the numerically computed phase velocity for $\tilde{k} \gtrsim 0.4$ as shown in Fig. 2.7.

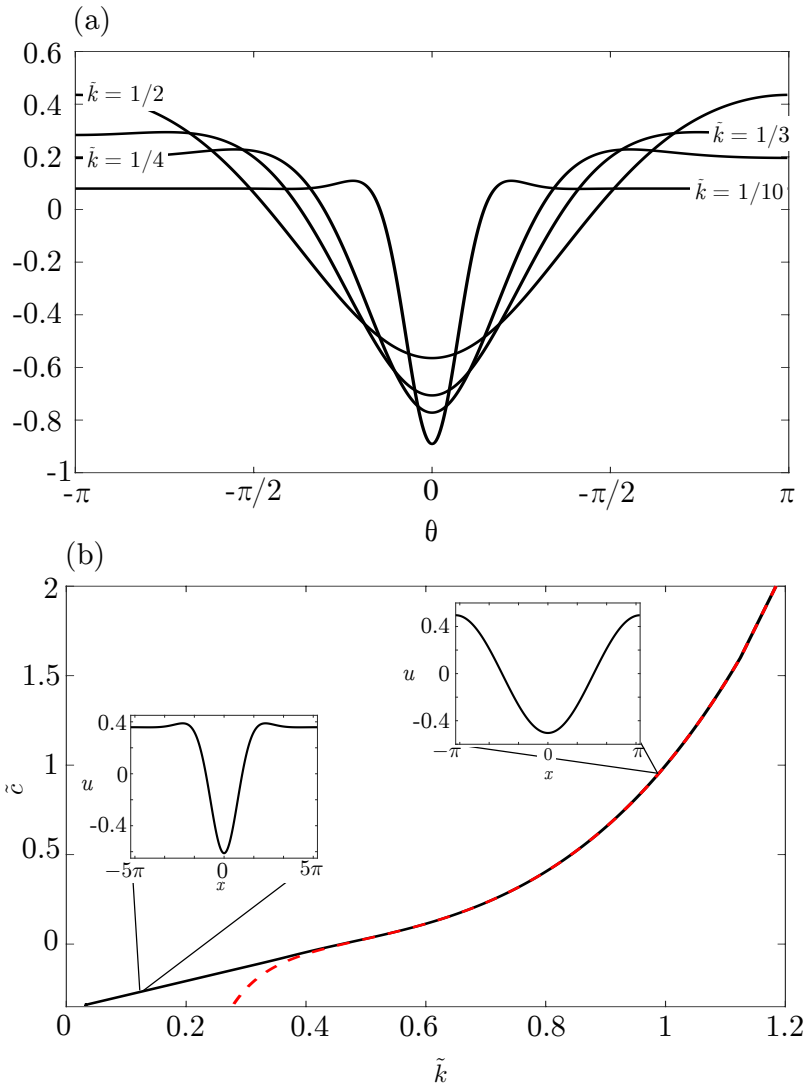

Figure 2.7: Numerically computed periodic traveling waves $\tilde{\varphi}(\theta, \tilde{k})$ with zero mean and unit amplitude. (a) Example periodic waves. (b) Comparison of numerically computed phase velocity $\tilde{c}$ for the family of periodic waves (black solid curve) compared with the Stokes approximation Eq. (2.41) (red dashed curve). Insets: example zero mean, unit amplitude periodic traveling waves for two different phase velocities.

Chapter 3

Whitham modulation equations for the Kawahara and KdV5 equations

Many of the results presented in this thesis are obtained by analyzing the Whitham modulation equations, a set of quasilinear PDEs that describe the slow evolution of a modulated nonlinear, periodic traveling wave [138, 140, 47, 71]. For the dispersive, scalar partial differential equations considered here, periodic traveling wave solutions can be uniquely identified by three independent parameters, the mean $\overline{u}$, amplitude a and wavenumber k. The underpinnings of Whitham modulation theory are as follows [140]. Rather than solving initial value problems for a dispersive, nonlinear equation we investigate IVPs for a first order, quasilinear system of PDEs for the wave parameters $\overline{u}, a, k$ that prescribes the approximate long time evolution is analyzed. As such, the structure of the Whitham modulation equations provide insight into the slow dynamics of a periodic wave. The results presented in this chapter draw upon works by the author [64, 122].

Asymptotic representations of periodic solutions outlined in Chapter 2 are leveraged to obtain the Kawahara-Whitham equations in the weakly nonlinear limit. The additional scaling symmetry from the reduction to the KdV5 equation allows us to utilize the one parameter family of numerically computed periodic solutions to study the KdV5-Whitham modulation equations well outside the weakly nonlinear regime.

Consider 2π-periodic traveling wave solutions to either the Kawahara (1.10) or KdV5 ((1.10) with $\sigma = 0$) equations in the form

$$f(\xi) = \varphi(\theta; \overline{u}, a, k), \quad \varphi(\theta + 2\pi; \overline{u}, a, k) = \varphi(\theta; \overline{u}, a, k), \tag{3.1}$$

where $\theta = k\xi$ is the phase variable and φ possesses three distinct parameters identified in Figure 3.1 and defined as

$$\begin{aligned} \text{wavenumber:} \quad & k, \\ \text{wave mean:} \quad & \overline{u} = \frac{1}{2\pi}\int_0^{2\pi} \varphi(\theta)d\theta, \\ \text{wave amplitude:} \quad & a = \max_{\theta\in[-\pi,\pi)} \varphi(\theta) - \min_{\theta\in[-\pi,\pi)} \varphi(\theta), \end{aligned}$$

and wave frequency $\omega = ck$, with velocity $c = c(\overline{u}, a, k)$. We now derive the Kawahara-Whitham modulation modulation equations.

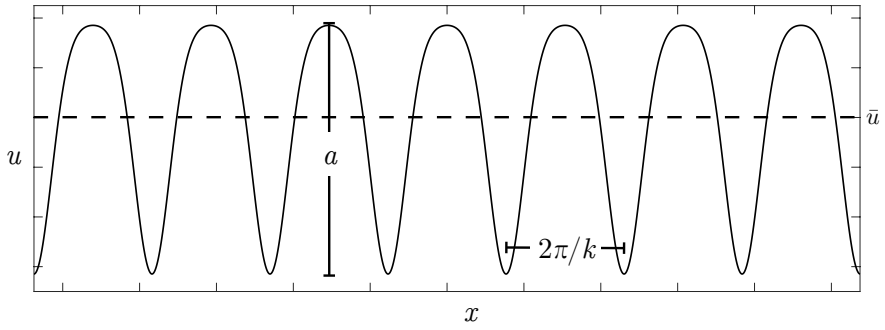

Figure 3.1: Sketch of a nonlinear periodic wave with modulation parameters identified graphically.

3.1 Whitham modulation equations: Derivation

Various methodologies can be utilized to derive the Whitham modulation equations. The first method introduced by Whitham [138] consisted of averaging conservation laws of the governing PDE and was applied to the Klein-Gordon and KdV equations. In the subsequent two years, Whitham formulated an equivalent approach to derive the modulation equations by averaging a Lagrangian density over a wave period [141] and taking variations with respect to wave amplitude, wavenumber, and wave frequency. Further developments by Luke [92] demonstrated that both methods to derive the modulation equations by Whitham

are equivalent to a multiple scales approach applied to the governing equation. Due to his seminal contributions, we refer to the obtained first order quasilinear system of PDEs as the Whitham equations. Here we will implement the two methods first introduced by Whitham to obtain the Kawahara-Whitham equations and demonstrate their equivalence in the weakly nonlinear regime.

3.1.1 Averaged conservation laws

Conservation laws define quantities whose values remain constant throughout the evolution defined by the governing partial differential equation. Here we require two conservation laws for the Kawahara equation (1.3). For the following calculation, we assume u is a sufficiently smooth function with rapid decay in itself and its derivatives as $x \to \pm\infty$ so that differentiation and integration of functions of u can be interchanged. The first conservation law of the Kawahara equation (1.3) is the system itself which specifies the conservation of the total "mass"

$$\begin{aligned}\frac{d}{dt}\int_{-\infty}^{\infty} u dx &= \int_{-\infty}^{\infty} u_t dx \\ &= \int_{-\infty}^{\infty} -\left[\frac{1}{2}u^2 + \sigma u_{xx} + u_{xxxx}\right]_x dx \\ &= 0,\end{aligned}$$

where the integral of the perfect derivative evaluates to 0 due to the rapid decay of u and its spatial derivatives in the far-field. The second conservation law for the total "momentum" is found by evaluating

$$\begin{aligned}\frac{d}{dt}\int_{-\infty}^{\infty} \frac{1}{2}u^2 dx &= \int_{-\infty}^{\infty} u u_t dx \\ &= -\int_{-\infty}^{\infty} u\left[\frac{1}{2}u^2 + \sigma u_{xx} + u_{xxxx}\right]_x dx, \\ &= -\int_{-\infty}^{\infty} \left[\frac{1}{3}u^3 + \sigma u u_{xx} - \frac{\sigma}{2}(u_x)^2 + u u_{xxxx} - u_x u_{xxx} + \frac{1}{2}(u_{xx})^2\right]_x dx \\ &= 0,\end{aligned}$$

which is again, zero due to the assumed decay of u and its derivatives. The conservation laws for the densities u and u^2 are

$$(u)_t + \left(\frac{1}{2}u^2 + \sigma u_{xx} + u_{xxxx}\right)_x = 0, \tag{3.2}$$

$$\left(\frac{1}{2}u^2\right)_t + \left(\frac{1}{3}u^3 + \sigma u u_{xx} - \frac{\sigma}{2}u_x^2 + u u_{xxxx} - u_x u_{xxx} + \frac{1}{2}u_{xx}^2\right)_x = 0. \tag{3.3}$$

The Whitham modulation equations are realized by computing a period-average of the conservation laws along the traveling wave manifold [138]. We derive the modulation equations by introducing the rapid phase variable $\theta = S(X,T)/\epsilon$ that satisfies

$$k = \theta_x = S_X, \quad \omega = -\theta_t = -S_T$$

where $X = \epsilon x$ and $T = \epsilon t$ are long space and slow time scales with $0 < \epsilon \ll 1$. We then seek an asymptotic solution in the form

$$u(x,t) = \varphi(\theta; \overline{u}, a, k) + \epsilon u_1(\theta, X, T) + \mathcal{O}(\epsilon^2), \tag{3.4}$$

with a leading order periodic traveling wave whose parameters $\overline{u}$, a, k depend on the slow variables X and T and each of the u_n are 2π-periodic in θ. Consequently, the derivatives in (3.2) and (3.3) transform according to

$$\frac{\partial}{\partial x} = k\frac{\partial}{\partial \theta} + \epsilon\frac{\partial}{\partial X}, \quad \frac{\partial}{\partial t} = -\omega\frac{\partial}{\partial \theta} + \epsilon\frac{\partial}{\partial T}.$$

We now introduce averaging of the quantity $F[u(x,t); X, T]$ according to

$$\overline{F} = \frac{1}{2\pi}\int_0^{2\pi} F \, d\theta. \tag{3.5}$$

Then, substituting the asymptotic series (3.4) for u into F results in

$$\overline{\frac{\partial F}{\partial t}} = \epsilon\frac{\partial \overline{F}}{\partial T} + \mathcal{O}(\epsilon^2), \quad \overline{\frac{\partial F}{\partial x}} = \epsilon\frac{\partial \overline{F}}{\partial X} + \mathcal{O}(\epsilon^2),$$

owing to the fact that the period average of an exact θ derivative is zero for periodic functions. Applying the averaging operator (3.5) to the conservation laws (3.2), (3.3) with the

asymptotic series (3.4) for u, we obtain

$$(\overline{u})_T + \left(\frac{1}{2}\overline{\varphi^2} + \sigma k^2 \overline{\varphi_{\theta\theta}} + k^4 \overline{\varphi_{\theta\theta\theta\theta}}\right)_X = 0, \tag{3.6}$$

$$\left(\frac{1}{2}\overline{\varphi^2}\right)_T + \left(\frac{1}{3}\overline{\varphi^3} + \sigma k^2 \overline{\varphi\varphi_{\theta\theta}} - k^2\frac{\sigma}{2}\overline{\varphi_\theta^2} + k^4\overline{\varphi\varphi_{\theta\theta\theta\theta}} - k^4\overline{\varphi_\theta\varphi_{\theta\theta\theta}} + \frac{1}{2}k^4\overline{\varphi_{\theta\theta}^2}\right)_X = 0, \tag{3.7}$$

subject to $\mathcal{O}(\epsilon)$ corrections that vanish in the zero dispersion limit. The modulation system is closed by the phase compatibility condition $S_{XT} = S_{TX}$, yielding the conservation of waves

$$k_T + (ck)_X = 0. \tag{3.8}$$

If initial data for Eqs. (3.6), (3.7), and (3.8) are invariant to the hydrodynamic scaling transformation $X \to bX$, $T \to bT$ (e.g., the step initial data to be considered in Chapters 4 and 5) then an equivalent alternative to the zero dispersion limit is the long time limit of Eqs. (3.6), (3.7), and (3.8) with the unscaled independent variables $x = X/\epsilon$, $t = T/\epsilon$. In fact, we will be considering smooth step-like initial data so that the long-time limit not equivalent exactly to the zero dispersion limit, but is approximately so.

The conservation laws (3.6), (3.7) are simplified via direct integration and integration by parts

$$\begin{aligned}
\overline{\varphi_{\theta\theta}} &= 0 \\
\overline{\varphi_{\theta\theta\theta\theta}} &= 0 \\
\overline{\varphi\varphi_{\theta\theta}} &= -\overline{\varphi_\theta^2}, \\
\overline{\varphi\varphi_{\theta\theta\theta\theta}} &= \overline{\varphi_{\theta\theta}^2}, \\
\overline{\varphi_\theta\varphi_{\theta\theta\theta}} &= -\overline{\varphi_{\theta\theta}^2}.
\end{aligned}$$

These identities, along with a return to the unscaled variables x, t, imply that the Whitham

equations in conservative form can be written compactly as

$$\overline{u}_t + \left(\frac{1}{2}\overline{\varphi^2}\right)_x = 0, \tag{3.9}$$

$$\left(\frac{1}{2}\overline{\varphi^2}\right)_t + \left(\frac{1}{3}\overline{\varphi^3} - \frac{3}{2}\sigma k^2\overline{\varphi_\theta^2} + \frac{5}{2}k^4\overline{\varphi_{\theta\theta}^2}\right)_x = 0, \tag{3.10}$$

$$k_t + (ck)_x = 0. \tag{3.11}$$

We now insert the periodic solution φ. For our purposes here, we utilize the Stokes wave (2.40) given here for convenience by

$$\varphi \sim \overline{\varphi} + \frac{a}{2}\cos\theta + \frac{a^2}{48k^2\left(\sigma - 5k^2\right)}\cos 2\theta,$$

and its nonlinear dispersion relation (2.41)

$$\omega \sim \overline{u}k - \sigma k^3 + k^5 + \frac{a^2}{96k^2\left(5k^2 - \sigma\right)},$$

which are asymptotically valid provided

$$\frac{1}{k^2|\sigma - 5k^2|} \ll a \ll 1.$$

The conservative form of the modulation equations, up to $\mathcal{O}(a^2)$, are then given by

$$\overline{u}_t + \left(\frac{\overline{u}^2}{2} + \frac{a^2}{16}\right)_x = 0, \tag{3.12}$$

$$\left(\frac{\overline{u}^2}{2} + \frac{a^2}{16}\right)_t + \left(\frac{\overline{u}^3}{3} + \frac{\overline{u}a^2}{8} - \sigma\frac{3a^2k^2}{16} + \frac{5a^2k^4}{16}\right)_x = 0, \tag{3.13}$$

$$k_t + \left(\overline{u}k - \sigma k^3 + k^5 - \frac{a^2}{96k\left(5k^2 - \sigma\right)}\right)_x = 0. \tag{3.14}$$

Carrying out the partial derivatives of the density and flux terms in the conservative form of the Whitham equations, we find

$$\begin{bmatrix} 1 & 0 & 0 \\ \overline{u} & \frac{a}{8} & 0 \\ 0 & 0 & 1 \end{bmatrix}\mathbf{q}_t + \begin{bmatrix} \overline{u} & \frac{a}{8} & 0 \\ \frac{a^2}{8} + \overline{u}^2 & \frac{a}{8}\left(5k^4 - 3\sigma k^2 + 2\overline{u}\right) & \frac{a^2k}{8}\left(10k^2 - 3\sigma\right) \\ k & -\frac{a}{240k^3 - 48k\sigma} & 5k^4 - 3\sigma k^2 + \overline{u} + \frac{a^2\left(15k^2 - \sigma\right)}{96(k\sigma - 5k^3)^2} \end{bmatrix}\mathbf{q}_x = 0 \tag{3.15}$$

where $\mathbf{q} = [\overline{u}, a, k]^{\mathrm{T}}$ is a vector of the periodic wave parameters. As long as $a \neq 0$, we can invert the first coefficient matrix and obtain the quasilinear form of the modulation equations

$$\mathbf{q}_t + \mathcal{A}\mathbf{q}_x = 0, \tag{3.16}$$

$$\mathcal{A} = \begin{bmatrix} \overline{u} & \frac{a}{8} & 0 \\ a & 5k^4 - 3\sigma k^2 + \overline{u} & ak\left(10k^2 - 3\sigma\right) \\ k & -\frac{a}{240k^3 - 48k\sigma} & 5k^4 - 3\sigma k^2 + \overline{u} + \frac{a^2\left(15k^2 - \sigma\right)}{96(k\sigma - 5k^3)^2} \end{bmatrix} \tag{3.17}$$

Setting $\sigma = 0$ yields the weakly nonlinear KdV5-Whitham modulation equations [122, 64].

3.1.2 Averaged Lagrangian

We now carry out an equivalent method to derive the Whitham modulation equations, though we will restrict ourselves to the weakly nonlinear limit for this calculation. The Kawahara equation (1.3) possesses a Lagrangian formulation in terms of the potential Φ such that

$$u = \frac{\partial \Phi}{\partial x}. \tag{3.18}$$

The Lagrangian density is

$$L = \frac{1}{2}\Phi_t\Phi_x + \Phi_x^3 - \frac{\sigma}{2}\Phi_{xx}^2 + \frac{1}{2}\Phi_{xxx}^2. \tag{3.19}$$

Critical points of the Lagrangian $\int L \, \mathrm{d}x\mathrm{d}t$ satisfy the Euler-Lagrange equations

$$(L_{\Phi_t})_t + (L_{\Phi_x})_x - (L_{\Phi_{xx}})_{xx} + (L_{\Phi_{xxx}})_{xxx} = 0,$$

which is exactly the Kawahara equation (1.3) upon identifying $\Phi_x = u$. The Whitham modulation equations are obtained by integrating the Lagrangian density (3.19) over the family of periodic traveling waves and taking variations with respect to the periodic wave parameters, thus yielding a closed system of equations that describes the modulated periodic wave [140, 141]. The procedure is made explicit in the weakly nonlinear limit by again

approximating the periodic traveling wave solution of equation (1.3) in the weakly nonlinear limit with the Stokes wave (2.40). We therefore seek the Lagrangian potential (3.19) of the form

$$\Phi(\theta) = \overline{u}x - \gamma t + \Psi(\theta) \tag{3.20}$$

where $\Psi(\theta)$ denotes the zero mean portion of the periodic wave potential such that $\varphi = \overline{u} + k\Psi_\theta$. Here, φ is the periodic solution that will be approximated by the Stokes wave (2.40) and whose parameters vary slowly in x and t. The modulation wavenumber and frequency are again defined in terms of the phase θ by $k = \theta_x$ and $\omega = -\theta_t$. Substituting the modulated wavetrain (3.20) into the Lagrangian density (3.19) gives

$$L = \frac{1}{2}\left[-\gamma + \frac{\omega}{k}\overline{u}\right]\varphi - \frac{1}{2}\frac{\omega}{k}\varphi^2 + \frac{1}{6}\varphi^3 - \frac{\sigma k^2}{2}\varphi_\theta^2 + \frac{k^4}{2}\varphi_{\theta\theta}^2, \tag{3.21}$$

The averaged Lagrangian is now obtained by substituting the Stokes expansion (2.40) into the Lagrangian (3.21) and averaging by integrating over a wave period [138]. The averaged Lagrangian is given by

$$\overline{L} = \frac{1}{2\pi}\int_0^{2\pi} L dx = -\frac{1}{2}\gamma\overline{u} + \frac{1}{6}\overline{u}^3 + \left(\frac{k^5 - \sigma k^3 + k\overline{u} - \omega}{16k}\right)a^2 + \mathcal{O}(a^4). \tag{3.22}$$

The modulation equations for the slowly varying parameters of the Stokes wave are now obtained by taking variations of this averaged Lagrangian with respect to the phase θ, the mean phase, ψ and the amplitude a. For simplicity, we only retain terms up to $\mathcal{O}(a^2)$ in the variations, though one can continue to higher orders if necessary. Amplitude variation, $\overline{L}_a = 0$, yields the linear dispersion relation $\omega = \overline{u}k + k^5$. Mean phase variation $-(\overline{L}_\gamma)_t + (\overline{L}_{\overline{u}})_x = 0$ determines the mean flow modulation

$$\overline{u}_t + \left(\frac{1}{2}\overline{u}^2 + \frac{a^2}{16}\right)_x = 0, \tag{3.23}$$

by virtue of the identity $-\gamma_x = u_t$. Phase variation $-(\overline{L}_\omega)_t + (\overline{L}_k)_x = 0$ leads to the conservation of wave action

$$\left[\frac{a^2}{k}\right]_t + \left[\frac{a^2}{k}\left(\overline{u} - 3\sigma k^2 + 5k^4\right)\right]_x = 0. \tag{3.24}$$

This modulation system is closed by the conservation of waves $\theta_{tx} = \theta_{xt}$

$$k_t + \left[\overline{u}k - \sigma k^3 + k^5 - \frac{a^2}{96k^2(5k^2-\sigma)}\right]_x = 0. \tag{3.25}$$

The weakly nonlinear modulation equations (3.23)–(3.25) are valid up to order a^2.

Again, we can cast the modulation system into quasilinear form, where we recover the system (3.16) with flux matrix $\mathcal{A}$ given by Eq. (3.17). Therefore, we have proved that the averaged conservation law and averaged Lagrangian approaches yield equivalent modulation systems in the weakly nonlinear limit.

3.2 Properties of the weakly nonlinear Whitham Modulation equations

The modulation equations derived in Sections 3.1.1 and 3.1.2 form a quasilinear system whose structure provides important information about the evolution of initial value problems. For instance, the eigenvalues of the matrix in quasilinear form, cf. (3.16) in the weakly nonlinear limit, reveal the hyperbolicity/ellipticity of the Whitham equations. If the eigenvalues of the Whitham equations are purely real, then the system is hyperbolic and the initial value problem can, in principle, be solved. However, if the eigenvalues have nonzero imaginary part, then the modulation equations are elliptic, and the initial value problem becomes ill-posed and the underlying periodic traveling wave is modulationally unstable [16].

3.2.1 Hyperbolicity/ellipticity

In the small amplitude regime, we may compute the eigenvalues of $\mathcal{A}$ in (3.16) perturbatively using the wave amplitude a as a small parameter. The eigenvalues, or characteristic velocities of the hyperbolic system are then given by the three distinct eigenvalues λ_i,

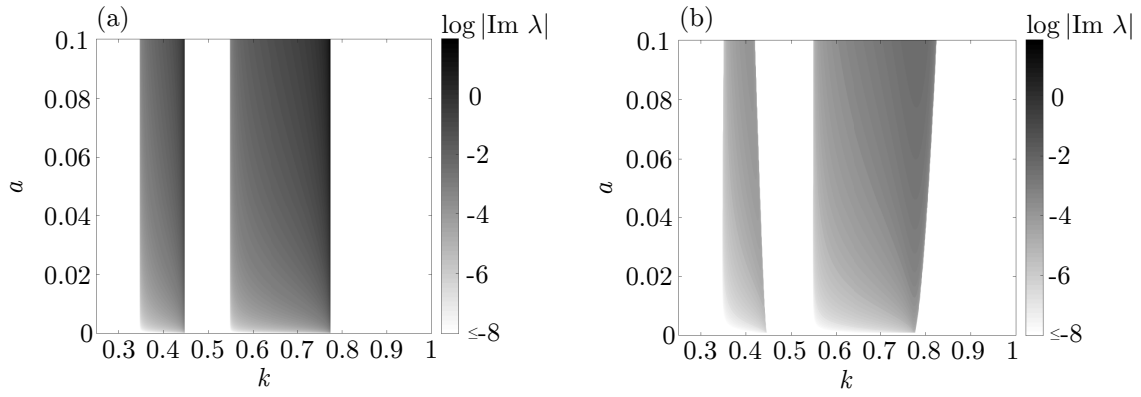

Figure 3.2: Magnitude of imaginary part of the eigenvalues of the weakly nonlinear modulation equations of the Kawahara equation. (a) imaginary part of the eigenvalues expansions (3.27)–(3.28) (b) eigenvalues of the coefficient matrix (3.17).

$i = 1, 2, 3$

$$\lambda_1 = \overline{u} + \mathcal{O}(a^2), \tag{3.26}$$

$$\lambda_2 = \overline{u} - 3\sigma k^2 + 5k^4 - a\sqrt{3 - 5k^2\left(\frac{6}{3\sigma - 5k^2} + \frac{1}{\sigma - 5k^2}\right)} + \mathcal{O}(a^2), \tag{3.27}$$

$$\lambda_3 = \overline{u} - 3\sigma k^2 + 5k^4 + a\sqrt{3 - 5k^2\left(\frac{6}{3\sigma - 5k^2} + \frac{1}{\sigma - 5k^2}\right)} + \mathcal{O}(a^2)., \tag{3.28}$$

For the case $\sigma = -1$ small amplitude periodic waves are modulationally stable in the weakly nonlinear limit due to the hyperbolicity of the Whitham equations [16]. On the other hand, periodic waves on an arbitrary background mean are modulationally unstable for $\sigma = 1$ for wavenumbers $k \in \left(\frac{\sqrt{3}}{5}, \frac{1}{\sqrt{5}}\right) \cup \left(\sqrt{\frac{3}{10}}, \sqrt{\frac{3}{5}}\right)$. Figure 3.2 shows the magnitude of the imaginary part of the eigenvalues for $\sigma = 1$ in the (k, a)-plane. The imaginary part of the eigenvalues of $\mathcal{A}$ in (3.17) are a proxy for the growth rate of the instability. This will be relevant in our investigation of DSW solutions of the Kawahara equation in Chapter 4.

For the KdV5 equation, we may take $\sigma = 0$. Therefore the characteristic velocities of

the KdV5-Whitham equations are

$$\lambda_1 = \overline{u} + \mathcal{O}(a^2), \tag{3.29}$$

$$\lambda_2 = \overline{u} + 5k^4 - \sqrt{\frac{5}{24}}a + \mathcal{O}(a^2), \tag{3.30}$$

$$\lambda_3 = \overline{u} + 5k^4 + \sqrt{\frac{5}{24}}a + \mathcal{O}(a^2), \tag{3.31}$$

of the flux Jacobian matrix, so that we may conclude that the modulation equations are strictly hyperbolic in the weakly nonlinear limit.

3.2.2 Genuine nonlinearity

The genuine nonlinearity of the modulation equations enables the existence of simple wave solutions across all of the parameter space, which are imperative in the construction of DSWs [47, 62, 91]. Simple wave solutions of the modulation equations and will play a crucial role in the construction of DSW solutions to the KdV5 equation (1.4) in Chapter 6 (cf. Fig. 1.6). For regions of parameter space where the modulation equations are hyperbolic, genuine nonlinearity is determined by the three eigenpairs $\{\lambda_j, \mathbf{r}_j\}$ where $\mathbf{r}_j$ is the right eigenvector corresponding to λ_j. The quantity

$$\mu_j = \nabla_{\mathbf{q}}\lambda_j \cdot \mathbf{r}_j,$$

determines if the characteristic field λ_j is genuinely nonlinear. If $\mu_j \neq 0$, then the modulation equations are genuinely nonlinear. Calculations are simplified by considering the KdV5-Whitham equations with $\sigma = 0$ in (3.16) since the KdV5-Whitham equations are strictly hyperbolic in the weakly nonlinear limit (cf. the eigenvalues (3.29)–(3.31) with $\sigma = 0$). The

eigenvectors of the flux matrix are

$$\mathbf{r}_1 = \begin{pmatrix} -5k^3 \\ 0 \\ 1 \end{pmatrix} - a \begin{pmatrix} 0 \\ \frac{1}{k} \\ 0 \end{pmatrix} + \mathcal{O}(a^2) \tag{3.32}$$

$$\mathbf{r}_2 = \begin{pmatrix} 0 \\ -4\sqrt{30}k^3 \\ 1 \end{pmatrix} + a \begin{pmatrix} -\frac{\sqrt{3}}{\sqrt{10}k} \\ \frac{33}{20k} \\ 0 \end{pmatrix} + \mathcal{O}(a^2) \tag{3.33}$$

$$\mathbf{r}_3 = \begin{pmatrix} 0 \\ 4\sqrt{30}k^3 \\ 1 \end{pmatrix} + a \begin{pmatrix} \frac{\sqrt{3}}{\sqrt{10}k} \\ \frac{33}{20k} \\ 0 \end{pmatrix} + \mathcal{O}(a^2) \tag{3.34}$$

It is possible to obtain expressions for the eigenvectors of the Kawahara-Whitham equations ($\sigma \neq 0$), although the expressions are quite complicated and not included here for brevity. The parameter, μ_j determines the genuine nonlinearity and can be computed for each eigenpair $\{\lambda_i, \mathbf{r}_i\}$ to be approximately

$$\begin{aligned} \mu_1 &= -5k^3 - \frac{13a^2}{96k^5} \\ \mu_2 &= 30k^3 - \frac{13}{8}\sqrt{\frac{3}{10}}\frac{a}{k} - \frac{241a^2}{12800k^5} + o(a^2) \\ \mu_3 &= 30k^3 + \frac{13}{8}\sqrt{\frac{3}{10}}\frac{a}{k} - \frac{241a^2}{12800k^5} + o(a^2). \end{aligned}$$

To respect asymptotic ordering obeyed by the Stokes approximation, we must enforce that $k \gg a^{1/4}$ so that for all $j = 1, 2, 3$, μ_j remains nonzero within this asymptotic regime. Therefore, we conclude that in the weakly nonlinear limit, the KdV5-Whitham modulation equations are genuinely nonlinear and we can construct integral curves across the regime $0 < a \ll 1$, $k \gg a^{1/4}$. We describe the computation of integral curves, i.e. simple waves, in the following section.

3.2.3 Simple waves

The Whitham modulation system (3.9)–(3.11) is readily solved for a special class of solutions. We seek the simple wave solution which varies in only one characteristic family, while the others remain constant [36]. When the modulation equations are hyperbolic and genuinely nonlinear, we compute wave curves that parameterize self-similar solutions to the modulation equations (3.36). These wave curves will be applied to the solution of Riemann problems in Chapter 6. The j-th wave curve is the integral curve in the direction of $\mathbf{r}_j$ [36]. We introduce the self similar parameterization $s = x/t$ so that $\mathbf{q} = \mathbf{q}(s)$. Along the $j - th$ characteristic, $s = \lambda_j$ so that the wave parameters are determined by

$$\frac{\mathrm{d}\mathbf{q}}{\mathrm{d}s} = \frac{\mathbf{r}_j}{\mu_j}. \tag{3.35}$$

3.3 Whitham modulation equations for the KdV5 equation

The periodic traveling wave solutions of the KdV5 equation can characterized up to scaling and Galilean symmetries (2.44) and (2.43) entirely by a one parameter family of periodic waves. For our purposes, we use a family of unit amplitude, zero mean periodic traveling wave solutions with arbitrary wavenumber. We will lean on these numerical computations in Chapter 5. A similar approach could be carried out to compute the Kawahara-Whitham modulation equations, but the Kawahara equation lacks a scaling invariance; hence the Kawahara periodic traveling waves form a 2-parameter family up to Galilean symmetry. This leads to additional complexities when computing the Kawahara-Whitham modulation equations numerically. See Ref. [94] for a similar numerical computation of the Whitham modulation equations for the so-called conduit equation.

3.3.1 Numerical computations of fully nonlinear KdV5-Whitham modulation equations

In Section 3.1.1, we demonstrated the simplest methodology to derive the KdV5-Whitham equations (3.9)–(3.11) via averaging conservation laws of the KdV5 equation. As in the weakly nonlinear limit, we may cast the modulation equations in quasilinear form for the modulation variables $\mathbf{q} = [\overline{u}, a, k]^{\mathrm{T}}$

$$\mathbf{q}_t + \mathcal{A}\mathbf{q}_x = 0 \tag{3.36}$$

where

$$\mathcal{A} = \begin{bmatrix} 1 & 0 & 0 \\ \frac{1}{2}\frac{\partial\overline{\varphi^2}}{\partial\overline{u}} & \frac{1}{2}\frac{\partial\overline{\varphi^2}}{\partial a} & \frac{1}{2}\frac{\partial\overline{\varphi^2}}{\partial k} \\ 0 & 0 & 1 \end{bmatrix}^{-1} \begin{bmatrix} \frac{1}{2}\frac{\partial\overline{\varphi^2}}{\partial\overline{u}} & \frac{1}{2}\frac{\partial\overline{\varphi^2}}{\partial a} & \frac{1}{2}\frac{\partial\overline{\varphi^2}}{\partial k} \\ \frac{1}{3}\frac{\partial\overline{\varphi^3}}{\partial\overline{u}} + \frac{5}{2}k^4\frac{\partial\overline{\varphi^2_{\theta\theta}}}{\partial\overline{u}} & \frac{1}{3}\frac{\partial\overline{\varphi^3}}{\partial a} + \frac{5}{2}k^4\frac{\partial\overline{\varphi^2_{\theta\theta}}}{\partial a} & \frac{1}{3}\frac{\partial\overline{\varphi^3}}{\partial k} + \frac{5}{2}\frac{\partial(k^4\overline{\varphi^2_{\theta\theta}})}{\partial\overline{u}} \\ k\frac{\partial c}{\partial\overline{u}} & k\frac{\partial c}{\partial a} & \frac{\partial(ck)}{\partial\overline{u}} \end{bmatrix},$$

which is valid provided the matrix inverse exists. For every computation performed throughout this thesis, $\mathcal{A}$ is well-defined. The symmetries (2.43), (2.44) of solutions to the KdV5 equation can be used to directly compute the averaged integrals' dependence on the mean $\overline{u}$ and amplitude a. We define the averaging integrals

$$I_n(\overline{u}, a, k) = \frac{1}{2\pi}\int_0^{2\pi} \varphi^n(\theta; \overline{u}, a, k)\, d\theta, \quad J_2(\overline{u}, a, k) = \frac{1}{2\pi}\int_0^{2\pi} \varphi^2_{\theta\theta}(\theta; \overline{u}, a, k)\, d\theta.$$

These integrals can be written explicitly in terms of period averages over the one-parameter family of periodic traveling waves solutions $\tilde{\varphi}(\theta; \tilde{k})$ using Eq. (2.45)

$$\begin{aligned} I_2(\overline{u}, a, k) &= \overline{u}^2 + a^2\tilde{I}_2(a^{-1/4}k), \\ I_3(\overline{u}, a, k) &= \overline{u}^3 + 3\overline{u}a^2\tilde{I}_2(a^{-1/4}k) + a^3\tilde{I}_3(a^{-1/4}k), \\ J_2(\overline{u}, a, k) &= a^2\tilde{J}_2(a^{-1/4}k), \end{aligned} \tag{3.37}$$

where we have introduced the $\tilde{\cdot}$ variables to denote averaging integrals of unit amplitude, zero mean periodic traveling wave solutions. Derivatives in the remaining parameter k are computed approximately via an unequally spaced, fourth-order finite difference scheme [51].

We now investigate the hyperbolicity/ellipticity and genuine nonlinearity of the modulation equations, which again depend solely upon the eigenvalues $\tilde{\lambda}_j$ and right eigenvectors $\tilde{\mathbf{r}}_j$ of $\mathcal{A}$. The $\tilde{\lambda}_j$ connote the eigenvalues of the Whitham modulation equation flux matrix $\mathcal{A}$ evaluated with unit amplitude, zero mean periodic waves. The eigenvalues of $\mathcal{A}$ for more general periodic traveling wave solutions can be determined from this family by using the scaling symmetries (2.44) so that

$$\lambda_j(\overline{u}, a, k) = \overline{u} + a\tilde{\lambda}_j(a^{-1/4}k) \tag{3.38}$$

$$\mathbf{r}_j(\overline{u}, a, k) = \begin{bmatrix} a^{3/4} & 0 & 0 \\ 0 & a^{3/4} & 0 \\ 0 & 0 & 1 \end{bmatrix} \tilde{\mathbf{r}}_j(a^{-1/4}k). \tag{3.39}$$

Numerical computation of the characteristic velocities, $\tilde{\lambda}_j(\tilde{k})$ depicted in Figure 3.3 illustrate hyperbolicity of the modulation equations for a range of $\tilde{k}$. When $0.41 \lesssim \tilde{k} \lesssim 0.65$ and $0.25 \lesssim \tilde{k} \lesssim 0.3$, two complex conjugate characteristic velocities with nonzero imaginary part emerge, so that corresponding periodic traveling waves are modulationally unstable. It is further shown in Fig. 3.3 that the weakly nonlinear calculations for the characteristic velocities Eqs. (3.29)–(3.31) are in excellent agreement with the numerical calculations for $\tilde{k} \gtrsim 0.7$.

In a similar manner, we utilize the eigenvalues and eigenvectors to determine regions of genuine nonlinearity for the modulation equations (3.9)–(3.11) by computing the quantities

$$\mu_j = \nabla\lambda_j \cdot \mathbf{r}_j, \quad j = 1, 2, 3. \tag{3.40}$$

For waves of unit amplitude and zero mean, we find points of non-genuine nonlinearity where $\mu_1 \approx \mu_2 \approx 0$, which are identified by the red points in the lower panel of Fig. 3.3(a). Our numerical computations suggest that both the first and second characteristic fields are not genuinely nonlinear at these select points $\tilde{k} \in \{0.167, 0.185, 0.222, 0.370\}$.

We directly compute simple waves by integrating (3.35) with the right hand side replaced by the numerically computed eigenpairs. Illustrative 2-wave curves are displayed

in Figs. 3.3(b) and (c) and correspond to the shaded regions in Fig. 3.3(a) (lower panel) on the left and right respectively. In these figures, we project the three dimensional curve $(\overline{u}(s), a(s), k(s))$ onto both the $\overline{u}$-a plane and the $\overline{u}$-k plane. We normalize the wave curves to emanate from the zero mean, unit amplitude state $\overline{u} = 0$, $a = 1$. For this visualization, we should note that $\overline{u}(s)$ is a monotonically decreasing function in s.

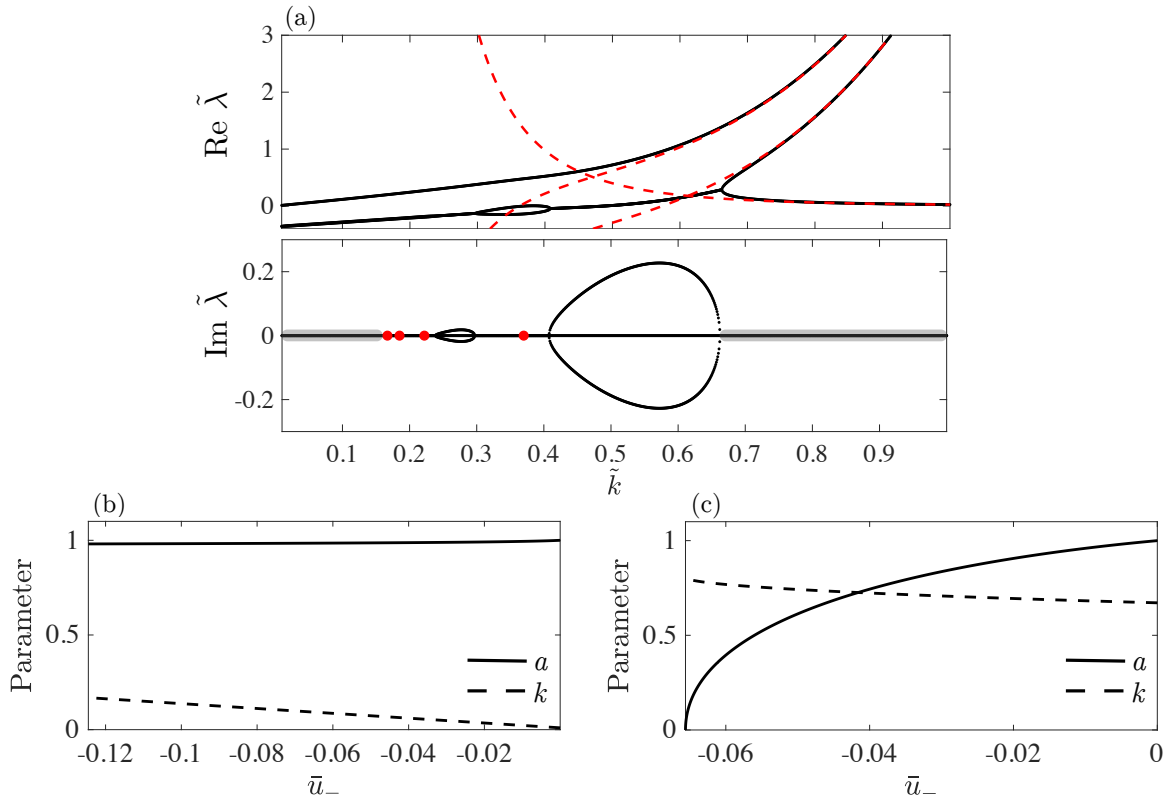

Figure 3.3: (a) Eigenvalues of $\mathcal{A}$ for $\overline{u} = 0$, and $a = 1$ as a function of wavenumber $\tilde{k}$ shown in black curves. The eigenvalues from weakly nonlinear theory (3.29)–(3.31) are identified by dashed red curves. Gray, banded regions denote the domain of the 2-wave curves, which solve the ODE (3.35) in (b) and (c). (b) Example 2-wave curve for $0 < \tilde{k} \lesssim 0.15$. (c) Example 2-wave curve for $0.65 \lesssim \tilde{k} < 1$.

3.4 Conclusions

Here we derived the Whitham modulation equations in conservative form for the Kawahara equation (3.9)–(3.11) using averaged conservation laws. Inserting the weakly nonlinear

Stokes wave expansion we demonstrated that the conservative system is equivalent to a quasilinear system that is obtained by taking variations of an averaged Lagrangian density (3.21). In the weakly nonlinear limit, we showed that the Kawahara-Whitham modulation equations can become elliptic for certain periodic traveling wave parameters meaning that the periodic traveling wave will be modulationally unstable. We simplified calculations of genuine nonlinearity by considering the KdV5 equation (1.4), which is the Kawahara equation (1.3) with no third order dispersion term. Here we found that the KdV5 modulation equations are hyperbolic and genuinely nonlinear in regimes where the weakly nonlinear Stokes' expansion is asymptotically valid.

We further investigated the structure of the KdV5-Whitham modulation equation using a one-parameter family of periodic traveling waves computed in Chapter 2. Within continuous bands in parameter space, the fully nonlinear KdV5-Whitham modulation equations are elliptic and at isolated points the modulation equations lose genuine nonlinearity.

Chapter 4

Numerical and asymptotic studies of wavebreaking in the Kawahara equation

In this chapter, we summarize results from the manuscript [121]. Dispersive shock waves (DSWs) arise from the dispersive resolution of gradient catastrophe, or wavebreaking [47]. Within the context of Whitham modulation theory, classical DSW is characterized by a modulated, nonlinear periodic traveling wave that gradually transitions from a finite amplitude solitary wave at one edge to a vanishing amplitude harmonic wave at the other. In this chapter, we characterize the long term behavior of DSWs that arise from the initial value problem

$$u_t + uu_x + \sigma u_{xxx} + u_{xxxxx} = 0 \qquad u(x,0) = \frac{\Delta}{2}\left(1 - \tanh\left(\frac{x}{w}\right)\right), \tag{4.1}$$

where $\Delta > 0$ is the amplitude of the approximate initial step with width w.

In related works, authors consider a higher order nonlinear Schrödinger equation with applications to fiber optics [31, 32, 33, 34, 95, 48, 120] where the authors observe a structural change in the DSW as the amplitude of the jump is varied or as the strength of the higher order dispersion is increased relative to lower order terms. The Gurevich-Pitaevskii (GP) problem for the Kawahara equation (4.1) provides a simpler test bed, relative to its bidirectional analogs, to better understand how higher order dispersion affects DSW structure. Using the initial value problem (4.1) as the canonical problem of interest, we observe new classes of DSWs that depend both on the amplitude of the initial step, Δ, and the sign of third order dispersion $\sigma = \pm 1$. We begin by briefly summarizing the novel DSW structures

observed in this chapter as well as identify their defining characteristics. Detailed numerical and asymptotic investigations of these waves will make up the remainder of this chapter.

In the small amplitude regime, gradient catastrophe from the step-like initial data evolves to a radiating DSW (**RDSW**). The RDSW is described asymptotically as a perturbed KdV DSW with small amplitude dispersive waves or radiation in resonance with the long waves within the DSW. The radiation is attributed to the existence of solitary wave solutions of the Kawahara equation embedded in the linear spectrum [126]. Further increase in fifth order dispersion strength results in a more complex, incoherent regime where we observe strong forward and backward propagation of waves. At a threshold jump height, backward wave propagation is arrested and a new coherent wave structure emerges, the traveling DSW or **TDSW**. The TDSW has a traveling wave component with a partial, non-monotonic solitary wave trailing edge connected to a modulated nonlinear periodic wavetrain. The modulated periodic wavetrain is terminated at the TDSW leading edge by a dispersively regularized envelope rarefaction wave—a partial DSW. The trailing wavetrain is identified numerically as a genuine traveling wave solution of the Kawahara equation which has a velocity determined by the traveling wave boundary conditions, and its velocity identified as a generalized Rankine-Hugoniot condition which is described in greater detail using the methods presented in Chapter 5.

Convex dispersion ($\sigma = -1$) is considered in Section 4.1.5 where we observe a classical KdV-like DSW. We apply DSW fitting theory [45] in order to determine the amplitude and speed of the trailing solitary wave and the wavenumber at the leading edge as a function of the initial jump height. For sufficiently large jump heights, fifth order dispersion dominates third order dispersion and a TDSW again emerges.

4.1 Dispersive shock waves in the Kawahara equation

We now study the structure of DSWs arising from the initial data (4.1) using a modification of that used to solve the modified KdV-Burgers equation [44]. The numerical method

is outlined in detail in Sec. 4.1.1.

We begin our investigation of Kawahara DSWs with the non-convex dispersion case $\sigma = +1$. The dynamics can be grouped into three qualitatively distinct regimes, loosely characterized by the dispersion relation and soliton solutions. These regimes are identified in Fig. 4.1 along with representative numerical solutions. Small to large jump heights generate waves with predominantly small to large wavenumbers, respectively. The regime of negative dispersion curvature for small k can be associated with elevation solitary waves embedded in the linear spectrum, hence naturally appear as a constituent part of radiating DSWs. Oscillatory, depression solitary waves coincide with the non-convex dispersion and are associated with traveling DSWs. The crossover regime straddles the dispersion inflection point and the solitary wave band gap, in which no localized solitary waves exist (see the discussion in Sec 2.2.1).

We now conduct a more thorough analysis of the large amplitude regime and the generation of non-classical traveling DSWs.

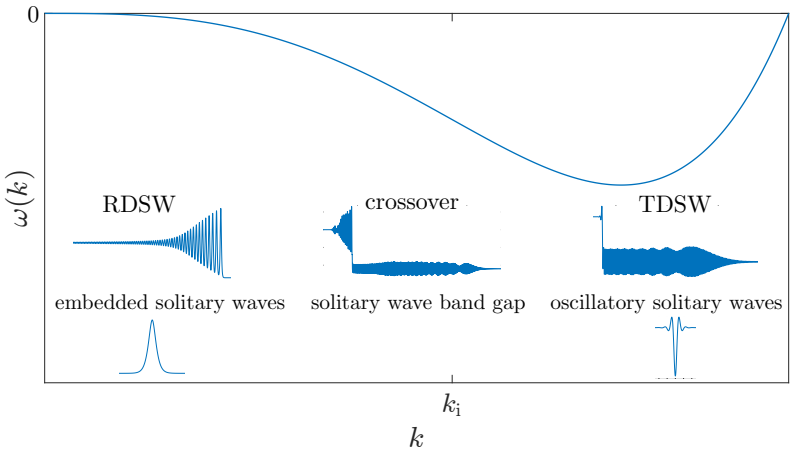

Figure 4.1: Non-convex Kawahara dispersion relation for $\sigma = +1$ along with example numerical simulations for step initial data. The RDSW, crossover regime, and TDSW can be identified with properties of the dispersion curvature and the existence of solitary wave structures.

4.1.1 Numerical evolution of step-like initial data

Here we outline the numerical method to integrate the smoothed, step-like initial value problem (4.1). We implement a pseudospectral spatial discretization by differentiating the equation and initial data (4.1) with respect to x. Let $v = \frac{\partial u}{\partial x}$, so that v satisfies the initial value problem

$$v_t + (uv)_x + \sigma v_{xxx} + v_{xxxxx} = 0, \quad v(x,0) = -\frac{\Delta}{2w}\text{sech}^2\left(\frac{x}{w}\right) \tag{4.2}$$

The rapid decay of v initially allows us to take the Fourier transform of the above equation to obtain

$$\hat{v}_t + ik\widehat{(uv)} + \omega(k)\hat{v} = 0. \tag{4.3}$$

Numerically, v is represented by its Fourier series on the computational domain $x \in [-L, L]$ by

$$v(x,t) = \sum_n \hat{v}_n(t) e^{\frac{in\pi}{L}x}, \tag{4.4}$$

where $\hat{v}_n(t) = \hat{v}\left(\frac{\pi n}{L}, t\right)$.

We solve (4.3) by inserting the Fourier series (4.4) and time-step with an integrating factor fourth order Runge-Kutta (RK4) scheme [127]. We recover the solution, u, at each time step via

$$u(x,t) = \sum_{n\neq 0} \frac{L}{in\pi}\hat{v}_n e^{\frac{in\pi}{L}x} - \frac{1}{2L}\int_{-L}^{L} xv(x,t)dx + (x+L)\frac{\Delta}{2L} + u_l, \tag{4.5}$$

where the integral can be computed with spectral accuracy via the trapezoidal rule due to the rapid decay of v.

Long time numerical simulations reported in the subsequent sections are performed on a spatial domain of length $L = 5 \times 10^3$ and$N = 2^{14}$ Fourier modes. The initial data width ranges from $w = 1$ to $w = 10$. The center of the step may be chosen to minimize wave–boundary interactions. The fast propagation of small amplitude dispersive waves due

to fifth order dispersion necessitate such a large computational domain. Various aspects of the approximate solutions were tested in order to ensure robustness of the numerical method as well as accuracy of the solution. In particular, all solutions reported exhibit boundary deviations less than 10^{-3}. The Fourier coefficients of v all decay to 10^{-10} or less in normalized amplitude and the mass satisfies the conservation property

$$\int_{-L}^{L} u(x,t)dx - \int_{-} L^{L}u(x,0)dx = -\frac{t\Delta^2}{2},$$

maintained below a relative error of 10^{-3}, which is only approached for long times $t = O(100)$ as a result of the small amplitude oscillations at the boundaries. Typical simulations presented in this section maintained a relative error below 10^{-4}.

4.1.2 Non-convex dispersion with large jumps: TDSWs

If the amplitude of the initial step Δ is sufficiently large, the long term evolution gives rise to a non-classical traveling DSW. The crossover to this large jump regime from jumps of modest amplitude will be made more precise in Section 4.1.4. Figure 4.2 is a simulation with initial jump $\Delta = 1$. We observe a sharp, non-monotonic transition from a constant to a nearly periodic wavetrain. The wavetrain exhibits some envelope modulations that eventually terminate at the leading edge with small amplitude oscillations. This coherent wavetrain is the TDSW. We begin our analysis by verifying two DSW-like properties of the dynamics:

(1) a near solitary wave trailing edge

(2) a harmonic wave leading edge.

First, we plot the amplitude-speed relations for both the trailing edge of TDSWs with varying $\Delta > 0$, extracted from numerical simulations, and Kawahara solitary waves in Figure 4.3(a) that exhibit good agreement. Furthermore, in 4.3(b), we overlay a Kawahara depression solitary wave with the same speed as the TDSW trailing edge (cf. the lower

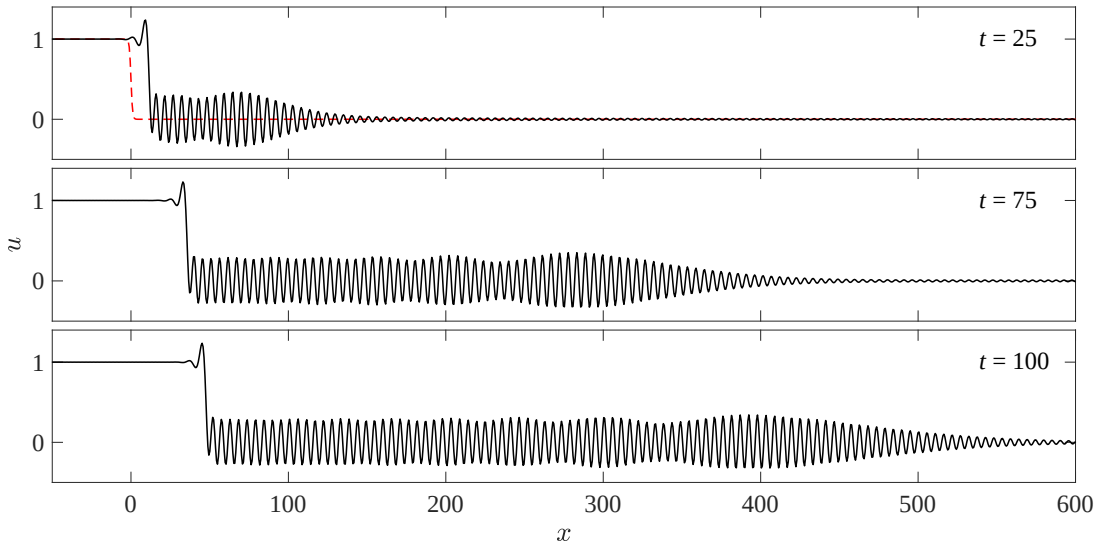

Figure 4.2: Kawahara traveling DSW resulting from the initial step $\Delta = 1$ for the non-convex case $\sigma = +1$. Initial data is shown in the top figure with the dashed curve.

branch of solitary waves computed in Fig. 2.2). A portion of the solitary wave correctly captures the non-monotonic structure of the rapid transition.

Next, we numerically extract the leading edge wavenumber from numerical simulations. We extract the leading edge wavenumber by averaging the wavenumbers extracted from ten peaks above a specified small amplitude threshold of $\frac{\Delta}{10}$. The leading edge velocity is also numerically extracted and compared with the linear wave group velocity evaluated at k_+. We observe excellent agreement between solitary waves and the leading edge group velocity, which is shown in Fig. 4.4.

These two numerical observations lend support to the identification of the TDSW solitary and harmonic wave edges, typical of classical DSWs [47]. But that is where the analogy ends. As we will now show, the TDSW exhibits unique, non-classical features.

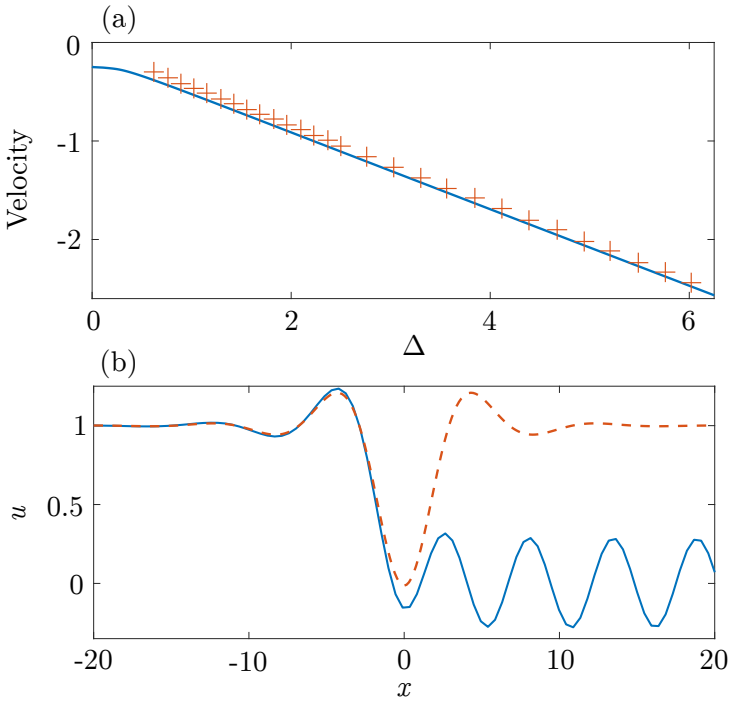

Figure 4.3: Trailing edge comparison with Kawahara ($\sigma = +1$) solitary waves. (a) Computed TDSW (pluses) and solitary wave (solid) amplitude-speed relations. (b) Overlay of solitary wave on TDSW leading edge with $\Delta = 1$.

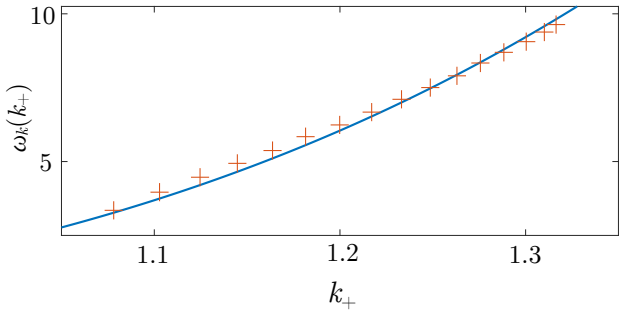

Figure 4.4: (+) Comparison of TDSW harmonic leading edge speed extracted from numerical simulations with the linear group velocity (solid).

4.1.2.1 TDSW trailing edge traveling wave

Further scrutiny of the trailing edge shows what appears to be the development of a nonlinear, periodic wavetrain co-propagating with the partial, trailing solitary wave. A zoom of the trailing wave is shown in Fig. 4.5. We take multiple approaches to determining this traveling wave:

(1) Assume the leading periodic wave has zero mean ($\overline{u} = 0$) and approximate the periodic wave by a Stokes wave (2.40).

(2) Assuming $\overline{u} = 0$ and numerically compute a traveling wave satisfying the requisite boundary conditions.

(3) Obtain the whole TDSW as a shock-rarefaction solution of the Kawahara-Whitham equations (3.9)–(3.11) in the weakly nonlinear regime.

We study the first two options here while the third option is addressed in Chapter 6. A more exhaustive study of the TDSW is performed for the KdV5 equation (1.4) in Chapters 5 and 6.

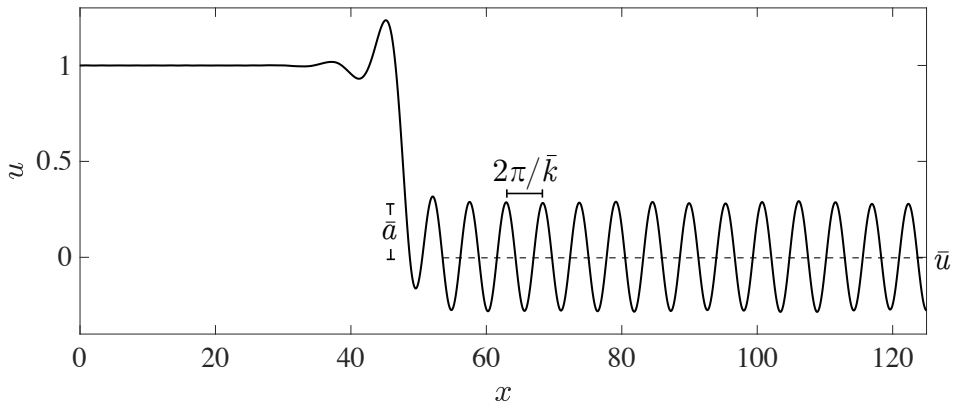

Figure 4.5: Trailing edge of the TDSW evolving from the GP problem (4.1) with $\Delta = 1$ at $t = 100$. The parameters of the nonlinearly resonant periodic wave are identified: mean $\overline{u}$, amplitude $\bar{a}$ and wavenumber $\bar{k}$.

The approximately periodic wavetrain oscillates about a mean value that is approximately 0. This suggests seeking a one-parameter family of Kawahara traveling waves $u(x,t) = f(\xi)$, $\xi = x - ct$ that satisfy the traveling wave ODE (1.10). subject to the boundary conditions (BCs)

$$\text{equilibrium BCs:} \quad \left\{ \lim_{\xi \to -\infty} f(\xi) = f'(\xi) = f''(\xi) = f'''(\xi) = f''''(\xi) = 0, \right. \tag{4.6}$$

$$\text{periodic orbit BC:} \quad \begin{cases} \lim\limits_{\xi \to \infty} |f(\xi) - F(\xi)| \to 0, \quad F(\xi + P) = F(\xi), \quad \xi \in \mathbb{R}, \\ \qquad\qquad\qquad\qquad \dfrac{1}{P}\displaystyle\int_0^P F(\xi) d\xi = 0, \end{cases} \tag{4.7}$$

where $P = \frac{2\pi}{k}$ is the wavetrain's period. Inserting the traveling wave ansatz into the Kawahara equation (1.3), we can integrate once and apply the boundary conditions at $\xi \to -\infty$ to obtain the same fourth order ODE (1.10) obtained for the computation of solitary and periodic waves in Chapter 2 where the integration constant A is determined by the enforcing the equilibrium boundary condition (4.6)

$$-cf + \frac{1}{2}f^2 + f'' + f^{(4)} = -c\Delta + \frac{\Delta^2}{2}. \tag{4.8}$$

The traveling wave has two free parameters c and P that should be parameterized by the initial jump height Δ. One relation is the zero mean requirement in (4.7). Another relation is obtained by integrating (4.8) again and applying the boundary conditions (4.6) to obtain the **zero energy integral**

$$-\frac{c}{2}f^2 + \frac{1}{6}f^3 + \frac{\sigma}{2}(f')^2 + f'f''' - \frac{1}{2}(f'')^2 = \left(\frac{\Delta}{2} - c\right)\Delta f - \frac{\Delta^3}{3}. \tag{4.9}$$

To determine the periodic orbit $F(\xi)$, we begin with an approximate, weakly nonlinear calculation. We consider a small amplitude $0 < \bar{a} \ll 1$ expansion of F and c as in the classical Stokes expansion [140]

$$F(\xi) = F_0(\theta) + \bar{a}F_1(\theta) + \bar{a}^2F_2(\theta) + \cdots, \quad \theta = \bar{k}\xi,$$

$$c = c_0 + \bar{a}^2 c_2 + \cdots,$$

where $\bar{k} = 2\pi/P$ is the wavenumber of the periodic orbit. Inserting the expansion into (4.8) and carrying out a standard perturbation calculation, we find

$$F = F_0 + \bar{a}\cos\theta + \bar{a}^2\left(2c_2 + \frac{1}{2(\Delta - F_0)} - \frac{1}{2(\Delta - F_0) - 16\bar{k}^2 + 64\bar{k}^4}\cos(2k\xi)\right) + o(\bar{a}^2) \tag{4.10}$$

$$c = \frac{F_0 + \Delta}{2} + \bar{a}^2 c_2 + o(\bar{a}^2) \tag{4.11}$$

$$\bar{k}^2 = \frac{1 + \sqrt{1 - 2F_0}}{2} \tag{4.12}$$

where

$$c_2 = \frac{1}{4}\left(\frac{1}{F_0 - \Delta - 8k^2 + 32k^4} + \frac{2}{F_0 - \Delta}\right), \tag{4.13}$$

and F_0 is a constant to be determined.

The zero mean requirement for the periodic orbit (4.7) applied to (4.10) yields

$$F_0 + a^2\left(2c_2 - \frac{1}{2(\Delta - F_0)}\right) = 0. \tag{4.14}$$

To account for the $\mathcal{O}(\bar{a}^2)$ terms in the mean, the background F_0 is expanded in the parameter $\bar{a}$ in the form $F_0 = F_{0,0} + \bar{a}^2 F_{0,2} + o(\bar{a}^2)$. Substitution of the asymptotic expansion yields

$$F_0 = a^2\left(\frac{1}{2\Delta} - 2c_2\right) \tag{4.15}$$

effectively canceling the $\mathcal{O}(\bar{a}^2)$ mean terms in (4.10). The only remaining free parameter is the wave amplitude $\bar{a}$, which can be approximated by inserting the expansion (4.10) into the zero energy estimate (4.9) and evaluating at a wave maximum, which yields

$$\bar{a} = \frac{\Delta^{3/2}}{\sqrt{3 + \frac{9\Delta}{2} + 3\sqrt{2\Delta + 1}}}. \tag{4.16}$$

Combining (4.15), (4.13), (4.12). and (4.11), we obtain an amplitude correction to the speed of the traveling wave

$$c = \frac{\Delta}{2} + \frac{\bar{a}^2}{4\Delta}, \tag{4.17}$$

and the square wavenumber of the wavetrain at leading order is given by

$$\bar{k}^2 = \frac{1+\sqrt{1+2\Delta}}{2}. \tag{4.18}$$

The accuracy of the approximate solutions is verified by directly computing zero mean, zero energy periodic orbits satisfying eqs. (4.8) and (4.9) using Matlab's boundary value solver bvp5c. Figure 4.6 shows the estimated and computed parameters c, $\bar{a}$, and $\bar{k}$ for zero mean periodic solutions. Good agreement is obtained for all values of Δ for which the traveling wave solutions were calculated.

We have shown the following. If a Kawahara traveling wave satisfying the BCs (4.6) and (4.7) exists, its velocity c is determined by the boundary conditions and, in particular, the jump height Δ. The first term in the velocity expansion $c_0 = \Delta/2$ is the Rankine-Hugoniot jump condition for classical shock waves. Therefore, we identify the traveling wave velocity c in (4.17) as a *generalized Rankine-Hugoniot condition* (gRH).

We now directly compute traveling waves satisfying the BCs (4.6), (4.7) and the zero energy integral (4.9). For a given jump height Δ and an associated zero mean far-field periodic solution $f(\xi)$, we compute solutions of the fourth order equation (4.8) with the four boundary conditions

$$f(0) = f'(0) = 0, \quad f(L) = f(0), \quad f''(L)^2 = -cf(L)^2 + \frac{1}{3}f(L)^3, \tag{4.19}$$

where L is sufficiently large so that the periodic orbit BC $F(\xi)$ has been reached. The third condition in (4.19) evaluates the periodic orbit at a maximum. The fourth condition evaluates the zero energy integral (4.15) at a maximum. We use Matlab's collocation method bvp5c with an initial guess extracted from the numerical simulation depicted in 4.2 that is then used to perform continuation to other values of Δ. The traveling wave velocity c is a parameter determined as part of the traveling wave computation.

The computed traveling wave solution for $\Delta = 1$ is superimposed on the TDSW determined by long-time integration of the GP problem, also for $\Delta = 1$, in Figure 4.7(a).

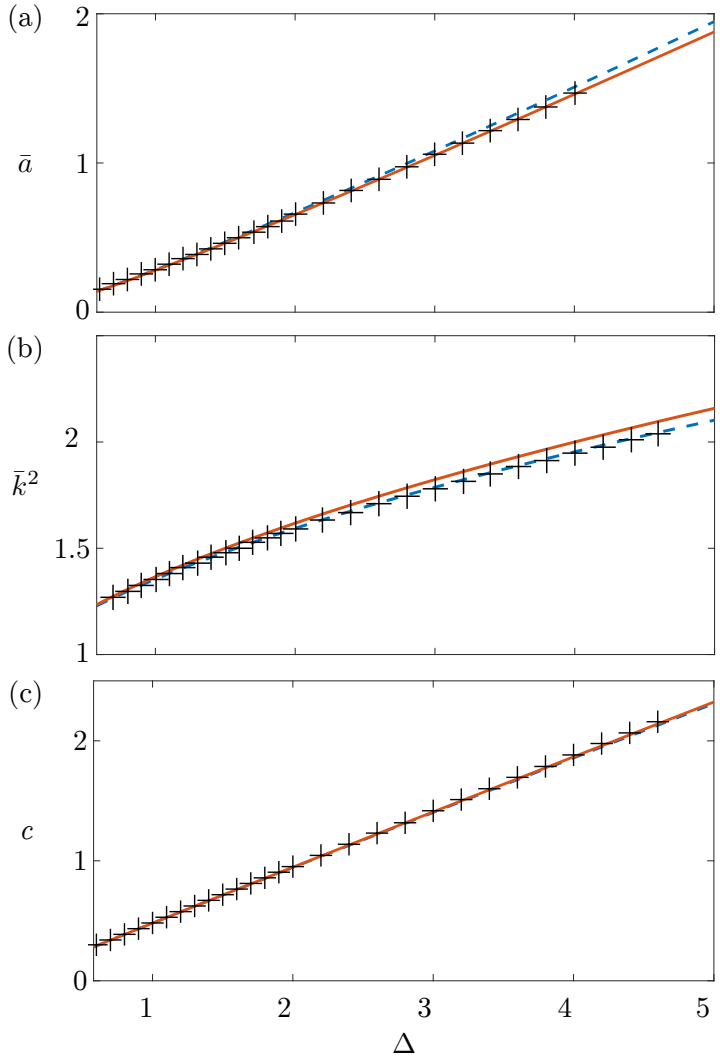

Figure 4.6: Comparisons of asymptotic predictions of nonlinear wavetrain features: (a) the amplitude of the nonlinear wavetrain, (b) the square of the wavenumber of the nonlinear wavetrain, and (c) the speed of the traveling wave. All figures compare values from computed traveling wave solutions (solid), asymptotic predictions (dashed), and data extracted from numerical simulations of the GP problem (pluses).

Sufficiently near the TDSW trailing edge, the two solutions are nearly indistinguishable. Figure 4.7(b) shows an absolute difference of at most 10^{-3} between these two solutions. This demonstrates that the TDSW trailing edge rapidly approaches a traveling wave, hence the terminology **traveling** DSW. The traveling wave at the trailing edge will be discussed in greater detail as it is described as a shock solution of the Whitham modulation equations in

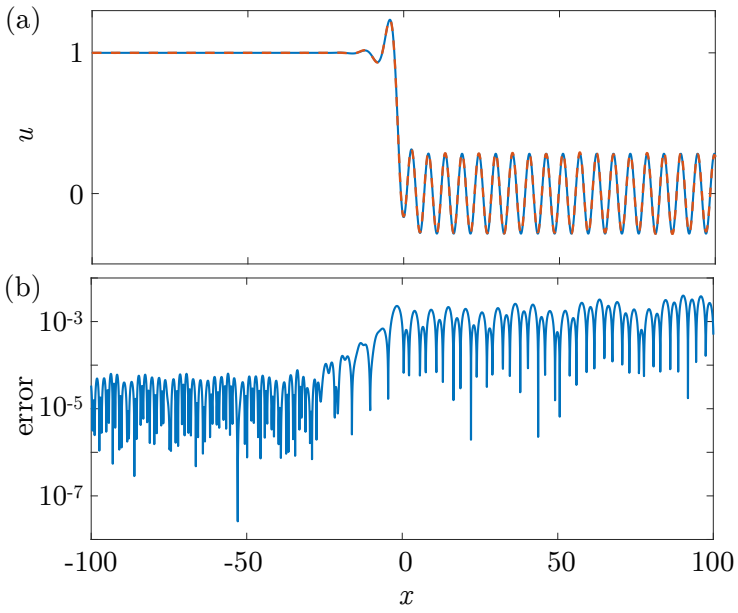

Figure 4.7: (a) Superimposed traveling wave solution to the dynamical system (4.8) with boundary conditions (4.19) (solid) on a TDSW computed from the GP problem with $\Delta = 1$ (dashed) at $t = 150$. (b) Absolute error between the two solutions.

Chapters 5 and 6 for the Kawahara (1.3) and KdV5 (1.4) equations.

We further examine properties of the TDSW by comparing the numerically extracted trailing edge velocity of the TDSW and the speed of the computed traveling wave, c, in Figure 4.6(c). We also compare the amplitude of the TDSW trailing edge wavetrain to the amplitude of the computed nonlinear wavetrain in the traveling wave $\bar{a}$ in Fig. 4.6(a). Both properties agree over a wide range of Δ.

Our traveling wave computations suggest that the solution is a heteroclinic connection between the equilibrium $f = \Delta$ and the mean 0 periodic orbit $f = F(\xi)$. We are able to accurately compute such solutions for $\Delta > \Delta_{\text{cr}} \approx 0.58$, suggesting a threshold for their existence. Such a threshold is consistent with the speed requirement $c < \Delta - \frac{1}{4}$ for non-monotonic Kawahara solitary waves (cf. Fig. 2.2), of which the TDSW trailing edge is approximately composed. We will examine the relationship between Δ_{cr} and the crossover to the TDSW regime in Section 4.1.4.

4.1.3 Non-convex dispersion with small jumps: RDSWs

We now consider the non-convex case of eq. (1.3) ($\sigma = +1$) in the small jump regime, $0 < \Delta \ll 1$. Introducing the scaling

$$u = \Delta U, \quad X = \Delta^{1/2} x, \quad T = \Delta^{3/2} t, \tag{4.20}$$

into Eq. (1.3) results in a perturbed KdV equation

$$U_T + U U_X + U_{XXX} = -\Delta U_{XXXXX}. \tag{4.21}$$

In the scaled variables (4.20), the initial conditions (4.1) become

$$U(X, 0) = \frac{1}{2}\left(1 - \tanh\left(\frac{X}{w}\right)\right), \tag{4.22}$$

Numerically, we evolve the scaled equation (4.21) subject to (4.22) but report the results for the unscaled field $u(x, t)$ through (4.20). Numerical results are shown in Fig. 4.8. Sufficiently small jumps lead to KdV-like, classical DSWs as Fig. 4.8(a) with $\Delta = 0.06$ attests. In this long-wave regime, the Kawahara linear dispersion relation is essentially concave with negative curvature so that the resulting DSWs exhibit positive polarity and orientation. The DSW leading edge is well approximated by an elevation Kawahara solitary wave as shown in 4.8(c). However, due to the embedding of the elevation solitary waves in the continuous spectrum [126, 14], the solitary wave emits small amplitude radiation ahead of the shock, a phenomenon demonstrated in Fig. 4.8(b). This DSW resonant radiation has also been observed in NLS-type models [31, 48, 10], so we introduce the nomenclature *radiating* DSW (RDSW) to describe this phenomenon.

For the analysis of RDSWs, we apply El's DSW fitting method [45] (see also [47]), which assumes the existence of a 2-wave solution of the Kawahara-Whitham modulation equations connecting a vanishing amplitude wave to a zero wavenumber wave. Under these conditions, the method yields the leading and trailing edge speeds as functions of the jump Δ. Additional macroscopic DSW properties that can be obtained are the solitary wave edge

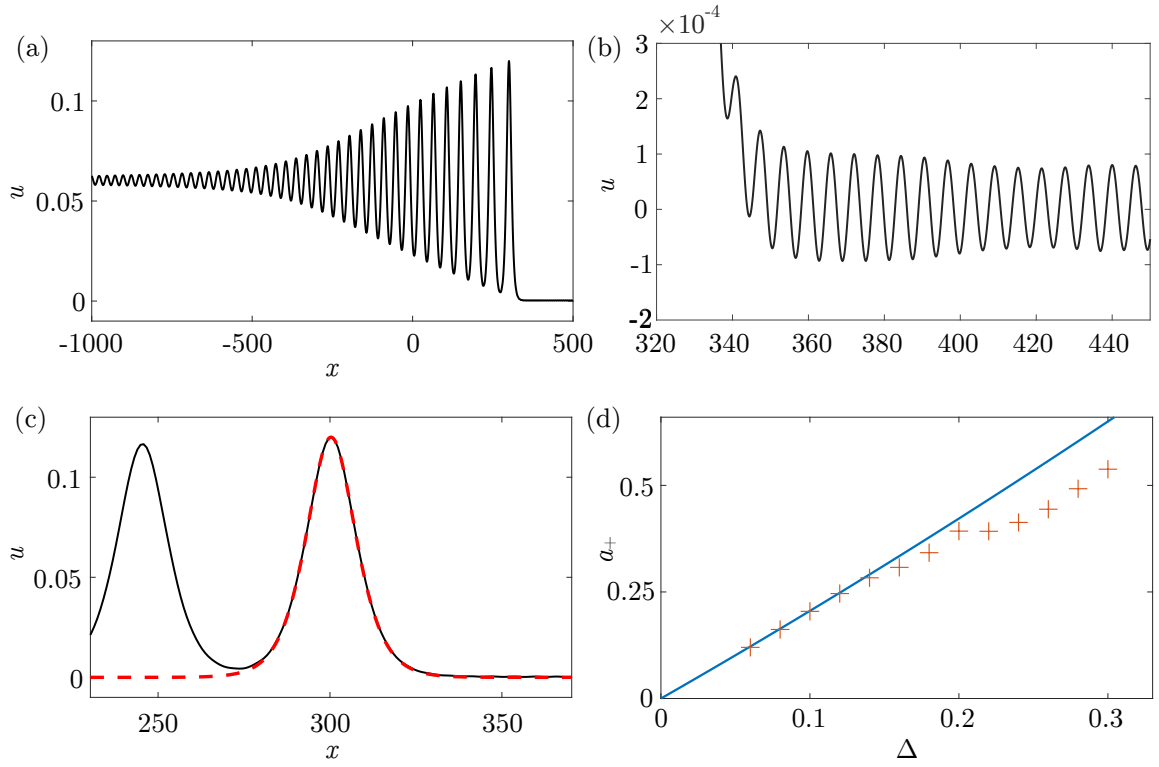

Figure 4.8: Numerically computed Kawahara radiating DSWs in the small jump regime. (a) The solution at $t \approx 8573$ for jump $\Delta = 0.06$. The radiation is not visible due to its small amplitude. (b) Zoomed in view of radiation for RDSW in panel (a). (c) RDSW leading edge from (a) with an overlay of a numerically computed Kawahara solitary wave of the same speed. (d) Comparison of the leading edge amplitude a_+ versus Δ incorporating predictions from Kawahara DSW fitting (solid) and extracted values from numerical simulations (pluses).

amplitude and the harmonic wave edge characteristic wavenumber. The fitting method can be carried out with knowledge of only the linear dispersion relation and the solitary wave amplitude-speed relation, both of which we know exactly or approximately. We note that the underlying assumptions for the validity of the DSW fitting method require additional considerations, which we do not fully explore here. Rather, we apply the method and compare the results with our numerical simulations.

The RDSW trailing edge wavenumber k_- is characterized by a simple wave solution of the Whitham modulation equations. This wavenumber can be determined from the solution

of the ODE

$$\frac{dk}{d\bar{u}} = \frac{\omega_{\bar{u}}}{\bar{u} - \omega_k} = \frac{1}{3k - 5k^3}, \quad k(0) = 0, \tag{4.23}$$

where

$$\omega = \overline{u}k - k^3 + k^5,$$

is the Kawahara linear dispersion relation. The modulation variable $\bar{u}$ corresponds to the period-mean of the modulated periodic traveling wave and the boundary condition $k(0) = 0$ is due to the vanishing of the modulation wavenumber at the RDSW solitary wave edge where $\bar{u} = \Delta$. The ODE (4.23) can be directly integrated, yielding

$$k(\bar{u})^2 = \frac{3 - \sqrt{9 - 20\bar{u}}}{5}. \tag{4.24}$$

The RDSW trailing edge wavenumber is determined by evaluating (4.24) at the RDSW trailing edge where $\bar{u} = 0$

$$k_- = k(\Delta) = \left(\frac{3 - \sqrt{9 - 20\Delta}}{5}\right)^{1/2} = \left(\frac{2\Delta}{3}\right)^{1/2} + \frac{5\Delta^{3/2}}{9\sqrt{6}} + \mathcal{O}(\Delta^{5/2}). \tag{4.25}$$

Reflecting the harmonic wave nature of the trailing edge, its velocity s_- is then determined by evaluating the Kawahara linear group velocity at the trailing edge

$$s_- = \frac{\partial \omega}{\partial k}(k_-, \Delta) = -2\Delta + \frac{(3 - \sqrt{9 - 20\Delta})^2}{10} = -2\Delta + \frac{10}{9}\Delta^2 + \mathcal{O}(\Delta^3). \tag{4.26}$$

There are several "barriers" to the DSW fitting analysis that constrain the admissible values of Δ [47]. The first barrier occurs at an extremum of the trailing edge speed as a function of jump height. The minimum of $s_-(\Delta)$ occurs when $\Delta = \Delta_{\mathrm{i}} = 27/80 \approx 0.34$. At this value of Δ, the trailing edge wavenumber $k_- = \sqrt{3/10}$ is precisely the zero dispersion point k_{i}. We cannot expect the DSW fitting method to accurately describe RDSWs for $\Delta > \Delta_{\mathrm{i}}$. In another model equation with non-convex dispersion, crossing this barrier led to DSW implosion [91]. Note that the jump height $\Delta = 9/20$, above which k_- becomes complex-valued in Eq. (4.25), exceeds the barrier Δ_{i}.

The second barrier occurs when the hyperbolic Whitham modulation system loses genuine nonlinearity at a linearly degenerate point. This barrier can be identified at the RDSW harmonic wave edge by finding the zero of $\omega_{k\bar{u}}(\bar{u}-\omega_k)+\omega_{kk}\omega_{\bar{u}}$ [47], which occurs at the jump height $\Delta = \Delta_{\mathrm{l}} = 1/4$. This second barrier occurs at a smaller jump height than the first. This sets an upper bound on the applicability of the DSW fitting method to $\Delta < 1/4$.

The speed at the DSW leading edge is calculated in a similar manner by first introducing conjugate variables $\tilde{k}$, and $\tilde{\omega}(\tilde{k},\bar{u}) = -i\omega(i\tilde{k},\bar{u})$, where $\tilde{k}$ acts as an amplitude parameter and $\tilde{\omega}$ is a "solitary wave dispersion relation". One now solves the ODE

$$\frac{d\tilde{k}}{d\bar{u}} = \frac{\tilde{\omega}_{\bar{u}}}{\bar{u}-\tilde{\omega}_{\tilde{k}}} = -\frac{1}{3\tilde{k}+5\tilde{k}^3}, \quad \tilde{k}(\Delta) = 0. \tag{4.27}$$

Integrating and evaluating the conjugate wavenumber at the solitary wave leading edge yields $\tilde{k}_+^2 = \tilde{k}(0)^2 = \frac{-3+\sqrt{9+20\Delta}}{5}$. The DSW leading edge speed s_+ is the conjugate phase velocity evaluated at the leading edge

$$\begin{aligned} s_+ &= \frac{\tilde{\omega}(\tilde{k}_+,0)}{\tilde{k}_-} = \frac{3}{25}+\frac{4}{5}\Delta-\frac{1}{25}\sqrt{9+20\Delta} \\ &= \frac{2}{3}\Delta+\frac{2}{27}\Delta^2+\mathcal{O}(\Delta^3). \end{aligned} \tag{4.28}$$

Utilizing the approximate Kawahara solitary wave amplitude-speed relation Eq. (2.39), we can obtain an estimate for the solitary wave edge amplitude a_+ by equating $s_+ = c(a_+)$ from Eq. (2.39) which gives the amplitude of the leading edge

$$a_+ = 2\Delta+\frac{5}{9}\Delta^2+\mathcal{O}(\Delta^3). \tag{4.29}$$

The leading solitary wave amplitude prediction from DSW fitting, Eq. (4.29), and the amplitude observed in numerical simulations are compared in Fig. 4.8. We observe good agreement with the DSW fitting result and numerical simulation for jump heights up to approximately $\Delta = 0.2$.

We note that all of the small Δ asymptotics in Eqs. (4.25), (4.26), (4.28), and (4.29) of the RDSW agree with the results for KdV at leading order in Δ [57]. However, the RDSW

exhibits an additional, radiative component. Using the RDSW analysis, we can estimate some of the properties of the forward, short-wave radiation. The resonance condition

$$s_+ = \frac{\omega(k_\mathrm{r}, 0)}{k_\mathrm{r}} = -k_\mathrm{r}^2 + k_\mathrm{r}^4, \tag{4.30}$$

equates the RDSW leading edge solitary wave speed (4.30) with the phase speed of linear waves, thus determining the resonant wavenumber k_r

$$\begin{aligned} k_\mathrm{r}^2 &= \frac{1}{2} + \frac{1}{10}\left(37 + 80\Delta - 4\sqrt{9 + 20\Delta}\right)^{1/2} \\ &= 1 + \frac{2}{3}\Delta + \mathcal{O}(\Delta^2). \end{aligned} \tag{4.31}$$

Because k_r exceeds the linear dispersion inflection point $k_\mathrm{i} = \sqrt{3/10}$, resonant radiation corresponds to the positive dispersion regime.

Pomeau et al. [111] and Benilov et al. [14] provide an asymptotic estimate for the amplitude a_r of the radiation from an unstable Kawahara solitary wave. Because a lone solitary wave decays due to this linear resonance, the amplitude a_r was found to be a time-dependent quantity. However, the RDSW leading edge approximate solitary wave is sustained so, using the results of [111, 14], we estimate the radiation amplitude

$$a_\mathrm{r} \sim K \exp\left(-\frac{3\pi}{2\sqrt{\Delta}}\right), \tag{4.32}$$

where $K \approx 752.85$ is a numerical constant. Figure 4.9 compares the numerically extracted RDSW radiation wavenumber k_r and amplitude a_r with the predictions of Eqs. (4.31) and (4.32). Due to fast dispersive propagation to the boundary, it becomes exceedingly difficult to numerically resolve the exponentially small radiation amplitude a_r for small Δ, likely the cause of the discrepancy in Fig. 4.9(b). This shows, and has been noted previously [48], that a DSW provides a means to effectively sustain a Kawahara solitary wave–which would otherwise decay due to linear resonance [14]–as part of a DSW. As Fig. 4.8(d) reveals, the RDSW leading edge amplitude closely follows the prediction in Eq. (4.29) until the jump exceeds about 0.2. One possible explanation for this could be the apparent loss of genuine

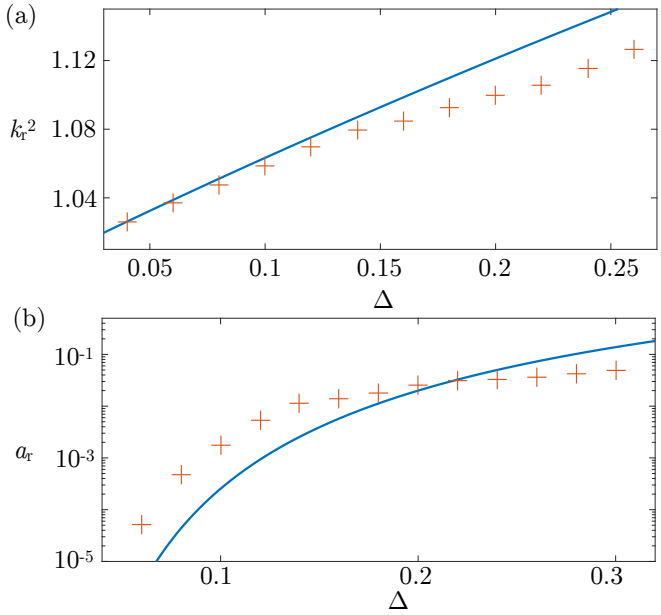

Figure 4.9: Comparison of amplitude of the radiation in the small amplitude RDSW with Analytical prediction from (4.32) (solid) and extracted values from numerical simulations (pluses).

nonlinearity in the Whitham equations when $\Delta > \Delta_l = 1/4$. At larger jumps, the RDSW solitary wave edge no longer resembles a Kawahara solitary elevation wave solution, but begins to share qualities with TDSWs. The dynamics begin to lose the rank ordered structure that is characteristic of classical DSWs. We now analyze the intermediate, crossover regime where the DSW structure gradually transitions from RDSWs to TDSWs.

4.1.4 Non-convex dispersion with intermediate jumps: crossover regime

As the magnitude of the jump initial data increases, the RDSW begins to lose KdV-like characteristics while gaining features of a TDSW. This transition between the RDSW with positive polarity and orientation (small jumps) and the TDSW with negative polarity and orientation (large jumps) occurs gradually as Δ is increased in magnitude. The evolution of the step-like initial value problem in Figure 4.10 is representative of the evolution of smooth step-like initial data in this intermediate, crossover regime with $\Delta = 0.3$ and displays

significant backward radiation adjacent to a recessed, large amplitude, oscillatory region. The structure of the oscillatory region exhibits slower amplitude decay and more of an amplitude separation from the leading edge than that of the smaller jump depicted in Fig. 4.8(a). The DSWs for values of Δ in this region are qualitatively characterized by this remnant of a small amplitude RDSW with positive polarity and orientation with superimposed small amplitude waves that imply incoherence. Such incoherence results in wave mixing that eliminates the rank-ordered structure of the RDSWs that occur for smaller jumps. The largest amplitude elevation wave does not appear to resemble any of the Kawahara solitary waves we have computed in Fig. 2.2 and waves propagate both ahead of and behind the peak. Just as we identify the leading edge of RDSWs resulting from small jumps with elevation solitary waves in Fig. 2.2 ($c > 0$) and the TDSW trailing edge for large jumps with non-monotonic elevation solitary waves ($c < \Delta - 1/4$), we interpret the intermediate jump transition region as corresponding to the solitary wave "band gap" for $-1/4 < c < 0$ in Fig. 2.2. For velocities in the band gap, solitary waves do not exist. However, we can compute periodic traveling waves in this region so a modulation description may be possible, but we do not pursue this further here. Rather, we seek to identify when the backward radiation on $u = \Delta$ emanating from the transition to $u = 0$ ceases, signifying the onset of the steady TDSW.

If these backward radiating waves were, in fact, linear then they could persist whenever the linear phase velocity on background Δ coincides with the edge speed, otherwise we expect a TDSW. The linear phase velocity $v_{\rm ph} = \omega(k, \Delta)/k = \Delta - k^2 + k^4$ attains a minimum value of $\Delta - 1/4$ precisely when the phase and group velocities coincide at $k = 1/\sqrt{2}$ and when the non-monotonic Kawahara solitary waves appear (cf. Fig. 2.2). Equating the minimum of $v_{\rm ph}$ to the TDSW leading order gRH (4.17), $c = \Delta/2$ gives the critical jump height $\Delta_{\rm cr} \sim \frac{1}{2}$, above which linear waves cannot propagate behind the TDSW. However, the numerical simulations show that waves continue to propagate backward even when $\Delta = 1/2$. Our numerical simulations have shown that this phenomenon persists up to jumps of $\Delta \approx 0.6$. Although close to the theoretical prediction, we argue that the true threshold criterion is

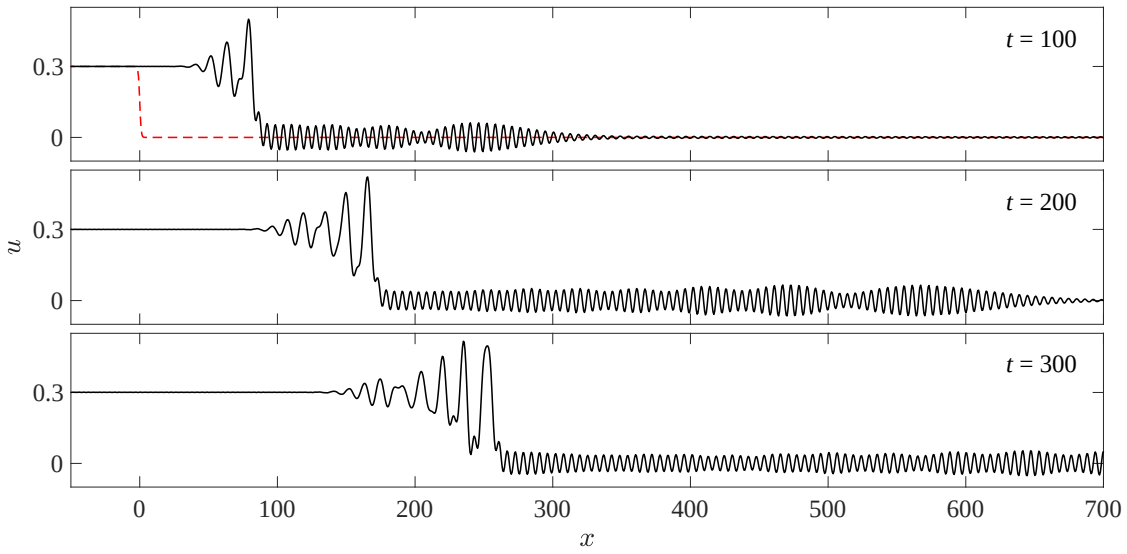

Figure 4.10: Crossover Kawahara DSW dynamics for the intermediate jump value $\Delta = 0.3$ with $\sigma = +1$. Initial data is the dashed curve.

the existence of the TDSW traveling wave. We found in Section 4.1.2.1 that we could no longer compute TDSWs for Δ below 0.58, very close to the observed transition to TDSWs at $\Delta = 0.6$. Therefore, the TDSW is a *threshold* phenomenon, only existing for $\Delta > \Delta_{\rm cr}$. For $\Delta < \Delta_{\rm cr}$, either a perturbed, classical DSWs are generated as in Section 4.1.3 (when $\Delta \lesssim 0.2$ from Fig. 4.8(d)) or a crossover, oscillatory state lacking a well-defined solitary wave edge is generated.

4.1.5 Convex dispersion

In the case where the sign of the third order term is negative ($\sigma = -1$), the Kawahara dispersion relation is a purely convex function of k. These are "convex dispersive hydrodynamics" so we may expect KdV-like DSWs. In this case, there are no linear resonances so that RDSW and the crossover regimes are not expected.

The numerical simulation shown in Fig. 4.11 depicts the temporal evolution of the GP-Riemann problem (4.1) for the Kawahara equation. This figure portrays the temporal

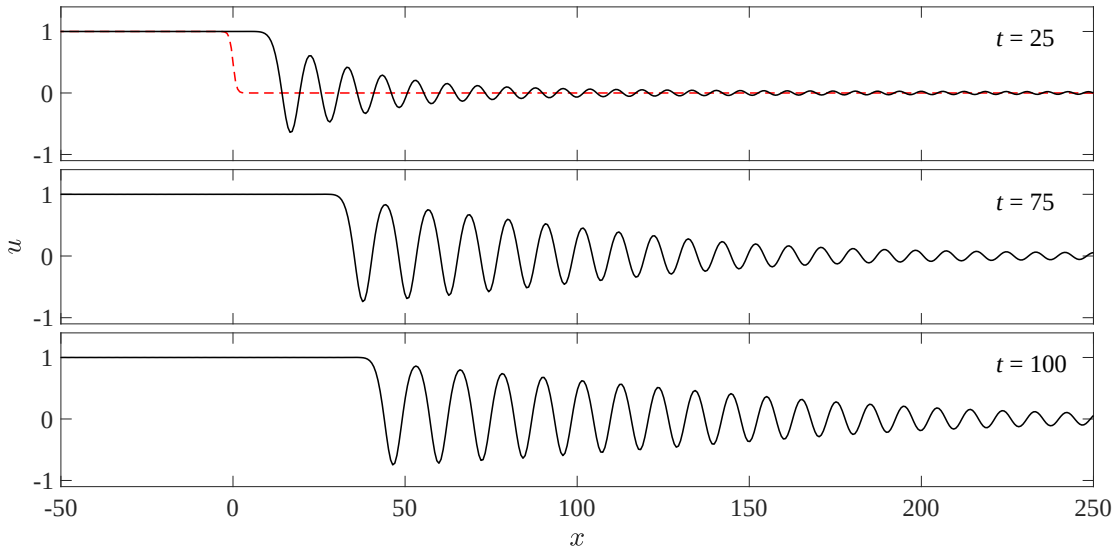

Figure 4.11: Development of a classical Kawahara DSW with initial jump $\Delta = 1$ and convex dispersion $\sigma = -1$. Approximate initial data is shown in the top figure with the dashed curve.

development of a DSW that is qualitatively similar to the classical KdV DSW. The addition of the fifth order term in Eq. (1.3) serves as a perturbation to the KdV equation that, in contrast to the non-convex case $\sigma = +1$, does not appear to qualitatively change the dynamics. The DSW trailing edge behaves like a solitary wave solution of the Kawahara equation as shown by Fig. 4.12(a) where the DSW trailing edge speed-amplitude relation, extracted from multiple simulations, is compared to the solitary wave amplitude speed relation from Fig. 2.1. A Kawahara solitary wave of velocity given by the trailing edge is superimposed on the DSW trailing edge in Fig. 4.12(b).

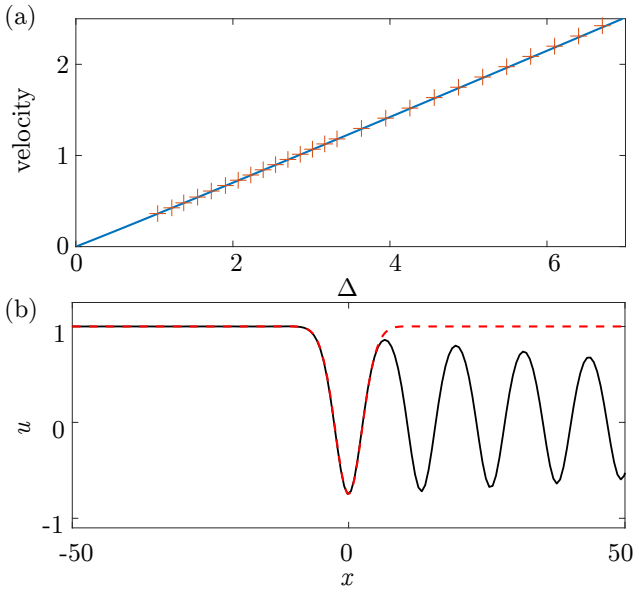

Figure 4.12: Comparison of DSW trailing edge properties to Kawahara solitary waves. (a) Speed-amplitude relation of Kawahara solitary wave (solid) and DSW trailing edge from numerical simulation (pluses) for $\sigma = +1$. (b) Overlay of numerically computed solitary wave with coincident velocity to the DSW trailing edge for $\Delta = 1$.

We now implement the DSW fitting method [45] (see also [47]). The implementation is essentially the same as that for the RDSW in Section 4.1.3 but we now use the dispersion relation and approximate solitary wave amplitude-speed relation, Eq. (2.39), both with $\sigma = -1$. The details are omitted since they are identical to the DSW fitting procedure for the RDSW in Sec. 4.1.3. The macroscopic DSW harmonic leading edge properties are the

characteristic wavenumber

$$k_+ = \left(\frac{-3+\sqrt{9+20\Delta}}{5}\right)^{1/2} = \left(\frac{2\Delta}{3}\right)^{1/2} - \frac{5\Delta^{3/2}}{9\sqrt{6}} + \mathcal{O}(\Delta^{5/2}), \tag{4.33}$$

and group velocity

$$s_+ = \frac{9}{5} + 4\Delta - \frac{3}{5}\sqrt{9+20\Delta} = 2\Delta + \frac{10}{9}\Delta^2 + \mathcal{O}(\Delta^3). \tag{4.34}$$

Fig. 4.13(a) shows the DSW harmonic edge wavenumber k_+ versus jump height. DSW fitting theory provides an excellent approximation of the trailing edge wavenumber, extracted from our numerical simulations. In particular, DSW fitting correctly captures the reduction of the trailing edge wavenumber relative to the leading order KdV result $k_+ = \sqrt{2\Delta/3}$. We see that higher order dispersion has a significant quantitative effect on the properties of the harmonic wave edge.

The macroscopic properties of the DSW solitary wave trailing edge include the velocity

$$s_- = \frac{3}{25} + \frac{1}{5}\Delta - \frac{1}{25}\sqrt{9-20\Delta} = \frac{\Delta}{3} + \frac{2}{27}\Delta^2 + \mathcal{O}(\Delta^3), \tag{4.35}$$

and the amplitude

$$a_- = 2\Delta - \frac{5}{9}\Delta^2 + \mathcal{O}(\Delta^3), \tag{4.36}$$

approximated by using Eq. 2.39 and equating $s_- = c(a_-)$. Although the trailing edge velocity is only defined for $0 < \Delta < 9/20$, the small Δ asymptotics agree with the KdV velocity (and amplitude a_+) to leading order [57]. The next order correction shows that the Kawahara DSW solitary wave edge velocity is above the corresponding KdV DSW velocity, which agrees with the numerical simulations shown in FIg. 4.13(b) for Δ below the critical value $9/20$. The DSW fitting method fails for $\Delta > 9/20$, even though numerical computations show a clear trend.

As the amplitude of the jump increases, fifth order dispersion dominates and a TDSW emerges in the long time dynamics. A numerical simulation of the smooth step-like initial data (4.1) with $w = 10$. For sufficiently large amplitude jumps, the modulated, periodic intermediate wavetrain characteristic of a TDSW emerges.

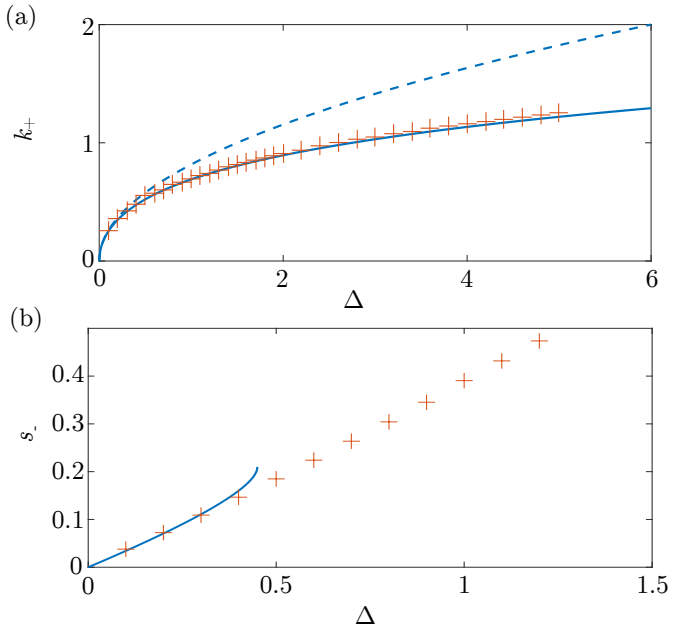

Figure 4.13: Kawahara DSW trailing edge wavenumber (a) and DSW leading edge speed, (b) for varying jump height. Comparison between Whitham theory predictions for the Kawahara equation (solid), Whitham theory for the KdV equation (dashed) and numerical simulation of the Kawahara equation (pluses).

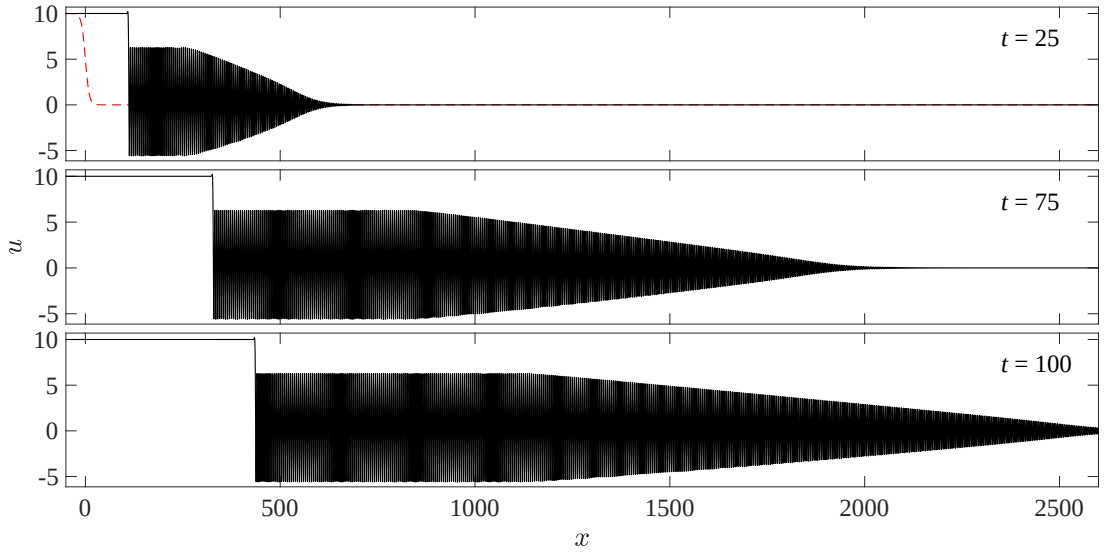

Figure 4.14: Development of a Kawahara TDSW with initial jump $\Delta = 5$ and convex dispersion $\sigma = -1$. Approximate initial data is shown in the top figure with the dashed curve.

4.2 Conclusions

In this chapter, we studied the long time evolution of the Gurevich-Pitaevskii step problem for the Kawahara equation. The classification carried out here reveals classical, KdV-like DSWs when the dispersion is convex and three distinct regimes for non-convex dispersion. These three regimes represent an intrinsic mechanism for the transition from convex to non-convex dispersive hydrodynamics. An example from shallow water waves (recall Section 2.1.2) illuminates this transition.

When gravity dominates surface tension effects, the Bond number B is small so that higher order dispersive effects continue to yield negative dispersion curvature for all but very short wavelengths. DSWs in this regime are therefore KdV-like, satisfying Eq. (1.3), with positive orientation and polarity as in Fig. 1.5(b). For B less than but close to $1/3$, where surface tension and gravity start to balance, the non-convexity of the dispersion relation manifests in the Kawahara equation with $\sigma = +1$. Small jumps still yield KdV-like DSWs with positive orientation and polarity but now they are accompanied by a resonance and small amplitude forward radiation. They are RDSWs. As the jump height is further increased, the forward radiation gets stronger at the expense of backward wave propagation until a critical jump height is reached. Above this threshold, a TDSW with negative orientation and polarity is generated, exhibiting a steady traveling wave structure at the trailing edge. Thus, the crossover from positive to negative DSW polarity and orientation manifests as an intrinsic feature of the Kawahara equation as the jump height is increased. For $B > 1/3$, $\sigma = -1$ and the DSWs are all KdV-like with negative polarity and orientation. Because the Bond number is inversely proportional to fluid depth, we expect to see these non-convex features for sufficiently shallow flows.

Higher order dispersive effects can play an important role in nonlinear fiber optics modeled by a higher order nonlinear Schrödinger equation as demonstrated in [95, 32, 31, 33]. The Kawahara equation is a simpler, scalar, unidirectional model in which to interpret the

dynamics of these works (cf. Section 2.1.3). In particular, the authors in [31] observed coherent structures consistent with RDSWs and TDSWs described in detail here. Solitary wave and DSW resonances modeled by a third order NLS equation were observed experimentally in [34]. This motivates further analysis of higher order NLS models as future work.

The TDSW is a non-classical DSW in the sense that it is not KdV-like; rather it satisfies a generalized Rankine-Hugoniot relation resulting from the far-field behavior of a constant in one direction and a periodic traveling wave in the other. The TDSW rapidly approaches a traveling wave solution of the Kawahara equation satisfying these far-field conditions, consisting of a coherent combination of a uniform wavetrain connected to the constant value through a partial, non-monotonic solitary wave. The fact that the Kawahara traveling wave ODE is fourth order enables this solution. It is natural to conjecture that the TDSW consists of a periodic orbit solution to the traveling wave ODE that is heteroclinic to an equilibrium, generalizing homoclinic and heteroclinic solutions studied previously [59]. An open question is the rigorous existence of a traveling wave solution of the Kawahara equation exhibiting this structure. Nonuniformity in the leading edge of the TDSW corresponds to a forward propagating wavepacket moving with the group velocity for a distinct wavenumber, approximately that of the periodic orbit. The uniform wavetrain acts as a channel for the effective dissipation of energy. Interestingly, the TDSW only exists for sufficiently large jumps $\Delta \gtrsim 0.60$, below which waves radiate forward and backward from the sharp transition region due to the Kawahara solitary wave band gap.

The generalized Rankine-Hugoniot condition is a kind of nonlinear resonance condition in the sense that the trailing edge solitary wave velocity coincides with the adjacent periodic traveling wave velocity. Such a condition has been assumed previously [31, 48] but here we show that it is inherent in the generation of a traveling wave structure within the TDSW.

Although a non-convex dispersion can give rise to TDSWs above threshold, it is not necessary. Another model equation, the conduit equation, also with non-convex dispersion, does not exhibit such solutions [91]. But that model, a Benjamin-Bona-Mahony (BBM)

type equation [15] with nonlinear dispersion, does display non-classical DSW dynamics at the DSW harmonic wave edge. Likely, the principle reason that TDSWs do not occur is the lack of a linear resonance at the DSW solitary wave edge.

A unique feature of the TDSW is its triple personality. On the one hand, it is similar to a dissipative shock wave in that it satisfies a generalized Rankine-Hugoniot condition and exhibits a steady character when viewed near the shock front. On the other hand, the TDSW is similar to a classical DSW, exhibiting two distinct limits: a small amplitude, harmonic edge moving with the group velocity and a large amplitude solitary wave edge moving with the phase velocity. But the TDSW is distinct in that the transition from a periodic wave to a solitary wave occurs almost instantaneously, setting it apart from DSWs in convex dispersive hydrodynamics and shock waves in dissipative hydrodynamics. In fact, numerical simulations of step initial data of the purely fifth order KdV equation, e.g. the Kawahara equation with $\sigma = 0$, demonstrates that the gradient catastrophe is resolved again by a TDSW [64] and can be interpreted as a shock solution of the Whitham modulation equations [122]. Chapter 5 explores the implications of this observation for the KdV5 equation. We revisit the TDSW solution of the Kawahara equation in Chapter 6 leveraging the results and methods presented in the next chapter.

Chapter 5

Discontinuous shock solutions of the KdV5-Whitham modulation equations

In this chapter, we present results that can be found in the manuscript [122]. The TDSW solution of the Kawahara equation presented in the previous chapter possesses a trailing edge with a depression solitary wave that brings the left equilibrium to a nearly uniform periodic wavetrain. In an effort to study the TDSW with the simplest requisite effects, we remove the third order dispersion term from the Kawahara equation (1.3). Setting $\sigma = 0$ in the Kawahara equation (1.3) yields the KdV5 equation

$$u_t + uu_x + u_{xxxxx} = 0. \tag{1.4}$$

Long time numerical evolution of a smoothed form of the initial data

$$u(x,0) = \frac{\Delta}{2}\left(1 - \tanh\left(\frac{x}{w}\right)\right), \tag{5.1}$$

with $w = 20$ results in the TDSW solution given in Figure 5.1. The original motivation for the work presented in this chapter was to fully describe the TDSW solutions in Fig. 5.1(a) and previous chapters in terms of modulation theory. Figure 5.1(b) is a zoom of the traveling wave at the trailing edge. The claim we make here is that within the context of modulation theory, this corresponds to a discontinuous shock solution of the KdV5-Whitham modulation equations. Since the Whitham modulation equations describe the dispersionless limit of the governing system, we demonstrate that the zero dispersion limit of heteroclinic traveling waves correspond precisely to the discontinuous shock solutions of the KdV5-Whitham modulation equations

In Chapter 6, we show that the TDSW solution of Fig. 5.1 is therefore described in terms of a shock-rarefaction solution to the KdV5-Whitham modulation system. However, our focus at the moment is to describe the heteroclinic wave at the trailing edge. The heteroclinic traveling wave moves at velocity c and is found by seeking a solution to the KdV5 equation (1.4) of the form $u(x,t) = f(\xi)$, $\xi = x - ct$, where

$$-cf' + ff' + f^{(5)} = 0. \tag{5.2}$$

During this research, a broader theme emerged and revealed a host of novel heteroclinic and homoclinic traveling wave solutions of Eq. (5.2) as well as a Whitham modulation theory framework to interpret them.

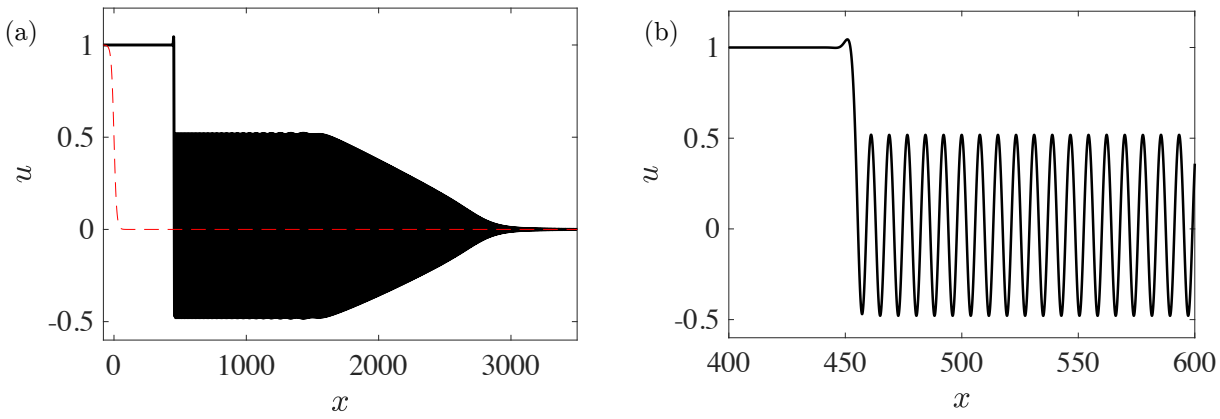

Figure 5.1: Numerical simulation of the Riemann problem (5.1) with $\Delta = 1$ for the KdV5 equation (1.4). (a) Solution at $t = 1000$ (solid) for a TDSW and the initial step (dashed). (b) A zoom in of the trailing edge that resembles an equilibrium heteroclinic to a periodic orbit traveling wave solution to the KdV5 equation [64].

5.1 Whitham shocks

We seek shock solutions of the conservative form of the KdV5-Whitham modulation equations (cf. Eqs. (3.9)–(3.11))

$$\overline{u}_t + \left(\frac{1}{2}\overline{\varphi^2}\right)_x = 0, \tag{5.3}$$

$$\left(\frac{1}{2}\overline{\varphi^2}\right)_t + \left(\frac{1}{3}\overline{\varphi^3} + \frac{5}{2}k^4\overline{\varphi^2_{\theta\theta}}\right)_x = 0, \tag{5.4}$$

$$k_t + (ck)_x = 0, \tag{5.5}$$

We recall that $\varphi(\theta) = \varphi(\theta, \overline{u}, a, k)$ is a modulated nonlinear periodic traveling wave solution of the KdV5 equation (1.4) with mean $\overline{u} = \overline{u}(x,t)$, amplitude $a = a(x,t)$ and wavenumber $k = k(x,t)$ and phase $\theta = \theta(x,t)$ such that $\theta_x = k(x,t)$, $\theta_t = -\omega(x,t)$.

In this section, we discuss the admissibility of shock solutions of the conservative modulation equations and their connections to heteroclinic traveling wave solutions of the KdV5 equation. Shock solutions of the modulation equations take the form of a moving discontinuity

$$\overline{u}(x,t) = \begin{cases} \overline{u}_- & x < Vt \\ \overline{u}_+ & x > Vt \end{cases} \qquad a(x,t) = \begin{cases} a_- & x < Vt \\ a_+ & x > Vt \end{cases} \qquad k(x,t) = \begin{cases} k_- & x < Vt \\ k_+ & x > Vt \end{cases}. \tag{5.6}$$

In order for the shock (5.6) to be a weak solution of (5.3)–(5.5), the left $(\overline{u}_-, a_-, k_-)$, right $(\overline{u}_+, a_+, k_+)$ states and the shock velocity V must satisfy the Rankine-Hugoniot jump conditions

$$-V[\![\mathbf{P}]\!] + [\![\mathbf{Q}]\!] = 0,$$

where $\mathbf{P}, \mathbf{Q} \in \mathbb{R}^3$ are the densities and fluxes in Eqs. (5.3)–(5.5) and $[\![\cdot]\!]$ represents the difference in the left and right values. Consequently, the jump conditions take the form

$$-V(\overline{u}_- - \overline{u}_+) + \frac{1}{2}\left(\overline{\varphi^2_-} - \overline{\varphi^2_+}\right) = 0, \tag{5.7}$$

$$-\frac{V}{2}\left(\overline{\varphi^2_-} - \overline{\varphi^2_+}\right) + \frac{1}{3}\left(\overline{\varphi^3_-} - \overline{\varphi^3_+}\right) + \frac{5}{2}\left(k_-^4\overline{\varphi^2_{-,\theta\theta}} - k_+^4\overline{\varphi^2_{+,\theta\theta}}\right) = 0, \tag{5.8}$$

$$-V(k_- - k_+) + (c_-k_- - c_+k_+) = 0. \tag{5.9}$$

where $\varphi_\pm = \varphi(\theta; \overline{u}_\pm, a_\pm, k_\pm)$ are the right $(+)$/left $(-)$ periodic traveling waves that compose the Whitham shock. We summarize this in the following.

Definition 5.1.1 (Whitham shock)**.** A discontinuity (5.6) moving with velocity V is called a **Whitham shock** when it is a weak solution of the Whitham modulation equations in conservative form (5.3)–(5.5). That is, the left $(\overline{u}_-, a_-, k_-)$ and right $(\overline{u}_+, a_+, k_+)$ states satisfy the Rankine-Hugoniot jump conditions (5.7)–(5.9).

In order to determine admissibility of Whitham shocks, we consider smooth heteroclinic traveling wave solutions to the KdV5 equation (1.4) that asymptote to distinct periodic waves as $x \to \pm\infty$

$$u(x,t) \to \begin{cases} \varphi_-(k_-x - \omega_-t + \theta_-) \equiv \varphi(k_-x - \omega_-t - \theta_-; \overline{u}_-, a_-, k_-) & x \to -\infty \\ \\ \varphi_+(k_+x - \omega_+t + \theta_+) \equiv \varphi(k_+x - \omega_+t - \theta_+; \overline{u}_+, a_+, k_+) & x \to \infty \end{cases}, \tag{5.10}$$

with each far-field periodic wave $(\varphi_\pm)$ characterized by the parameters $(\overline{u}_\pm, a_\pm, k_\pm)$ and phase shifts $\theta_\pm$.

Our main result states that KdV5 heteroclinic traveling wave solutions exhibiting the far field behavior (5.10) necessarily lie on the Whitham shock locus of states satisfying (5.7)–(5.9).

Theorem 1. *Suppose $f(\xi)$ with speed c ($\xi = x - ct$) is a traveling wave solution of the fifth order KdV equation* (5.2) *such that*

$$\inf_{\theta_\pm \in [0,2\pi)} |f(\xi) - \varphi_\pm(k_\pm\xi + \theta_\pm)| \to 0$$

uniformly as $\xi \to \pm\infty$, then the Rankine-Hugoniot relations (5.7)–(5.9) *for the KdV5-Whitham equations* (5.3)–(5.5) *are satisfied by the far-field periodic waves $\varphi_\pm$ with parameters $\overline{u}_\pm$, $a_\pm$, $k_\pm$. The traveling wave velocity is the shock velocity $c = V$ and coincides with the phase velocities $c = c_\pm$.*

Proof. By assumption, there exists some traveling wave profile $f(\xi)$ that solves the KdV5 equation (1.4) with the far-field behavior described by the boundary conditions (5.10). The factors $\theta_\pm$ are appropriate phase shifts so that the traveling wave matches the far-field periodic orbits $\varphi_\pm$. We define the averaging operators $\bar{\mathcal{L}}^\pm$ acting on a periodic, integrable function $F(\xi)$ as

$$\bar{\mathcal{L}}^\pm[F] = \lim_{\bar{x}\to\pm\infty} \frac{k_\pm}{2\pi} \int_{\bar{x}}^{\bar{x}+2\pi/k_\pm} F(\xi)d\xi.$$

Since $f \to \varphi_\pm$ uniformly, we can compute for $n = 1, 2, 3$

$$\begin{aligned}
\bar{\mathcal{L}}^\pm[f^n] &= \lim_{\bar{x}\to\pm\infty} \frac{k_\pm}{2\pi} \int_{\bar{x}}^{\bar{x}+2\pi/k_\pm} f^n(\xi)d\xi, \\
&= \frac{1}{2\pi} \int_0^{2\pi} \varphi_\pm^n(\theta)d\theta, \\
&= \overline{\varphi_\pm^n}
\end{aligned}$$

and

$$\begin{aligned}
\bar{\mathcal{L}}^\pm[(f'')^2] &= \lim_{\bar{x}\to\pm\infty} \frac{k_\pm}{2\pi} \int_{\bar{x}}^{\bar{x}+2\pi/k_\pm} (f''(\xi))^2 d\xi \\
&= \frac{k_\pm^4}{2\pi} \int_0^{2\pi} \left(\varphi_\pm''(\theta)\right)^2 d\theta \\
&= k_\pm^4 \overline{(\varphi_\pm'')^2}.
\end{aligned}$$

Since f is a traveling wave solution to (1.4) with two periodic wave limits, the phase speed of each must be the same, i.e.,

$$c = c_\pm. \tag{5.11}$$

This condition immediately implies the jump condition (5.9) with $c = V$ from the conservation of waves. All traveling wave solutions with speed c admit the first and second integrals of Eq. (5.2)

$$-cf + \frac{1}{2}f^2 + k^4 f^{(4)} = C_1, \tag{5.12}$$

$$-\frac{c}{2}u + f^2 + \frac{1}{6}f^3 + k^4 f' f''' - \frac{k^4}{2}(f'')^2 = C_1 f + C_2, \tag{5.13}$$

where derivatives are with respect to the variable $\theta = k\xi$. We now apply the operator $\bar{\mathcal{L}}^{\pm}$ to the first integral (5.12) to obtain

$$-c\overline{u}_{\pm} + \frac{1}{2}\overline{\varphi_{\pm}^2} = \frac{A}{2}, \tag{5.14}$$

where we used $\bar{\mathcal{L}}^{\pm}[f''''] = 0$ by virtue of periodicity in the far-field. Equating the two relations in (5.14) to eliminate A gives

$$-c(\overline{u}_{-} - \overline{u}_{+}) + \frac{1}{2}\left(\overline{\varphi_{-}^2} - \overline{\varphi_{+}^2}\right) = 0, \tag{5.15}$$

which is precisely the first jump condition (5.7) when we identify $V = c$. Applying the operator $\bar{\mathcal{L}}^{\pm}$ to the second integral (5.13) results in

$$k_{\pm}^4\overline{\varphi_{\pm}'''\varphi_{\pm}'} - \frac{k_{\pm}^4}{2}\overline{(\varphi_{\pm}'')^2} + \frac{1}{6}\overline{\varphi_{\pm}^3} - \frac{c}{2}\overline{\varphi_{\pm}^2} - \frac{A}{2}\overline{u}_{\pm} + B = 0, \tag{5.16}$$

where we used $\bar{\mathcal{L}}^{\pm}[f'''f'] = k_{\pm}^4\overline{\varphi_{\pm}'''\varphi_{\pm}'}$. Integrating by parts and applying (5.15) simplifies Eq. (5.16) to

$$\frac{c}{2}\overline{\varphi_{\pm}^2} - \frac{1}{3}\overline{\varphi_{\pm}^3} - \frac{5}{2}k_{\pm}^4\overline{(\varphi_{\pm}'')^2} = -B. \tag{5.17}$$

The third and final Rankine-Hugoniot condition (5.8) with $c = V$ is found by subtracting the $+$ and $-$ instances of Eq. (5.17) to eliminate B

$$-\frac{c}{2}\left(\overline{\varphi_{-}^2} - \overline{\varphi_{+}^2}\right) + \frac{1}{3}\left(\overline{\varphi_{-}^3} - \overline{\varphi_{+}^3}\right) + \frac{5}{2}\left(k_{-}^4\overline{(\varphi_{-}'')^2} - k_{+}^4\overline{(\varphi_{+}'')^2}\right) = 0, \tag{5.18}$$

thereby completing the proof. □

Theorem 1 motivates the following.

Definition 5.1.2 (admissibility)**.** A KdV5 Whitham shock (recall Def. 5.1.1) is **admissible** if there exists a heteroclinic traveling wave solution with speed $c = V$ to the KdV5 equation (1.4) satisfying Eq. (5.2) and the boundary conditions (5.10) corresponding to the left $(-)$/right $(+)$ states of the Whitham shock (5.6) and $V = c_{+} = c_{-}$.

In the following section, we provide extensive numerical computations of heteroclinic traveling wave solutions of the KdV5 equation (1.4) that imply the existence of admissible Whitham shocks for the KdV5-Whitham equations (5.3)–(5.5).

5.2 Heteroclinic and homoclinic traveling waves

In this section, we study admissible KdV5 Whitham shocks with increasing levels of complexity. First, we consider the case of a shock solution (5.6) to the modulation equations where one far-field state degenerates to zero wavenumber, i.e., a solitary wave. These results are then generalized to Whitham shocks in which two periodic waves satisfying the jump conditions propagate with identical phase velocities. The section culminates with computations of two co-propagating Whitham shocks where the corresponding traveling wave solutions are homoclinic, localized oscillatory patterns on an oscillatory or uniform background.

5.2.1 Solitary wave to periodic wave

We consider the case, without loss of generality, where the left periodic wave degenerates to a solitary wave ($k_- \to 0$) and the right periodic wave is of unit amplitude and zero mean ($a_+ = 1$, $\overline{u}_+ = 0$). The associated Whitham shock (5.6) is

$$\big(\overline{u}, a, k\big)(x,t) = \begin{cases} (\overline{u}_-, a_-, 0) & x < Vt \\ \\ (0, 1, k_+) & x \geq Vt \end{cases}. \tag{5.19}$$

In the solitary wave limit ($k \to 0$) of the modulation equations (5.3)–(5.5), the averaged quantities are

$$\overline{\varphi^2} = \overline{u}^2, \quad \overline{\varphi^3} = \overline{u}^3, \quad \overline{(\varphi'')^2} = 0.$$

Therefore, the jump conditions (5.7)–(5.9) with a solitary wave on the left are

$$-V\left(\overline{u}_-\right) + \left(\frac{1}{2}\overline{u}_-^2 - \frac{1}{2}\overline{\varphi_+^2}\right) = 0, \tag{5.20}$$

$$-\frac{V}{2}\left(\overline{u}_-^2 - \overline{\varphi_+^2}\right) + \left(\frac{1}{3}\overline{u}_-^3 - \frac{1}{3}\overline{\varphi_+^3} - \frac{5}{2}k_+^4\overline{\varphi_{+,\theta\theta}^2}\right) = 0, \tag{5.21}$$

$$V - c_+ = 0. \tag{5.22}$$

An illuminating calculation using the Stokes wave approximation (cf. Eq. (2.40) with $\sigma = 0$) for φ_+

$$\varphi_+ = \frac{1}{2}\cos\theta - \frac{a}{240k_+^4}\cos 2\theta \tag{5.23}$$

$$V = c_+ = k_+^4 - \frac{1}{480k_+^4}, \tag{5.24}$$

leads to explicit formulae. In this case, the jump conditions (5.20)–(5.22) are solved by

$$V = c_+ = \frac{\overline{u}_-}{2} - \frac{1}{16\overline{u}_-}, \quad k_+^4 = \frac{4\overline{u}_-^3 + 3\overline{u}_-}{15} - \frac{1}{80\overline{u}_-} \tag{5.25}$$

where $\overline{u}_-^2$ is a root of the polynomial

$$1024\left(\overline{u}_-^2\right)^4 - 384\left(\overline{u}_-^2\right)^3 - 720\left(\overline{u}_-^2\right)^2 + 168\left(\overline{u}_-^2\right) - 9 = 0, \tag{5.26}$$

which has three positive solutions $\overline{u}_-^2 \in \{0.08777, 0.1337, 0.9455\}$. The positive square roots are inserted into (5.25) to obtain the wavenumber k_+, shock velocity V and the right characteristic velocities (calculated for the weakly nonlinear Whitham equations and given by the eigenvalue expansions of the KdV5-Whitham Eqs. (3.29)–(3.31)) for three distinct shock loci. These calculations are summarized in Table 5.1. The left solitary wave amplitude a_- can be recovered from the solitary wave speed-amplitude relation by equating it to the shock velocity $c(\overline{u}_-, a_-, 0) = V$. The left characteristic speeds for the left solitary wave state are $\lambda_1^{(-)} = \overline{u}_-$, $\lambda_2^{(-)} = \lambda_3^{(-)} = V$. The reason that two of the characteristic velocities for the left state are the same is that two of the three modulation equations coincide in the solitary wave limit $k \to 0$, which is a well-known property of the Whitham equations [47]. The cases where $\overline{u}_-^2 < 0$ or $\overline{u}_- < 0$ in Eq. (5.26) can be dismissed because these choices result in a complex value for $\overline{u}_-$ or k_+ in Eq. (5.25).

We test the accuracy of the approximate Whitham shock loci reported in Table 5.1 by solving the jump conditions (5.20)–(5.22) with the one-parameter family of periodic traveling wave solutions obtained numerically in Chapter 2. Results from the numerical computations are given in Table 5.2. The Whitham shock locus with the largest root of Eq. (5.26) is

$\overline{u}_-$	V	k_+	$\lambda_1^{(+)}$	$\lambda_2^{(+)}$	$\lambda_3^{(+)}$
0.2963	-0.0628	0.3936	-0.7271	0.1858	1.0416
0.3657	0.0119	0.4775	-0.3768	0.4809	0.5360
0.9724	0.4219	0.8082	0.0586	1.6775	2.5904

Table 5.1: Three distinct Whitham shock loci and right (+) characteristic velocities for (5.19) when the right periodic wave φ_+ is approximated by a weakly nonlinear Stokes wave (5.23).

	$\overline{u}_-$	V	k_+	$\lambda_1^{(+)}$	$\lambda_2^{(+)}$	$\lambda_3^{(+)}$
▲	0.2522	-0.1133	0.3173	-0.1462	-0.0780	0.4056
●	0.3479	-0.0071	0.4496	0.6071	$-0.0237 - 0.1194i$	$-0.0237 + 0.1194i$
■	0.9726	0.4213	0.8080	0.0623	1.6472	2.5723

Table 5.2: Three distinct Whitham shock loci and right characteristic velocities using numerically computed periodic traveling waves. Compare with the approximate loci in Table 5.1.

well-approximated to three digits (denoted by ■). The corresponding right characteristic velocities on this locus are accurate to one or two digits. The two Whitham shock loci corresponding to the two smaller roots of Eq. (5.26) are less accurately approximated. The reason for this is the Stokes approximation restriction $k_+ \gg a_+^{1/4} = 1$ that requires a sufficiently large wavenumber k_+. The Whitham shock locus with the largest root $\overline{u}_-$ also exhibits the largest wavenumber k_+, hence is expected to be a better approximation to the true Whitham shock locus, although good agreement is notable given that $k_+ < 1$.

Two of the characteristic velocities for the locus denoted ● are complex, therefore we expect this locus to correspond to unstable Whitham shocks. We investigate stability questions in Sec. 5.2.3.

We now compute heteroclinic traveling wave solutions whose zero dispersion limit correspond to a Whitham shock from each of the loci reported in Table 5.2, hence demonstrating Whitham shock admissibility. See Appendix B for details on the computations. The obtained solutions are depicted in Fig. 5.2. All three traveling wave solutions visually look

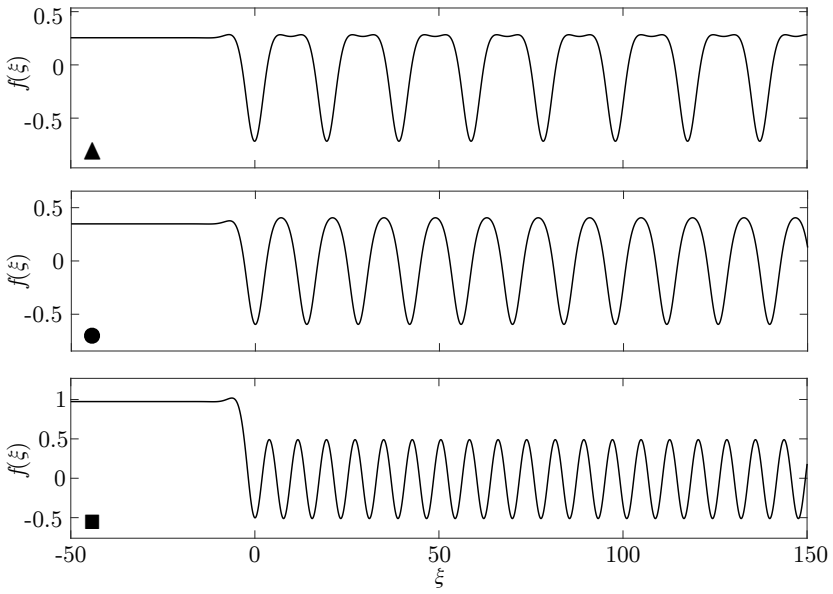

Figure 5.2: Computed traveling wave solutions corresponding to the periodic wave and mean values from the Whitham shock locus in Table 5.2, matched by the symbols in the lower left corner.

similar for $x < 0$, which corresponds to the left solitary wave $(\overline{u}_-, a_-, 0)$ of the Whitham shock (5.19). To investigate this further, we compare this portion of the heteroclinic traveling wave solutions with solitary wave solutions that move with the shock velocity V on the background $\overline{u}_-$ (the solitary wave amplitude a_- is obtained from $c(\overline{u}_-, a_-, 0) = V$). Figure 5.3 consists of the heteroclinic traveling wave solutions depicted in Fig. 5.2 overlaid with the left solitary wave (dashed red) and the right periodic wave $\varphi(\theta; 0, 1, k_+)$ (dashed blue) that form the corresponding admissible Whitham shock. Both the left solitary waves and the right periodic waves are visually indistinguishable from the heteroclinic traveling wave in their respective regions of validity. This corroborates our formulation and interpretation of the zero dispersion limit of heteroclinic traveling wave solutions as admissible Whitham shocks where the left wave is a solitary wave that rapidly transitions to a co-propagating finite amplitude periodic wave.

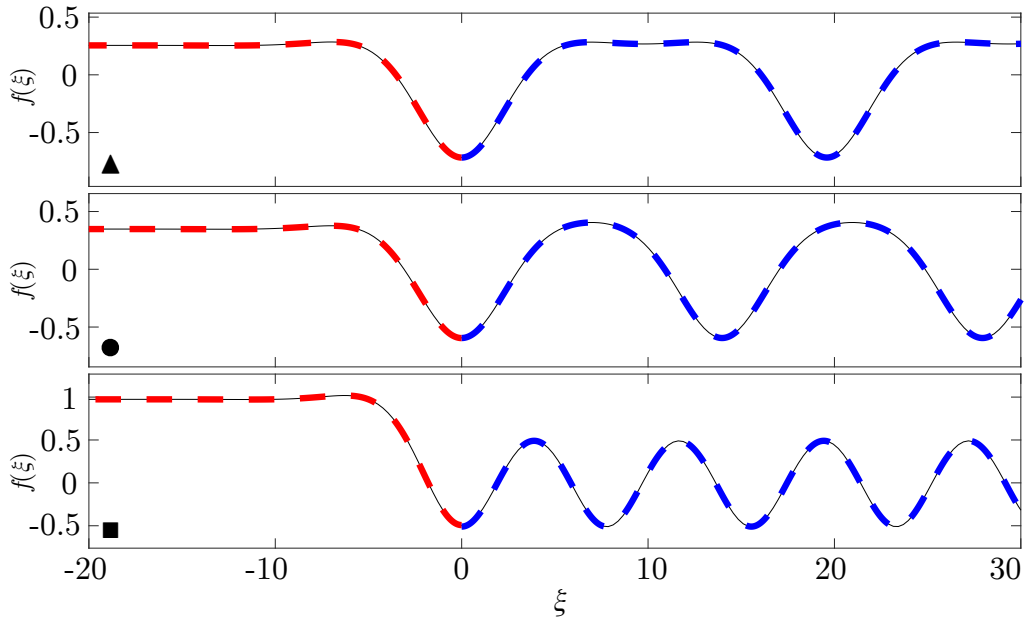

Figure 5.3: Whitham shock structure via heteroclinic TW solutions (solid). The left solitary wave (dashed red for $x < 0$) and right periodic wave (dashed blue for $x > 0$) from the Whitham shock loci reported in Table 5.2 are overlaid on the heteroclinic TW solution. The symbols in the lower left corners coincide with those in Fig. 5.2 and Table 5.2.

Admissible Whitham shock solutions and characteristics

$$\Gamma_j = \left\{ (x,t) \mid \frac{\mathrm{d}x}{\mathrm{d}t} = \lambda_j \right\}, \quad j = 1,2,3, \tag{5.27}$$

corresponding to the loci ▲ and ■ in Table 5.2 are shown in Figures 5.4 and 5.5, respectively. Both Whitham shocks with real characteristic velocities are weakly compressive in the first characteristic family Γ_1 because $\lambda_1^{(+)} < V = \lambda_1^{(-)}$, while the second characteristic family is weakly expansive $\lambda_2^{(-)} = V < \lambda_2^{(+)}$, and the third characteristic family passes through the Whitham shock, decelerating $V < \lambda_3^{(+)} < \lambda_3^{(-)}$ for ▲ and accelerating $V < \lambda_3^{(-)} < \lambda_3^{(+)}$ for ■ [36]. Consequently, we refer to this class of Whitham shock solutions as **weak 1-shocks**.

The degeneration of the periodic wave to a solitary wave on the left state in Fig. 5.2 allows us to obtain three additional admissible Whitham shock loci by reflecting the initial data (5.19) and the heteroclinic traveling wave across $x = 0$. These solutions are weakly

compressive in the second characteristic family, Γ_2, hence are called **weak 2-shocks**. Further implications of this observation are discussed in Sec. 5.2.3.

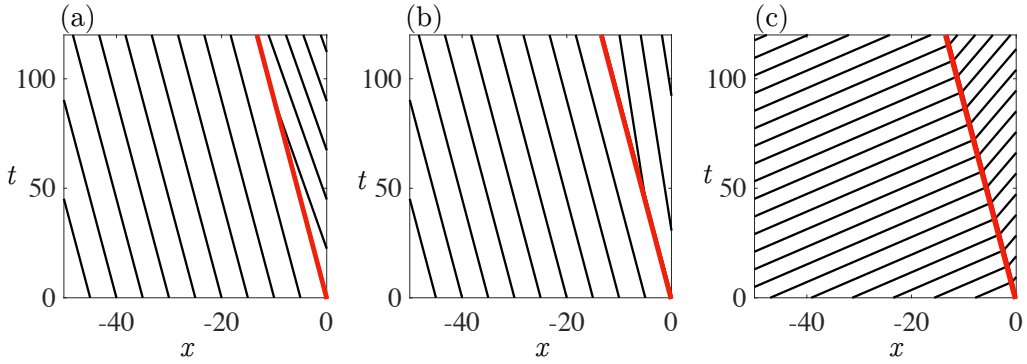

Figure 5.4: Characteristics of the KdV5-Whitham modulation equations for the Whitham shock locus ▲ in Table 5.2. (a) Weakly compressive 1-wave characteristics Γ_1, (b) Weakly expansive 2-wave characteristics Γ_2, and (c) Decelerating 3-wave characteristic family Γ_3. The shock is identified by the thick, red line.

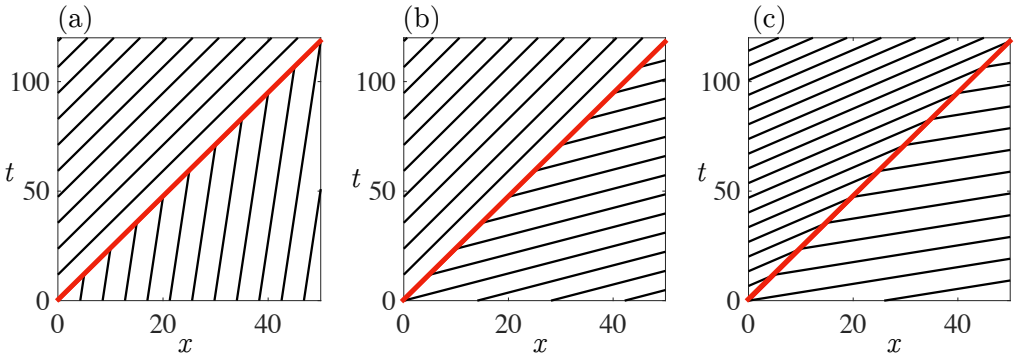

Figure 5.5: Characteristics of the KdV5-Whitham modulation equations for the solution ■ in Table 5.2. (a) Weakly compressive 1-wave characteristics Γ_1, (b) Weakly expansive 2-wave characteristics Γ_2, and (c) Accelerating 3-wave characteristic family Γ_3. The shock is identified by the thick, red line.

5.2.2 Periodic wave to periodic wave

Let us continue our computation of the jump conditions Eqs. (5.7)–(5.9) where we now consider shock solutions of the modulation equations corresponding to heteroclinic traveling

waves with one periodic wave connected to another. We slightly modify the Riemann problem (5.19) from the previous section where the left state is assumed to have zero wavenumber. In this section, we scale the Whitham shock (5.6) so that, without loss of generality, the left state consists of an arbitrary periodic wave, and the right state consists of a periodic wave with zero mean, unit amplitude and arbitrary wavenumber. This parameter set results in the shock solution

$$(\overline{u}, a, k)(x,t) = \begin{cases} (\overline{u}_-, a_-, k_-) & x < Vt \\ \\ (0, 1, k_+) & x \geq Vt \end{cases}, \tag{5.28}$$

where $V = c_\pm$ is the phase velocity of right $(+)$, left $(-)$ periodic waves. The Rankine-Hugoniot jump relations (5.7)–(5.9) are a nonlinear system of three equations that relate the five parameters: k_+, $\overline{u}_-$, a_-, k_-, and V. We use $\overline{u}_-$ as the continuation parameter to obtain the one-parameter family of Whitham shock loci

$$k_+ = k_+(\overline{u}_-), \quad a_- = a_-(\overline{u}_-), \quad k_- = k_-(\overline{u}_-), \quad V = V(\overline{u}_-).$$

Note that the far-field behavior of the heteroclinic traveling wave therefore reveals the structure of the Whitham shock, since admissible shocks take the form of (5.28) where the left and right states are given precisely by the periodic wave's parameters.

Attempts to solve the jump conditions (5.7)–(5.9) approximately by using the Stokes wave approximation (5.23) yield no nontrivial, asymptotically valid solutions, aside from the solitary wave to periodic shocks discussed previously. As a result, we rely on numerical continuation along the parameterized curves $(k_+, a_-, k_-, V)(\overline{u}_-)$ where we start from the three Whitham shock loci calculated in Section 5.2.1 so that $k_- = 0$ and $\overline{u}_-$, k_+, V are initialized from Table 5.2 (a_- satisfies $c(\overline{u}_-, a_-, 0) = V$). We numerically continue solutions to the jump conditions (5.7)–(5.9) with Matlab's fsolve function for decreasing values of $\overline{u}_-$. Continuation is terminated when the value $k_+(\overline{u}_-) < 10^{-3}$ is reached, indicating that the oscillatory wavetrain in the left far-field is nearly a solitary wave. Figures 5.6(a), (c) and (e)

present the three Whitham shock loci parameterized by the left mean $\overline{u}_-$. We also compute heteroclinic traveling wave solutions for select points on the locus and plot them in Figures 5.6(b), (d), and (f). Details of the numerical computation of periodic-periodic heteroclinic traveling waves can be found in Appendix B. Consequently, we find that all three computed periodic to periodic Whitham shock loci are admissible.

We now investigate dynamic stability of admissible Whitham shocks. Modulational stability is determined by the hyperbolicity of the Whitham modulation equations (recall Fig. 3.3). Whitham shocks with real characteristic velocities are identified by the white background in Fig. 5.6 (a), (c), and (e) while the gray background denotes complex characteristic velocities $\mathrm{Im}\lambda_1 \neq 0$ and $\mathrm{Im}\lambda_2 \neq 0$. This means that either the left or right periodic waves that comprise the heteroclinic traveling wave is modulationally unstable and we expect the heteroclinic solution to be unstable as well. The implications of this will be investigated further in Sec. 5.2.3.

In Figure 5.7, we plot the numerically computed characteristic curves Γ_j, $j = 1, 2, 3$ and the shock trajectory for the periodic to periodic Whitham shock in Fig. 5.6(a) where $\overline{u}_- = 0.6$ (the corresponding heteroclinic traveling wave is shown in Fig. 5.6(b)). We observe that all characteristic families pass through the shock and satisfy

$$\lambda_1^{(\pm)} < V < \lambda_2^{(\pm)} < \lambda_3^{(\pm)}. \tag{5.29}$$

Shocks that are not compressive in any characteristic family violate the Lax entropy conditions. In the conservation law community, non-Lax shocks can be identified as admissible when they are, for example, the limit of vanishing dissipative-dispersive heteroclinic traveling waves [68, 85]. In such cases, they are referred to as **undercompressive**. Here, we find that the vanishing dispersion limit of heteroclinic periodic to periodic traveling waves generally converge to undercompressive Whitham shocks. To prove this, consider Fig. 5.8 where the scaled characteristic velocities $(\lambda_j - \overline{u})/a$, $j = 1, 2$ and shock velocity $(V - \overline{u})/a$ are plotted in the scaled coordinate $\tilde{k} = a^{-1/4}k$. Since $\lambda_3 > \lambda_2$, we see that all admissible

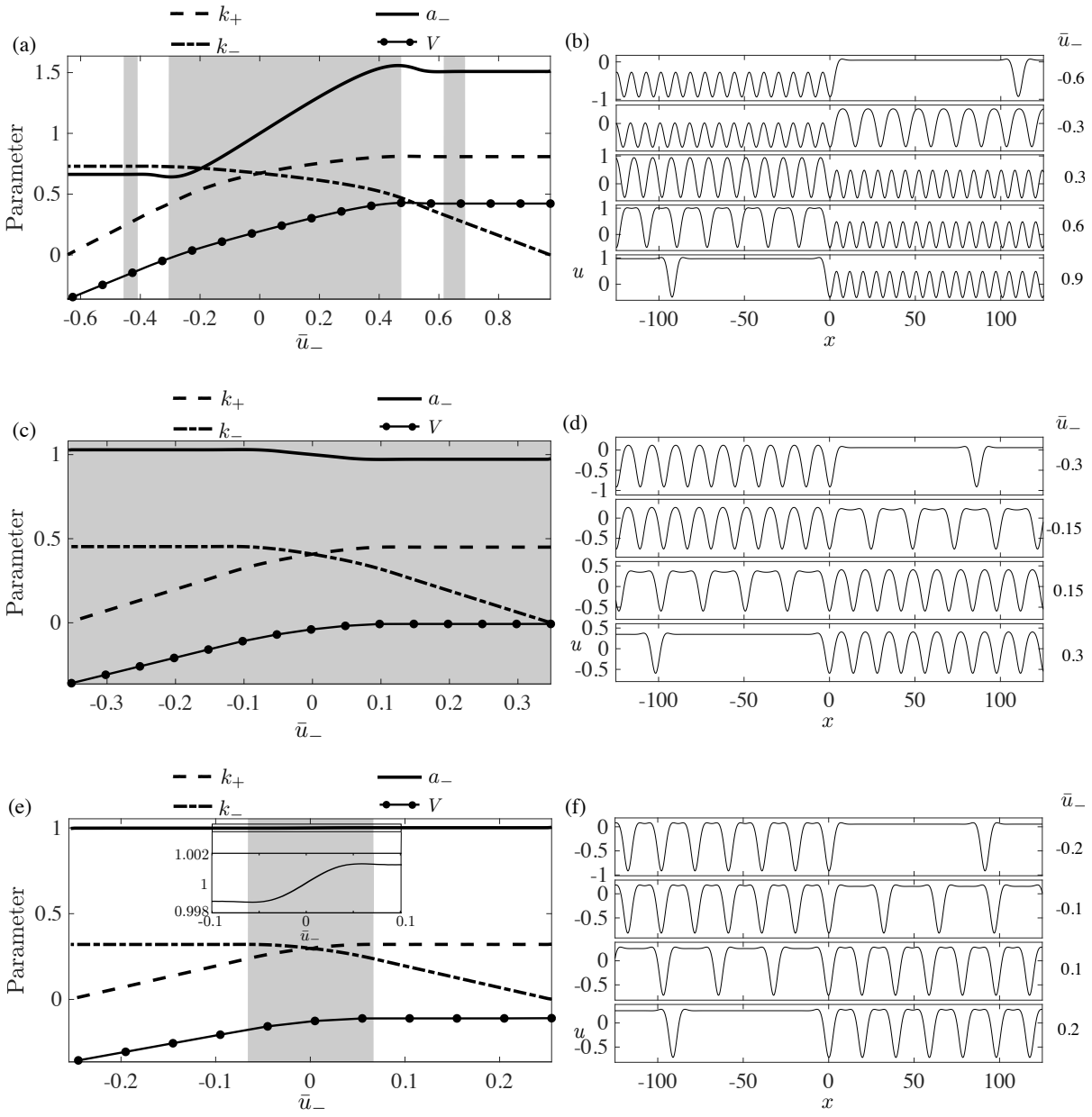

Figure 5.6: Continuation curves of admissible periodic to periodic Whitham shock solutions (5.28) and corresponding heteroclinic traveling wave solutions. (a),(c),(e) Shock loci for the periodic wave parameters $k_-(\overline{u}_-)$, $a_+(\overline{u}_-)$, $k_+(\overline{u}_-)$, and $V(\overline{u}_-)$. (b), (d), (f) Example heteroclinic solutions corresponding to the shock curves (a), (c), and (e) respectively. Gray, shaded areas in (a), (c) and (e) correspond to complex characteristic velocities and modulational instability. The zoomed-in inset in Figure (e) demonstrates that the amplitude is not constant across the solution curve.

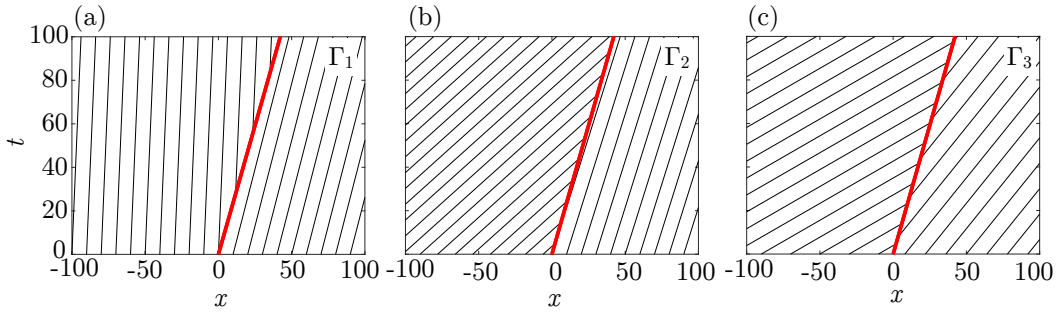

Figure 5.7: (a)-(c) Characteristic families of the undercompressive Whitham shock in Fig. 5.6(b) with $\overline{u}_+ = 0.6$ where $\lambda_1^{(\pm)} < V < \lambda_2^{(\pm)} < \lambda_3^{(\pm)}$. The shock trajectory is depicted with the thick red curve.

Whitham shocks with real characteristic velocities exhibit the undercompressive relations (5.29) except for the very narrow band of waves $0.662 \lesssim ka^{-1/4} \lesssim 0.672$. Because this band is so narrow in parameter space, we do not investigate solutions in this regime any further. Undercompressive shocks were first described for general 2×2 systems in [119] and have since been observed, for example, in fluid dynamics [17].

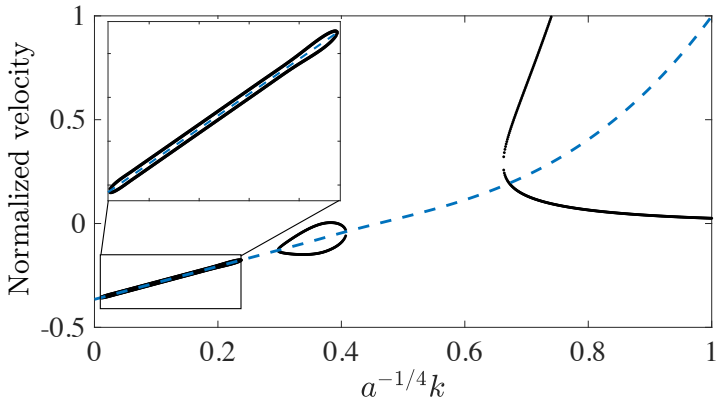

Figure 5.8: Numerically computed normalized Whitham shock velocity $(V - \overline{u})/a$ (blue, dashed) and normalized, purely real characteristic velocities $(\lambda_1 - \overline{u})/a < (\lambda_2 - \overline{u})/a$ (black dots). The inset is a zoomed in view of the phase velocity and characteristics velocities for small $a^{-1/4}k$.

We now utilize the heteroclinic solutions to construct symmetric, homoclinic, traveling

waves that can be described by two copropagating Whitham shock solutions.

5.2.3 Two copropagating shock solutions

In Sections 5.2.1 and 5.2.2 we established the admissibility of KdV5-Whitham shocks by computing heteroclinic traveling wave solutions to the KdV5 equation (1.4). Each locus of admissible Whitham shocks depicted in Fig. 5.6(a), (c), (e) include, up to scaling and Galilean symmetries, pairs of shocks with reflected + and − states. The implication of this observation is that it is possible to arrange for co-propagating Whitham shocks with the same equilibrium on the left and right, respectively, as well as the periodic wave on the right and left, respectively. Can we compute homoclinic TWs consisting of two co-propagating Whitham shocks? Furthermore, can this construction be extended to solutions tending to a periodic wave in the far-field? We affirmatively answer these questions now.

We formulate the double Whitham shock problem as a locally periodic wave that terminates after a finite number of oscillation periods and transitions to a different periodic wave, possibly a solitary wave, in the far field. To this end, let us consider solutions of the form

$$(\overline{u}, a, k)(x,t) = \begin{cases} (0, 1, k_{\mathrm{i}}) & |x - Vt| \leq \frac{n\pi}{k_{\mathrm{i}}} \\ (\overline{u}_{\mathrm{o}}, a_{\mathrm{o}}, k_{\mathrm{o}}) & |x - Vt| \geq \frac{n\pi}{k_{\mathrm{i}}} \end{cases}, \tag{5.30}$$

where the subscript i refers to the inner periodic wave with n oscillations and subscript o denotes the outer periodic wave in the far field. Following the normalization in Sec. 5.2.2, we have normalized the inner periodic solution to have zero mean and unit amplitude.

Figure 5.9 depicts the structure of an example homoclinic TW solution in the physical plane overlaid with co-propagating weak 1-shock and weak 2-shock solutions that satisfy the jump conditions for zero wavenumber in the far field, i.e., $k_{\mathrm{o}} = 0$. In general, the far-field periodic wave can be chosen from a continuous set of nonzero wavenumbers (cf. Fig. 5.6 for the range of possible values, equating $k_{\mathrm{o}} = k_{-}$).

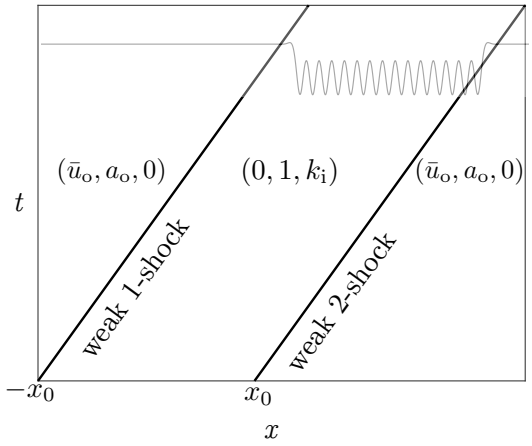

Figure 5.9: Double Whitham shock solution satisfying the jump conditions (5.7)–(5.9) from the interior periodic wave $(0, 1, k_{\rm i})$ to the outer solitary wave $(\overline{u}_{\rm o}, a_{\rm o}, 0)$. The shocks are identified by the solid black curves and the solution (shock structure) in physical space is shown in gray.

Utilizing the three Whitham shock loci in Table 5.2, the scaling symmetries (2.43) and (2.44), and double Whitham shock data (5.30), we compute homoclinic traveling wave profiles. The homoclinic traveling waves are periodic on the computational domain, and hence we observe their dynamic stability by solving the KdV5 equation (1.4) numerically using a pseudospectral Fourier discretization and time-integrating with fourth order Runge-Kutta. Solutions are initialized with band-limited noise to elucidate possible instabilities. Further details can be found in Appendix B. The time evolution of the perturbed homoclinic traveling wave solutions then allows us to corroborate our hypothesis that traveling waves comprised of modulationally (un)stable portions will be (un)stable. Indeed, in Fig. 5.10, we depict the evolution of three distinct homoclinic solutions with $n = 25$ oscillation periods. Note that our computational approach enables the construction of homoclinic solutions with any number of oscillation periods. The intermediate periodic wave in Fig. 5.10(b) lies on the Whitham shock locus ● in Table 5.2, which exhibits complex characteristic velocities. As we predict, the homoclinic traveling wave solution is unstable. In Figs. 5.10 (a) and (c),

the homoclinic oscillatory defect is comprised of periodic waves on the Whitham shock loci ▲ and ■ in Table 5.2, respectively, where the modulation equations are strictly hyperbolic. Perturbed homoclinic traveling waves are numerically stable over a long integration time.

These homoclinic traveling waves are similar to solutions obtained in the investigation of reversible Hamiltonian systems [21, 29], though we have presented an alternative approach by which multi-pulse solutions with an arbitrary number of peaks can be computed from the Whitham shock loci in Table 5.2.

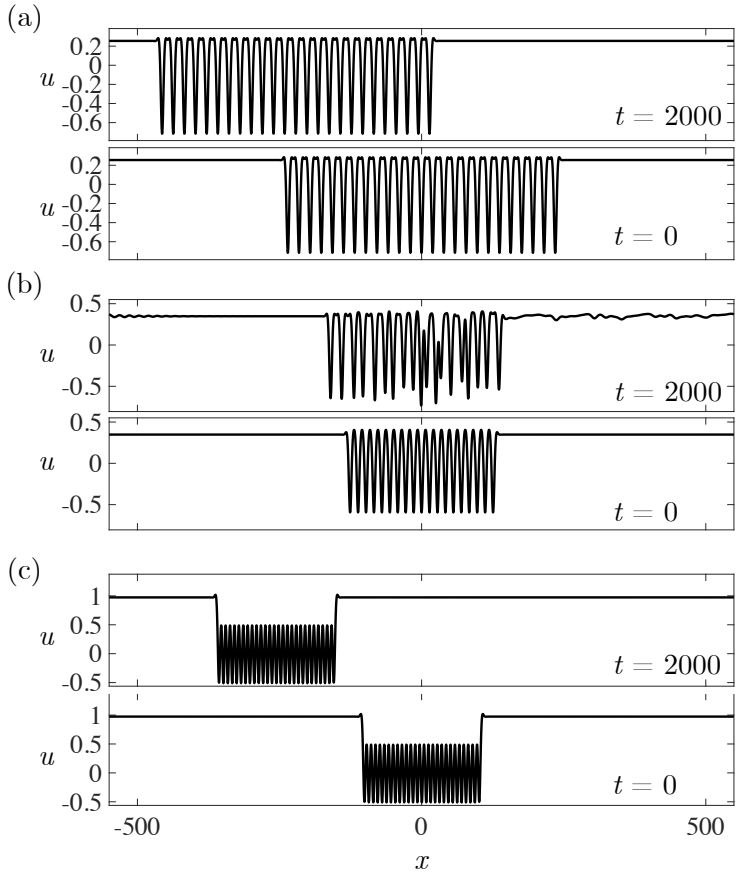

Figure 5.10: Evolution of perturbed homoclinic traveling wave solutions whose oscillatory parameters in Eq. (5.30) with $n = 25$ lie on the Whitham shock loci in Table 5.2. Initial data at $t = 0$ is evolved to $t = 2000$. (a) Double Whitham shocks ▲ in Table 5.2 with real characteristics. (b) Double Whitham shocks ● with complex characteristics. (c) Double Whitham shocks ■ with real characteristics.

Similarly, homoclinic traveling waves consisting of distinct inner and outer periodic

waves can be constructed from Whitham shock loci shown in Fig. 5.6. Numerical computations of initially perturbed homoclinic traveling waves of this type along with their long time evolution are displayed in Fig. 5.11, again revealing numerically stable evolution for those solutions with all real characteristic velocities—Fig. 5.11(a,d)—and numerically unstable evolution for those double Whitham shocks that exhibit complex characteristic velocities—Fig. 5.11(b,c).

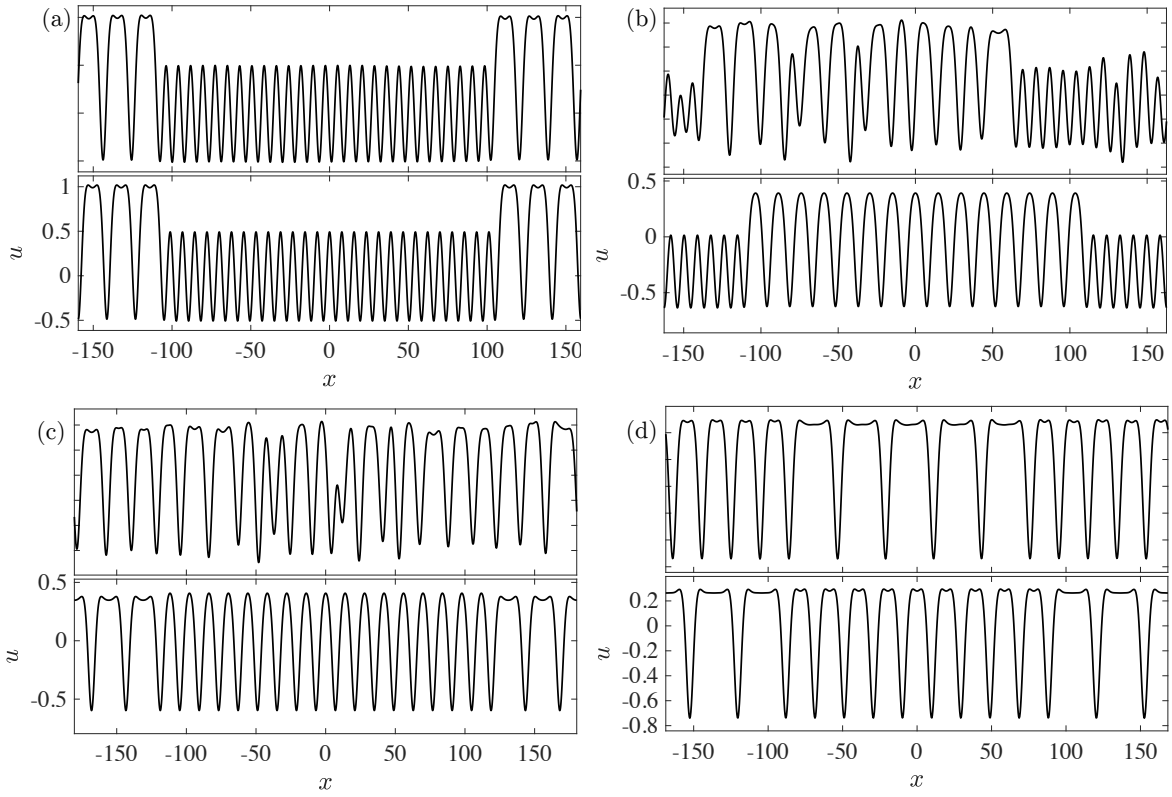

Figure 5.11: Evolution of perturbed traveling waves corresponding to co-propagating Whitham shocks shown at initial time $t = 0$ and final time $t = 1500$. Parameter values are selected from those depicted in Figure 5.6. (a) traveling wave with parameters in Fig. 5.6(a) with $\overline{u}_{\rm o} = \overline{u}_{-} = 0.6$. (b) traveling wave with parameters in Fig. 5.6(a) with $\overline{u}_{\rm o} = \overline{u}_{-} = -0.3$. (c) traveling wave with parameters in Fig. 5.6(c) with $\overline{u}_{\rm o} = \overline{u}_{-} = 0.15$. (d) traveling wave with parameters in Fig. 5.6(e) with $\overline{u}_{\rm o} = \overline{u}_{-} = 0.1$.

5.3 Conclusions

The fifth order KdV equation (1.4) is shown in this chapter to have a plethora of novel traveling wave solutions. The heteroclinic traveling wave solutions studied here consist of two periodic waves that co-propagate and transition between one another on a length scale comparable with the length scale of a single wave period. Utilizing the framework of Whitham modulation theory that describes the zero dispersion limit of nonlinear oscillatory wavetrains via the Whitham system of conservation laws, we establish that these heteroclinic traveling wave solutions limit to discontinuous shock solutions of the Whitham modulation equations, i.e., **Whitham shocks**. Despite the apparent contradiction of the use of the Whitham modulation equations to describe a rapid transition in periodic wave parameters, we argue that the shock solutions of the modulation equations describe the zero dispersion limit of the periodic wave solution of the governing differential equation.

Within this framework, we prove that a heteroclinic traveling wave solution of the KdV5 equation (1.4) connecting disparate periodic waves necessarily satisfies the Rankine-Hugoniot jump conditions of the Whitham equations in conservative form. The jump conditions reveal *admissible* Whitham shock loci—far-field periodic wave parameters that are then used as candidate traveling wave solutions of the governing PDE.

Numerical computations of the characteristic velocities in tandem with the novel traveling wave profiles allow us to specify the characteristic structure of Whitham shocks and deduce their stability. These computations reveal that, but for a negligibly small portion of parameter space, admissible Whitham shocks are undercompressive, i.e., each characteristic family passes through the shock and therefore violates the Lax entropy condition. The characteristic velocities of the modulation equations also reveal the stability of heteroclinic traveling wave solutions. Since the hyperbolicity of the Whitham modulation equations is a necessary condition for the stability of periodic solutions [16], the stability of traveling wave solutions considered in this manuscript are determined by the stability of the periodic

waves that constitute them, which can be readily checked by examining the Whitham shock velocities.

A prominent contributing feature to the emergence of novel heteroclinic traveling waves and admissible Whitham shocks found in this manuscript is the presence of higher order dispersive effects. In Chapter 6, we will provide numerical evidence of Whitham shocks in other systems by studying a nonlocal model for free-surface gravity-capillary water waves. To further analytically study these heteroclinic traveling waves connecting two far-field periodic waves, one promising route is to investigate integrable higher order nonlinear, dispersive systems [4] so that heteroclinic traveling waves may be understood in the context of the inverse scattering transform. For instance, the mathematical structure underlying these traveling waves could be elucidated though a detailed study of the Lax equation [135, 80]

$$u_t + 30u^2u_x + 20u_xu_{xx} + 10uu_{xxx} + u_{xxxxx} = 0, \tag{5.31}$$

an integrable equation with higher order dispersive terms.

Of related importance is the extensive literature describing spontaneous, localized pattern formation in **dissipative** systems, where the prototypical example is the Swift-Hohenberg equation that leads to a fourth order ODE for stationary solutions that resemble the ODE for traveling waves of the KdV5 equation [75, 23, 22, 12, 40]. Here, stationary solutions of the governing equation have been computed in which an equilibrium state spontaneously transitions to a localized periodic state and back to equilibrium, the stationary, dissipative analog of the homoclinic traveling waves limiting to double Whitham shocks computed here. The results have since been extended to consider steady solutions in which a large, localized periodic pattern persists on a small amplitude oscillatory background [76]. A promising avenue for further study is the consideration of modulation dynamics in the Swift-Hohenberg equation. Of course, the ensuing dynamics and stability of these solutions will differ from the dynamics studied here because the regularizing mechanisms in each case—dissipation or dispersion respectively—are wholly different. From this point of view,

traveling wave solutions occurring in higher order dispersive systems could serve as a bridge between conservative Hamiltonian systems and dissipative pattern forming systems.

Chapter 6

Applications and Extensions

In this chapter, we discuss applications of the work in this thesis , in particular leveraging the results presented in Chapter 5. Further reading from the results in this section are found in the manuscript [122].

We begin by revisiting the impetus for the investigation of Whitham shocks and construct the modulation solution for the TDSW solution of the KdV5 equation. We also reexamine the heteroclinic traveling wave portion of the TDSW solution of the Kawahara equation and compare the oscillatory wave's parameters to the values given by the jump conditions of the Kawahara-Whitham modulation equations. The jump conditions of the Kawahara-Whitham equations are in excellent agreement with numerical computations of heteroclinic traveling waves (see Section 4.1.2 and and Ref. [121]). This chapter concludes with numerical experiments simulating the Riemann problem for the Whitham equation [140, 139], which describes weakly nonlinear, fully dispersive gravity-capillary water waves.

6.1 Dam break problem for the KdV5-Whitham modulation equations: traveling dispersive shock waves revisited

In this section, we revisit the traveling DSW (TDSW) solution of the KdV5 equation (cf. Figures 1.6 and 5.1). The TDSW is identified by two distinct regions. At the left, trailing edge of the TDSW, there is a heteroclinic traveling wave corresponding to an admissible Whitham shock solution of the modulation equations, such as those discussed in Chapter 5.

The heteroclinic traveling wave terminates at a partial DSW described by a continuous, simple wave solution of the modulation equations (cf. Section 3.2.3) at the leading edge to the right. Since the modulated leading edge initiates from an oscillatory wavetrain, rather than a solitary wave, it is termed a partial DSW. Similar partial DSWs have been observed in the initial boundary value problem of nonlinear systems with lower order dispersion, though they arise from a forcing boundary [63, 99].

We restate the initial value problem whose solution is described by a Whitham shock-rarefaction modulation solution of the KdV5 equation (1.4) with unit step initial data (5.1)

$$u_t + uu_x + u_{xxxxx} = 0, \tag{1.4}$$

$$u(x,0) = \frac{\Delta}{2}\left[1 - \tanh\left(\frac{x}{w}\right)\right] \tag{6.1}$$

where we take the initial data with $\Delta = 1$ and width $w = 10$.

A direct numerical simulation of the unit step initial data (5.1) to (1.4) is shown in Fig. 6.1 where the solution is evolved to $t = 1000$ and we identify the two distinct regions of the solution. These regions are bounded by a line in the x-t plane with the inverse slopes

$V_{\rm s}$: The Whitham shock velocity corresponding to the velocity of the trailing heteroclinic traveling wave,

V_i: The intermediate velocity at which the partial DSW terminates into the oscillatory portion of the trailing heteroclinic traveling wave,

V_+: The velocity of the leading harmonic edge envelope where the TDSW terminates as the modulated wave amplitude.

We denote the parameters of the periodic portion of the heteroclinic wave by $(\overline{u}_{\rm i}, a_{\rm i}, k_{\rm i})$ and the leading harmonic wave edge wavenumber by k_+, then $V_i = \lambda_2(\overline{u}_{\rm i}, a_{\rm i}, k_{\rm i})$ and $V_+ = \lambda_2(0, 0, k_+)$, where λ_2 is defined in Eq. (3.30). The TDSW traveling wave portion bears a striking resemblance to the traveling wave that is identified by the symbol ■ in Fig. 5.2.

Since the Whitham shock locus for this solution in Table 5.2 is well approximated using a Stokes wave, we scale the solution using (2.43) and (2.44) so that the far-field mean values of the heteroclinic wave are $\overline{u}_- = 1$ and $\overline{u}_\mathrm{i}$ is a to-be-determined parameter. The intermediate periodic wave properties are then given as a one parameter family

$$a_\mathrm{i} = \frac{1}{\zeta}(1-\overline{u}_\mathrm{i}), \quad k_\mathrm{i}^4 = \left[\frac{4\zeta^2+3}{15} - \frac{1}{80\zeta^2}\right](1-\overline{u}_\mathrm{i}) \quad V_s = \left[\frac{1}{2} - \frac{1}{16\zeta^2}\right](1-\overline{u}_\mathrm{i}) + \overline{u}_\mathrm{i}, \quad (6.2)$$

where $\zeta \approx 0.9724$ is the positive square root of the largest, positive real root of the quartic polynomial (5.26), and $\overline{u}_\mathrm{i}$ is the mean to be determined by matching to a simple wave describing the transition from the oscillatory wavetrain to the leading, constant level, $\overline{u}_+ = 0$ propagating with velocity V_+. The computation of the simple wave can be acheived by casting the KdV5-Whitham modulation equations into an approximate Riemann invariant form (cf. Reference [64])

$$r_{1,t} + \lambda_i r_{1,x} = 0,$$

with $i = 1, 2, 3$. The Riemann invariants r_i, constant along their respective characteristics, λ_i are, to their leading order correction in amplitude

$$r_1 = \overline{u} - \frac{a^2}{80k^4} \qquad \lambda_1 = \overline{u}, \quad (6.3)$$

$$r_2 = \overline{u} - \frac{5}{4\sqrt{30}}a + \frac{5}{4}k^4 \qquad \lambda_2 = \overline{u} + 5k^4 - \sqrt{\frac{5}{24}}a, \quad (6.4)$$

$$r_3 = \overline{u} + \frac{5}{4\sqrt{30}}a + \frac{5}{4}k^4 \qquad \lambda_3 = \overline{u} + 5k^4 + \sqrt{\frac{5}{24}}a. \quad (6.5)$$

The modulated, leading periodic wave is approximated by a 2-wave curve of the modulation system, so that r_1 and r_3 remain constant giving the relations

$$\overline{u}_\mathrm{i} = \frac{a_\mathrm{i}^2}{80k_\mathrm{i}^4}, \quad k_+^4 = \overline{u}_\mathrm{i} + \frac{5}{4\sqrt{30}}a_\mathrm{i} + \frac{5}{4}k_\mathrm{i}^4,$$

so that the intermediate periodic wave parameters and the leading edge wavenumber are given *explicitly* in terms of the largest root, ζ, of the polynomial Eq. (5.26). The expansion

fan in the second characteristic that describes the leading, modulated periodic wave on the interval $V_{\rm i} \leq x/t \leq V_+$

$$r_2(x/t) = \begin{cases} \overline{u}_{\rm i} - \frac{5}{4\sqrt{30}} a_{\rm i} + \frac{5}{4} k_{\rm i}^4 & V_{\rm i} < x/t \\ \lambda_2^{-1}(x/t) & V_{\rm i} \leq x/t \leq V_+ \\ \frac{5}{4} k_+^4 & V_+ > x/t \end{cases},$$

We can determine the self-similar dynamics of the modulation variables by then solving $\mathbf{q} = \mathbf{q}(r_1, r_2(x,t), r_3)$.

The Whitham shock locus, 2-wave curve and the far-field mean values completely determine the Whitham shock-rarefaction modulation solution

$$(\overline{u}, a, k)(x,t) = \begin{cases} (1, a_-, 0) & V_{\rm s} t < x \\ (\overline{u}_{\rm i}, a_{\rm i}, k_{\rm i}) & V_{\rm s} t \leq x < V_{\rm i} t \\ \mathbf{q}(r_1, r_2(x,t), r_3) & V_{\rm i} t \leq x < V_+ t \\ (0, 0, k_+) & V_+ t \leq x \end{cases}.$$

This shock-rarefaction solution can be viewed as the higher dispersion analog of the shock-rarefaction solution for the shallow water dam break problem or the gas dynamics piston problem [86].

In Figure 6.1, we compare the Whitham shock-rarefaction solution of the modulation equations with numerical simulations of smoothed step initial data. Numerically extracted values of the modulation parameters exhibit excellent agreement with the Whitham shock-rarefaction modulation solution. The small oscillations in the modulation variables that occur along the intermediate equilibrium state are due to higher order dispersive effects that are not captured by leading order modulation theory.

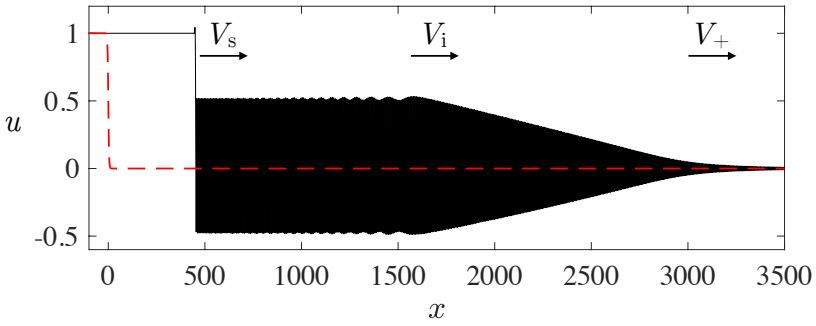

Figure 6.1: Direct numerical simulation the initial value problem (5.1) with smoothed step data (dashed red) at $t = 1000$ (solid black). Three distinct velocities V_s, V_i, and V_+ are identified.

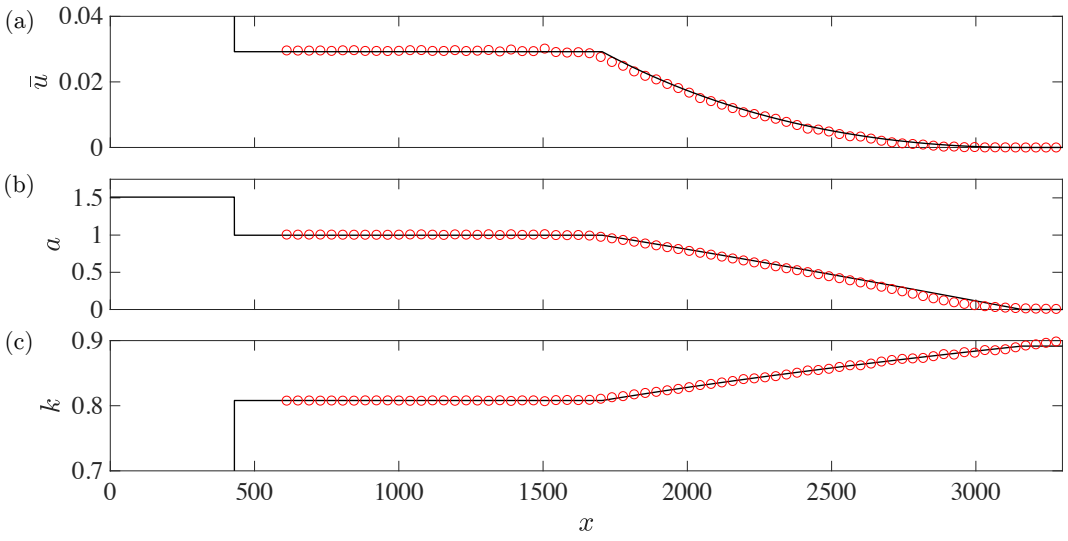

Figure 6.2: Extracted modulation parameters (a) mean, (b) amplitude, and (c) wavenumber extracted from numerical simulations of (5.1) (circles) with the shock-rarefaction solution of the Whitham modulation equations at $t = 1000$ (solid curves).

6.2 Traveling waves in gravity-capillary water waves

In this section, we consider two models of gravity-capillary water waves that incorporate higher order dispersive effects. We recall the linear dispersion relation for right-moving water waves on a constant, normalized depth with surface tension is given in nondimensional form

by

$$\begin{aligned}\omega(k) &= \sqrt{k(1+Bk^2)\tanh(k)},\\ &\sim k + \frac{1}{6}\left(B-\frac{1}{3}\right)k^3 + \frac{1}{360}\left(19-30B-45B^2\right)k^5 + \mathcal{O}(k^7).\end{aligned}$$

In this section, we are motivated by the physical problem in which B is sufficiently close to $1/3$, so that $B - 1/3 \sim k^2$ when $k \ll 1$ so that third and fifth order dispersion are in competition.

6.2.0.1 Kawahara equation

Let us now reexamine the heteroclinic traveling wave solutions of the Kawahara equation (1.3) computed in Section 4.1.2 that arise from the initial value problem (1.15) with Δ sufficiently large. Since the numerically computed traveling waves were indistinguishable from the TDSW trailing edge, we now compare the trailing heteroclinic traveling wave's parameters to values given by the Whitham shock loci of the modulation system. We will utilize the Stokes approximation so that calculations may be made explicit as in the previous section.

The Kawahara Whitham modulation equations (3.9)–(3.11) derived in Chapter 3 and are given here with the third order dispersion parameter $\sigma = +1$

$$\begin{aligned}(\overline{u})_t + \left(\frac{1}{2}\overline{\varphi^2}\right)_x &= 0,\\ \left(\frac{1}{2}\overline{\varphi^2}\right)_t + \left(\frac{1}{3}\overline{\varphi^3} - \frac{3}{2}k^2\overline{\varphi_\theta^2} + \frac{5}{2}k^4\overline{\varphi_{\theta\theta}^2}\right)_x &= 0,\\ k_t + (ck)_x &= 0,\end{aligned} \tag{6.6}$$

where $\varphi = \varphi(\theta)$ is a periodic, traveling wave solution to (1.3). Based on numerical computations in Chapter 4 and [121], we expect that a heteroclinic traveling wave solution exists whereby a solitary wave and periodic wave are connected and propagate with the same velocity. This heteroclinic traveling wave can therefore be described by a Whitham-shock solution

to Eqs. (6.6) with shock velocity $V = c_\pm$, the phase velocity of the left and right states. The Rankine-Hugoniot jump conditions are therefore given by

$$-V\overline{u}_- + \left(\frac{\overline{u}_-^2}{2} - \frac{1}{2}\overline{\varphi_+^2}\right) = 0, \tag{6.7}$$

$$-V\left(\overline{u}_-^2 - \overline{\varphi_+^2}\right) + \left(\frac{\overline{u}_-^3}{3} - \frac{1}{3}\overline{\varphi_+^3} + \frac{3}{2}k_+^2\overline{\varphi_{+,\theta}^2} - \frac{5}{2}k_+^4\overline{\varphi_{+,\theta\theta}^2}\right) = 0, \tag{6.8}$$

$$-Vk_+ + \omega_+ = 0. \tag{6.9}$$

Inserting the Stokes wave expansion (2.40) with nonlinear velocity (2.41)

$$\varphi_+ = \overline{u}_+ + \frac{a_+}{2}\cos\theta + \frac{a_+^2}{48k_+^2\left(1-5k_+^2\right)}\cos 2\theta,$$
$$V = c_+ = \overline{u}_+ - k_+^2 + k_+^4 - \frac{a_+^2}{96k_+^2\left(5k_+^2-1\right)},$$

for the leading periodic wave (see Appendix A for the derivation) into the jump conditions (6.7)–(6.9), we then solve the algebraic system

$$-V\overline{u}_- + \left(\frac{\overline{u}_-^2}{2} - \frac{a_+^2}{4}\right) = 0,$$
$$-\frac{V}{2}\left(\frac{\overline{u}_-^2}{2} - \frac{a^2}{4}\right) + \left(\frac{\overline{u}_-^3}{3} + \frac{3}{4}k_+^2a_+^2 - \frac{5}{4}k_+^4a_+^2\right) = 0,$$
$$-Vk_+ + \left(\overline{u}_+k_+ - k_+^3 + k_+^5 - \frac{a_+^2}{96k_+\left(5k_+^2-1\right)}\right) = 0,$$

numerically for a fixed value of $\overline{u}_- = \Delta$ and the ensuing wave parameters are then compared to numerical computations of heteroclinic traveling waves (cf. Figure 4.7). In Figure 6.3, we compare the periodic wave parameter values from the jump conditions and those obtained from numerical computations of heteroclinic traveling waves using Matlab's bvp5c that were presented in Chapter 4.

Since we are using the Stokes approximation for the leading periodic wave, we only expect agreement with numerical simulations for sufficiently small wave amplitude. However, the results depicted in Fig. 6.3 demonstrate that even for quite large values of a_+, the Stokes approximation remains very accurate. Notice further that the numerical computations of

traveling waves, whose parameters are depicted by the red dots, cease for $\Delta \lesssim 0.58$, the observed cutoff for the numerical existence of the traveling wave solution (cf. Chapter 4 or Ref. [121]). Here, numerical fixed point computations of traveling waves do not converge, yet the Whitham shock locus continues well past this point. We interpret these computations as evidence of **inadmissible Whitham shocks** for the Kawahara equation. The mere existence of a Whitham shock is not a sufficient condition to guarantee the existence of a traveling wave solution.

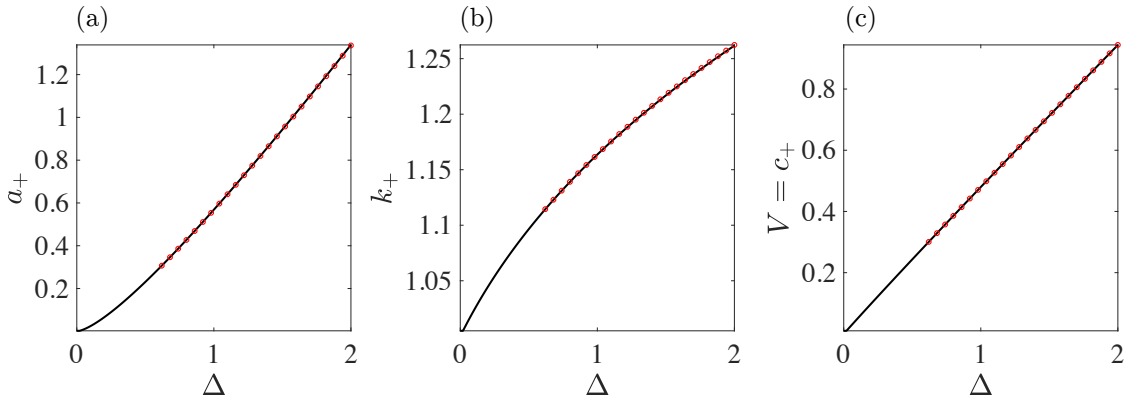

Figure 6.3: (a)-(c)Traveling wave parameter values, a_+, k_+ and V, respectively from computations of the jump conditions (6.7)–(6.9) (solid, black curves) compared against numerical computations of traveling waves from [121] (red circles).

6.2.0.2 Gravity-capillary Whitham equation

In 1967, Whitham proposed a model equation that captures the full dispersive properties of a physical system via a convolution term [139]. The so-called Whitham equation takes the form

$$u_t + uu_x + \mathcal{K} * u_x = 0, \tag{6.10}$$
$$\mathcal{K} = \frac{1}{2\pi}\int_{\mathbb{R}} c(k)e^{ikx}dk,$$

where $c(k)$ is the phase velocity. The equation (6.10) is a model for unidirectional right-moving gravity-capillary water waves if we let $c(k) = \sqrt{\frac{(1+Bk^2)\tanh k}{k}}$ (cf. Eq. (2.27)).

Solutions similar to those appearing in the KdV5 equation (1.4) and the Kawahara equation (1.3) are expected to also persist for the Whitham equation when the Bond number B, is sufficiently close to $1/3$ because a small wavenumber expansion of the water wave dispersion relation (2.28) reveals that third and fifth order dispersion are in balance (recall Section 2.1.4.1). We revisit our original motivation for investigating traveling wave solutions to the KdV5 equation (1.4) by conducting direct numerical simulations of the smoothed, step-like initial data (5.1) with $\Delta = 0.25$ and $w = 20$. The results of the simulations at $t = 2000$ are shown in Figure 6.4 for different values of the Bond number, B. The simulations indicate that for B near $1/3$ (e.g., $0.3 \leq B \leq 0.375$), where third order dispersion is weak, familiar TDSW-looking dynamics emerge (cf. Fig. 5.1). The trailing edge resembles a nearly uniform traveling wave and the leading portion resembles a partial DSW terminating into the intermediate nonlinear wavetrain. These numerical simulations suggest that the Whitham shocks described in this manuscript are, in fact, quite general. With that being said, the numerical simulations depicted in Figure 6.4 for $B = 0.4$ and $B = 0.425$ no longer resemble TDSWs; instead they look like classical, convex, KdV-like DSWs. In this regime lower order dispersion dominates, preventing the higher order dispersive balance that appears to be needed for the existence of admissible Whitham shocks. A future avenue of research will be to understand the transition from solutions discussed throughout this manuscript to the classical convex, KdV-type DSW solutions arising from step initial data.

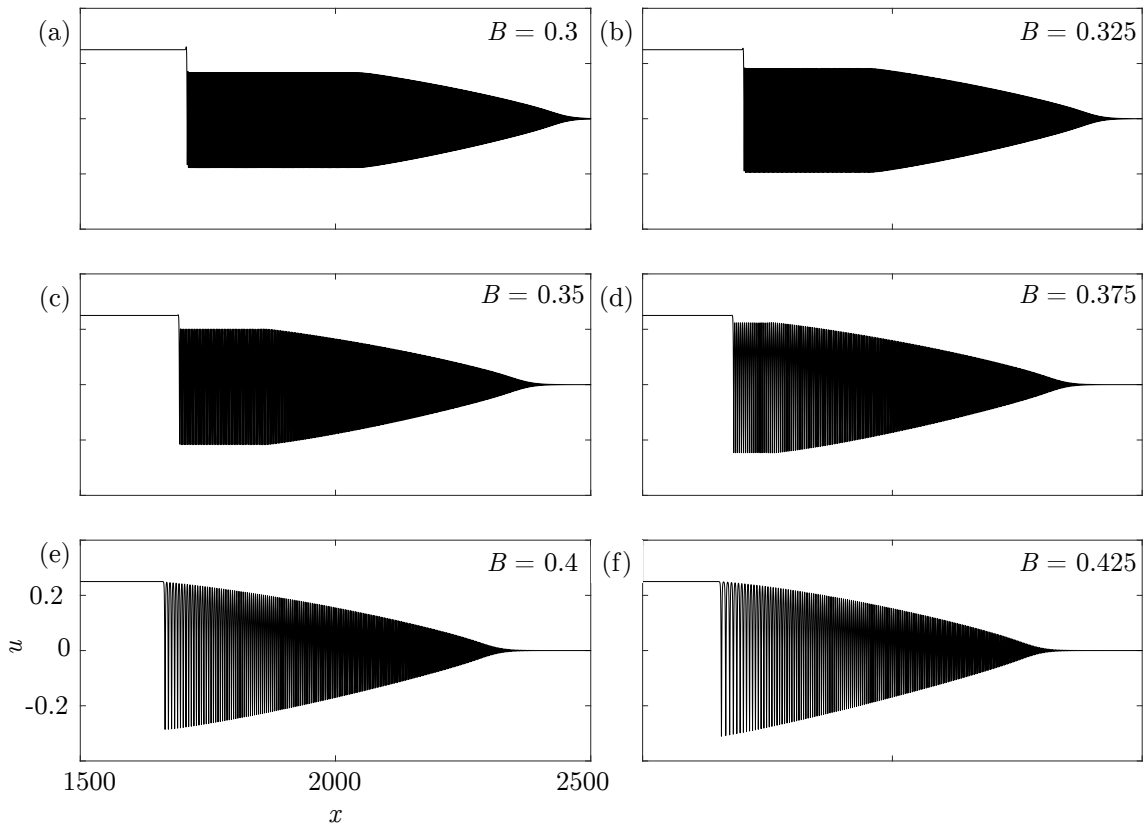

Figure 6.4: Solutions arising from step-like initial data (5.10) for the Whitham equation (6.10) matching the phase velocity, $c(k)$ for linear gravity-capillary water waves. The initial step has an amplitude of $\Delta = 0.25$ at $x = 0$ and the simulations are shown on the same axes at $t = 2000$ for various Bond numbers, B, specified in each subfigure.

Chapter 7

Hydrodynamic optical soliton tunneling

In this chapter, we shift focus and discuss the interaction of a solitary wave with an evolving potential using the Nonlinear Schrödinger equation as the model system based on the manuscript [123].

7.1 Background

The tunneling of wavepackets incident upon a potential barrier is a defining quantum mechanical property [79]. The linear phenomenon can be extended to nonlinear solitonic wavepackets or solitons–localized, unchanging waveforms in which nonlinear and dispersive effects are in balance. In the original consideration of a soliton incident upon a potential barrier, it was found that the soliton can losslessly pass, or tunnel, through a localized repulsive or attractive potential [104]. The connection of this so-called soliton tunneling with quantum mechanical tunneling was established in an optical setting in [116] where a bright optical pulse propagating in an optical fiber with anomalous dispersion was transmitted through a localized defective region of normal dispersion–the analog of a potential barrier.

Soliton tunneling has been studied theoretically in some detail in recent years in various physical systems including optical media [7, 147, 134, 144], nematic liquid crystals [8, 106] and matter waves in Bose-Einstein condensates (BEC) [114, 90]. Recent experiments observed the nonlinear analogs of some linear quantum features including nonlinear scattering [89], reflection and ejection [11] and soliton tunneling [101]. In a related vein, analogies between

soliton tunneling and other physical effects were considered in [13, 115, 117].

In the focusing (anomalous dispersion) regime, nonlinear optical plane wave propagation is subject to modulational instability with respect to long wavelength perturbations [146]. In contrast, plane wave propagation in the normal dispersion (defocusing) regime is stable and, remarkably, exhibits many features characteristic of fluid motion [28]. The dispersive effects in such a "fluid of light" are due to diffractive or chromatic properties of the medium. The dispersive hydrodynamic behavior of light propagation has been considered and observed in a number of works, see, e.g., [133, 53, 142].

Robust features of the diffraction of laser light in a nonlinear, defocusing medium and matter waves in a repulsive BEC include dark solitons, which are moving depression waves whose width is proportional to the coherence length l of the medium. In addition to solitons, DSWs also persist in optical systems [47]. Optical DSWs have been observed in both bulk media [133] and optical fibers [35]. While the DSW oscillatory length scale is also the medium's microscopic coherence length l, DSWs exhibit expanding, rank-ordered oscillations spanning a larger, macroscopic coherence length scale L, which increases with time. The latter length scale also characterizes non-oscillatory hydrodynamic flows such as expansion or rarefaction waves (RWs) and compressive Riemann waves that have recently been observed in optical fibers in the context of wavebreaking control [137]. The scale separation $l \ll L$, a natural characterization of dispersive hydrodynamics [19], enables a mathematical description of DSWs via nonlinear wave, Whitham averaging [140, 47], while RWs are described by the long-wave, dispersionless limit of the original equations.

Despite the fact that solitons, RWs and DSWs are well known, fundamental features of dispersive media, soliton-RW and soliton-DSW interactions, have been mostly overlooked. As we show, these interactions motivate an alternative notion of optical tunneling whereby a dark soliton incident upon a spatially extended hydrodynamic barrier in the form of a DSW or a RW can penetrate through to the other side of the evolving hydrodynamic structure. Thus, in contrast to the traditional notion of soliton tunneling through an externally

imposed barrier, hydrodynamic soliton tunneling corresponds to the full penetration and emergence of the soliton through an intrinsic hydrodynamic state that evolves **according to the same equation as the soliton**. This generalizes the understanding of a soliton as a coherent, particle-like entity that can interact elastically with other solitons [145] and dispersive radiation [2] to one that can also interact with nonlinear hydrodynamic states and emerge intact, i.e., without fissioning or radiation, albeit with a different amplitude that results from a change in the background mean flow.

In this section, we study the tunneling of solitons through hydrodynamic states within the framework of the integrable, defocusing nonlinear Schrödinger (NLS) equation, which is an accurate model for nonlinear light propagation in single mode optical fibers with normal dispersion [20]. We invoke the scale separation $l \ll L$ inherent to Whitham modulation theory in order to derive a system of asymptotic equations that describe the interaction between narrow dark solitons and evolving, broad hydrodynamic barriers. We obtain the conditions on the incident soliton amplitude and hydrodynamic mean flow density and velocity for tunneling. One of the fundamental properties of hydrodynamic soliton tunneling is **hydrodynamic reciprocity** whereby the tunneling through RWs and DSWs is described by the same set of conditions in spite of the very different interaction dynamics. This general property of solitonic hydrodynamics has been recently formulated for scalar models and experimentally confirmed for a fluid system [93]. We also show that tunneling is not always possible and that the soliton can be absorbed or trapped within the hydrodynamic flow. Moreover, we find that soliton interaction with hydrodynamic states can lead to reversal of the soliton's propagation direction and spontaneous soliton cavitation.

The particular case of optical hydrodynamic soliton tunneling considered here could be observed, for example, within the experimental setting described in [142] for the generation of DSWs and RWs in optical fibers.

7.2 Problem formulation

We consider the defocusing NLS equation

$$i\psi_t = -\frac{1}{2}\psi_{xx} + |\psi|^2\psi, \tag{7.1}$$

where in the context of fiber optic propagation, t is the longitudinal coordinate in the fiber, x is the retarded time, and $\psi(x,t)$ is the complex-valued, slowly-varying envelope of the electric field. All variables are nondimensionalized to their typical values. See, e.g., [142] for a detailed description of NLS normalizations and typical values of physical parameters pertinent to the regimes considered here.

Equation (7.1) can be written in dispersive hydrodynamic form via the transformation $\psi = \sqrt{\rho}e^{i\phi}$, $u = \phi_x$

$$\begin{aligned} \rho_t + (\rho u)_x &= 0, \\ u_t + uu_x + \rho_x &= \left(\frac{\rho_{xx}}{4\rho} - \frac{\rho_x^2}{8\rho^2}\right)_x, \end{aligned} \tag{7.2}$$

where ρ is the optical power and u is the chirp. In terms of the hydrodynamic interpretation of these quantities, we will refer to ρ as a mass density and u as a flow velocity (see, e.g., [47]). Within this setting, the normalized coherence length is $l = \rho_0^{-1/2}$ where ρ_0 is a typical density scale. The coherence length is an intrinsic scale that, along with the coherence time $\tau = \rho_0^{-1}$, corresponds to a scaling invariance of the hydrodynamic equations (7.2). In BECs, l is known as the healing length [109].

Equations (7.2) admit the localized, dark soliton solution

$$\begin{aligned} \rho(x,t) &= \overline{\rho} - a\,\mathrm{sech}^2[\sqrt{a}(x - ct - x_0)], \\ u(x,t) &= \overline{u} \pm \sqrt{\overline{\rho} - a}[1 - \overline{\rho}/\rho(x,t)], \end{aligned} \tag{7.3}$$

where a is the maximum deviation from the mean density $\overline{\rho}$, $\overline{u}$ is the mean flow velocity, and $c = \overline{u} \pm \sqrt{\overline{\rho} - a}$ is the soliton amplitude-speed relation. The $\pm$ in (7.3) is due to the bi-directional nature of the NLS equation as a dispersive hydrodynamic system (7.2). When

$a = \overline{\rho}$, the soliton is called a black soliton because its minimum is a zero density, cavitation point.

The typical tunneling problem consists of a soliton incident on a fixed potential barrier, either due to a change in the medium or an external effect. However, the spatiotemporal barriers considered here evolve according to the same equation that describes the dynamics of the medium. For an optical fiber with homogeneous, normal dispersion, this corresponds to a time-dependent input signal that results in both a soliton and a large-scale barrier. We assume that the hydrodynamic mean flow $(\overline{\rho}, \overline{u})$ that develops from the initial data varies on much longer length and time scales $L \gg l$, $T \gg \tau$, respectively. Due to the slow evolution of the mean flow, this is the regime in which Whitham modulation theory is operable. We will now briefly derive the NLS-Whitham modulation equations.

7.2.1 NLS-Whitham modulation equations

To describe how the mean flow couples to the soliton amplitude during the interaction, we utilize Whitham modulation theory [140]. To apply Whitham modulation theory, we first derive a periodic solution to (7.2), by seeking a solution of the form

$$\rho(x,t) = \rho(\xi), \tag{7.4}$$

$$u(x,t) = u(\xi), \qquad \xi = x - ct \tag{7.5}$$

Inserting into the hydrodynamic system (7.2) we obtain the system of ordinary differential equations

$$-c\rho' + (\rho u)' = 0, \tag{7.6}$$

$$-cu' + uu' + \rho' = \left(\frac{\rho''}{4\rho} - \frac{(\rho')^2}{8\rho}\right)', \tag{7.7}$$

where $'$ denotes differentiation with respect to ξ. Integrating equation (7.6) with respect to ξ results in

$$u = c + \frac{c_1}{\rho}, \tag{7.8}$$

where c_1 is a constant of integration. Inserting this expression into Eq. (7.7) and integrating once more gives

$$-\frac{c}{2}+c_2+\frac{c_1^2}{2\rho^2}+\rho+\frac{(\rho')^2}{8\rho^2}-\frac{\rho''}{4\rho}=0, \tag{7.9}$$

where c_2 is a constant of integration. An integrating factor for the ODE (7.9) is ρ', which can be utilized to integrate once more. Integrating and simplifying we find a first order differential equation for ρ

$$\begin{aligned}(\rho')^2 &= 4\rho^3+\left(8c_2-4c^2\right)\rho^2+8c_3\rho-4c_1^2,\\ &= 4(\rho-\lambda_1)(\rho-\lambda_2)(\rho-\lambda_3),\end{aligned} \tag{7.10}$$

where c_3 is the final constant of integration and the cubic is simplified by factoring with roots $\lambda_1\le\lambda_2\le\lambda_3$. Equation (7.10) is solved in terms of Jacobi elliptic functions [24]

$$\rho=\lambda_1+(\lambda_2-\lambda_1)\mathrm{sn}^2\left(\sqrt{\lambda_3-\lambda_1}\xi,m\right) \tag{7.11}$$

$$u=c\pm\frac{\sqrt{\lambda_1\lambda_2\lambda_3}}{\rho},\qquad m=\frac{\lambda_2-\lambda_1}{\lambda_3-\lambda_1}. \tag{7.12}$$

For the NLS-Whitham modulation equations, it is useful to express the periodic solution in terms of the parameters $r_1\le r_2\le r_3\le r_4$ such that [47]

$$\rho=\frac{1}{4}(r_4-r_3-r_2+r_1)^2+(r_4-r_3)(r_2-r_1)\mathrm{sn}\left(\sqrt{(r_4-r_2)(r_3-r_1)}\xi;m\right), \tag{7.13}$$

$$u=c-\frac{\mathcal{C}}{\rho},\qquad m=\frac{(r_2-r_1)(r_4-r_3)}{(r_4-r_2)(r_3-r_1)} \tag{7.14}$$

where

$$c=\frac{1}{2}\left(r_1+r_2+r_3+r_4\right),$$

and

$$\mathcal{C}=\frac{1}{8}\left(-r_1-r_2+r_3+r_4\right)\left(-r_1+r_2-r_3+r_4\right)\left(r_1-r_2-r_3+r_4\right).$$

The NLS modulation equations can be derived via methods similar to those in Chapter 3, though they consist of a system of the four variables r_1,r_2,r_3,r_4. The parameters r_i form

a vector of **Riemann invariants** so that the NLS-Whitham modulation equations are a system of four equations that can be written in diagonal form [105, 50, 71, 47]

$$\frac{\partial r_i}{\partial t} + V_i(\mathbf{r})\frac{\partial r_i}{\partial x} = 0, \quad i = 1, \ldots, 4. \tag{7.15}$$

The Riemann invariants $\mathbf{r}$ vary on the much larger spatiotemporal scales L and T than the scales l and τ of the soliton (7.3). The characteristic velocities are

$$V_1 = \frac{1}{2}\sum_{i=1}^{4} r_i + \frac{(r_1 - r_2)(r_1 - r_4)}{(r_1 - r_4) + (r_4 - r_2)\mu(m)} \tag{7.16}$$

$$V_2 = \frac{1}{2}\sum_{i=1}^{4} r_i + \frac{(r_1 - r_2)(r_2 - r_3)}{(r_3 - r_2) + (r_1 - r_3)\mu(m)} \tag{7.17}$$

$$V_3 = \frac{1}{2}\sum_{i=1}^{4} r_i + \frac{(r_2 - r_3)(r_3 - r_4)}{(r_2 - r_3) + (r_4 - r_2)\mu(m)} \tag{7.18}$$

$$V_4 = \frac{1}{2}\sum_{i=1}^{4} r_i + \frac{(r_1 - r_4)(r_4 - r_3)}{(r_1 - r_4) + (r_3 - r_1)\mu(m)}, \tag{7.19}$$

where $\mu = \frac{E(m)}{K(m)}$ and $K(m)$ and $E(m)$ are the complete elliptic integrals of the first and second kind, respectively. The characteristic velocities exhibit the ordering $V_i \leq V_j$ if $1 \leq i \leq j \leq 4$. The wavelength, L and amplitude a of the periodic wave are given by

$$L = \frac{2K(m)}{\sqrt{(r_4 - r_2)(r_3 - r_1)}}, \tag{7.20}$$

$$a = (r_2 - r_1)(r_4 - r_3). \tag{7.21}$$

7.2.2 Hydrodynamic soliton tunneling: setup

We consider the problem of a dark soliton (7.3) incident upon a barrier that evolves from step initial data in the mean flow $\overline{\rho}(x,0)$, $\overline{u}(x,0)$, where

$$\overline{\rho}(x,0) = \begin{cases} \overline{\rho}_- & x < 0 \\ \overline{\rho}_+ & x > 0 \end{cases}, \quad \overline{u}(x,0) = \begin{cases} \overline{u}_- & x < 0 \\ \overline{u}_+ & x > 0 \end{cases}. \tag{7.22}$$

As we will show, the long-time evolution of soliton-hydrodynamic barrier interaction is determined by the far-field flow conditions $\overline{\rho}_{\pm}$ and $\overline{u}_{\pm}$. Therefore, our theory generalizes to soliton tunneling through arbitrary hydrodynamic barriers with given far-field conditions.

The step initial conditions (7.22) generally evolve into a combination of two waves: RWs and/or DSWs each characterized by a simple-wave locus of the dispersionless limit of the system (7.2) [46, 47]. This is equivalent to the Whitham system (7.15) with $r_2 = r_3 = 0$. Therefore, we shall be imposing a simple-wave constraint on the initial mean flow data (7.22), i.e., we assume that either r_1 or r_4 is constant across $x = 0$ so that the mean flow will evolve into a single expanding hydrodynamic wave, either a RW or a DSW. Due to the bi-directional nature of the NLS equation, there are four distinct configurations, defined by the direction of the jump (up or down) of the Riemann invariant r_1 or r_4 across $x = 0$. We will focus on the two cases that result in a RW or a DSW when r_1 is constant. These two configurations along with an incident dark soliton moving to the left or right define four basic cases of hydrodynamic soliton tunneling considered here and shown in Fig. 7.1.

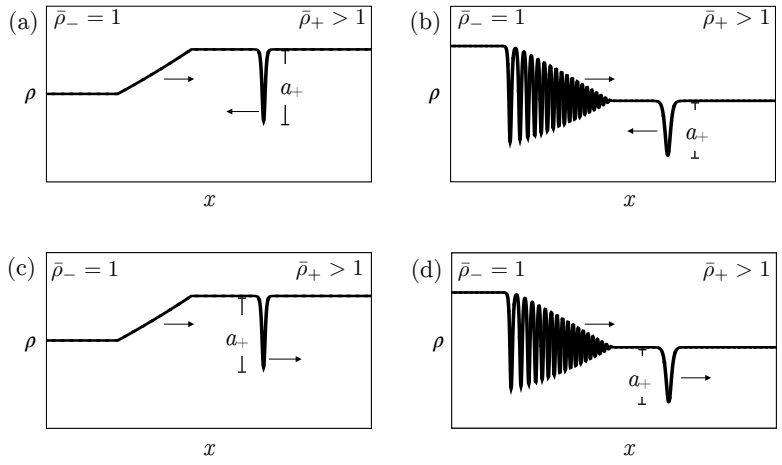

Figure 7.1: Hydrodynamic soliton tunneling configurations. (a) soliton-RW collision (b) soliton-DSW collision (c) RW overtaking soliton (d) DSW overtaking soliton.

The RW and DSW depicted in Fig. 7.1 are referred to as a 4-RW and a 4-DSW,

respectively because their characteristic wave speeds degenerate to the *fastest* long wave speed $\overline{u}_0 + \sqrt{\overline{\rho}_0}$ when $\overline{\rho}_+, \overline{\rho}_- \to \overline{\rho}_0$, $\overline{u}_+, \overline{u}_- \to \overline{u}_0$. The other two cases where $r_4(x,0)$ is constant correspond to a 1-RW or a 1-DSW because their speeds degenerate to the slowest long wave speed $\overline{u}_0 - \sqrt{\overline{\rho}_0}$. These 1-waves can be obtained from the 4-waves considered here with the reflection invariance $x \to -x$, $u \to -u$ of Eqs. (7.2).

Soliton-mean field interaction is described by the soliton limit of the NLS-Whitham Eqs. (7.15), which is achieved when $r_2 = r_3$ (see, e.g., [47]). By analyzing the expressions (7.16)–(7.19) for the characteristic velocities in the soliton limit $r_2 = r_3$, it is possible to establish that the limiting modulation system consists of shallow water equations [86]

$$\begin{aligned} \overline{r}_t + \frac{1}{2}\left(3\overline{r} + \overline{s}\right)_x = 0, \\ \overline{s}_t + \frac{1}{2}\left(\overline{r} + 3\overline{s}\right)_x = 0, \end{aligned} \tag{7.23}$$

where $\overline{s} = r_4$, $\overline{r} = r_1$ and the equation for the merged Riemann invariant r_3 is [47]

$$r_{3,t} + \frac{1}{2}(\overline{r} + 2r_3 + \overline{s})r_{3,x} = 0, \tag{7.24}$$

with

$$r_3 = \bar{u}/2 \pm \sqrt{\overline{\rho} - a}, \tag{7.25}$$

where the two signs are due to bi-directionality (cf., the second formula in Eq. (7.3)) and a is the soliton amplitude.

Eq. (7.24) is therefore the equation for the soliton amplitude $a(x,t)$. Crucially for our consideration, the soliton amplitude here is a spatiotemporal *field*, satisfying a PDE, while in standard soliton perturbation theories [74], the soliton amplitude has only a temporal dependence that satisfies an ODE along the soliton trajectory. The trajectory and dynamics of a single soliton from the amplitude field can be interpreted as the introduction of a fictitious train of non-interacting solitons of the same amplitude and some small wavenumber $0 < k \ll 1$, which necessarily satisfies the wave conservation equation

$$k_t + (ck)_x = 0, \tag{7.26}$$

with $c = \frac{1}{2}(\overline{r} + 2r_3 + \overline{s})$, the soliton amplitude-speed relation. Using the limiting system (7.23), (7.24), the wave conservation equation (7.26) can be written in diagonal, Riemann invariant form if we assume that r_3 is constant

$$\begin{aligned} (kp)_t + c\,(kp)_x &= 0, \\ p = \exp\left(-\int_{\overline{s}_0}^{\overline{s}} \frac{\frac{dc_s}{d\overline{s}}}{\frac{1}{2}(\overline{r} + 3s) - c} ds \right), \end{aligned} \tag{7.27}$$

where $\overline{s}_0$ is some fixed reference value, e.g., $\overline{s}_-$.

Thus, the initial conditions (7.22) for the hydrodynamic barrier should be complemented by similar conditions for the soliton amplitude field and the small wavenumber,

$$a(x,0) = \begin{cases} a_- & x < 0 \\ \\ a_+ & x > 0 \end{cases}, \quad k(x,0) = \begin{cases} k_- & x < 0 \\ \\ k_+ & x > 0 \end{cases}, \tag{7.28}$$

where only the incident amplitude a_+ is given at the onset (recall the configurations in Fig. 7.1). The soliton-hydrodynamic wave interaction now takes the form of a **generalized Riemann problem**. However, here we only consider continuous solutions to the initial value problem, so the shock solutions discussed in previous chapters are not at play.

The hydrodynamic soliton tunneling problem then consists of finding (i) the transmitted soliton amplitude a_- and (ii) the stretching (contraction) coefficient k_+/k_- for the soliton train that determines the soliton phase shift due to tunneling.

Concluding this section, we note that the long wave limit of the Whitham equations demonstrates that while the soliton amplitude is coupled to the evolving mean flow, the mean flow itself evolves **independently** of additional localized nonlinear waves.

7.3 Hydrodynamic soliton tunneling: results

We shall consider the basic tunneling configurations depicted in Fig. 7.1, which are defined by constancy of one of the hydrodynamic Riemann invariants $\overline{r}, \overline{s}$ in the step initial

data (7.22). Without loss of generality, one can choose $(\overline{\rho}_-, \overline{u}_-) = (1, 0)$, the remaining configurations can be deduced from scaling, Galilean shifts, and reflection symmetries associated with Eq. (7.1).

We note that, given step initial conditions, the hydrodynamic system (7.23) is valid only if the resulting wave is a RW. This implies that the reduced single-phase modulation system (7.23), (7.24), (7.27) describes only soliton-RW interactions (cases (a) and (c) in Fig. 7.1). Indeed, soliton DSW interaction is more complicated and generally requires consideration of two-phase NLS modulation equations [50]. Remarkably, however, we will show that the soliton-DSW tunneling conditions for cases (b) and (d) can be found from the soliton-RW tunneling conditions via **hydrodynamic reciprocity** [93, 123].

Let us assume that $\overline{r}(x, 0)$ has no jump across $x = 0$ and the jump in $\overline{s}(x, 0)$ resolves into a RW. The modulation equations (7.23), (7.24), (7.27) with step initial conditions for $\overline{s}$, r_3 and kp found from (7.22), (7.28) imply the simple wave solution in which $\overline{r} = r_1$, r_3, and kp are constant for all (x, t) but $\overline{s} = r_4$ is varying in a self-similar fashion, $\overline{s} = \overline{s}(x/t)$. This 4-wave modulation solution describes the hydrodynamic tunneling configurations (a) and (c) in Fig. 7.1. An example 4-wave evolution is shown in Fig. 7.2.

The tunneling problem now essentially reduces to finding the constant values of r_3 and kp given the constant value of

$$\overline{r} = \overline{u}_+/2 - \sqrt{\overline{\rho}_+} = \overline{u}_-/2 - \sqrt{\overline{\rho}_-} = -1,$$

and the initial jump for $\overline{s}$ found from (7.22) so that the Riemann invariants resemble those in Fig. 7.2. The solution for $\overline{s}(x/t)$ will then define the soliton trajectory through a hydrodynamic RW barrier.

The requirement of constancy of r_3 defined by Eq. (7.25) when evaluated with (7.22) and (7.28) yields a simple algebraic expression for the transmitted soliton amplitude through a RW

$$a_- = a_+ - 2(\sqrt{\rho_+} \pm \sqrt{\overline{\rho}_+ - a_+})(\sqrt{\rho_+} - 1). \tag{7.29}$$

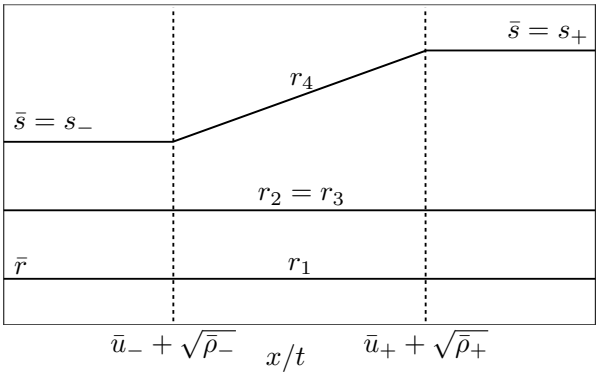

Figure 7.2: Hydrodynamic soliton tunneling configuration of the Riemann invariants for soliton-RW interactions.

Importantly, tunneling through the hydrodynamic barrier requires $0 < a_- \leq 1$. The $\pm$ in Eq. (7.29) corresponds to the two branches of r_3 with "$-$" corresponding to the collision case depicted in Fig. 7.1(a) and "$+$" the overtaking case depicted in Fig. 7.1(c). The transmitted, or tunneled, soliton amplitude-speed relation is then

$$\begin{aligned} c_- &= \pm\sqrt{1 - a_-} \\ &= \frac{1}{2}\left(\overline{r} + r_3 + \overline{s}_-\right), \end{aligned} \tag{7.30}$$

with a_- given by Eq. (7.29). The expression for the soliton velocity c_- in terms of Riemann invariants is a convenient representation that inherently incorporates the appropriate sign $\pm$. We shall also explore implications of constancy of kp.

The formulae (7.29) and (7.30), in spite of their simplicity, exhibit a number of remarkable implications. These include soliton tunneling, soliton trapping, the spontaneous emergence of a cavitation point, and soliton direction reversal. Furthermore, the obtained conditions incorporate the fundamental notion of hydrodynamic reciprocity established for uni-directional systems of the Korteweg-de Vries (KdV) type in [93]. This states that the tunneling conditions **are the same for both the RW and DSW**. This concept enables the application of Eqs. (7.29) and (7.30) to soliton-DSW interaction.

To extend the reciprocity result of [93] to the hydrodynamic optical tunneling con-

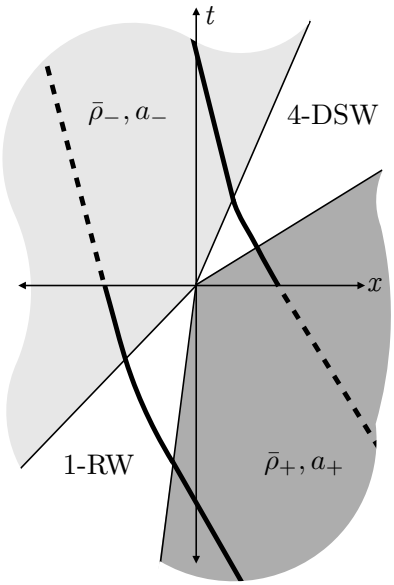

Figure 7.3: Time reversibility of initial data $(\overline{\rho}_+, a_+)$ and $(\overline{\rho}_-, a_+)$ with $\overline{\rho}_+ < \overline{\rho}_-$. Forward temporal evolution results in soliton interaction with a 4-DSW (upper half plane) and backward evolution results in soliton interaction with a 1-RW. Soliton trajectories are depicted with solid and dashed curves.

sidered here, we consider a general case where the left background state is $(\overline{\rho}_-, \overline{u}_-)$ (not necessarily $(1, 0)$) and take either $\overline{r}(x, 0)$ or $\overline{s}(x, 0)$ constant. This generalization will require consideration of both branches of r_3 in Eq. (7.25) and in the tunneling condition (7.29). Hydrodynamic reciprocity ultimately results from the time and space reversibility of the NLS equation (7.1).

We first consider the soliton-DSW interaction case where $\overline{\rho}_- > \overline{\rho}_+$ so that the DSW is known as a 4-DSW [47]. The soliton is initially located to the right of the DSW so that the hydrodynamic transition across the DSW satisfies a 4-wave modulation curve in which $\overline{r} = r_1 = const$ (see [46, 47]) and thus

$$\overline{u}_- - \overline{u}_+ = 2(\sqrt{\overline{\rho}_-} - \sqrt{\overline{\rho}_+}). \tag{7.31}$$

The nonlinear superposition of a soliton and a DSW can be achieved by considering the modulation of two-phase (quasi-periodic) solutions of the NLS equation (7.1) [50]. Therefore, a description of the full soliton-DSW modulation would require integration of the two-phase

Whitham equations. However, we can determine all the results of soliton-DSW interaction by invoking continuity of the modulation solution for negative time.

If we now consider $t \to -t$ for the Whitham modulation equations (7.15), then the characteristic velocities $-V_i$ are re-ordered. The same initial data $\overline{\rho}_- > \overline{\rho}_+$ and the locus (7.31) corresponds to the generation of a 1-RW. If a soliton of amplitude a_- is initialized to the left of the RW, then soliton-RW interaction is determined by the constancy of r_3 so that the tunneled soliton amplitude satisfies

$$a_+ = a_- - 2\left(\sqrt{\overline{\rho}_-} \pm \sqrt{\overline{\rho}_- - a_-}\right)\left(\sqrt{\overline{\rho}_-} - \sqrt{\overline{\rho}_+}\right), \tag{7.32}$$

where the $\pm$ corresponds to the same branch of r_3 that is taken. The relation (7.32) corresponds to a 1-wave modulation of the time-reversed Whitham equations. This is a global relationship that must also hold for the corresponding 4-wave soliton-DSW modulation of the non-reversed Whitham equations due to continuity of the modulation solution away from the origin. This analysis is pictured in Fig. 7.3 where, for negative time, a soliton-RW interaction is pictured and a soliton-DSW interaction is shown for positive time.

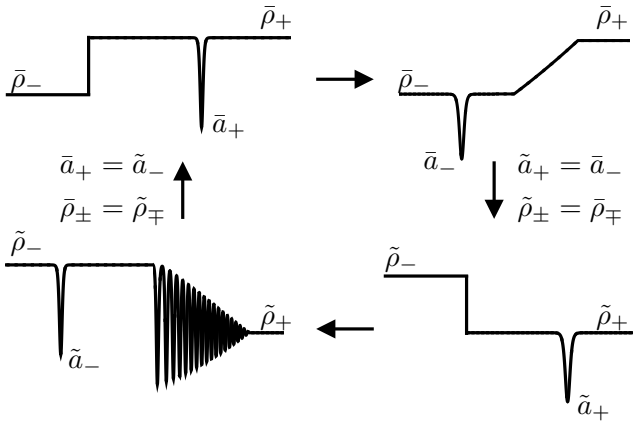

Figure 7.4: Sketch of configurations demonstrating hydrodynamic reciprocity. Horizontal arrows refer to temporal evolution and vertical arrows connote the transformation to the reciprocal initial condition.

Equation (7.32) can be inverted to obtain a_- in terms of a_+ and $\overline{\rho}_\pm$. If we set $\overline{\rho}_- = 1$

and $\overline{u}_- = 0$, then Eq. (7.32) and Eq. (7.29) are equivalent. The tunneling condition (7.29) is the same for both soliton-RW and soliton-DSW interaction.

Another way to understand hydrodynamic reciprocity is schematically pictured in Fig. 7.4. Rather than reversing time, this Figure depicts spatial reversal. A soliton of amplitude a_+ initially placed to the right of a jump with $\overline{\rho}_- < \overline{\rho}_+$ results in soliton interaction with a 4-RW and a_- satisfying Eq. (7.32). Now, consider a spatially reversed jump with $\tilde{\rho}_\pm = \overline{\rho}_\mp$ so that $\tilde{\rho}_- > \tilde{\rho}_+$. With a soliton of amplitude $\tilde{a}_+ = a_-$ initially placed on the right, the soliton interaction with a 4-DSW results in the tunneled amplitude $\tilde{a}_- = a_+$. This is the bi-directional generalization of the uni-directional hydrodynamic reciprocity condition noted in [93].

In what follows, we compare the modulation theory predictions for hydrodynamic optical soliton tunneling with numerical simulations of Eq. (7.1) for initial data comprised of a smoothed step Eq. (7.23) and a soliton. We use a standard 6th order finite difference spatial discretization with Dirichlet boundary conditions. Time evolution is achieved with the standard 4th order Runge-Kutta method. The numerical evolution was validated by the numerical evolution of the exact solitary wave solution on a uniform background Eq. (7.3).

Comparisons between the transmitted soliton amplitude predicted by Eq. (7.29) and numerical simulations are given in Fig. 7.3, showing excellent agreement. When the tunneling relation (7.29) is not satisfied for $a_\pm > 0$, the soliton will become trapped within the spatially extended hydrodynamic state. Trapping then results in the soliton acting as a nonlinear modulation of the hydrodynamic structure. Examples of a soliton trapped in a hydrodynamic barrier are shown in Fig. 7.6 where the soliton was unable to pass through the RW or DSW for long simulation times. Soliton-DSW trapping can be viewed as the formation of a "defect" in the locally periodic DSW structure, analogous to the soliton defects of KdV cnoidal waves considered in [78]. In contrast to classical optical soliton tunneling in which the localized pulse can be reflected by a barrier with sufficient energy, this is not possible in the context of hydrodynamic optical tunneling.

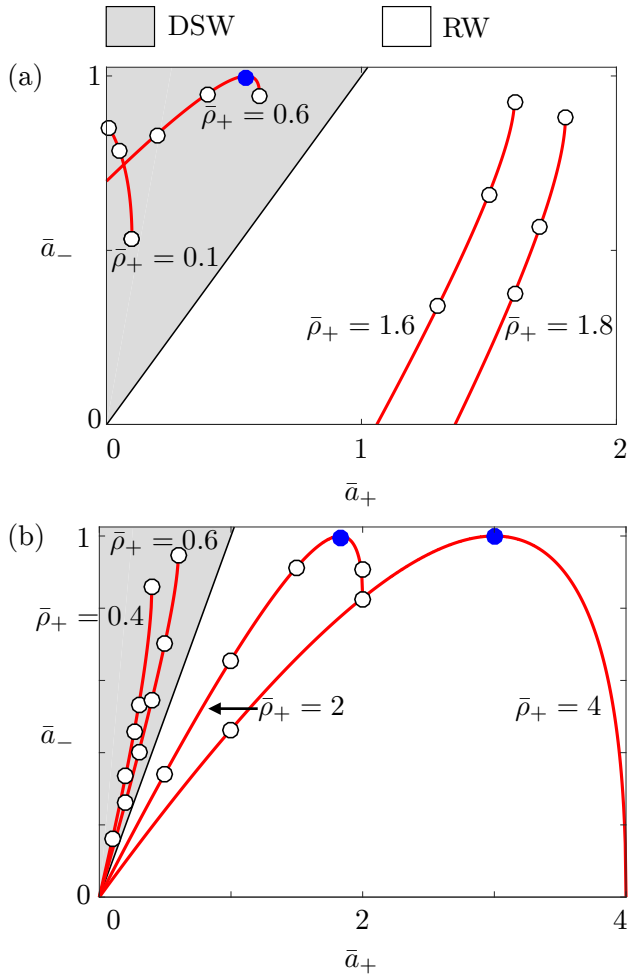

Figure 7.5: Comparison between the tunneling relation (7.29) (solid curves) and direct numerical simulations of the NLS equation (dots) with smoothed, step initial data defined by $\overline{\rho}_+ > 0$ and a soliton of amplitude a_+. (a) The overtaking cases in Fig. 7.1(c,d). (b) The collision cases in Fig. 7.1(a,b). Filled dots correspond to the emergence of a black soliton. The grey regions correspond to soliton-DSW tunneling and white regions correspond to soliton-RW tunneling.

The simplest tunneling configuration is that of a solitary wave though a RW because the evolution of the macroscopic structure of the RW can be determined by standard methods applied to the modulation Eqs. (7.23) and (7.24). The RW evolution, in terms of the Riemann invariants is

$$\overline{s}_{\mathrm{RW}}(x,t) = \begin{cases} \overline{s}_- & x < V_- t \\ \frac{1}{3}\left(2\frac{x}{t} - \overline{r}\right) & V_- t \le x \le V_+ t \\ \overline{s}_+ & V_+ t < x \end{cases}, \tag{7.33}$$

where $V(\overline{s},\overline{r}) = \frac{1}{2}(3\overline{s}+\overline{r})$ and $V_\pm = V(\overline{s}_\pm,\overline{r})$ are the edge speeds of the centered RW [86]. We note that small amplitude linear oscillations may be present at an edge of the RW in the full NLS dynamics due to dispersive regularization but these oscillations decay and have negligible influence on the asymptotic RW behavior. The trajectory of the soliton center x_{s} is a characteristic (2- or 3-characteristic) of the Whitham modulation equations (7.15) that satisfies the initial value problem

$$\frac{dx_{\mathrm{s}}}{dt} = c\left(\overline{r},\overline{s},r_3\right), \quad x_{\mathrm{s}}(0) = x_+. \tag{7.34}$$

Here, x_+ is the location of the solitary wave at $t = 0$ and the location of the step (7.22) is taken to be $x = 0$; c is the soliton amplitude-speed relation (7.30) written in terms of Riemann invariants. A direct integration of (7.34) results in the location of the solitary wave tunneling through a rarefaction wave

$$x_{\mathrm{s}}(t) = \begin{cases} x_+ + c_+ t & x \le t_1 \\ \dfrac{(\overline{r}+r_3)t + 3\left(\overline{s}_+ - r_3\right)t_1^{2/3}t^{1/3}}{2} & t_1 < x < t_2 \\ x_- + c_- t & t \ge t_2 \end{cases}, \tag{7.35}$$

where

$$
\begin{aligned}
t_1 &= x_+/(\overline{s}_+ - r_3),\\
t_2 &= (\overline{s}_+ - r_3)^{3/2}(\overline{s}_- - r_3)^{-3/2}t_1,\\
x_- &= (\overline{s}_+ - r_3)^{1/2}(\overline{s}_- - r_3)^{-1/2}x_+,\\
c_\pm &= \frac{1}{2}\left(\overline{r} + 2r_3 + \overline{s}_\pm\right).
\end{aligned}
$$

The effective phase shift of the soliton center through a RW is given by the difference in the x-intercepts of the linear soliton trajectories post and pre-hydrodynamic interaction.

$$
x_+ - x_- = \left(1 - \sqrt{\frac{\overline{s}_+ - r_3}{\overline{s}_- - r_3}}\right) x_+. \tag{7.36}
$$

Example comparisons of the predicted soliton trajectory through a rarefaction wave from Eq. (7.35) with numerical simulations are given in Figs. 7.7(a) and (c) and are in excellent agreement.

An alternative, instructive way to determine the interaction phase shift is to analyze the additional modulation equation (7.27) that describes the evolution of the wavenumber $0 < k \ll 1$ in a train of well separated, non-interacting solitons with the amplitude field $a(x,t)$. Given the mean flow $\overline{s}_{\mathrm{RW}}(x,t)$ in (7.33), the amplitude field $a(x,t)$ is determined by the constancy of $\overline{r}$ and r_3 in Eq. (7.25). The soliton phase shift now follows from the requirement of constancy of the Riemann invariant pk of Eq. (7.27) across the initial step (7.22), (7.28). Indeed, equating the values of pk at both sides of the initial step we find the ratio $k_+/k_- = x_-/x_+$, which determines the stretching (contraction) of the soliton wavetrain at leading order [93],

$$
\begin{aligned}
\frac{k_+}{k_-} = \frac{x_-}{x_+} &= \exp \int_{\overline{s}_-}^{\overline{s}_+} \frac{\dfrac{dc}{d\overline{s}}}{\frac{1}{2}\left(\overline{r} + 3\overline{s}\right) - c} d\overline{s},\\
&= \sqrt{\frac{\overline{s}_+ - r_3}{\overline{s}_- - r_3}},
\end{aligned} \tag{7.37}
$$

where the first term in the denominator is the characteristic speed associated with $\overline{s}$. This simpler approach yields the same result as that obtained from Eq. (7.35).

We can now invoke the notion of hydrodynamic reciprocity—the surprising fact that the interaction of the soliton with a RW is the same as that with a DSW at the macroscopic level [93, 123]. In addition to the tunneling relation (7.29), the phase shift (7.36) also applies to soliton-DSW interaction. The macroscopic properties of the DSW itself–leading harmonic edge speed and trailing soliton edge speed–are determined by an analysis of the single phase Whitham equations in place of the direct integration that was possible in the RW case. The distinguished edge speeds of the DSW are given by [56]

$$\begin{aligned} V_{-,\mathrm{DSW}} &= 2\sqrt{\overline{\rho}_+} - 1, \\ V_{+,\mathrm{DSW}} &= \overline{u}_+ + \frac{\overline{\rho}_+ - 8\sqrt{\overline{\rho}_+} + 8}{2 - \sqrt{\overline{\rho}_+}}. \end{aligned} \tag{7.38}$$

Incorporating the soliton phase shift Eq. (7.37) results in the soliton trajectory before and after interaction

$$x_{s,\mathrm{DSW}} = \begin{cases} x_+ + \frac{1}{2}\left(\overline{r} + 2r_3 + \overline{s}_+\right) t & x \le t_1 \\ x_- + \frac{1}{2}\left(\overline{r} + 2r_3 + \overline{s}_-\right) t & x \ge t_2. \end{cases}, \tag{7.39}$$

where now, t_1, t_2 are determined by equating the pre and post-interaction soliton trajectories with the appropriate DSW edge velocities from Eq. (7.38). Comparisons with numerical simulations of soliton-DSW interactions are shown in Figs. 7.7(b,d) with excellent agreement. The trajectory prediction Eq. (7.39) also correctly captures the phenomenon of soliton direction reversal shown in Fig. 7.7(d).

The transition to a different mean flow across the hydrodynamic barrier not only results in a controllable soliton trajectory but also the generation of transmitted solitons of prespecified amplitudes (cf., Eq. (7.29)). For specific initial configurations of the tunneling problem, we predict and numerically observe the spontaneous development of a black soliton that exhibits cavitation or a null in the density at the soliton minimum. Black soliton

solutions are characterized in the normalization considered here by an amplitude $a_- = 1$ with an associated π phase jump across the soliton minimum. In the reference frame chosen, the soliton velocity on the left flow is given by $c_- = 0$. The phenomenon of so-called self cavitation of dispersive shock waves was theoretically predicted in [46] and both a zero density point and the associated π phase jump was observed experimentally for the dam break problem of spin waves in a defocusing magnetic material [69]. Zero density points were also observed in an optical "photon fluid" [142]. The interaction of a dark soliton with a mean flow then gives a fundamentally new mechanism for generating a cavitation point in the flow. Example numerical simulations demonstrating spontaneous cavitation following the interaction are shown in Fig. 7.8.

7.4 Conclusions

In this chapter, we have introduced a new notion of hydrodynamic optical soliton tunneling where a localized, depression wave or dark soliton is incident on a spatiotemporal hydrodynamic barrier. Under the assumptions of nonlinear wave, Whitham modulation theory, the evolution of the inhomogeneous mean flow decouples from the soliton so that, at the leading order macroscopic level, the flow is wholly unaltered by the presence of the local pulse. The solution is found to be a self-similar simple wave of a system of quasilinear partial differential equations whose characteristics determine both the mean flow and the soliton trajectory. The self-similar simple wave obtained evolves from an initial step in the flow to either a single DSW or a RW but the approach generalizes to any initial state that limits to different constants as $x \to \pm\infty$, which define soliton tunneling conditions.

The main result of this chapter is encompassed in the tunneling and phase relations given by Eqs. (7.29) and (7.37). They determine the transmitted soliton amplitude, speed, and position in terms of only the incident soliton amplitude, its position, and the hydrodynamic flow in the far-field. The known soliton trajectory and amplitude following interaction provide a mechanism for soliton control via interaction with a spatially extended mean flow.

The notion of hydrodynamic reciprocity identified earlier in [93] for scalar, KdV type systems and generalized here to the NLS case allows one to investigate a complex soliton-DSW interaction by studying the simpler case of soliton-RW interaction. Reciprocity implies that, although the tunneling of a soliton through a DSW involves a complex interaction with rapid nonlinear oscillations, they are unimportant for determining the resulting amplitude, velocity and shift of the solitary wave post interaction. The methodology presented here to track the trajectory of the soliton only requires knowledge of the far field boundary conditions and hence this approach can be extended to more general initial configurations.We also note that the developed theory is not restricted to integrable NLS dynamics and can be generalized to more general cases of hydrodynamic optical soliton tunneling described by non-integrable versions of the defocusing NLS equation, e.g. with saturable nonlinearity, using the methods of [45, 62, 47]

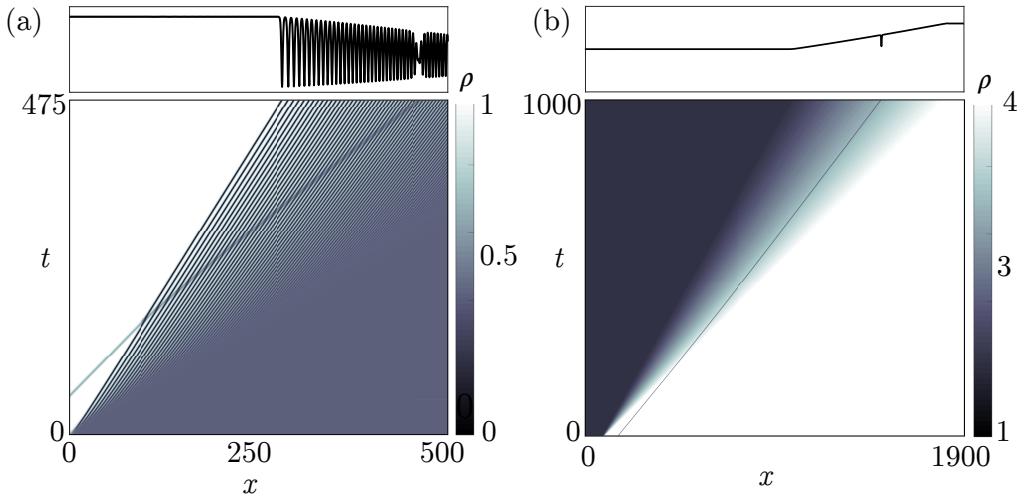

Figure 7.6: Numerical simulation of hydrodynamically trapped solitons. (a) Soliton of amplitude $a_- = 0.25$ sent into a 4-DSW with $\overline{\rho}_+ = 0.5$. (b) Soliton of amplitude $a_+ = 1$ overtaken by RW with $\rho_+ = 4$.

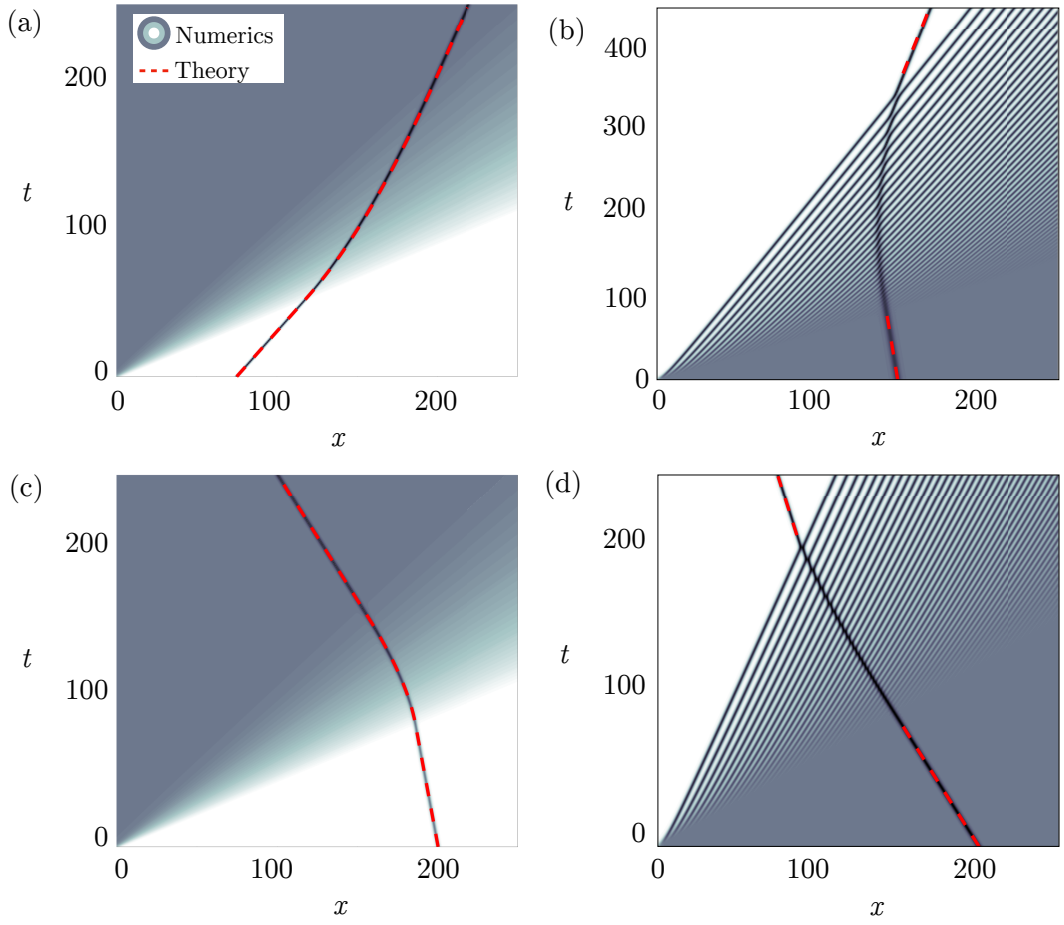

Figure 7.7: Tracking a soliton through a RW and DSW via equations (7.35) and (7.39). (a) $\overline{\rho}_+ = 2$, $a_+ = 1$ and the sign of r_3 in Eq. (7.25) is "−". (b) $\overline{\rho}_+ = 0.5$, $a_+ = 0.5$, the r_3 sign is "−". (c) $\overline{\rho}_+ = 2$, $a_+ = 2$, the sign of r_3 is "+". (d) $\overline{\rho}_+ = 0.5$, $a_+ = 0.4$, the sign of r_3 is "+". Predictions from Eqs. (7.35) and (7.39) are the red dashed curves, the contours are from direct numerical simulation of Eq. (7.1).

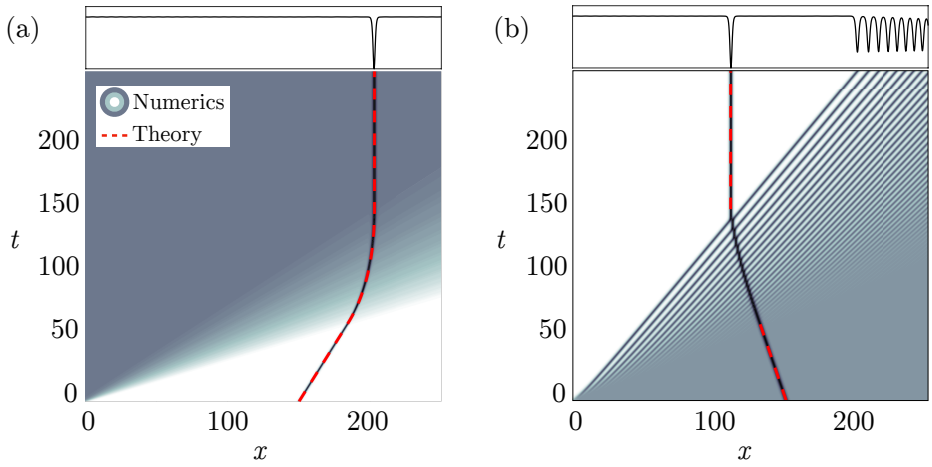

Figure 7.8: Examples of the emergence of a black soliton after tunneling in the characteristic plane. The initial configurations are (a) RW collision case with $\overline{\rho}_+ = 2$, (b) DSW overtaking case with $\overline{\rho}_+ = 0.6$. Initial soliton amplitudes are chosen so that $a_- = 1$ in (7.29). Numerically computed soliton trajectories (contours) are compared against theoretical predictions of Eqs. (7.35) and (7.39). The snapshots of the intensity ρ at $t = 225$ are shown above the contour plots.

Chapter 8

Conclusions and Future work

In this thesis, we investigated a variety of problems in dispersive hydrodynamics both in scalar systems with higher order dispersion and in the bi-directional Nonlinear Schrödinger equation. We will now recap the primary results presented and discuss future directions for research and open questions.

In Chapter 2, we showed that if parameters in a dispersive Eulerian system are such that third order, long wave dispersion is sufficiently small, then the fifth order Kawahara equation is the universal, asymptotic model. We went on to discuss its solitary wave and periodic wave solutions and compute them numerically using the methods outlined in Appendix B. In Chapter 3, we derived the Whitham modulation equations for weakly nonlinear solutions of the Kawahara equation and determined parameter ranges in which they are hyperbolic/elliptic, which determined the modulational stability or instability of periodic waves. In more detail, we discussed the structure of the KdV5-Whitham modulation equation by utilizing a numerically computed one-parameter family of periodic solutions. Here we found that for small bands of wavenumber, unit amplitude periodic solutions with zero mean are modulationally unstable, which has implications for the dynamics of heteroclinic and homoclinic traveling waves computed in Chapter 5.

Our study of step-like initial data posed to Kawahara equation in Chapter 4 revealed a rich collection of DSWs. We divided our investigation into two regimes: the linearly resonant case and the linearly nonresonant case. When the sign of third order dispersion

and fifth order dispersion are the same ($\sigma = 1$ in Eq. (1.3)), two distinct wavenumbers are resonant–e.g. their phase velocities are the same. In this case we observed three distinct DSW regimes that depend on the amplitude of the initial smoothed jump. The radiating DSW (**RDSW**) occurs for small initial jumps. The RDSW is a perturbed KdV DSW, where the leading, elevation solitary wave is embedded in the linear wave spectrum and the DSW emits fast, small amplitude, short wave radiation. For large amplitude jumps in the step-like data, the backward propagating waves are arrested and the initial data is resolved by a traveling DSW (**TDSW**). The TDSW occurs when fifth order dispersion dominates and is characterized by a depression solitary wave at the trailing edge that brings the left equilibrium to a nearly uniform periodic wavetrain. The wavetrain is brought to the leading equilibrium via a partial DSW. The trailing edge of the TDSW is identified as a heteroclinic traveling wave solution of the Kawahara equation. For initial jumps of moderate amplitude, the smoothed discontinuity is resolved by a crossover DSW, which shares features with both the RDSW and the TDSW but is difficult to study due to complex nonlinear wave mixing resulting from nonlinear resonances throughout the wave structure. In the case of convex, positive dispersion ($\sigma = -1$ in Equation (1.3)) the DSWs resemble KdV DSWs for modest amplitude initial steps, but transition to a TDSW as the initial jump increases further. We utilized the asymptotic DSW fitting method to determine the macroscopic DSW properties and find that the method yields unphysical results for sufficiently large jumps.

Our investigation of the Kawahara equation motivated numerical simulations of the Gurevich-Pitaevskii problem for the KdV5 equation (1.4) [64] where smooth, step-like initial data is resolved by a TDSW. In Chapter 5, we used the KdV5 equation as a model that admits heteroclinic traveling wave solutions consisting of disparate periodic traveling waves in the left and right far-fields. We found that the trailing, heteroclinic traveling wave of the TDSW is described by a discontinuous shock solution of the Whitham modulation equations (3.9)–(3.11). These discontinuous solutions correspond to a **generalized Riemann problem** of the Whitham modulation equations and are referred to as **Whitham shocks**. The

Rankine-Hugoniot jump conditions give necessary algebraic constraints on far-field periodic wave parameters which comprise the heteroclinic wave. Note that the physical relevance and admissibility of discontinuous shocks in the Whitham modulation equations had not been identified before this study. We compute heteroclinic waves whose parameters satisfy the Rankine-Hugoniot relations, and identify these traveling waves with **admissible** Whitham shocks. We further computed homoclinic traveling waves—periodic waves with a localized, periodic wave defect, that corresponds to two co-propagating Whitham shocks. Numerical simulations allow us to observe the modulational stability or instability of the traveling waves which is predicted by the hyperbolicity/ellipticity of the KdV5-Whitham modulation equations.

We further explored heteroclinic traveling waves corresponding to Whitham shocks in Chapter 6. We used an equilibrium-to-periodic heteroclinic traveling wave to describe the trailing edge of the TDSW solution of the KdV5 equation and compute the partial DSW via a simple wave solution of the modulation equations—therefore constructing the KdV5 TDSW solution entirely in terms of Whitham modulation theory. We revisited the heteroclinic traveling wave solutions of the Kawahara equation (1.3) (recall Section 4.1.2) and find that their parameters satisfy the Rankine-Hugoniot relations of the Kawahara-Whitham modulation equations. However, the jump conditions suggest that there are Whitham shock solutions beyond the parameter values for which we were successful in the computation of traveling waves. We interpret these computations as evidence of **inadmissible Whitham shocks** for the Kawahara equation. The mere existence of a Whitham shock is not a sufficient condition to guarantee the existence of a traveling wave solution.

Chapter 7 shifts focus from the previous chapters' study of higher order dispersive, scalar equations. In this chapter, we investigated the interaction of a solitary wave with an evolving background in bi-directional systems. Here we considered applications in optics where the defocusing nonlinear Schrödinger equation is a universal model. A dark soliton incident upon a rarefaction wave is posed as a generalized Riemann problem, whose charac-

teristics determine the evolution of the mean flow, soliton amplitude, and soliton trajectory. The notion of **hydrodynamic reciprocity**–e.g. the continuity of the Whitham modulation equations allow us to generalize our results to the case where a dark soliton interacts with a DSW as well, and can determine the soliton amplitude before and after interaction.

We will briefly comment on open problems related to questions raised by this thesis. The novel nonclassical DSWs and novel heteroclinic traveling waves investigated in Chapters 4–6 were focused on scalar model equations with higher order, or even nonlocal dispersion. Despite the extensive study of the KdV5 equation, there are still various open questions. The study of admissible Whitham shocks thus far focused on traveling waves such that the shock velocity coincides with the left and right periodic wave velocity. Is it possible to compute Whitham shocks that do not correspond to heteroclinic traveling waves?

The existence of nonlinearly resonant solutions similar to those studied in this thesis in bi-directional, NLS type equations is suggested by numerical and experimental studies in optics[31, 33]. In future projects, we will explore the following. What novel traveling waves can be computed in bi-directional systems? Are they different from those computed in scalar systems, such as those presented in this thesis?

The study of nonclassical DSWs along with the notion of hydrodynamic tunneling poses an additional avenue for future research. The NLS-soliton tunneling investigated in chapter 7 relied on the concept of hydrodynamic reciprocity to establish a criterion for the tunneling of a localized pulse through a DSW. This problem is solved due to the continuity of the Whitham equations in the description of a classical DSW. Since the TDSW is described by a discontinuous shock solution of the modulation equations, we can no longer invoke this property. This begs the following question: how does a solitary wave interact with a TDSW? More generally, we may investigate the interaction of a solitary wave with a localized homoclinic traveling wave, or even the interaction of two homoclinic, localized traveling waves.

Bibliography

[1] M. J. Ablowitz, Nonlinear Dispersive Waves: Asymptotic Analysis and Solitons, Cambridge Texts in Applied Mathematics, Cambridge University Press, Cambridge, UK ; New York, 1 edition ed., Oct. 2011.

[2] M. J. Ablowitz and Y. Kodama, Note on asymptotic solutions of the Korteweg-de Vries equation with solitons, Studies in Applied Mathematics, 66 (1982), pp. 159–170.

[3] M. J. Ablowitz and Z. H. Musslimani, Spectral renormalization method for computing self-localized solutions to nonlinear systems, Optics Letters, 30 (2005), p. 2140.

[4] M. J. Ablowitz and H. Segur, Solitons and inverse scattering transform, SIAM, Philadelphia, 1981.

[5] V. Achilleos, D. J. Frantzeskakis, P. G. Kevrekidis, and D. E. Pelinovsky, Matter-Wave Bright Solitons in Spin-Orbit Coupled Bose-Einstein Condensates, Physical Review Letters, 110 (2013).

[6] T. R. Akylas and R. H. J. Grimshaw, Solitary internal waves with oscillatory tails, Journal of Fluid Mechanics, 242 (1992), p. 279.

[7] D. Anderson, M. Lisak, B. Malomed, and M. Quiroga-Teixeiro, Tunneling of an optical soliton through a fiber junction, Journal of the Optical Society of America B, 11 (1994), pp. 2380–2384.

[8] G. Assanto, A. A. Minzoni, M. Peccianti, and N. F. Smyth, Optical solitary waves escaping a wide trapping potential in nematic liquid crystals: Modulation theory, Physical Review A, 79 (2009), p. 033837.

[9] I. Bakholdin, Non-dissipative discontinuities in continuum mechanics, FIZMATLIT, Moscow, 2004.

[10] S. Baqer and N. F. Smyth, Modulation theory and resonant regimes for dispersive shock waves in nematic liquid crystals, (2019). preprint.

[11] A. Barak, O. Peleg, C. Stucchio, A. Soffer, and M. Segev, Observation of Soliton Tunneling Phenomena and Soliton Ejection, Physical Review Letters, 100 (2008), p. 153901.

[12] M. Beck, J. Knobloch, D. J. B. Lloyd, B. Sandstede, and T. Wagenknecht, Snakes, Ladders, and Isolas of Localized Patterns, SIAM Journal on Mathematical Analysis, 41 (2009), pp. 936–972.

[13] T. L. Belyaeva and V. N. Serkin, Wave-particle duality of solitons and solitonic analog of the Ramsauer-Townsend effect, The European Physical Journal D, 66 (2012).

[14] E. S. Benilov, R. Grimshaw, and E. P. Kuznetsova, The generation of radiating waves in a singularly-perturbed Korteweg-de Vries equation, Physica D: Nonlinear Phenomena, 69 (1993), pp. 270–278.

[15] T. B. Benjamin, J. L. Bona, and J. J. Mahony, Model Equations for Long Waves in Nonlinear Dispersive Systems, Philosophical Transactions of the Royal Society of London. Series A, Mathematical and Physical Sciences, 272 (1972), pp. 47–78. ArticleType: research-article / Full publication date: Mar. 30, 1972 / Copyright 1972 The Royal Society.

[16] S. Benzoni-Gavage, P. Noble, and L. M. Rodrigues, Slow Modulations of Periodic Waves in Hamiltonian PDEs, with Application to Capillary Fluids, Journal of Nonlinear Science, 24 (2014), pp. 711–768.

[17] A. Bertozzi, A. Mnch, and M. Shearer, Undercompressive shocks in thin film flows, Physica D: Nonlinear Phenomena, 134 (1999), pp. 431–464.

[18] A. L. Binswanger, Nonclassical, Oblique Dispersive Shock Waves in Steady Shallow Water Flows, 2019.

[19] G. Biondini, G. El, M. Hoefer, and P. Miller, Dispersive hydrodynamics: Preface, Physica D: Nonlinear Phenomena, 333 (2016), pp. 1–5.

[20] R. W. Boyd, Nonlinear Optics, Academic Press, Oct. 2013.

[21] B. Buffoni, A. R. Champneys, J. F. Toland, C. Down, B. Ay, and U. \. U, Bifurcation and coalescence of a plethora of homoclinic orbits for a Hamiltonian system, tech. rep., J. Dyn. Diff. Eq, 1994.

[22] J. Burke and E. Knobloch, Localized states in the generalized Swift-Hohenberg equation, Physical Review E, 73 (2006).

[23] ——, Homoclinic snaking: Structure and stability, Chaos: An Interdisciplinary Journal of Nonlinear Science, 17 (2007), p. 037102.

[24] P. F. Byrd and M. D. Friedman, Handbook of Elliptic Integrals for Engineers and Scientists, 1971.

[25] D. C. Calvo, T.-S. Yang, and T. R. Akylas, On the stability of solitary waves with decaying oscillatory tails, in Proceedings of the Royal Society of London A: Mathematical, Physical and Engineering Sciences, vol. 456, The Royal Society, 2000, pp. 469–487.

[26] J. D. Carter, Bidirectional Whitham equations as models of waves on shallow water, Wave Motion, 82 (2018), pp. 51–61.

[27] J. D. Carter and M. Rozman, Stability of Periodic, Traveling-Wave Solutions to theCapillary Whitham Equation, Fluids, 4 (2019), p. 58.

[28] I. Carusotto and C. Ciuti, Quantum fluids of light, Reviews of Modern Physics, 85 (2013), pp. 299–366.

[29] A. Champneys, Homoclinic orbits in reversible systems and their applications in mechanics, fluids and optics, Physica D: Nonlinear Phenomena, 112 (1998), pp. 158–186.

[30] D. Clamond, D. Dutykh, and A. Durn, A plethora of generalised solitary gravitycapillary water waves, Journal of Fluid Mechanics, 784 (2015), pp. 664–680.

[31] M. Conforti, F. Baronio, and S. Trillo, Resonant radiation shed by dispersive shock waves, Physical Review A, 89 (2014), p. 013807.

[32] M. Conforti and S. Trillo, Dispersive wave emission from wave breaking, Optics Letters, 38 (2013), p. 3815.

[33] ——, Radiative effects driven by shock waves in cavity-less four-wave mixing combs, Optics Letters, 39 (2014), p. 5760.

[34] M. Conforti, S. Trillo, A. Mussot, and A. Kudlinski, Parametric excitation of multiple resonant radiations from localized wavepackets, Scientific Reports, 5 (2015), p. 9433.

[35] C. Conti, A. Fratalocchi, M. Peccianti, G. Ruocco, and S. Trillo, Observation of a Gradient Catastrophe Generating Solitons, Physical Review Letters, 102 (2009), p. 083902.

[36] C. M. Dafermos, Hyperbolic Conservation Laws in Continuum Physics, Springer, Berlin, 4th ed. ed., 2016.

[37] F. Dias and P. Milewski, On the fully-nonlinear shallow-water generalized Serre equations, Physics Letters A, 374 (2010), pp. 1049–1053.

[38] E. Dinvay, H. Kalisch, D. Moldabayev, and E. I. Pru, The Whitham equation for hydroelastic waves, Applied Ocean Research, 89 (2019), pp. 202–210.

[39] E. Dinvay, D. Moldabayev, D. Dutykh, and H. Kalisch, The Whitham equation with surface tension, Nonlinear Dynamics, 88 (2017), pp. 1125–1138.

[40] A. Doelman, B. Sandstede, A. Scheel, and G. Schneider, The dynamics of modulated wave trains, vol. 199 of Memoirs of the AMS, American Mathematical Society, Providence, RI, 2009.

[41] B. Dubrovin, On Hamiltonian Perturbations of Hyperbolic Systems of Conservation Laws, II: Universality of Critical Behaviour, Communications in Mathematical Physics, 267 (2006), pp. 117–139.

[42] B. Dubrovin, S.-Q. Liu, and Y. Zhang, On Hamiltonian perturbations of hyperbolic systems of conservation laws I: Quasi-Triviality of bi-Hamiltonian perturbations, Communications on Pure and Applied Mathematics, 59 (2006), pp. 559–615.

[43] M. Ehrnstrm, M. D. Groves, and E. Wahln, On the existence and stability of solitary-wave solutions to a class of evolution equations of Whitham type, Nonlinearity, 25 (2012), pp. 2903–2936.

[44] G. El, M. Hoefer, and M. Shearer, Dispersive and Diffusive-Dispersive Shock Waves for Nonconvex Conservation Laws, SIAM Review, 59 (2017), pp. 3–61.

[45] G. A. El, Resolution of a shock in hyperbolic systems modified by weak dispersion, Chaos, 15 (2005), p. 037103.

[46] G. A. El, V. V. Geogjaev, A. V. Gurevich, and A. L. Krylov, Decay of an initial discontinuity in the defocusing NLS hydrodynamics, Physica D, 87 (1995), pp. 186–192.

[47] G. A. El and M. A. Hoefer, Dispersive shock waves and modulation theory, Physica D, 333 (2016), pp. 11–65.

[48] G. A. El and N. F. Smyth, Radiating dispersive shock waves in non-local optical media, Proceedings of the Royal Society A: Mathematical, Physical and Engineering Science, 472 (2016), p. 20150633.

[49] H. Flaschka, M. G. Forest, and D. W. McLaughlin, Multiphase averaging and the inverse spectral solution of the Korteweg-de Vries equation, Comm. Pure Appl. Math., 33 (1980), pp. 739–784.

[50] M. G. Forest and J. Lee, Geometry and modulation theory for the periodic nonlinear Schrödinger equation, in Oscillation Theory, Computation, and Methods of Compensated Compactness, vol. 2, Springer, 1986, pp. 35–69.

[51] B. Fornberg, Generation of Finite Difference Formulas on Arbitrarily Spaced Grids, Mathematics of Computation, 51 (1988), p. 8.

[52] T. Gao, Z. Wang, and J.-M. Vanden-Broeck, On asymmetric generalized solitary gravitycapillary waves in finite depth, Proceedings of the Royal Society A, 472 (2016), p. 20160454.

[53] J. Garnier, G. Xu, S. Trillo, and A. Picozzi, Incoherent Dispersive Shocks in the Spectral Evolution of Random Waves, Physical Review Letters, 111 (2013), p. 113902.

[54] A. Green and P. Naghdi, A derivation of equations for wave propagation in water of variable depth, Journal of Fluid Mechanics, 78 (1976), pp. 237–246.

[55] R. Grimshaw, B. Malomed, and E. Benilov, Solitary waves with damped oscillatory tails: an analysis of the fifth-order Korteweg-de Vries equation, Physica D, 77 (1994), pp. 473–485.

[56] A. V. Gurevich and A. L. Krylov, Dissipationless shock waves in media with positive dispersion, Sov. Phys. JETP, 65 (1987), pp. 944–953.

[57] A. V. Gurevich and L. P. Pitaevskii, Nonstationary structure of a collisionless shock wave, Sov. Phys. JETP, 38 (1974), pp. 291–297.

[58] P. Guyenne and E. I. Pru, Forced and Unforced Flexural-gravity Solitary Waves, Procedia IUTAM, 11 (2014), pp. 44–57.

[59] M. Haragus and G. Iooss, Local Bifurcations, Center Manifolds, and Normal Forms in Infinite-Dimensional Dynamical Systems, Springer London, London, 2011.

[60] M. Haragus, E. Lombardi, and A. Scheel, Spectral stability of wave trains in the Kawahara equation, Journal of Mathematical Fluid Mechanics, 8 (2006), pp. 482–509.

[61] W. Hereman, P. P. Banerjee, A. Korpel, G. Assanto, A. v. Immerzeele, and A. Meerpoel, Exact solitary wave solutions of nonlinear evolution and wave equations using a direct algebraic method, Journal of Physics A, 19 (1986), pp. 607–628.

[62] M. A. Hoefer, Shock Waves in Dispersive Eulerian Fluids, Journal of Nonlinear Science, 24 (2014), pp. 525–577.

[63] M. A. Hoefer, M. J. Ablowitz, and P. Engels, Piston dispersive shock wave problem, Physical Review Letters, 100 (2008), p. 084504.

[64] M. A. Hoefer, N. F. Smyth, and P. Sprenger, Modulation theory solution for nonlinearly resonant, fifth-order Korteweg-de Vries, nonclassical, traveling dispersive shock waves, Studies in Applied Mathematics, 142 (2019), pp. 219–240.

[65] J. K. Hunter and J. Scheurle, Existence of perturbed solitary wave solutions to a model equation for water waves, Physica D: Nonlinear Phenomena, 32 (1988), pp. 253–268.

[66] J. K. Hunter and J.-M. Vanden-Broeck, Solitary and periodic gravitycapillary waves of finite amplitude, Journal of Fluid Mechanics, 134 (1983), p. 205.

[67] A. T. Ilichev and V. Y. Tomashpolskii, Soliton-like structures on a liquid surface under an ice cover, Theoretical and Mathematical Physics, 182 (2015), pp. 231–245.

[68] D. Jacobs, B. McKinney, and M. Shearer, Travelling wave solutions of the modified Korteweg-deVries-Burgers equation, Journal of Differential Equations, 116 (1995), pp. 448–467.

[69] P. P. Janantha, P. Sprenger, M. Hoefer, and M. Wu, Observation of Self-Cavitating Envelope Dispersive Shock Waves in Yttrium Iron Garnet Thin Films, Physical Review Letters, 119 (2017), p. 024101.

[70] R. S. Johnson, A Modern Introduction to the Mathematical Theory of Water Waves by R. S. Johnson, Oct. 1997.

[71] A. M. Kamchatnov, Nonlinear periodic waves and their modulations: an introductory course, World Scientific, 2000.

[72] T. Kawahara, Oscillatory Solitary Waves in Dispersive Media, Journal of the Physical Society of Japan, 33 (1972), pp. 260–264.

[73] M. Khamehchi, K. Hossain, M. Mossman, Y. Zhang, T. Busch, M. M. Forbes, and P. Engels, Negative-Mass Hydrodynamics in a Spin-Orbit Coupled Bose-Einstein Condensate, Physical Review Letters, 118 (2017), p. 155301.

[74] Y. S. Kivshar and B. A. Malomed, Dynamics of solitons in nearly integrable systems, Reviews of Modern Physics, 61 (1989), pp. 763–915.

[75] E. Knobloch, Spatially localized structures in dissipative systems: open problems, Nonlinearity, 21 (2008), pp. T45–T60.

[76] E. Knobloch, H. Uecker, and D. Wetzel, A multitude of localized patterns in SH357, arXiv:1904.01100 [nlin], (2019). arXiv: 1904.01100.

[77] N. A. Kudryashov, A note on new exact solutions for the Kawahara equation using Exp-function method, Journal of Computational and Applied Mathematics, 234 (2010), pp. 3511–3512.

[78] E. A. Kuznetsov and A. V. Mikhailov, Stability of stationary waves in nonlinear weakly dispersive media, Sov. Phys. JETP, 40 (1975), pp. 855–859.

[79] L. Landau and E. Lifshitz, Quantum mechanics, Pergamon Press, 1965.

[80] P. Lax, Integrals of nonlinear equations of evolution and solitary waves, Comm. Pur. Appl. Math., 21 (1968), pp. 467–490.

[81] P. D. Lax, Hyperbolic systems of conservation laws and the mathematical theory of shock waves, SIAM, 1973.

[82] P. D. Lax and C. D. Levermore, The small dispersion limit of the {Korteweg-de Vries} equation: 1-3, Communications on Pure and Applied Mathematics, 36 (1983), pp. 253–290; 571–593; 809–830.

[83] ——, The small dispersion limit of the {Korteweg-de Vries} equation: 2, Communications on Pure and Applied Mathematics, 36 (1983), pp. 571–593.

[84] ——, The small dispersion limit of the {Korteweg-de Vries} equation: 3, Communications on Pure and Applied Mathematics, 36 (1983), pp. 809–830.

[85] P. G. LeFloch, Hyperbolic systems of conservation laws, Birkhauser, 2002.

[86] R. J. LeVeque, Finite volume methods for hyperbolic problems, Cambridge University Press, 2002.

[87] Y.-J. Lin, R. L. Compton, K. Jimnez-Garca, J. V. Porto, and I. B. Spielman, Synthetic magnetic fields for ultracold neutral atoms, Nature, 462 (2009), pp. 628–632.

[88] Y.-J. Lin, K. Jimnez-Garca, and I. B. Spielman, Spin-orbit-coupled Bose-Einstein condensates, Nature, 471 (2011), pp. 83–86.

[89] Y. Linzon, R. Morandotti, M. Volatier, V. Aimez, R. Ares, and S. Bar-Ad, Nonlinear Scattering and Trapping by Local Photonic Potentials, Physical Review Letters, 99 (2007).

[90] S. Loomba, H. Kaur, R. Gupta, C. N. Kumar, and T. S. Raju, Controlling rogue waves in inhomogeneous Bose-Einstein condensates, Physical Review E, 89 (2014), p. 052915.

[91] N. K. Lowman and M. A. Hoefer, Dispersive shock waves in viscously deformable media, Journal of Fluid Mechanics, 718 (2013), pp. 524–557.

[92] J. C. Luke, A perturbation method for nonlinear dispersive wave problems, Proceedings of the Royal Society of London Series A, 292 (1966), pp. 403–412.

[93] M. D. Maiden, D. V. Anderson, N. A. Franco, G. A. El, and M. A. Hoefer, Solitonic Dispersive Hydrodynamics: Theory and Observation, Physical Review Letters, 120 (2018), p. 144101.

[94] M. D. Maiden and M. A. Hoefer, Modulations of viscous fluid conduit periodic waves, Proc. R. Soc. A, 472 (2016), p. 20160533.

[95] S. Malaguti, M. Conforti, and S. Trillo, Dispersive radiation induced by shock waves in passive resonators, Optics Letters, 39 (2014), p. 5626.

[96] B. Malomed and J. Vanden-Broeck, Solitary wave interactions for the fifth-order kdv equation, Contemporary Mathematics, 200 (1996), pp. 133–144.

[97] S. C. Mancas, Traveling Wave Solutions to Kawahara and Related Equations, Differential Equations and Dynamical Systems, 27 (2019), pp. 19–37.

[98] S. C. Mancas and W. A. Hereman, Traveling Wave Solutions to Fifth- and Seventh-order Korteweg–de Vries Equations: Sech and Cn Solutions, Journal of the Physical Society of Japan, 87 (2018), p. 114002.

[99] T. R. Marchant and N. F. Smyth, The initial boundary problem for the Korteweg-de Vries equation on the negative quarter-plane, Proceedings of the Royal Society of London A, 458 (2002), pp. 857–871.

[100] A. Marchenko, Long waves in shallow liquid under ice cover, Journal of Applied Mathematics and Mechanics, 52 (1988), pp. 180–183.

[101] T. Marest, F. Braud, M. Conforti, S. Wabnitz, A. Mussot, and A. Kudlinski, Longitudinal soliton tunneling in optical fiber, Optics Letters, 42 (2017), pp. 2350–2353.

[102] Y. Matsuno, Hamiltonian formulation of the extended GreenNaghdi equations, Physica D, 301302 (2015), pp. 1–7.

[103] J. W. Miles, The Korteweg-de Vries equation: a historical essay, Journal of Fluid Mechanics, 106 (1981), p. 131.

[104] A. C. Newell, Nonlinear tunnelling, Journal of Mathematical Physics, 19 (1978), pp. 1126–1133.

[105] M. V. Pavlov, Nonlinear Schrödinger equation and the Bogolyubov-Whitham method of averaging, Teor. Mat. Fiz., 71 (1987), pp. 584–588. English translation in Theor. Math. Phys.

[106] M. Peccianti, A. Dyadyusha, M. Kaczmarek, and G. Assanto, Escaping Solitons from a Trapping Potential, Physical Review Letters, 101 (2008), p. 153902.

[107] D. E. Pelinovsky and Y. A. Stepanyants, Convergence of Petviashvili's Iteration Method for Numerical Approximation of Stationary Solutions of Nonlinear Wave Equations, SIAM Journal on Numerical Analysis, 42 (2004), pp. 1110–1127.

[108] V. I. Petviashvili, Equation of an extraordinary soliton, Fizika Plazmy, 2 (1976), p. 469.

[109] L. P. Pitaevskii and S. Stringari, Bose-Einstein condensation, Clarendon, 2003.

[110] S. D. Poisson, Mémoire sur la théorie du son,, J. Ecole Polytech. Paris, 7 (1808), pp. 319–370.

[111] Y. Pomeau, A. Ramani, and B. Grammaticos, Structural stability of the Korteweg-de Vries solitons under a singular perturbation, Physica D, 31 (1988), pp. 127–134.

[112] F. Remonato and H. Kalisch, Numerical bifurcation for the capillary Whitham equation, Physica D, 343 (2017), pp. 51–62.

[113] D. Richardson, B. A. Kalinikos, L. D. Carr, and M. Wu, Spontaneous Exact Spin-Wave Fractals in Magnonic Crystals, Physical Review Letters, 121 (2018), p. 107204.

[114] M. I. Rodas-Verde, H. Michinel, and V. M. Prez-Garca, Controllable Soliton Emission from a Bose-Einstein Condensate, Physical Review Letters, 95 (2005).

[115] V. Serkin, A. Hasegawa, and T. Belyaeva, Geiger-Nuttall law for Schrödinger solitons, Journal of Modern Optics, 60 (2013), pp. 116–127.

[116] V. Serkin, V. Vysloukh, and J. Taylor, Soliton spectral tunnelling effect, Electronics Letters, 29 (1993), pp. 12–13.

[117] V. N. Serkin, A. Hasegawa, and T. L. Belyaeva, Soliton self-induced sub-barrier transparency and the controllable shooting out effect, Journal of Modern Optics, 60 (2013), pp. 444–451.

[118] F. Serre, Contribution l tude des coulements permanents et variables dans les canaux., La Houille Blanche, (1953), pp. 374–388, 830–872.

[119] M. Shearer, D. G. Schaeffer, D. Marchesin, and P. L. Paes-Leme, Solution of the riemann problem for a prototype 2x2 system of non-strictly hyperbolic conservation laws, Archive for Rational Mechanics and Analysis, 97 (1987), pp. 299–320.

[120] N. F. Smyth, Dispersive shock waves in nematic liquid crystals, Physica D, 333 (2016), pp. 301–309.

[121] P. Sprenger and M. Hoefer, Shock Waves in Dispersive Hydrodynamics with Nonconvex Dispersion, SIAM Journal on Applied Mathematics, 77 (2017), pp. 26–50.

[122] P. Sprenger and M. A. Hoefer, Discontinuous shock solutions of the Whitham modulation equations as dispersionless limits of traveling waves, arXiv:1907.09329 [nlin], (2019). arXiv: 1907.09329.

[123] P. Sprenger, M. A. Hoefer, and G. A. El, Hydrodynamic optical soliton tunneling, Physical Review E, 97 (2018).

[124] C. Su and C. S. Gardner, Korteweg-de Vries equation and generalizations. III. Derivation of the Korteweg-de Vries and Burgers equation, Journal of Mathematical Physics, 10 (1969), pp. 536 – 539.

[125] E. Tadmor, Burgers' Equation with Vanishing Hyper-Viscosity, Communications in Mathematical Sciences, 2 (2004), pp. 317–324.

[126] Y. Tan, J. Yang, and D. E. Pelinovsky, Semi-stability of embedded solitons in the general fifth-order KdV equation, Wave Motion, 36 (2002), pp. 241–255.

[127] L. Trefethen, Spectral Methods in MATLAB, SIAM, Jan. 2000.

[128] O. Trichtchenko, B. Deconinck, and J. Wilkening, The instability of Wilton ripples, Wave Motion, 66 (2016), pp. 147–155.

[129] O. Trichtchenko, P. Milewski, E. Pru, and J.-M. VandenBroeck, Stability of periodic traveling flexural-gravity waves in two dimensions, Studies in Applied Mathematics, 142 (2019), pp. 65–90.

[130] S. Venakides, The zero-dispersion limit of the Korteweg-de Vries equation with non-trivial reflection coefficient, Communications on Pure and Applied Mathematics, 38 (1985), pp. 125–155.

[131] S. Venakides, The korteweg-de vries equation with small dispersion: Higher order lax-levermore theory, Communications on Pure and Applied Mathematics, 43 (1990), pp. 335–361.

[132] P. K. A. Wai, C. R. Menyuk, Y. C. Lee, and H. H. Chen, Nonlinear pulse propagation in the neighborhood of the zero-dispersion wavelength of monomode optical fibers, Optics Letters, 11 (1986), p. 464.

[133] W. Wan, S. Jia, and J. W. Fleischer, Dispersive superfluid-like shock waves in nonlinear optics, Nature Physics, 3 (2007), pp. 46–51.

[134] J. Wang, L. Li, and S. Jia, Nonlinear tunneling of optical similaritons in nonlinear waveguides, Journal of the Optical Society of America B, 25 (2008), pp. 1254–1260.

[135] A.-M. Wazwaz, Partial differential equations and solitary waves theory, Nonlinear physical science, Higher Education Press ; Springer, Beijing : Berlin, 2009.

[136] K. E. Webb, Y. Q. Xu, M. Erkintalo, and S. G. Murdoch, Generalized dispersive wave emission in nonlinear fiber optics, Optics Letters, 38 (2013), p. 151.

[137] B. Wetzel, D. Bongiovanni, M. Kues, Y. Hu, Z. Chen, S. Trillo, J. M. Dudley, S. Wabnitz, and R. Morandotti, Experimental Generation of Riemann Waves in Optics: A Route to Shock Wave Control, Physical Review Letters, 117 (2016).

[138] G. B. Whitham, Non-linear dispersive waves, Proceedings of the Royal Society of London Series A, 283 (1965), pp. 238–261.

[139] G. B. Whitham, Variational methods and applications to water waves, Proceedings of the Royal Society of London. Series A, 299 (1967), pp. 6–25.

[140] G. B. Whitham, Linear and nonlinear waves, Wiley, New York, 1974.

[141] Whitham Gerald Beresford and Lighthill Michael James, Variational methods and applications to water waves, Proceedings of the Royal Society of London. Series A. Mathematical and Physical Sciences, 299 (1967), pp. 6–25.

[142] G. Xu, M. Conforti, A. Kudlinski, A. Mussot, and S. Trillo, Dispersive Dam-Break Flow of a Photon Fluid, Physical Review Letters, 118 (2017), p. 254101.

[143] J. Yang, Newton-conjugate-gradient methods for solitary wave computations, Journal of Computational Physics, 228 (2009), pp. 7007–7024.

[144] R. Yang and X. Wu, Spatial soliton tunneling, compression and splitting, Optics Express, 16 (2008), pp. 17759–17767.

[145] N. J. Zabusky and M. D. Kruskal, Interaction of "Solitons" in a Collisionless Plasma and the Recurrence of Initial States, Physical Review Letters, 15 (1965), p. 240.

[146] V. Zakharov and L. Ostrovsky, Modulation instability: The beginning, Physica D, 238 (2009), pp. 540–548.

[147] W.-P. Zhong and M. R. Beli, Soliton tunneling in the nonlinear Schrödinger equation with variable coefficients and an external harmonic potential, Physical Review E, 81 (2010), p. 056604.

Appendix A

Stokes wave approximation

Here we provide computation of the Stokes' approximation for weakly nonlinear periodic solutions to the Kawahara equation

$$u_t + uu_x + \sigma u_{xxx} + u_{xxxxx} = 0. \tag{A.1}$$

We seek a 2π periodic solution $u = \varphi(\theta)$ where $\theta = kx - \omega t$. The periodic solution satisfies the ordinary differential equation

$$-c\varphi' + \varphi\varphi' + \sigma k^2 \varphi''' + k^4 \varphi^{(5)} = 0, \tag{A.2}$$

where $c = \frac{\omega}{k}$ is the phase velocity and derivatives are with respect to the independent variable θ. We seek a solution with a small, finite amplitude $0 < a \ll 1$ so that the periodic wave, φ, and its velocity, c, may be expressed by

$$\varphi(\theta) = \overline{\varphi} + \frac{a}{2}\varphi_1(\theta) + a^2\varphi_2(\theta) + \dots,$$
$$c = c_0 + ac_1 + a^2 c_2 + \dots,$$

where $\bar{\varphi}$ is the mean of the periodic wave. The calculation is carried out by gathering terms at increasing orders of a and solving the linear problem at each increasing order.

The first nontrivial problem at $\mathcal{O}(a)$ is

$$-c_0\varphi_1' + \overline{\varphi}\varphi_1' + \sigma\varphi_1''' + \varphi_1^{(5)} = 0,$$
$$\mathcal{L}\{\varphi_1\} = 0,$$

where $\mathcal{L}$ is the linear differential operator defined on sufficiently differentiable functions on $[0, 2\pi)$ to be $\mathcal{L}\{f\} = \left(-c_0\partial_\theta + \overline{\varphi}\partial_\theta + \sigma k^2\partial_\theta^3 + k^4\partial_\theta^5\right) f$. The leading order problem admits the solution

$$\varphi_1 = \cos\theta,$$

which then immediately implies that

$$c_0 = \overline{u} - \sigma k^2 + k^4,$$

the linear phase velocity.

Carrying on to $\mathcal{O}(a^2)$ we have the nonhomogeneous problem

$$\begin{aligned}\mathcal{L}\{\varphi_2\} &= c_1\varphi_1 - \varphi_1\varphi_1' \\ &= c_1\sin\theta + \frac{1}{2}\sin 2\theta.\end{aligned}$$

A brief calculation shows that the adjoint operator is $\mathcal{L}^\dagger = -\mathcal{L}$, and in order for the $\mathcal{O}(a^2)$ equation to have a solution, the right hand side must be orthogonal to the kernel of $\mathcal{L}^\dagger$. This implies that $c_1 = 0$. Solving for φ_2 gives

$$\varphi_2 = -\frac{\cos 2\theta}{60k^4 - 12\sigma k^2},$$

where we require $k \notin \left\{0, \sqrt{\frac{\sigma}{5}}\right\}$. Continuing to $\mathcal{O}(a^3)$ we have

$$\begin{aligned}\mathcal{L}\{\varphi_3\} &= c_2\varphi_1 - \varphi_2\varphi_1' - \varphi_1\varphi_2' \\ &= \left(\frac{c_2}{2} + \frac{1}{192k^2\left(5k^2 - \sigma\right)}\right)\sin\theta + \left(\frac{3}{192k^2\left(5k^2 - \sigma\right)}\right)\sin 3\theta,\end{aligned}$$

The solvability condition is applied and we find the amplitude correction to the phase velocity

$$c_2 = -\frac{1}{96k^2\left(5k^2 - \sigma\right)}.$$

For clarity, we now provide the form of the periodic solution along with its phase velocity.

$$\varphi = \overline{\varphi} + \frac{a}{2}\cos\theta + \frac{a^2}{48k^2\left(\sigma - 5k^2\right)}\cos 2\theta \tag{A.3}$$

$$c = \overline{u} - \sigma k^2 + k^4 - \frac{a^2}{96k^2\left(5k^2 - \sigma\right)}. \tag{A.4}$$

For the asymptotic series to remain well ordered, we require that $\varphi_2 \ll \varphi_1$ so that

$$a \ll k^2|\sigma - 5k^2|.$$

If we set $\sigma = 0$, we have the weakly nonlinear solution to the KdV5 equation (1.4)

$$\varphi = \overline{\varphi} + \frac{a}{2}\cos\theta - \frac{a^2}{240k^4}\cos 2\theta$$
$$c = \overline{u} + k^4 - \frac{a^2}{480k^4},$$

which is identical to the result given in Ref. [122]. Note that in this limit we require

$$a \ll k^4,$$

to maintain asymptotic ordering.

Appendix B

Numerical methods

In this appendix, we outline the numerical methods we use throughout this thesis.

B.1 Traveling wave computations

Numerical computations of traveling waves are leveraged throughout this thesis for a variety of purposes. In the following section, we outline the various methods utilized to compute periodic and solitary waves solutions to general classes of nonlinear, scalar dispersive PDEs. We begin our discussion with the computation of periodic waves.

B.1.1 Periodic solutions

Periodic solutions of the KdV5 equation (1.4) are of the form $u = \varphi(\theta)$ where φ is a solution to

$$-c\varphi + \frac{1}{2}\varphi^2 + k^4\varphi^{(4)} = A, \tag{B.1}$$

where $A \in \mathbb{R}$ is a constant of integration. Formally, we may perform the Galilean shift $\varphi \to \tilde{\varphi} + c + \sqrt{2A + c^2}$ and set $\tilde{c} = -\sqrt{2A + c^2}$ to set $A = 0$. Solutions to the ODE (B.1) can be represented by a Fourier series. The method applied here follow those presented by Erhström and Kalisch [43]. For the computation of periodic solutions to the KdV5 equation (1.4) we fix the wavelength of the solution so that $k = 1$ (the period of the solution is therefore 2π) and use the velocity c as a continuation parameter. The Fourier series is truncated to

approximate the solution in $L^2([0, 2\pi])$

$$\varphi \approx \varphi_N = \sum_{n=-N}^{N-1} \hat{\varphi}_n e^{-inx}, \tag{B.2}$$

The Fourier coefficients are denoted by $\hat{\varphi}_n$. We find the coefficients by solving the algebraic equation

$$-c\varphi_N + \frac{1}{2}\varphi_N^2 + \left(\frac{2\pi n}{L}\right)^4 \varphi_N. \tag{B.3}$$

The nonlinear system of equations is solved via Matlab's fsolve routine with gives accurate results. The periodic solution is reconstructed from (B.2). Scaling symmetries (2.43), (2.44) allow us to rescale the periodic wave to have zero mean and unit amplitude, and arbitrary wavenumber, $\tilde{k}$. The periodic solutions then form the one parameter family

$$\left\{\tilde{\varphi}(\theta; 0, 1, \tilde{k})\right\}_{\tilde{k}>0}$$

We validate the numerical method by computing approximate periodic solutions of the KdV equation (1.2), and compare to the elliptic function solution (1.7). We find that the solutions differ by at most $O(10^{-7})$.

B.1.2 Solitary wave solutions

For the computation of solitary waves, we utilize various accurate and efficient methods. As for the computation of periodic waves, we utilize a Fourier based method, which is a good approximation of solitary waves so long as the solutions are sufficiently localized. Here we will present the methods in a quite general setting for linearly dispersive ODEs with KdV-like nonlinearity

$$u_t + uu_x + \mathcal{K} * u_x = 0, \tag{B.4}$$

where

$$\mathcal{K} * u_x = \frac{1}{2\pi}\left[\int_{\mathbb{R}} e^{ikx}\left(\frac{\omega(k)}{k}\right) dk\right] * u_x. \tag{B.5}$$

The operation $*$ is the convolution

$$(f * g)(x) = \int_{\mathbb{R}} f(y)g(x-y)dy$$

and ω is a specified linear dispersion relation. Traveling, solitary waves that limit to zero then take the form $u = u(\xi)$, where $\xi = x - ct$ and satisfy the ODE

$$-cu + \frac{1}{2}u^2 + \mathcal{K} * u = 0. \tag{B.6}$$

with far-field boundary conditions

$$u^{(n)}(\theta) \to 0, \quad \text{as } |\theta| \to \infty,$$

.

B.1.2.1 Spectral renormalization

The spectral renormalization method was originally introduced by Ablowitz and Musslimani [3] to compute spatial or temporal soliton solutions of equations modeling nonlinear fiber optics and is a generalization of the Petviashvilli method [108]. The method to compute localized solutions to Eq. (B.6) is outlined as follows.

Since u is assumed to decay rapidly, we may take the Fourier transform of the ODE (B.6), denoting the Fourier transform by $\hat{u}$. The convolution term then becomes multiplicative in the Fourier domain so that we have

$$-c\hat{u} + \frac{1}{2}\hat{u^2} + \frac{\omega(k)}{k}\hat{u} = 0.$$

Some algebraic manipulation yields

$$\hat{u} = \frac{\frac{1}{2}\hat{u^2}}{c - \frac{\omega(k)}{k}}. \tag{B.7}$$

A naive iterative solve has no guarantee that solutions remain nontrivial (or even bounded). This is mitigated by the introduction of a new variable $u = \lambda w$ where $\lambda \neq 0$ is a to be

determined constant that is introduced to prevent the solution from tending to zero. The fixed point problem then becomes

$$\hat{w} = \frac{\frac{\lambda}{2}\hat{w^2}}{c - \frac{\omega(k)}{k}}. \tag{B.8}$$

We determine λ by multiplying Eq. (B.8) by $\hat{w}^*$ and integrating over k

$$\lambda = \frac{\int_{\mathbb{R}} |\hat{w}(k)|^2 dk}{\int_{\mathbb{R}} \frac{\frac{1}{2}\widehat{w^2}\hat{w}^*}{c - \frac{\omega(k)}{k}} dk}$$

where $c - \frac{\omega(k)}{k}$ is assumed to be nonzero, so that no solitary waves are embedded in the linear spectrum. We find solutions to (B.8) iteratively by

$$\hat{w}_{m+1} = \frac{\frac{\lambda_m}{2}\hat{w_m^2}}{c - \frac{\omega(k)}{k}}, \qquad \lambda_m = \frac{\int_{\mathbb{R}} |\hat{w_m}(k)|^2 dk}{\int_{\mathbb{R}} \frac{\frac{1}{2}\widehat{w_m^2} w_m^*}{c - \frac{\omega(k)}{k}} dk}$$

with the initial guess $w_0 = e^{-\frac{1}{10}x^2}$ and $\lambda_0 = 1$. We halt iterations when the relative error between iterations is

$$\max_k |\hat{w}_m - \hat{w}_{m-1}| < \mathcal{E},$$

where $\mathcal{E}$ is a parameter, typically chosen to be on the order of 10^{-14} to 10^{-12}.

Figure B.1 demonstrates the spectral renormalization method applied to the KdV equation (1.2), which possesses the solitary wave solution (2.37). We numerically approximate the solitary wave solution with velocity $c = 1/3$ on the domain $[-50\pi, 50\pi]$ with $N = 2^{12}$ Fourier modes. Figure B.1(a) is a qualitative comparison of the numerically computed soliton and the true solution while Fig. B.1(b) shows that the solutions differ by at most 10^{-15} (the maximum error is approximately 2.5×10^{-15}). Fig. B.1(c) demonstrates that the numerically computed solution is spectrally accurate and Fig. B.1(d) shows that the method converges linearly to the true solution [107].

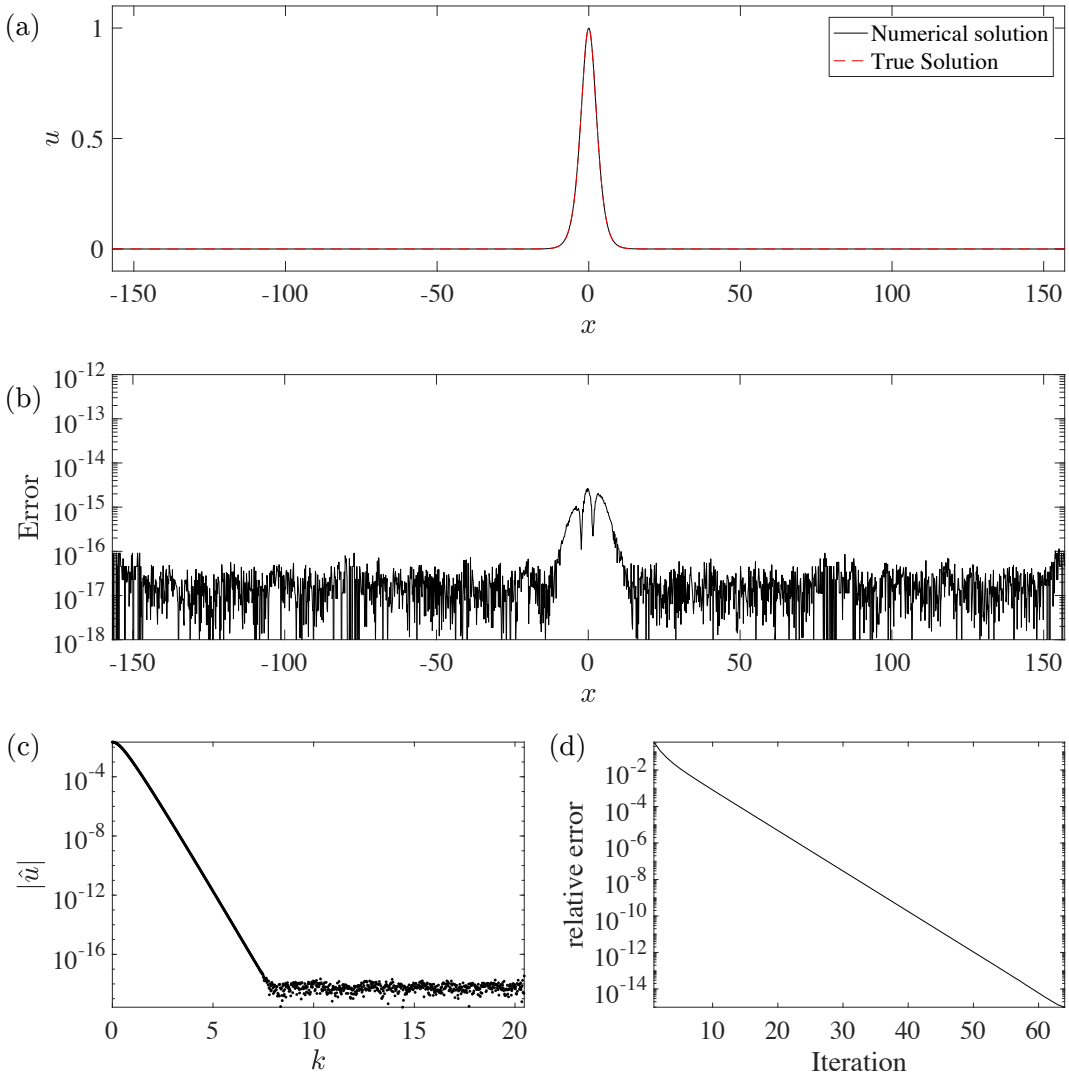

Figure B.1: Validation of the spectral renormalization method for computing the soliton solution of the KdV equation (2.37) with $c = 1/3$. (a) Numerically computed solitary wave solution (black, solid) superimposed with the true solution (dashed, red). (b) The absolute error between the numerically computed solution and the true solution depicted in panel (a). (c) The amplitude of the Fourier coefficients of the numerically computed solution, $|\hat{u}|$ as a function of wavenumber k. (d) The relative error between iterations, $\max_k |\hat{w}_m - \hat{w}_{m-1}|$.

B.1.2.2 Newton-Conjugate-Gradient

In this section we provide an alternative, robust method for computing localized solutions of Eq. (B.6) [143]. The basic principle of the Newton-CG method to compute solitary waves is the following: utilize Newton iterations to solve the linear system for the Fourier coefficients of the nonlinear wave equation while using conjugate gradient methods at each step of the Newton iteration to speed up iterations.

Let u_n denote the approximate solution at an iterative step, sufficiently close to the true solution. Following Yang [143], we define the iterative scheme for approximate solitary wave solutions

$$u_{n+1} = u_n + \varepsilon_n. \tag{B.9}$$

Where the function update ε_n is a solution to the linear, nonhomogeneous problem

$$L_{1,n}\left[\varepsilon_n\right] = -L_0\left[u_n\right], \tag{B.10}$$

where

$$L_{1,n}\left[f\right] = -cf + u_n f + \mathcal{K} * f, \tag{B.11}$$

$$L_0\left[g\right] = -cg + \frac{1}{2}g^2 + \mathcal{K} * g. \tag{B.12}$$

The convolution terms $L_{1,n}$ and L_0 are computed rapidly using the FFT in Matlab. The linear system is solved using the conjugate gradient (CG) method to determine ε_n. We always initialize $\varepsilon_n = 0$ and repeat conjugate gradient iteration until the maximal residual

$$R = \max\left|L_{1,n}\left[\varepsilon_n\right] - L_0[u_n]\right|, \tag{B.13}$$

is below a specified tolerance. Typically, we repeat CG iterations until $R < 10^{-3}$ and update the approximate solution via Eq. (B.9). We halt the procedure when $L_0\left[u_n\right]$ is smaller than a specified tolerance, typically on the order of 10^{-12} or lower.

To validate the procedure, we implement the Newton-CG method to compute approximate solitary wave solutions of the KdV equation with velocity $c = 1/3$, as in the previous

section. We initialize the iterative scheme with $u_0 = \mathrm{sech}(x)$ and approximate the solution on a uniform grid in $[-50\pi, 50\pi]$ using $N = 2^{11}$ points. The iterative procedure is halted when $L_0[u_n] < 10^{-13}$ and the CG procedure used to compute ε_n are compete when $R < 10^{-3}$ as defined by Eq. (B.13). Figure B.2 shows the results of the iterative method. Figure B.2(a) is a qualitative comparison of the true solution and the numerically computed solitary wave and are indistinguishable. In fact, Fig. B.2 shows that the computed soliton and the true solution differ by only slightly above machine precision. In Fig. B.2(c), we show the rapid convergence of the method, showing that only 8 iterations of Eq. (B.10) were required, however, this does not account for the CG steps. In practice, the Newton-CG method is quite sensitive to the initial guess, and the solution often tends to zero rapidly for poor initial guesses.

B.2 Heteroclinic and homoclinic traveling waves

The numerical computation of heteroclinic traveling waves limiting to a constant is implemented implemented using the iterative Newton-conjugate gradient method that was described previously in Appendix B.1.2.2. We first consider the case of a heteroclinic traveling wave corresponding to a Whitham shock where the left state has zero wavenumber (cf. Section 5.2.1), $\varphi_- = \varphi_-(\theta; \overline{u}_-, a_-, 0)$ and the right wave is chosen to have zero mean and unit amplitude $\varphi_+ = \varphi_+(0, 1, k_+)$. We construct an approximate heteroclinic traveling wave solution by using a constant to approximate the solitary wave at the left state and the right state is approximated by a numerically computed periodic wave (cf. Appendix B.1.1) with a fixed number of oscillations. To implement the Newton-CG method, we use an even reflection of our initial guess across a minimum of the periodic wave so that the initial guess decays rapidly and is amenable to a description in terms of a Fourier series. An example of the initial guess for the iterative solver is shown in Fig. B.3, where intermediate periodic wave wavenumber is determined by the jump conditions (5.7)–(5.9). Outside the oscillatory region in the initial guess, the solution abruptly transitions to the known far-field

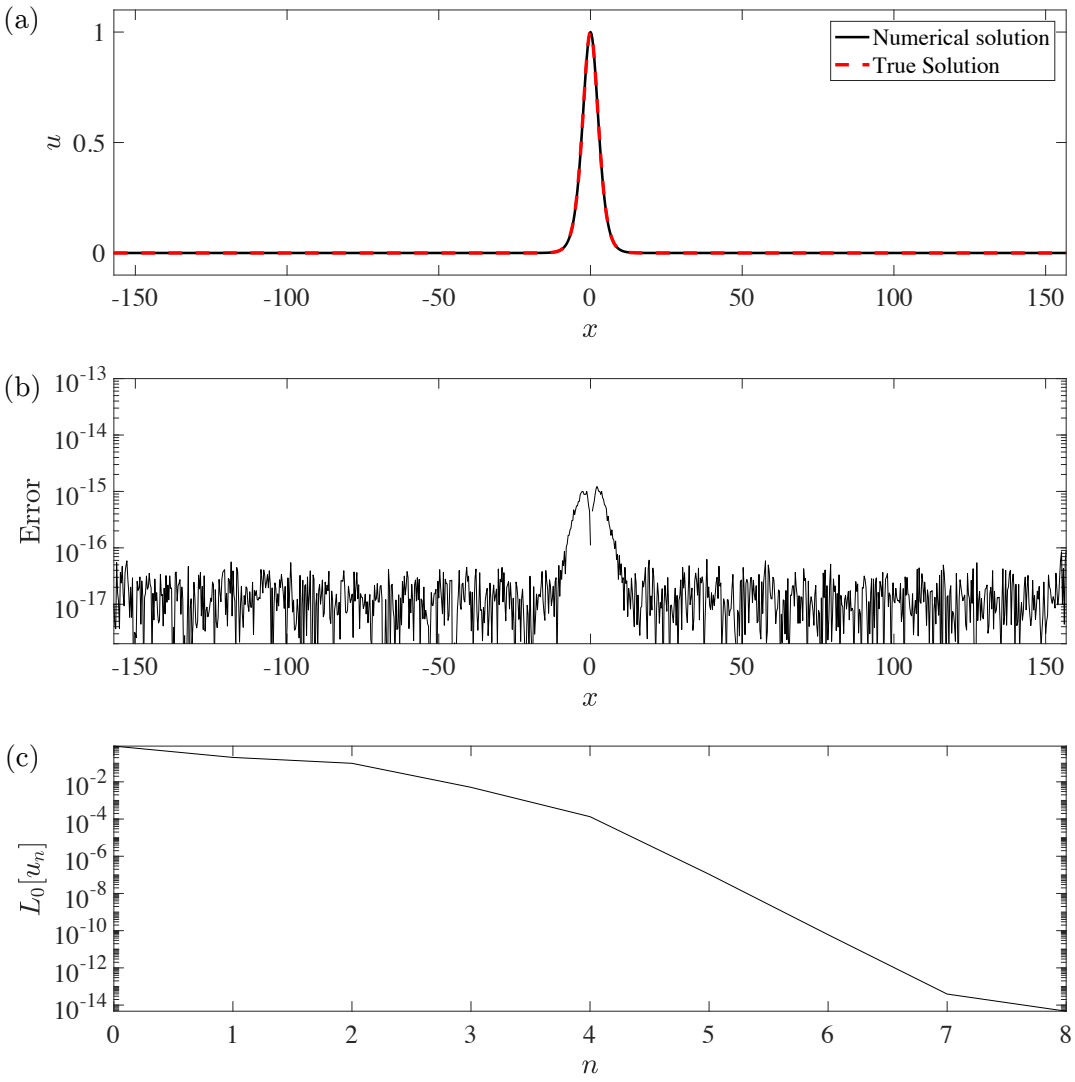

Figure B.2: Example of the use of the Newton-CG method to compute the soliton solution of the KdV equation with velocity $c = 1/3$. (a) Numerically computed solitary wave solution (black, solid) superimposed with the true solution (dashed, red). (b) The absolute error between the numerically computed solution and the true solution depicted in panel (a). (c) The residual of $L_0[u_n]$ at each step of the iterative scheme (B.9), n.

constant value determined by the same jump conditions. The initial guess is then given to the Newton-CG and a traveling wave with velocity V, determined by the jump conditions,

is then computed.

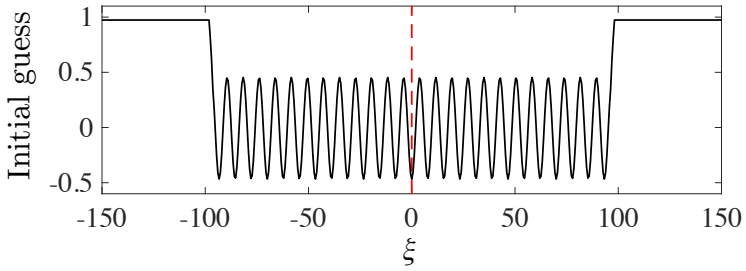

Figure B.3: Depiction of initial guess given to numerical method with an even reflection across the origin, identified by the vertical, dashed line.

Periodic-periodic heteroclinic traveling waves discussed in Section 5.2.2 are computed with Matlab's fifth order collocation method bvp5c. The heteroclinic traveling waves consist of left and right periodic waves $\varphi(x - Vt; \overline{u}_\pm, a_\pm, k_\pm)$ where the far-field periodic waves with the same velocity have parameters that satisfy the Rankine-Hugoniot relations of the KdV5-Whitham equations (5.7)–(5.9) with $\overline{u}_+ = 0$ and $a_+ = 1$.

A heteroclinic traveling wave with coordinate $\xi = x - Vt$ satisfies the fifth order dynamical system

$$\frac{d}{d\xi}\begin{bmatrix} u_1 \\ u_2 \\ u_3 \\ u_4 \\ u_5 \end{bmatrix} = \begin{bmatrix} u_2 \\ u_3 \\ u_4 \\ u_5 \\ Vu_2 - u_1u_2 \end{bmatrix}, \tag{B.14}$$

where the traveling wave profile is identified by $u = u_1(\xi)$.

In numerical computations, we specify an integer number of oscillations on the left and right of the origin denoted by n_- and n_+, respectively. The computational domain is therefore fixed to be $\xi \in [L_-, L_+]$ where

$$L_\pm = \pm 2(n_\pm + \frac{1}{2})\pi/k_\pm,$$

where $k_\pm$ denotes the wavenumber of the right $(+)$, left $(-)$ periodic waves. The $1/2$ term in $L_\pm$ owes to the fact that the left and right periodic waves are "glued" at their minima, halfway through one oscillation period. Furthermore, the computational domain is defined in such a way that the left and right periodic waves reach their maxima at $L_\pm$. Periodic-periodic heteroclinic solutions satisfy the boundary conditions

$$\begin{aligned} u_1(L_+) &= \varphi_+\left(\frac{2\pi n_+}{k_+}\right) & u_1(L_-) &= \varphi_-\left(\frac{2\pi n_-}{k_-}\right) \\ u_2(L_+) &= u_4(L_+) = 0 & u_2(L_-) &= 0. \end{aligned} \tag{B.15}$$

We briefly discuss the construction of the the initial guess provided to Matlab's fifth order collocation method. From the jump conditions, Eqs. (5.7)–(5.9), we are given the parameters of far-field periodic waves $\varphi_\pm = \varphi_\pm(\theta; \overline{u}_\pm, a_\pm, k_\pm, V)$ where the right periodic wave, φ_+, is normalized to have zero mean $\overline{u}_+ = 0$ and unit amplitude $a_+ = 1$. The remaining parameters k_+, $\overline{u}_+$, a_+ and k_+ are given by the jump conditions (cf. the shock loci shown in Fig. 5.6). The initial guess is comprised of $\frac{n_+ + 1}{2}$ wave periods emanating from the origin and terminating at $\xi = L_+$. The same construction is used for the left periodic wave, which is valued for negative values of ξ from the left boundary $\xi = L_-$ and terminating at $\xi = 0$. An example heteroclinic periodic-periodic solution to (B.14) satisfying boundary conditions (B.15) is shown in Fig. B.2. The solution depicted in Fig. B.2 required 1438 unequally spaced collocation points on the interval $[L_-, L_+]$ to achieve an maximum residual of 10^{-9}. However, if we increase the computational domain so that our initial guess contains oscillations $n_- = 8$ and $n_+ = 40$ while keeping all other far-field periodic wave parameters equal, we require 4483 unequally spaced mesh points to meet the same accuracy requirements. We illustrate the relation between the number of collocation points versus the maximum residual error achieved by numerical computations in Fig. B.2. Note that with a somewhat number of collocation points, we are able to achieve errors below 10^{-13} for the sample heteroclinic traveling waves.

Homoclinic traveling waves corresponding to two, co-propagating Whitham shocks are computed by solving Eq. (B.1) with periodic boundary conditions via Matlab's fifth order

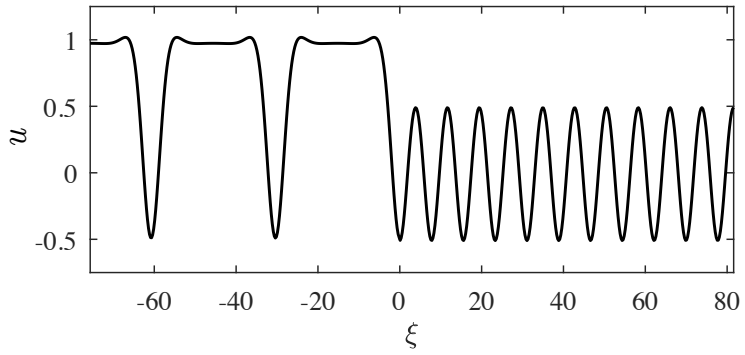

Figure B.4: Numerically computed periodic-to-periodic heteroclinic traveling wave corresponding to Whitham shock with parameters $\overline{u}_- = 0.75$, $a_- \approx 1.51$, $k_- \approx 0.206$, $k_+ \approx .809$. The number of oscillation periods are $n_- = 2$ and $n_+ = 10$.

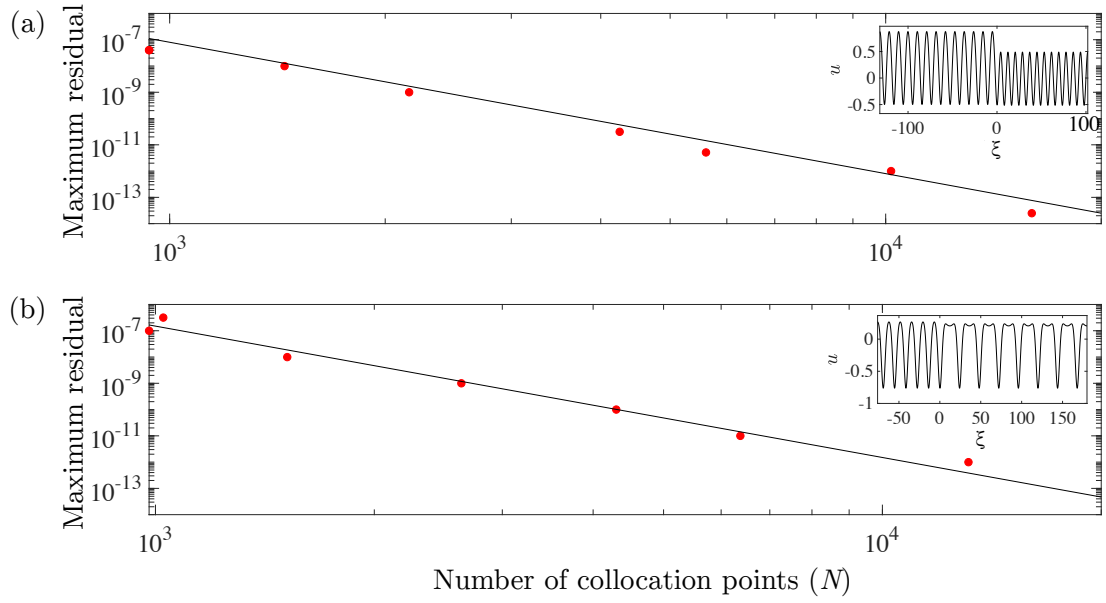

Figure B.5: Number of collocation points versus maximum residual error (red dots) for various periodic-periodic heteroclinic traveling waves plotted versus a reference line N^{-5} to demonstrate fifth order convergence. (a) Maximum residual error of a periodic-periodic heteroclinic traveling wave with approximate parameters $(\overline{u}_-, a_-, k_-) \approx (0.25, 1.37, 0.59)$ and $(\overline{u}_+, a_+, k_+) \approx (0, 1, 0.77)$ with $n_- = 12$ and $n_+ = 12$. (b) Maximum residual error of a periodic-periodic heteroclinic traveling wave with approximate parameters $(\overline{u}_-, a_-, k_-) \approx (-0.15, 1.02, 0.45)$ and $(\overline{u}_+, a_+, k_+) \approx (0, 1, 0.26)$ with $n_- = 5$ and $n_+ = 7$. Insets are computed heteroclinic traveling wave solutions with the smallest residual reported.

collocation method bvp5c. The length of the computational domain is chosen so that a

user specified number of oscillations of interior and exterior periodic waves can satisfy the periodic boundary conditions. The interior and exterior periodic waves' parameters are approximately given by points on the Whitham shock loci.

Homoclinic traveling waves are evolved using the integrating factor fourth order Runge-Kutta method[127] applied to Eq. (1.4). The method is the same as that implemented to compute the long time evolution of smoothed, step-like initial data, though we do not need to initially differentiate the equation and the initial data. We implement a spatial, Fourier discretization so that Fourier modes decay to $\mathcal{O}(10^{-14})$ and time steps, Δt, of the explicit fourth order Runge-Kutta method are chosen in the range $\Delta t \in [10^{-4}, 10^{-3}]$. Evolution of various homoclinic traveling waves with small amplitude, band-limited noise are given in Fig. 5.9.